PROELECTROPHILE-NUCLEOPHILE ADDUCT FORMATION AND PERMANGANATE OXIDATION OF ALKENES: USE OF MODEL COMPOUNDS TO PROBE COMPLEX REACTION PATHWAYS

By

Phillip M. Flanders

A dissertation submitted to Johns Hopkins University in conformity with the requirements for the degree of Doctor of Philosophy

Baltimore, Maryland

February, 2014

Abstract

Laboratory studies of reactions between model compounds yield valuable insights into complex reaction chemistries that would be difficult if not impossible to observe directly in environmental media. We used model compounds to investigate two types of reaction pathways: adduct formation and permanganate oxidation.

First, we mimicked covalent bond forming reactions between nucleophilic contaminants and electrophilic sites within natural organic matter (NOM) or naturally occurring electrophilic toxicants. Initial studies modeled adduct formation at electrophilic NOM sites by reacting the model electrophiles p-benzoquinone and patulin with a suite of model nucleophiles. Further studies used MnO_2(s, pyrolusite)-oxidized hydroquinone proelectrophiles to simulate the highly electrophilic moieties that can be generated when NOM reacts with oxidants in a sediment or soil. Overall, our model compound studies demonstrated that added nucleophiles compete with H_2O/OH^- to form monoadducts, which can then undergo further oxidization and addition to form di- and triadducts. Mass spectra consistent with monoadducts from reactions between nine nucleophiles and MnO_2-oxidized gentisic acid were acquired by LC/MS. Separate experiments monitoring both the consumption of a model proelectrophile and a nucleophile (acetylhydroquinone and 4-ethylaniline, respectively) and the generation of Mn^{II} from reduction of MnO_2 provided indirect evidence for multiple oxidation-addition steps.

Second, we used model compounds to study permanganate oxidation of alkenes. Competition between hydrolysis and oxidation of a common intermediate leads to a distribution of products. To collect direct evidence of the influence of pH and oxidant dose on this product distribution, we selected *cis*-stilbenedicarboxylic acid as a model compound because it yields permanganate oxidation products amenable to LC/MS analysis. High permanganate dose favors highly oxidized products, while alkaline pH favors products from hydrolysis.

This dissertation demonstrates how strategic selection of model compounds can elucidate complex environmental contaminant removal pathways by providing an internally consistent system for the study of multiple reaction conditions and competitive reactions.

Advisor: Alan T. Stone

Readers: A. Lynn Roberts and Steven Rokita

Acknowledgments

I owe thanks and gratitude to many people who've helped me and been there for me during graduate school.

First I thank my parents, Jeff and Karen Flanders, for their love and support throughout these many years of education. They have always offered inspiration, guidance, and assistance whenever I needed it–whether I knew I needed it or not.

I'd like to thank my roommates who've lived with me during graduate school: John Sivey, Umut Aypar, Andrew Clayborne and Jennifer Ronald. They put up with my quirks over the years and were understanding front lines to the day-to-day stress of graduate school.

I thank my advisor, Prof. Alan Stone, for all of his guidance, patience, and detailed feedback. He has been an invaluable resource and imaginative thinker throughout this entire process.

I thank other professors at Johns Hopkins who have influenced me over the past few years: Lynn Roberts, Bill Ball, Ed Bouwer, Kai Loon Chen, and Dimitri Sverjensky. I thank my DQE committee: Alan Stone, Lynn Roberts, Ed Bouwer, and Kai Loon Chen. I thank my GBO committee: Alan Stone, Lynn Roberts, Gerry Meyer, Caren Meyers, and Gary Posner. Lastly, I thank my defense committee: Alan Stone, Lynn Roberts, and Steven Rokita.

I thank Penney Miller, my research advisor during my undergraduate years at Rose-Hulman Institute of Technology. She piqued my interest in environmental chemistry. Her mentorship provided me with a set of skills that have been invaluable in my doctoral research. She gave me real appreciation for HPLC and LC/MS. She built the foundation of my scientific writing, presentation, and experimental planning skills.

I thank Chris Higgins for teaching me how to operate the LC/MS, which I used extensively in my research. He also has been a continuing source of help and inspiration.

I thank Keith Ritchie for all of his time and effort making sure that the instruments and tools that I use were kept in working order. I'm also grateful for his help with the lab for the Experimental Methods course.

I thank the department's front office staff for all of their help making this dissertation happen: Joe, Joyce, Christine, Rob, Rok, Adena, Denise, and the student workers.

I thank the other members of Prof. Stone's research group during my time at Johns Hopkins: Zhi Shi, Nathan Boland, Grace Stokes, and Xiaomeng Xia. I also thank the other doctoral students who worked along with me in the labs: John Sivey, Kevin Bisceglia, Katie Onesios, Jessica Lawson, Amar Wadhawan, Andrew Graham, Pavlo Bohutskyi, Jin Yang, An Huynh, Peng Yi, Yaqi You, Shao-Yiu Hsu, and Stephanie Lau. The discussions, collaborations, and friendships I've had with all of you were an invaluable part of these years of my life.

Lastly, I need to thank the friends I have made in Baltimore for making sure that–when I have some free time–I always enjoyed myself! You guys are the best! I would also like to thank the Dissertation Support Group for your advice and inspiration.

Thanks to everyone who has been a part of my life these past six years!

This dissertation is dedicated to

the army of people who believed in me

and made it possible.

Contents

List of Tables

List of Figures

List of Symbols

AAS	Flame Atomic Absorption Spectrometry
An	4-Ethylaniline
CHES	N-Cyclohexyl-2-aminoethanesulfonic acid
DEPP	1,4-Diethylpiperazine
e^-	Electron
EDG	Electron Donating Group
EDTA	Ethylenediaminetetraacetic acid
EWG	Electron Withdrawing Group
HPLC	High Performance Liquid Chromatography
[i]	Concentration of i, in either mol/L or μMol/L
$[i]_0$	Initial concentration of i, in either mol/L or μMol/L
Im	4-Methylimidazole
k_{obs}	Observed Pseudo-First-Order Rate Constant
LC/MS	Liquid Chromatography with Mass Spectrometry
LOD	Limit of Detection
m/z	Mass to Charge ratio of a fragment detected in mass pectrometry

MES	2-(N-morpholino)ethanesulfonic acid
MOPS	3-(N-morpholino)propanesulfonic acid
$[M\text{-}COOH]^-$	Anionic fragment produced during ionization in LC/MS resulting from loss of a carboxylic acid functional group
$[M\text{-}H]^-$	Anionic fragment produced during ionization in LC/MS resulting from loss of a carboxylic acid functional group
NER	Non-Extractable Residue
NMR	Nuclear Magnetic Resonance
NOM	Natural Organic Matter
Nu	Nucleophile
OE	Oxidizing Equivalent
pK_a	Acid Dissociation Constant
UV/Vis	Ultraviolet/Visible Light Spectrophotometry
X-Nu	Monoadduct hydroquinone resulting from addition of an added nucleophile
X-OH	Monoadduct hydroquinone resulting from addition of H_2O or OH^-
XH_2	A *p*-dihydroxybenzene
XH_2(I)	Hydroquinone
XH_2(II)	Acetylhydroquinone
XH_2(III)	2,5-Dihydroxybenzoic acid
XH_2(IV)	2,5-Dihydroxyterephthalic acid
Z	A *p*-benzoquinone
Z-Nu	Monoadduct benzoquinone resulting from oxidation of X-Nu

Z-OH	Monoadduct benzoquinone resulting from oxidation of X-OH
Z(I)	*p*-Benzoquinone
Z(II)	Acetyl-*p*-benzoquinone
Z(III)	Carboxy-*p*-benzoquinone
Z(IV)	2,5-Dicarboxy-*p*-benzoquinone
ξ	Extent of reaction
ρ	Hammett reaction constant
σ	Hammett substituent constant

Chapter 1

Introduction

1.1 Motivation

Manganese can be an important oxidant in soils and sediments and in water and wastewater treatment systems. We will focus on $Mn^{III,IV}$ (hydr)oxides and permanganate (MnO_4^-). $Mn^{III,IV}$ (hydr)oxides are present in both sediments and soil and have high enough reduction potentials to oxidize many organic reductants such as hydroquinone and catechols, which could represent redox active moieties within natural organic matter (NOM).

Contaminants containing nucleophilic functional groups could be removed from the water column by undergoing nucleophilic addition reactions with electrophilic sites within NOM. Whether or not removal is irreversible depends on the reaction mechanism and the nature of that product that is ultimately generated. Most organic contaminants will partition into NOM based on their affinity for organic matter versus aqueous solution, however this "physical" partitioning phenomenon is reversible and can be described by partitioning coefficients that are often correlated to the octanol-water partition coefficient (K_{ow}). Mechanisms that lead to covalent bonds and thus irreversible sorption include radical coupling, nucleophilic substitution, and nucleophilic addition reactions. Nucleophilic

addition can form a bond between nucleophiles and carbonyl functional groups (ketones and aldehydes) or α,β-unsaturated carbonyls, also known as "Michael acceptors." Whether or not a contaminant will form an irreversible bond depends on the strength of the nucleophile and the ambient chemical conditions.

The importance of nucleophilic addition reactions in contaminant removal also depends on the strength of the electrophilic functional groups. NOM is thought to contain carbonyl and benzoquinone electrophilic functional groups (*1*, *2*). Nucleophilic addition to carbonyl functional groups, 1,2-addition, is reversible but Michael-type addition, 1,4-addition, to benzoquinones is irreversible (*3*, *4*). Both 1,2- and 1,4-addition will occur with NOM, but 1,4-addition to benzoquinone electrophiles leads to ultimate removal of the contaminant (*3*). The electrophilicity of a benzoquinone functional group changes based on whether it is a 1,4 or a 1,2 benzoquinone and on electron withdrawing and donating ability of the ring substituents (*5*). The NOM matrix to which a benzoquinone is attached will exert both electronic and steric effects on its electrophilicity. Benzoquinones deep within the NOM structure may be unavailable for reaction with nucleophiles from the water column for steric reasons. Benzoquinones bound to NOM via alkyl chains are inhibited by the electron donating properties of alkyl functional groups. However, carbonyl groups such as carboxylic acids are electron withdrawing and should increase the electrophilicity of nearby benzoquinones. Ratasuk et al. (*2*) suggested that quinone functional groups within NOM fall into two categories: reactive benzoquinones that possess electron-withdrawing groups, and sterically hindered benzoquinones that are bonded to electron-donating substituents (*2*).

Benzoquinone functional groups within NOM are also thought to be involved in the redox properties of NOM (*2*, *6–9*). For example, some microorganisms use NOM as an intermediate electron shuttle, allowing them to reduce insoluble Fe(III) to bioavailable Fe(II) (*9*, *10*). Benzoquinones are linked to catechol and hydroquinone moieties by reduction

and oxidation reactions: oxidation of NOM will transform catechol and hydroquinone moieties into benzoquinone, reduction of NOM transforms benzoquinones into phenols. This means that the presence of an oxidant will generate electrophilic benzoquinone moieties via oxidation of non-electrophilic catechol and hydroquinone moieties. We refer to catechol and hydroquinone moieties as "proelectrophiles" which are compounds that become electrophilic after oxidation. We therefore expect that oxidation of NOM will increase the number of electrophilic sites within NOM.

Beyond the number of electrophilic sites, we expect that oxidation will also increase the *electrophilicity* of NOM. Benzoquinones with electron-withdrawing substituents are highly unstable in the presence of water. For example, carboxy-*p*-benzoquinone cannot be synthesized (*11*) and is not commercially available. Carboxy-*p*-benzoquinone is so electrophilic that it quickly reacts with an available nucleophile. In aqueous solution, hydroxide ion and water itself can both react as nucleophiles. We refer to addition of water or hydroxide as "hydration." When a stronger nucleophile is available, addition products other than the hydration product will be formed. Oxidation could unlock highly reactive electrophilic sites within NOM by generating benzoquinone sites with electron-withdrawing substituents that can react with nucleophilic contaminants.

Permanganate (MnO_4^-) is used in many ways in water treatment and environmental remediation (*12*, *13*). MnO_4^- can remove Mn^{II} and Fe^{II} during drinking water treatment as well as remedy taste and odor problems. It can remove precursors to trihalomethanes and other disinfection byproducts. It can promote coagulation and flocculation improving removal of organic carbon. MnO_4^- can also be used as a chemical oxidant in groundwater remediation (*14*).

Although manganese is an essential nutrient and is found naturally in source waters, too much manganese in drinking water can cause problems with unpleasant taste or odor,

discoloration, and staining of plumbing fixtures, leading to customer complaints for drinking water suppliers (*15*, *16*). Excess iron leads to similar complaints. Water containing high concentrations of manganese usually comes from wells under reducing conditions where manganese and iron exist in their reduced and soluble forms: Mn^{2+} and Fe^{2+} (*17*).

Drinking water treatment plants remove excess manganese and iron by one of two methods. Adding an oxidant (such as MnO_4^-, ozone, or chlorine dioxide) will oxidize Mn^{2+} and Fe^{2+} to insoluble forms. The resulting particles can be removed by filtration or coagulation and sedimentation. A second method called "manganese green sands" involves a column filter loaded with $Mn^{III,IV}$ (hydr)oxide coated media. The $Mn^{III,IV}$ coating oxidizes Mn^{2+} and Fe^{2+} to insoluble forms that the filter media traps. Continuous or pulse addition of an oxidant (usually MnO_4^- or free chlorine) regenerates Mn^{IV} in the oxide coating (*17–21*).

Similarly, MnO_4^- can be used to help remove arsenic from drinking water. MnO_4^- oxidizes arsenite (As^{III}) to arsenate (As^{V}). Precipitation or adsorption can remove arsenate but arsenite is difficult to remove using these conventional techniques (*22*). Arsenic removal from drinking water is a critical public health issue. Chronic exposure to arsenic in drinking water at high concentrations can lead to skin or lung cancer, while at low concentrations it can cause chronic fatigue, hair loss, weight loss, variation in skin pigment, hyperkeratoses, and ulcerations (*22*, *23*).

Some water treatment plants use MnO_4^- to remove taste and odor problems from drinking water (*15*, *16*). Organic odor compounds of algal or bacterial origin such as β-cyclocitral (*24*, *25*) and dimethyl trisulfide (*26*) are degraded by MnO_4^-. MnO_4^- effectively treats source waters contaminated with hydrogen sulfide (*27*). MnO_4^- can also be used in industrial wastewater treatment. For example, it effectively decolorizes dye and textile industry wastewater (*28*).

Oxidation of organic matter in source waters can remove precursors that form trihalomethanes and other disinfection byproducts (*29–31*). Many of these byproducts, including trihalomethanes, are suspected carcinogens and are regulated by the Clean Water Act. In drinking water treatment, THMs are generated by oxidation of organic matter by free chlorine. As concern about disinfection byproducts in drinking water increases and regulatory limits tighten, permanganate pre-oxidation may be used in more drinking water treatment plants to control DBP formation.

Some "enhanced coagulation" techniques employ MnO_4^- oxidation, which improves aggregation during coagulation in water treatment plants, especially when the source water contains high levels of organic carbon. MnO_4^- aids aggregation in two ways: it breaks up organic matter into smaller fragments that are more easily adsorbed by coagulant (*32*), and it precipitates solid $Mn^{III,IV}$ oxyhydroxide particles that aid in adsorbing organic matter or that cause further oxidation (*33*, *34*).

"In-situ chemical oxidation" employs MnO_4^- or another oxidant for groundwater remediation. Oxidant solution is delivered by a pump and flood method where MnO_4^- reacts with the target contaminant (*35*). In-situ chemical oxidation using MnO_4^- as an oxidant can effectively treat many contaminants including chlorinated ethylenes (*36–38*), cyclotrimethylenetrinitramine (RDX, *39*, *40*), chlorophenols (*41*), and methyl-*tert*-butyl ether (*42*). Waldemer and Tratnyek (*43*) reported rate constants for 24 contaminants including some pesticides, substituted phenols, TNT, and methyl ethyl ketone.

Researchers are exploring the ability of MnO_4^- to remove micropollutants from water. Some micropollutants that are effectively removed by MnO_4^- include the cyanobacterial toxin microcystin-LR (*44–47*), endocrine-disrupting compounds related to estradiol (*48*), the antibacterial compound triclosan (*49*), and pesticides including aldrin, terbufos, metribuzin, permethrin (*50*), and dichlorvos (*51*).

1.2 Oxidation States of Manganese

The manganese atom in MnO_4^- is in the $+7$ oxidation state which is the highest oxidation state of manganese (Figure 1.1). The standard reduction potential of permanganate is based on which reduction product is generated which is thought to depend on solution pH (Table 1.1).

The $+3$ and $+4$ Mn oxidation states exist as solids in relevant aqueous conditions forming a variety of $Mn^{III,IV}$ (hydr)oxides that vary by crystal structure and Mn^{III} to Mn^{IV} ratio (*52*, *53*). These compounds are important in environmental reduction and oxidation reactions and are nearly ubiquitous in soils and sediments (*53*). Mn^{II} exists as a colorless and highly soluble ion, $Mn^{2+}(aq)$.

Mn^{V} and Mn^{VI} could be important species involved in reduction of MnO_4^-, but only transiently because they are generally not stable under conditions relevant to water and wastewater treatment. Manganate (Mn^{VI}) exists as an oxoanion, MnO_4^{2-}, that is unstable in water and disproportionates to MnO_2 and MnO_4^- (*54*).

$$3\,Mn^{VI}O_4^{2-} + 2\,H_2O \rightleftharpoons Mn^{IV}O_2 + 2\,Mn^{VII}O_4^- + 4\,OH^- \tag{1.1}$$

The equilibrium constant for Equation 1.1 favors MnO_2 and MnO_4^-. MnO_2 particles act as a heterogeneous catalyst and increase the rate of disproportionation (*55*). Hypomanganate (Mn^{V}) is stable as MnO_4^{3-} in highly alkaline solution, although the protonated species rapidly reacts via disproportionation which is catalyzed by MnO_2 solid (*56*). Additionally, one-electron oxidation of hypomanganate to manganate is "immeasurably fast at room temperature" (*56*).

$$MnO_4^- + MnO_4^{3-} \rightleftharpoons 2\,MnO_4^{2-} \tag{1.2}$$

Mn^{III} and Mn^{IV} precipitate as (hydr)oxide solids in aquatic conditions. Pyrolusite (β-MnO_2) is the most thermodynamically stable form under oxidizing conditions at circumneutral to alkaline pH (*52*). Pyrolusite (β-MnO_2), feitnechtite (β-MnOOH), manganite (γ-MnOOH), and birnessite (δ-MnO_2) all have high reduction potentials, making them powerful oxidants. Reduction potentials for some $Mn^{III,IV}$ (hydr)oxide are shown in Table 1.1.

In aquatic environments manganese cycles across the oxic/anoxic interface because of the differing properties of the +3/+4 and +2 oxidation states (Figure 1.2, *57*). $Mn^{III,IV}$ (hydr)oxides are stable in the oxic zone of the water column and settle to the top of sediments. Abiotic and microbial reactions reduce the (hydr)oxides to Mn^{2+}(aq) which is is highly soluble in water and readily diffuses back into the water column. Fluxes of Mn^{2+}(aq) from sediments have been measured in several different locations and range from 0.07 to 2.3 mmol m^{-2} day^{-1} (*58*). After returning to the oxic zone, Mn^{2+}(aq) is oxidized via both microbial and abiotic mechanisms into $Mn^{III,IV}$(hydr)oxide particles (*58*, *59*) to complete the cycle. Due to this redox cycling of manganese, each manganese atom is oxidized and reduced 100 to 300 times before ultimate burial (*60*).

$Mn^{III,IV}$(hydr)oxides can be reduced microbially (*61*, *62*), by sulfide below the oxic/anoxic interface (*63*), or by organic molecules (*64–66*). Reduction by dissolved Fe^{II} is also possible, but is inhibited by complexation of Fe^{2+} (*62*).

Oxidation of Mn^{2+}(aq) is favorable under oxidizing conditions at circumneutral pH (*52*). Oxidation by O_2 occurs slowly in solution or at a mineral surface (*67*). Microbial oxidation is several orders of magnitude faster, and increases with increasing concentration of dissolved O_2 (*68–71*).

1.3 Research Objectives and Thesis Outline

This research is focused on three reaction pathways: Michael addition of nucleophiles to benzoquinones and naturally occurring Michael acceptors, the proelectrophile reaction mechanism, and permanganate oxidation of alkenes. We are particularly interested in the effect of aqueous chemical conditions (especially pH) and initial concentrations on the resulting product distribution. We chose to work primarily with model compounds in clean laboratory conditions. Using model compounds allows us to directly study kinetics and mechanisms involved in all three pathways which is prohibitively difficult when using environmental samples. Also, working with model compounds decreases the complexity of the product distribution generated by these reactions.

In Chapter 2, we employ *p*-benzoquinone and patulin as model Michael acceptor electrophiles to improve our understanding of the kinetics and mechanism of the Michael addition reaction in neutral pH aqueous conditions. The rate of electrophile consumption under pseudo-first-order kinetic conditions gives a direct comparison of the nucleophilicity towards Michael addition of our model nucleophiles. We show that the Hammett relationship holds for para-substituted anilines for Michael addition, indicating the important of electronic effects on reaction rate.

Chapter 3 explores the proelectrophile pathway, which we expect will occur in sediments (*1*, *3*, *4*, *72*) and soils (*73*, *74*). Our model electrophiles are hydroquinones containing electron-withdrawing group substituents. The hydroquinone molecules are oxidized by MnO_2(s, pyrolusite) particles that are 98% Mn^{IV} and only 2% Mn^{III}, so we expect a one-to-one stoichiometry between hydroquinone and MnO_2. Oxidation generates a highly electrophilic benzoquinone that quickly reacts with water to form a hydration product or an

added nucleophile to form an adduct. We prepared solutions containing nine nucleophiles and gentisic acid in the presence of MnO_2 and recorded LC/MS evidence for the resulting addition products. Because benzoquinone adducts and hydration products are themselves hydroquinones, they are subject to oxidation by MnO_2, yielding a second generation of benzoquinones that can undergo further hydration and nucleophilic reaction steps. It is, therefore, possible for one hydroquinone model compound to undergo oxidation and addition multiple times in the presence of excess oxidant. We show that the importance of second generation addition products depends on the initial concentration of nucleophile.

In Chapter 4, we employ cis-stilbenedicarboxylic acid as a model compound to understand product distribution resulting from alkene oxidation by MnO_4^-. The oxidation rate of alkene functional groups by MnO_4^- is fast and independent of pH for the rate-determining step which is thought to be attack of MnO_4^- attacks on the alkene resulting in an unstable intermediate. The product distribution results from a complex system of reactions that break down the intermediate. Several pathways are possible and which of the pathways dominates depends on competition between hydrolysis and further oxidation steps. The possible organic oxidation and Mn reduction products differ by the extent of oxidation that occurs. The organic oxidation products range from diols to a pair of carboxylic acids from C=C bond-cleavage. We use LC/MS to monitor organic reactants and products including products for which authentic standards are not available. We propose a modified iodometric titration method to measure MnO_4^-, $Mn^{III,IV}$ solids, and Mn^{2+}. We vary the pH, the buffer system, and reductant to oxidation concentration ratio to explore their effects on the product ratios.

References

(1) K. A. Thorn, P. Pettigrew, W. S. Goldenberg, E. J. Weber. Covalent binding of aniline to humic substances. 2. ^{15}N NMR studies of nucleophilic addition reactions. *Environmental Science and Technology* **1996**, *30*, 2764–2775.

(2) N. Ratasuk, M. A. Nanny. Characterization and quantification of reversible redox sites in humic substances. *Environmental Science and Technology* **2007**, *41*, 7844–7850.

(3) E. J. Weber, D. L. Spidle, K. A. Thorn. Covalent binding of aniline to humic substances. 1. Kinetic studies. *Environmental Science and Technology* **1996**, *30*, 2755–2763.

(4) G. E. Parris. Covalent binding of aromatic amines to humates. 1. Reactions with carbonyls and quinones. *Environmental Science and Technology* **1980**, *14*, 1099–1106.

(5) A. Kutyrev. Nucleophilic reactions of quinones. *Russian Chemical Reviews* **1991**, *60*, 72–88.

(6) R. Sutton, G. Sposito. Molecular structure in soil humic substances: The new view. *Environmental Science and Technology* **2005**, *39*, 9009–9015.

(7) Z. Struyk, G. Sposito. Redox properties of standard humic acids. *Geoderma* **2001**, *102*, 329–346.

(8) J. Nurmi, P. G. Tratnyek. Electrochemical properties of natural organic matter (NOM), fractions of NOM, and model biogeochemical electron shuttles. *Environmental Science and Technology* **2002**, *36*, 617–624.

(9) D. Scott, D. McKnight, E. Blunt-Harris, S. Kolesar, D. Lovley. Quinone moieties act as electron acceptors in the reduction of humic substances by humics-reducing microorganisms. *Environmental Science and Technology* **1998**, *32*, 2984–2989.

(10) D. R. Lovley, J. D. Coates, E. L. Blunt-Harris, E. J. P. Phillips, J. C. Woodward. Humic substances as electron acceptors for microbial respiration. *Nature* **1996**, *382*, 445–448.

(11) T. J. Holmes, V. John, J. Vennerstrom, K. E. Choi. Solution characterization of carboxybenzoquinone and the isolation of derived quinhydrones. *The Journal of Organic Chemistry* **1984**, *49*, 4736–4738.

(12) J. Walton, P. Labine, A. Reidies, *The Chemistry of Permanganate in degradative oxidations* in *Chemical Oxidation: Technologies for the Nineties*, W. W. Eckenfelder, J. A. Roth, A. R. Bowers (Eds.), CRC Press, Lancaster, **1992**, pp. 205–230.

(13) U.S. EPA Office of Ground Water and Drinking Water; Alternative Disinfectants and Oxidants Guidance Manual. **1999**.

(14) R. L. Siegrist, M. A. Urynowicz, O. R. West, M. L. Crimi, K. S. Lowe, *Principles and Practices of In Situ Chemical Oxidation Using Permanganate*, Batelle Press, Columbus, OH, **2001**.

(15) A. M. Dietrich. Aesthetic issues for drinking water. *Journal of Water and Health* **2006**, *4*, 11–16.

(16) J. M. Cerrato, Reyes, L.P., C. N. Alvarado, A. M. Dietrich. Effect of PVC and iron materials on Mn(II) deposition in drinking water distribution systems. *Water Research* **2006**, *40*, 2720–2726.

(17) L. Rader. How to operate and maintain manganese greensand treatment units. *On Tap* **2003**, *2*, 31–32.

(18) B. F. Willey, H. Jennings. Iron and Manganese Removal with Potassium Permanganate. *Journal (American Water Works Association)* **1963**, *55*, 729–734.

(19) A. A. Islam, J. E. Goodwill, R. Bouchard, J. E. Tobiason, W. R. Knocke. Characterization of filter media MnOx(s) surfaces and Mn removal capability. *Journal (American Water Works Association)* **2010**, *102*, 71–83.

(20) R. Raveendran, B. Chatelier, K. Williams. Oxidation of manganese in drinking water systems using potassium permanganate. *Water Science and Technology: Water Supply* **2002**, *2*, 173–178.

(21) J. M. Cerrato, M. F. Hochella Jr, W. R. Knocke, A. M. Dietrich, T. F. Cromer. Use of XPS to identify the oxidation state of Mn in solid surfaces of filtration media oxide samples from drinking water treatment plants. *Environmental Science and Technology* **2010**, *44*, 5881–5886.

(22) S. Sorlini, F. Gialdini. Conventional oxidation treatments for the removal of arsenic with chlorine dioxide, hypochlorite, potassium permanganate and monochloramine. *Water Research* **2010**, *44*, 5653–5659.

(23) F. W. Pontius, K. G. Brown, C.-J. Chen. Health implications of arsenic in drinking water. *Journal (American Water Works Association)* **1994**, *86*, 52–63.

(24) K. J. Zhang, N. Y. Gao, H. K. Yen, Y. T. Chiu, T. F. Lin. Degradation and formation of wood odorant β-cyclocitral during permanganate oxidation. *Journal of Hazardous Materials* **2011**, *194*, 362–368.

(25) A. M. Dietrich, R. C. Hoehn, L. C. Dufresne, L. W. Buffin, D. M. C. Rashash, B. C. Parker. Oxidation of odorous and nonodorous algal metabolites by permanganate, chlorine, and chlorine dioxide. *Water Science and Technology* **1995**, *31*, 223–228.

(26) X. Ma, S. Hu, H. Wang, J. Li, J. Huang, Y. Zhang, W. Lu, Q. Li. Kinetics of oxidation of dimethyl trisulfide by potassium permanganate in drinking water. *Frontiers of Environmental Science and Engineering in China* **2012**, *6*, 171–176.

(27) S. Edwards, R. Alharthi, A. E. Ghaly. Removal of hydrogen sulphide from water. *American Journal of Environmental Sciences* **2011**, *7*, 295–305.

(28) X. R. Xu, H. B. Li, W. H. Wang, J. D. Gu. Decolorization of dyes and textile wastewater by potassium permanganate. *Chemosphere* **2005**, *59*, 893–898.

(29) B. Moyers, J. S. Wu. Removal of organic precursors by permanganate oxidation and alum coagulation. *Water Research* **1985**, *19*, 309–314.

(30) K. J. Ficek, J. E. Boll. Potassium permanganate: an alternative to prechlorination. *Aqua* **1980**.

(31) S. Miller. Disinfection Products In Water Treatment. *Environmental Science and Technology* **1993**, *27*, 2292–2294.

(32) W. Z. Yu, J. Gregory, T. Liu, Y. L. Yang, M. Sun, G. B. Li. Effect of enhanced coagulation by $KMnO_4$ on the fouling of ultrafiltration membranes. *Water Science and Technology* **2011**, *64*, 1497–1502.

(33) J. Ma, G. Li. Laboratory and full-scale plant studies of permanganate oxidation as an aid in coagulation. *Water Science and Technology* **1993**, *27*, 47–54.

(34) J. Ma, G. B. Li, Z. L. Chen, G. R. Xu, G. Q. Cai. Enhanced coagulation of surface waters with high organic content by permanganate preoxidation. *Water Science and Technology: Water Supply* **2001**, *1*, 51–61.

(35) Y. Seol, H. Zhang, F. W. Schwartz. A Review of In Situ Chemical Oxidation and Heterogeneity. *Environmental and Engineering Geoscience* **2003**, *9*, 37–49.

(36) M. Schnarr, C. Truax, G. Farquhar, E. Hood, T. Gonullu, B. Stickney. Laboratory and controlled field experiments using potassium permanganate to remediate trichloroethylene and perchloroethylene DNAPLs in porous media. *Journal of Contaminant Hydrology* **1998**, *29*, 205–224.

(37) Y. E. Yan, F. W. Schwartz. Oxidative degradation and kinetics of chlorinated ethylenes by potassium permanganate. *Journal of Contaminant Hydrology* **1999**, *37*, 343–365.

(38) Y. E. Yan, F. W. Schwartz. Kinetics and Mechanisms for TCE Oxidation by Permanganate. *Environmental Science and Technology* **2000**, *34*, 2535–2541.

(39) J. Albano, S. Comfort, V. Zlotnik, T. Halihan, M. Burbach, C. Chokejaroenrat, S. Onanong, W. Clayton. In situ chemical oxidation of RDX-Contaminated groundwater with permanganate at the nebraska ordnance plant. *Ground Water Monitoring and Remediation* **2010**, *30*, 96–106.

(40) T. Halihan, J. Albano, S. Comfort, V. A. Zlotnik. Electrical resistivity imaging of a permanganate injection during in situ treatment of RDX-contaminated groundwater. *Ground Water Monitoring and Remediation* **2012**, *32*, 43–52.

(41) S. M. G. Hossain, R. G. McLaughlan. Oxidation of Chlorophenols in Aqueous Solution by Excess Potassium Permanganate. *Water, Air, and Soil Pollution* **2011**, *223*, 1429–1435.

(42) J. H. Damm, C. Hardacre, R. M. Kalin, K. P. Walsh. Kinetics of the oxidation of methyl tert-butyl ether (MTBE) by potassium permanganate. *Water Research* **2002**, *36*, 3638–3646.

(43) R. Waldemer, P. G. Tratnyek. Kinetics of contaminant degradation by permanganate. *Environmental Science and Technology* **2006**, *40*, 1055–1061.

(44) W. Li, J. Duan, D. Mulcahy. Kinetic characteristics of oxidation of microcystin-LR at low concentration by chlorine and permanganate. *Journal Of Water Supply Research And Technology-Aqua* **2012**, *61*, 82–93.

(45) J. Acero, E. Rodríguez, M. E. Majado, A. Sordo, J. Meriluoto. Oxidation of microcystin-LR with chlorine and permanganate during drinking water treatment. *Journal Of Water Supply Research And Technology-Aqua* **2008**, *57*, 371–380.

(46) E. Rodríguez, J. Acero, L. Spoof, J. Meriluoto. Oxidation of MC-LR and -RR with chlorine and potassium permanganate: Toxicity of the reaction products. *Water Research* **2008**, *42*, 1744–1752.

(47) G. D. Onstad, S. Strauch, J. Meriluoto, G. A. Codd, U. von Gunten. Selective oxidation of key functional groups in cyanotoxins during drinking water ozonation. *Environmental Science and Technology* **2007**, *41*, 4397–4404.

(48) J. Jiang, S.-Y. Pang, J. Ma, H. Liu. Oxidation of phenolic endocrine disrupting chemicals by potassium permanganate in synthetic and real waters. *Environmental Science and Technology* **2012**, *46*, 1774–1781.

(49) J. Jiang, S.-Y. Pang, J. Ma. Oxidation of triclosan by permanganate (Mn(VII)): Importance of ligands and in situ formed manganese oxides. *Environmental Science and Technology* **2009**, *43*, 8326–8331.

(50) E. Chamberlain, H. Shi, T. Wang, Y. Ma, A. Fulmer, C. Adams. Comprehensive screening study of pesticide degradation via oxidation and hydrolysis. *Journal of Agricultural and Food Chemistry* **2012**, *60*, 354–363.

(51) C. Liu, Z. Qiang, C. Adams, F. Tian, T. Zhang. Kinetics and mechanism for degradation of dichlorvos by permanganate in drinking water treatment. *Water Research* **2009**, *43*, 3435–3442.

(52) O. Bricker. Some Stability Relations in the System Mn-O_2-H_2O at 25°C and One Atmosphere Total Pressure. *American Mineralogist* **1965**, *50*, 1296–1354.

(53) J. E. Post. Manganese oxide minerals: Crystal structures and economic and environmental significance. *Proceedings Of The National Academy Of Sciences Of The United States Of America* **1999**, *96*, 3447–3454.

(54) H. I. Schlesinger, H. B. Siems. The solubility product of barium manganate and the equilibrium between manganate and permanganate ions. *The Journal of the American Chemical Society* **1924**, *46*, 1965–1978.

(55) F. R. Duke. The disproportionation of manganate ion. Manganese dioxide as heterogeneous catalyst. *Journal of Physical Chemistry* **1952**, *56*, 882–884.

(56) A. Carrington, M. C. R. Symons. Structure and reactivity of the oxy-anions of transition metals. Part I. The manganese oxy-anions. *Journal of The Chemical Society (Resumed)* **1956**, 3373–3380.

(57) K. Nealson, D. Saffarini. Iron and manganese in anaerobic respiration: Environmental significance, physiology, and regulation. *Annual Review of Microbiology* **1994**, *48*, 311–343.

(58) C. Johnson, M. Ulrich, L. Sigg, D. M. Imboden. A mathematical model of the manganese cycle in a seasonally anoxic lake. *Limnology & Oceanography* **1991**, *36*, 1415–1426.

(59) P. van Cappellen, Y. Wang. Cycling of iron and manganese in surface sediments: A general theory for the coupled transport and reaction of carbon, oxygen, nitrogen, sulfur, iron, and manganese. *American Journal of Science* **1996**, *296*, 197–243.

(60) D. Canfield, B. Thamdrup, J. Hansen. The anaerobic degradation of organic matter in Danish coastal sediments: Iron reduction, manganese reduction, and sulfate reduction. *Geochimica et Cosmochimica Acta* **1993**, *57*, 3867–3883.

(61) C. R. Myers, K. Nealson. Bacterial Manganese Reduction And Growth With Manganese Oxide As The Sole Electron-Acceptor. *Science* **1988**, *240*, 1319–1321.

(62) C. R. Myers, K. Nealson. Microbial Reduction Of Manganese Oxides - Interactions With Iron And Sulfur. *Geochimica et Cosmochimica Acta* **1988**, *52*, 2727–2732.

(63) D. J. Burdige, K. Nealson. Chemical And Microbiological Studies Of Sulfide-Mediated Manganese Reduction. *Geomicrobiology Journal* **1986**, *4*, 361–387.

(64) H. Ulrich, A. T. Stone. Oxidation of chlorophenols adsorbed to manganese oxide surfaces. *Environmental Science and Technology* **1989**, *23*, 421–428.

(65) Y. Wang, A. T. Stone. The citric acid-(MnO2)-O-III,IV(birnessite) reaction. Electron transfer, complex formation, and autocatalytic feedback. *Geochimica et Cosmochimica Acta* **2006**, *70*, 4463–4476.

(66) Y. Wang, A. T. Stone. Reaction of Mn-III,Mn-IV (hydr)oxides with oxalic acid, glyoxylic acid, phosphonoformic acid, and structurally-related organic compounds. *Geochimica et Cosmochimica Acta* **2006**, *70*, 4477–4490.

(67) S. Davies, J. J. Morgan. Manganese(II) oxidation kinetics on metal oxide surfaces. *Journal of Colloid and Interface Science* **1989**, *129*, 63–77.

(68) S. Emerson, S. Kalhorn, L. Jacobs, B. Tebo, K. Nealson, R. Rosson. Environmental oxidation rate of manganese(II): bacterial catalysis. *Geochimica et Cosmochimica Acta* **1982**, *46*, 1073–1079.

(69) B. Tebo, K. Nealson, S. Emerson, L. Jacobs. Microbial mediation of Mn(II) and Co(II) precipitation at the O2/H2S interfaces in two anoxic fjords. *Limnology & Oceanography* **1984**, *29*, 1247–1258.

(70) B. Tebo, S. Emerson. Effect of oxygen tension, Mn(II) concentration, and temperature on the microbially catalyzed Mn(II) oxidation rate in a marine fjord. *Applied And Environmental Microbiology* **1985**, *50*, 1268–1273.

(71) B. Tebo, S. Emerson. Microbial manganese(II) oxidation in the marine environment: a quantitative study. *Biogeochemistry* **1986**, *2*, 149–161.

(72) D. Colon, E. J. Weber, G. Baughman. Sediment-associated reactions of aromatic amines. 2. QSAR development. *Environmental Science and Technology* **2002**, *36*, 2443–2450.

(73) H. Li, L. Lee. Sorption and abiotic transformation of aniline and α-naphthylamine by surface soils. *Environmental Science and Technology* **1999**, *33*, 1864–1870.

(74) H. Li, L. Lee, D. Schulze, C. A. Guest. Role of soil manganese in the oxidation of aromatic amines. *Environmental Science and Technology* **2003**, *37*, 2686–2693.

(75) A. T. Stone, J. J. Morgan. Reduction and dissolution of manganese (III) and manganese (IV) oxides by organics. 1. Reaction with hydroquinone. *Environmental Science and Technology* **1984**, *18*, 450–456.

(76) J. D. Hem, C. E. Roberson, R. B. Fournier. Stability Of Beta MnOOH and Manganese Oxide Deposition from Springwater. *Water Resources Research* **1982**, *18*, 563–570.

Table 1.1. Reduction half-reactions and standard reduction potentials for environmentally and water/wastewater treatment relevant manganese species (*37*, *52*, *56*, *75*, *76*). For MnO_4^- the relevant pH range is given (*37*, *56*).

Reduction Half-Reaction	E° (V)	relevant pH range
$MnO_4^- + e^- \rightleftharpoons MnO_4^{2-}$	+0.56	> 12
$MnO_4^- + 3\,e^- + 2\,H_2O \rightleftharpoons MnO_2 + 4\,OH^-$	+0.59	7–12
$MnO_4^- + 3\,e^- + 4\,H^+ \rightleftharpoons MnO_2 + 2\,H_2O$	+1.70	3.5–7
$MnO_4^- + 5\,e^- + 8\,H^+ \rightleftharpoons Mn^{2+} + 4\,H_2O$	+1.51	< 3.5
$\beta-MnOOH(s) + 3\,H^+ + e^- \rightleftharpoons Mn^{2+}(aq) + 2\,H_2O$	+1.65	
$\gamma-MnOOH(s) + 3\,H^+ + e^- \rightleftharpoons Mn^{2+}(aq) + 2\,H_2O$	+1.50	
½ $\delta-MnO_2(s) + 2\,H^+ + e^- \rightleftharpoons$ ½ $Mn^{2+}(aq) + H_2O$	+1.29	

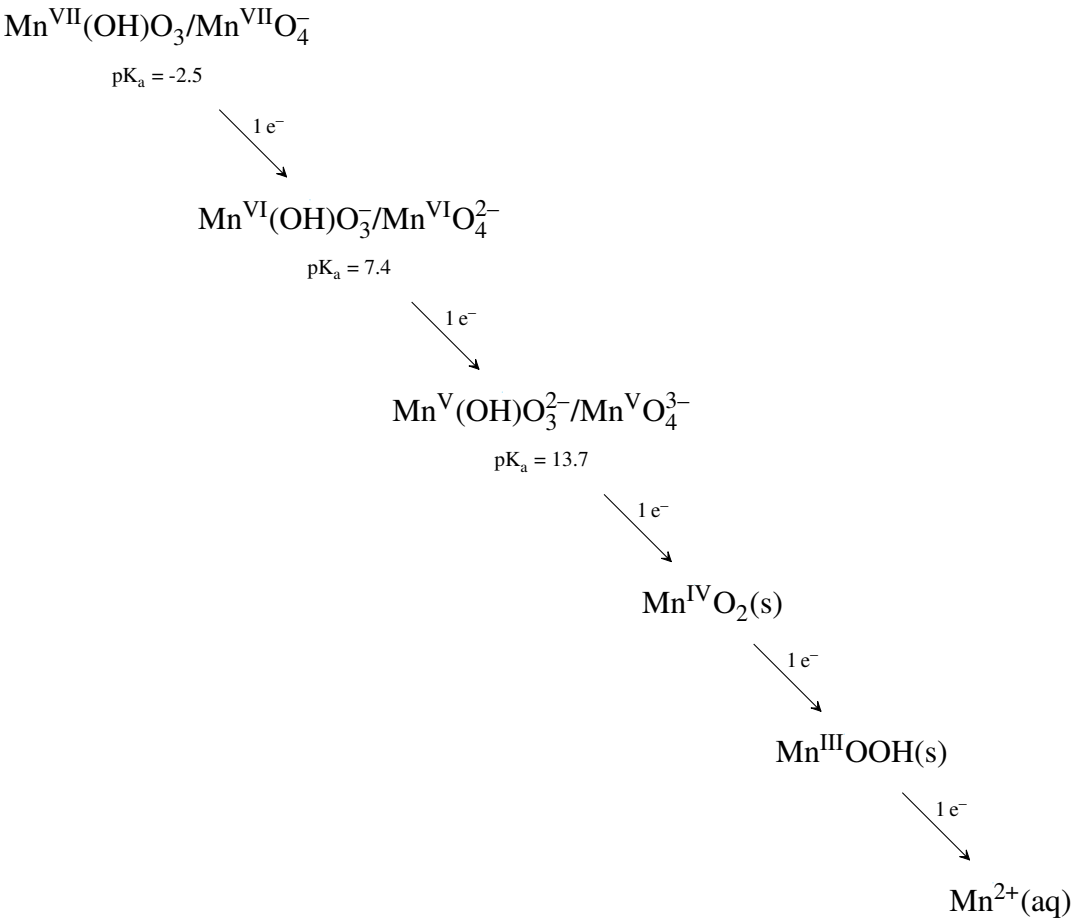

Figure 1.1. Oxidation states of manganese relevant to environmental and water/wastewater treatment conditions.

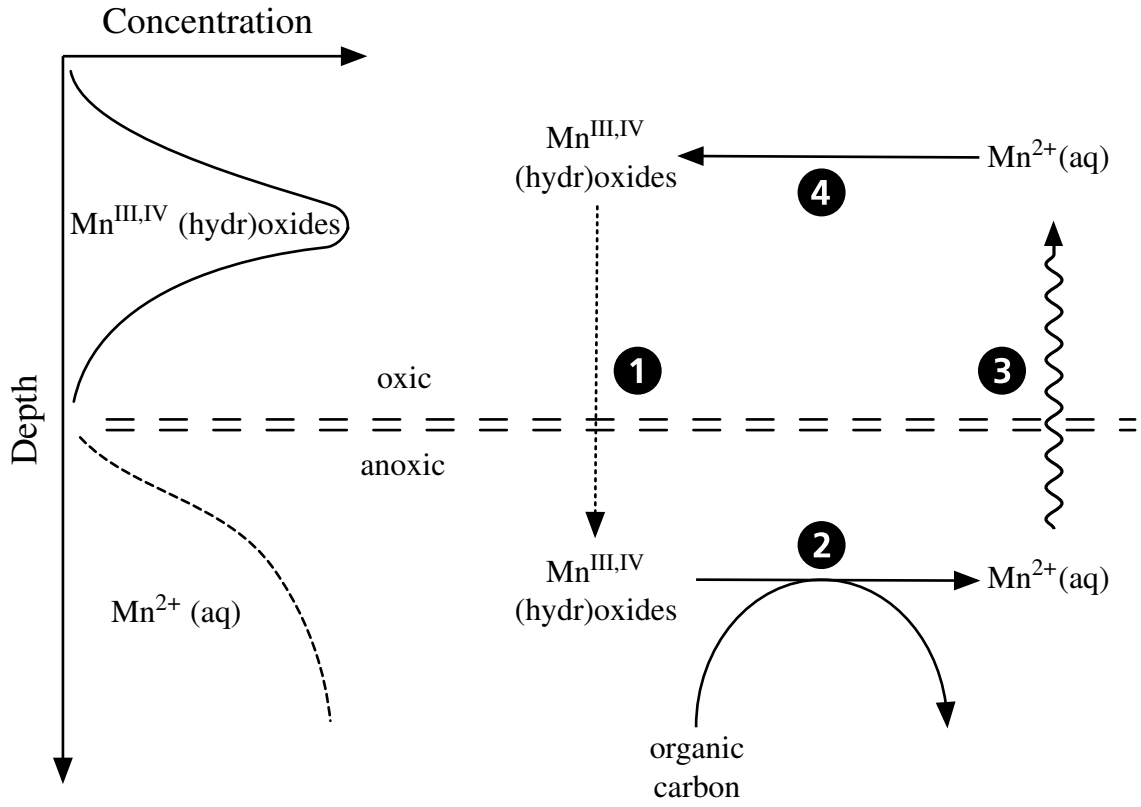

Figure 1.2. Manganese distribution (Left) and cycle around the oxic/anoxic interface (right, *57*). 1) gravitational settling causes $Mn^{III,IV}$ (hydr)oxide particles sink below the interface. 2) There, they are reduced by microorganisms or abiotically to Mn^{2+}(aq). 3) Highly soluble Mn^{2+}(aq) readily diffuses into the oxic zone. 4) Once in the oxic zone, Mn^{2+}(aq) can be oxidized back to $Mn^{III,IV}$ solids by microorganisms or O_2.

Chapter 2

Aqueous Addition Reactions of Patulin and *p*-Benzoquinone: Competition Between Added Nucleophiles, Water, and Buffers

2.1 Introduction

Organic contaminant interactions with natural organic matter (NOM) can occur via several different mechanisms including ionic, hydrogen and covalent bonding, charge-transfer or electron donor-acceptor mechanisms, van der Waal forces, ligand exchange, hydrophobic effects, or partitioning (*1*). Contaminants that cannot be recovered from a soil by extraction are called bound residues or nonextractable residues (NER). Relative to the parent contaminant, NER have lower bioavailability and mobility and their formation could represent a safe and effective removal mechanism for some contaminants (*1–3*).

Contaminants containing nucleophilic functional groups like aniline, phenol, and N-heterocycles could form NER via covalent bonding, and the extent of NER formation is sensitive to molecular structure of the contaminant (*1*, *4*). Based on kinetic data for pesticides, those containing phenol or aniline nucleophilic functional groups exhibit greater

NER formation than those containing N-heterocycles (*4*). In one study where ^{14}C-labeled pyridine and aniline were incubated with a sediment sample, pyridine was almost completely recovered by multiple extractions but aniline could only be partially recovered (*5*). Aniline loss is thought to occur via both reversible mass-transfer sorption interactions, cation exchange reactions, and covalent bond forming reactions representing NER formation (*5*, *6*). Aniline contains an amine functional group and could form covalent bonds via a nucleophilic addition reaction, while pyridine is a poorer nucleophile (*5*). NMR and mass spectrometric studies confirmed the formation of covalent bonds between NOM and aniline (*7*).

Michael addition is one pathway that could lead to irreversible covalent bond formation between nucleophilic contaminants and NOM (*8–11*). The Michael addition reaction occurs between a nucleophile and a "Michael acceptor" electrophile containing an α,β-unsaturated carbonyl substructure (–C=C–C=O). This reaction can also be called 1,4-addition because the nucleophilic attack occurs at the β carbon, but the donated electrons are transferred to the oxygen atom that is four atoms away.

(2.1)

where Nu is the nucleophile. Figure 2.1 depicts Michael addition to *p*-benzoquinone (*8*). The reaction is initiated by nucleophilic attack at the β-carbon. Proton transfer and keto-enol tautomerization reactions lead to the final products. The molecular structure of both the nucleophile and the Michael acceptor affect rates of Michael addition. The strength of a nucleophile is related to the electron density at the atom that donates electrons during the attack step. This atom is called the nucleophilic center. Structure effects that increase electron density at the electrophilic atom should increase the rate of Michael addition

reactions. The reverse is true for Michael acceptors, the carbonyl withdraws electron-density at the receptor site making them electron deficient.

NOM is thought to contain *o*- and *p*-benzoquinone moieties that could be active participants in many biogeochemical cycles (*12*, *13*). Similarities between NOM samples and model quinones have been reported as evidence of benzoquinone moieties using cyclic voltammetry (*14*), redox titration (*15*), cyclic O_2 oxidation and H_2/Pd reduction experiments (*16*), and fluorescence spectroscopy (*17*).

A nucleophile could form an irreversible bonds to an α,β-unsaturated carbonyl in a benzoquinone moiety within NOM via Michael addition. ^{15}N NMR and kinetic studies provide evidence for bond formation by aniline nucleophiles (*7*, *8*). Direct evidence of benzoquinone moieties can be obtained by ^{15}N and ^{13}C NMR spectroscopy of fulvic and humic acid samples that have reacted with ^{15}N-labeled hydroxylamine (*18*). Although the less stable *ortho*-benzoquinone isomer is more likely to be present in NOM, we will employ *p*-benzoquinone as a convenient model electrophile for laboratory experiments (*19*). *p*-Benzoquinone could be present in receiving waters of disinfected wastewater as a result of chlorination of municipal wastewater containing acetominophen (*20*).

The mycotoxin patulin (Figure 2.2) is used as a second model Michael acceptor electrophile. Patulin is a naturally-occurring electrophilic toxic compound arising from certain *Penicillium* and *Aspergillus* fungal species that grow on rotting crops, especially apples and pears (*21–24*). Mycotoxins can leach into surface water from from decaying agricultural fields (*25*, *26*). Patulin is carcinogenic and teratogenic (*27*, *28*) and can induce intestinal injuries such as degeneration of epithelial cells, inflammation, ulceration, and hemorrhages (*27*). Nucleophilic addition reactions of patulin with biological thiol nucleophiles such as cysteine and glutathione provide protection from toxicity of patulin and generate less toxic adducts (*27–29*).

Our study employs model nucleophiles, para-substituted anilines, 4-methoxyphenol, hydroxylamine, and 4-methylimidazole, to study nucleophilic addition reactions. These model compounds serve to represent aromatic amine, phenolic, and heterocyclic nitrogen functional groups that can impart nucleophilicity to organic contaminants. 4-Methylimidazole serves as a model for histidine and similar heterocyclic nitrogen compounds. These model nucleophiles are experimentally convenient because they contain only one Lewis base group that could donate lone-pair electrons during nucleophilic attack. More complicated compounds can contain two or more nucleophilic sites. For example, the herbicides clopyralid, chloramben and aminopyralid contain potentially nucleophilic pyridine-like and aniline-like functional groups and may form NERs via Michael addition. Clopyralid and aminopyralid are used to control broadleaf weeds (*30*, *31*). Clopyralid (*30*) and aminopyralid (*31*) do not leach from test agricultural plots, do not hydrolyze, and do not significantly volatilize, but they cannot be detected in the soil within months of application. In these field studies the loss of clopyralid and aminopyralid was credited to biodegradation. However, an abiotic mechanism involving covalent bond formation with soil organic matter could have evaded the detection method. In order to determine if herbicides like clopyralid and aminopyralid are lost by nucleophilic addition reactions, it would be useful to know how nucleophilic these compounds are. We propose that rate of loss of *p*-benzoquinone measured in a simple laboratory experiment could be used as a tool to assess nucleophilicity towards addition by complicated nucleophiles that may correlate with reaction rate with NOM.

We apply the Hammett relationship to describe the effect of electronic structure on rate constant (k_{Nu^-}) for loss of *p*-benzoquinone in the presence of para-substituted anilines. These nucleophiles have only one Lewis base group allowing a Hammett relationship to be developed to describe substituent effects on rate of loss of electrophile. The Hammett relationship (*32*, *33*) can be applied to many thermodynamic or kinetic constants by relating

the log of a rate or equilibrium constant to a reaction constant (ρ) and substituent constants (σ). We use it for second-order rate constants of Michael acceptor loss attributed to the nucleophiles deprotonated form k_{Nu^-}:

$$\log\left(k_{\mathrm{Nu}^-}\right) = \rho\sigma \tag{2.2}$$

The reaction constant is determined from the slope of Equation 2.2 and is used as a way to quantify electronic structure sensitivity of Michael addition reactions with *p*-benzoquinone and patulin model Michael acceptors and para-substituted aniline nucleophiles. Some Hammett ρ values are available in the literature for reaction of para-substituted anilines with soil samples (*8*, *11*, *34*) and with model electrophiles (*8*, *35*). Colón and coworkers (*11*) observed biphasic kinetics characterized by a fast first step and a second slow step for loss of a suite of aromatic amines added to sediment samples. They found good correlation between Hammett substituent constants and rate of loss of substituted anilines to a sediment sample for the initial rapid step, but for the second slow step, they reported a much weaker correlation. In contrast, Li et al. (*36*) reported a strong correlation between Hammett constants and irreversible binding to soil samples.

Anilines can form imines with *p*-benzoquinone via a reaction with water as a byproduct (*37*). The imine may be an important product in nonaqueous solution, but in aqueous solution imines are readily hydrolyzed back to the starting reactants. In literature reports (*7*, *8*), the final isolatable product is reported to result from Michael addition. Although, it is not possible to distinguish imine products from Michael addition products without authentic standards, our experiments are conducted in aqueous solution over long time periods so predominantly Michael addition products are expected under these conditions.

Addition products and NERs can also result from radical addition mechanisms (*1*). Thomson (*38*) suggested that thiol compounds add to juglone via a radical addition mechanism. Later, Perlinger et al. (*39*) reported that Michael addition and radical addition were both active in the reaction of bisulfide and juglone to form mercapto substituted juglone. They reasoned that increasing pH favors the radical pathway because the radical pathway involves loss of a proton where Michael addition requires gain of a proton and EPR (electron paramagnetic resonance) detected increasing yield of semiquinone radical with increasing pH (*39*). In these studies, radical generation occurred via redox mechanisms. Our experimental solutions contain no added oxidants or reductants and are sparged with N_2(g) to minimize dissolved O_2 concentration. The intent of these measures is to mitigate redox reactions in our reaction solutions and suppress radical formation.

In this study, we examine loss of *p*-benzoquinone and patulin in the presence of model nucleophilic contaminants. We will also discuss complications associated with loss of *p*-benzoquinone or patulin in the absence of an added nucleophile, where we expect H_2O, OH^-, and buffer compounds to be the most important potential nucleophiles. A series of substituted anilines are used to develop a Hammett relationship and explore the effect of electronic effect on rate of nucleophilic attack. Lastly, loss of *p*-benzoquinone in the presence of complicated nucleophiles such as aminopyralid, chloramben, and clopyralid is discussed as a means to assess nucleophilicity.

2.2 Materials and Methods

All aqueous solutions were prepared from reagent grade chemicals and distilled, deionized water (Milli-Q water, 18 M-cm resistivity, Millipore Corp., Milford, MA). All bottles

and glassware were rinsed with distilled water, soaked in 5 M nitric acid overnight, rinsed with distilled water and Milli-Q water and air-dried.

2.2.1 Chemicals

3-(N-Morpholino)propanesulfonic acid (MOPS), 2-(N-morpholino)ethanesulfonic acid monohydrate (MES), sodium acetate, and ascorbic acid were purchased from Sigma (St. Louis, MO). *p*-Benzoquinone, 4-methylimidazole, aniline, maleic acid, N-cyclohexyl-2-aminoethanesulfonic acid (CHES), 4-aminophenol, 4-methoxyphenol, 4-ethylaniline, and ethylenediaminetetraacetic acid disodium salt dihydrate (EDTA) were purchased from Aldrich (St. Louis, MO). *p*-Benzoquinone was purified by sublimation before use. Patulin was purchased from A. G. Scientific (San Diego, CA). 4-Methoxyaniline (p-anisidine), 4′-aminoacetophenone, hydroxylamine hydrochloride, and 4-nitroaniline were purchased from Alfa Aesar (Pelham, NH). 1,4-Diethylpiperazine (DEPP), chloramben, (3-amino-2,5-dichlorobenzoic acid), and NaCl were purchased from Acros (Fair Lawn, NJ). HPLC grade methanol and HCl were purchased from Fisher Scientific (Pittsburgh, PA). Clopyralid (3,6-dichloro-2-pyridinecarboxylic acid) and ammonium acetate were purchased from Fluka (Buchs, Switzerland). 1,2,4-Trihydroxybenzene was purchased from TCI America (Portland, OR). Aminopyralid (4-amino-3,6-dichloropyridine-2-carboxylic acid) was purchased from Chem Service (West Chester, PA). NaOH was purchased from J. T. Baker (Phillipsburg, NJ). 3-Hydroxypyridine was purchased from Lancaster Synthesis (Morecombe, UK).

2.2.2 Experimental Design

Stock solutions were prepared freshly each day. Stocks (10 mM) of Michael acceptor electrophile (patulin or *p*-benzoquinone) were prepared in methanol because of their low

aqueous solubility. Stock solutions of MOPS buffer, NaCl, and nucleophile of interest were prepared in Milli-Q water. The MOPS buffer stock was adjusted to pH 7.0 using NaOH and HCl. Sufficient volume of nucleophile, MOPS, NaCl, and Michael acceptor stocks were pipetted into a 25 mL volumetric flask to give a solution consisting of 100 μM Michael acceptor electrophile, 1.0 mM or 10 mM nucleophile, 5 mM MOPS, and 10 mM ionic strength when diluted to the mark. This solution was sparged with N_2(g) for 30 min to remove O_2. Then sufficient stock of Michael acceptor electrophile was added to initiate reaction, the solution was diluted to the mark, and the time of addition was recorded. These reaction solutions contained less than 1% methanol. A separate solution containing no added nucleophile served as a control. Working as quickly as possible following addition of the electrophile, aliquots of each solution were pipetted into separate autosampler vials. The vials were sealed with Teflon septa and loaded into an autosampler for HPLC analysis. Inside the autosampler, the samples were held in the dark and at room temperature (22 – 23°C). Each vial was injected into the HPLC only once and the time of injection was recorded. The time point for a sample on a time course plot was the difference between the time of reaction initiation and the time of injection. Most time courses lasted 4 hours. One exception is patulin loss time course data in the absence of an added nucleophile. These solutions were prepared as described above and placed in open polypropylene bottles in a constant temperature bath held at 25±1°C and were continuously sparged with N_2(g). Samples were withdrawn periodically transferred to autosampler vials that were then analyzed by HPLC.

2.2.3 Instrumentation and Analysis

p-Benzoquinone and patulin concentration was monitored using reversed-phase HPLC (Waters Corp., Milford, MA) run in isocratic mode with 85% 5 mM ammonium acetate and

15% methanol (by volume) at a flow rate of 1.0 mL min^{-1}. The column was a Spherisorb ODS2 5μm 5.6 × 150 mm (Waters Corp., Milford, MA). UV detection was used for *p*-benzoquinone at 245 nm and at 280 nm for patulin. Visible light absorbance at 510 nm and spectra were recorded using a Shimadzu UV-1800 spectrophotometer with 1 cm quartz cuvettes.

LC/MS with electrospray ionization was used in an attempt to observe 1,2,4-trihydroxybenzene in experiments with *p*-benzoquinone. LC separation was conducted using a Waters 2795 separation module (Milford, MA) with a 4.6 x 100 mm, 5 μm particle size, Atlantis T3 column (Waters, Milford, MA) run in isocratic mode with 70% 5 mM ammonium acetate and 30% methanol at 200 μL min^{-1} as the eluent. LC/MS was able to detect authentic standards of 1,2,4-trihydroxybenzene to a detection limit of 5 μM, but this analyte was not detected in any experimental samples.

In our experimental solutions, the added nucleophile concentration is 10 times greater than the concentration of *p*-benzoquinone or patulin. Under these conditions, an observed rate constant (k_{obs}) can be obtained from fitting time course data to a pseudo-first-order model:

$$\frac{d[\mathrm{Z}]}{dt} = -k_{\mathrm{obs}}[\mathrm{Z}] \tag{2.3}$$

where Z is the Michael acceptor. Pseudo-first order conditions apply because the nucleophile is present in greater than order-of-magnitude excess of the Michael acceptor. Both slope and initial concentration in the integrated form of Equation 2.3 were used as fitting parameters. Second-order rate constants are calculated by normalizing the pseudo-first-order rate constants by the initial concentration of the nucleophile. These rate constants are normalized by the initial concentration of the deprotonated form of the nucleophile rather than the total

nucleophile concentration:

$$k_{\mathrm{Nu}^-} = \frac{k_{\mathrm{obs}}\mathrm{K_a}\mathrm{Nu_T}}{\mathrm{K_a} + [\mathrm{H}^+]}. \tag{2.4}$$

where k_{Nu^-} is the corrected second-order rate constant, and $\mathrm{K_a}$ is the acid dissociation constant of the nucleophile.

Increase in absorbance at 510 nm over time will also be used to determine a pseudo-first-order rate constants. In this case, consider the concentration of the product of a $\mathrm{Z} \longrightarrow \mathrm{P}$ first-order reaction (*40*, p. 27)

$$[\mathrm{P}] = [\mathrm{P}]_0 + [\mathrm{Z}]_0 \left(1 - e^{-k_{\mathrm{obs}}t}\right) \tag{2.5}$$

where is P is the reaction product. Assuming that Beer's law holds for P at 510 nm, the concentration of P is related to the absorbance ($abs_{510\ \mathrm{nm}}$) by the extinction coefficient of P at 510 nm (ϵ_P).

$$abs_{510\ \mathrm{nm}} = \epsilon_{\mathrm{P}}\ell[\mathrm{P}] \tag{2.6}$$

Combining Equations 2.5 and 2.6 gives

$$abs_{510\ \mathrm{nm}} = \epsilon_{\mathrm{P}}\ell[\mathrm{P}]_0 + \epsilon_{\mathrm{P}}\ell[\mathrm{Z}]_0 \left(1 - e^{-k_{\mathrm{obs}}t}\right) \tag{2.7}$$

Equation 2.7 can be used to determine pseudo-first-order rate constants for time course plots of 510 nm absorbance. The second-order rate constant of generation of a product of an added nucleophile and *p*-benzoquinone that absorbs at 510 nm was determined from a series of experiments with initial concentration of *p*-benzoquinone of 100 μM and increasing concentration of added nucleophile. The relationship between k_{obs} and the initial

concentration of added nucleophile ($[Nu]_0$) is linear

$$k_{obs} = k[Nu]_0 \tag{2.8}$$

and the slope determined by linear regression gives the second order rate constant (k).

2.3 Results and Discussion

2.3.1 *p*-Benzoquinone

Time courses showing loss of *p*-benzoquinone time courses in the presence of 1 mM or 10 mM added nucleophiles are shown in Figure 2.3. Under the conditions of Figure 2.3, less than 5% loss of *p*-benzoquinone was observed in the absence of added nucleophile. See Section 2.5.2 in the Supporting Information for more information on our preliminary studies of loss of p-Benzoquinone in pH buffered solutions that do not contain an added nucleophile. These preliminary studies may suggest that a general base catalysis mechanism is active in DEPP, MES, and MOPS solutions but the evidence in the Supporting Information is insufficient to unequivocally reach that determination. Observed pseudo-first-order rate constants and k_{Nu^-} values are shown in Table S2.1 in the supporting information.

Whenever we add a nucleophile to solutions of *p*-benzoquinone, the added nucleophile competes with H_2O, OH^-, and buffer. The rate of reaction with the added nucleophile depends on how strong the nucleophile is and the concentration of its active, deprotonated form. Additionally, the added nucleophile must be strong enough and/or concentrated enough to outcompete other nucleophiles present in solution. In Figure 2.3, a high concentration (1 mM) of aniline and 4-methylimidazole readily outcompeted H_2O, OH^-, and MOPS

buffer for reaction with *p*-benzoquinone. However, because 1mM 4-methoxyphenol did not result in significantly greater loss of *p*-benzoquinone than in the control, we increased the concentration to 10 mM.

If the rate of p-benzoquinone loss were simply a function of pK_a, then we would expect 4-methoxyphenol would react more rapidly than 4-methylimidazole or aniline. However, we observed the opposite trend (Figure 2.3). At pH 7, 4-methoxyphenol is nearly 100% protonated, 4-methylimidazole is 77% protonated, and aniline is almost entirely protonated. The nucleophile with the highest proportion of deprotonated form leads to the fastest rate of loss of *p*-benzoquinone. The rate constants followed the same trend: 2.3×10^{-1} M^{-1} s^{-1} for aniline, 2.2×10^{-3} M^{-1} s^{-1} for 4-methylimidazole, and 7.06×10^{-4} M^{-1} s^{-1} for 4-methoxyphenol (Table S2.1). Based on these constants, aniline is a stronger nucleophile than 4-methylimidazole, which is stronger than 4-methoxyphenol.

We observed growth of an absorbance peak centered around 400 and 510 nm in UV/Vis spectra recorded in solutions of 100 μM *p*-benzoquinone and aniline at pH 7.0 in 5 mM MOPS buffer (Figure 2.4A). The 510 nm absorbance reached 0.4 absorbance units in 60 min in the absence of aniline (blank on Figure 2.4) which is could be attributed to hydration, but could also be due to adduct formation with MOPS. In the supporting information (section 2.5.2) we present results of preliminary experiments that may indicate adduct formation of MOPS. The expected hydration product of *p*-benzoquinone, 1,2,4-trihydroxybenzene, could not be detected by LC/MS. MOPS buffered solutions (5 mM at pH 7.0) of 1,2,4-trihydroxybenzene do quickly change color and exhibit absorbance at 510 nm (Figure S2.3 in the Supporting Information). The rate of increase of absorbance at 510 nm increased with increasing concentration of aniline. The concentration dependence of k_{obs} increased linearly with the initial concentration of aniline (Figure 2.4B). Pseudo-first-order rate constants were determined using Equation 2.7 and the second-order constant was obtained using 2.8. The

second-order rate constant was 3.8 ± 0.810^{-1} M^{-1} s^{-1}. Monitoring loss of *p*-benzoquinone yielded a similar but slightly smaller rate constant: 2.3×10^{-1} M^{-1} s^{-1}.

The rate constant determined from 510 nm absorbance (Figure 2.4) corresponds to only the generation of a *p*-benzoquinone and aniline reaction product if only that product absorbs at 510 nm. In the absence of aniline, we observed some absorbance at 510 nm in solutions of 100 μM *p*-benzoquinone in 5.0 mM MOPS (Figure S2.7) but less absorbance was observed than in solutions containing aniline (Figure 2.4). In the absence of *p*-benzoquinone, no absorbance is observed from solutions of aniline under the same conditions and timescale as Figure 2.4. Also, The linear relationship between observed rate constant and aniline concentration (Figure 2.4B) supports the conclusion that 510 nm absorbance comes from a reaction product of aniline.

2.3.2 Patulin

Time courses for loss of patulin in the presence of representative nucleophiles (para-substituted anilines, 4-methoxyphenol, and hydroxylamine) are shown in Figure 2.5. No significant loss of patulin was observed when 4-methylimidazole, 4-methoxyphenol, or 4-acetylphenol was added to serve as the nucleophile. No significant loss of patulin was observed in the absence of an added nucleophile in 5 mM MOPS at pH 7.0. Section 2.5.3 in the Supporting Information presents results of preliminary experiments of loss of patulin in solutions of varying pH and buffer.

2.3.3 Comparison of Electrophilicity: *p*-Benzoquinone and Patulin

The rate constants measured for reactions of nine nucleophiles with *p*-benzoquinone and six with patulin are summarized in Table 2.1. For nucleophiles where rate constants were

measured for both *p*-benzoquinone and patulin, the values are between 1 and 2 orders of magnitude larger for *p*-benzoquinone than for patulin.

For both *p*-benzoquinone and patulin the Hammett ρ value determined from the slope of the Hammett plot was negative (Figure 2.6). The Hammett σ values are taken from McDaniel et al. (*41*). The ρ value was greater in magnitude for *p*-benzoquinone (-2.1 ± 0.3) than for patulin (-1.2 ± 0.2). Para-substituted anilines react with *p*-benzoquinone 1–2 orders of magnitude faster than with patulin (Figure 2.6).

Negative ρ values mean that substituted anilines containing electron-donating substituents increase the rate of reaction relative to aniline. Electron-donating substituents increase electron density at the nucleophilic center atom making nucleophilic attack more favorable. Negative ρ values also imply build-up of positive charge in the transition state, which is stabilized by increased electron density at the nucleophilic center. Both of these findings are consistent with the Michael addition mechanism where the nucleophile donates two electrons to the Michael acceptor (Figure 2.1). Table 2.2 compares the ρ values obtained in this study with those available in the literature. Colón et al. (*11*) reported ρ values from biphasic kinetics of loss of aromatic amines to sediment samples: the ρ value was -1.7 for the "fast" first step and -0.4 for the "slow" second step. Our ρ value for *p*-benzoquinone (-2.1 ± 0.3) is larger in magnitude, but supports the conclusion that Michael type nucleophilic addition is involved in irreversible binding of anilines. Parris (*8*) reported a Hammett ρ value of -1.5 for *p*-benzoquinone reaction with 4-methylaniline, aniline, 4-chloroaniline, and 3,4-dichloroaniline. His reaction conditions differed slightly from those reported here: his solutions contained 71% methanol and no buffer (*8*), where the results reported here used less than 1% methanol and were buffered using 5 mM MOPS adjusted to pH 7.0. Solvent and pH effects may explain why our ρ value is larger in magnitude than the value reported by Parris.

One explanation for the higher rate constants observed for *p*-benzoquinone than patulin (Table 2.1) is that nucleophiles react faster with *p*-benzoquinone than with patulin because of structural differences: *p*-benzoquinone undergoes 1,4-addition while patulin must undergo 1,6-addition. In 1,4-addition the electrophilic site is two atoms closer to the electronegative oxygen atom that ultimately accepts the electrons from the nucleophile. In 1,6-addition addition these electrons must traverse an additional carbon-carbon double bond. Electron density at electrophilic site in Michael acceptors is withdrawn by the oxygen atom, and should be withdrawn more strongly when it is two atoms away instead of four. Also, there are four possible Michael addition sites on *p*-benzoquinone where patulin has one. So, *p*-benzoquinone could be four times as likely to react with a nucleophile than patulin at the same concentration.

2.3.4 Assessing Nucleophilicity: Aminopyralid, Chloramben, and Clopyralid

In the previous sections, we were primarily interested in loss of the Michael acceptor in the presence of simple model nucleophiles that only contained one Lewis base group. We could assess and compare nucleophilicity of compounds based on observed *p*-benzoquinone loss rate at a given pH and buffer. This approach could also be valuable for complicated nucleophiles. Consider the rate of *p*-benzoquinone loss observed in the presence of 1 mM clopyralid, aminopyralid, or chloramben (Figure 2.7). These solutions were buffered with 5.0 mM MOPS adjusted to pH 7.0. Aminopyralid and clopyralid react at similar rates, with rate constants of 1.69×10^{-3} and 1.84×10^{-3} M^{-1} s^{-1}, respectively. Chloramben reacted significantly faster, the rate constant was 1.2×10^{-2} M^{-1} s^{-1}.

The structures of the three herbicides differ in whether or not they include an aniline-like amine nitrogen or a pyridine-like heterocyclic nitrogen (Figure 2.2). These compounds are more complicated than our model nucleophiles because they contain multiple potential nucleophilic sites. Heterocyclic nitrogen atoms are not as strongly nucleophilic as aniline: 4-methylimidazole reacted much more slowly than aniline with *p*-benzoquinone (Figure 2.3) and pyridine was reported to form no covalent bonds with NOM (*5*).

Based on these simple experiments, chloramben is the most nucleophilic of the three herbicides that we tested. We anticipate that nucleophilicity measured this way will correlate with the rate of loss to irreversible binding to organic matter in soils or sediments. If this were true, then chloramben would be a more environmentally friendly pesticide choice than aminopyralid or clopyralid because it would quickly become biologically unavailable. Although making this conclusion is not possible with our current limited data set, future research work could explore the nature of the relationship between *p*-benzoquinone loss rates and rate of loss via irreversible binding to organic matter. This could inform both choice and design of environmentally friendly chemicals and development of fate and transport models that properly account for this loss mechanism.

2.4 Conclusions

We examined time course data for loss of *p*-benzoquinone and patulin Michael acceptor electrophiles in the presence of several added nucleophiles under pseudo-first-order conditions. Under these conditions, we tentatively attribute loss of *p*-benzoquinone and patulin primarily to Michael-type nucleophilic addition. Even in the absence of an added nucleophile, loss of *p*-benzoquinone and patulin was observed in buffered solutions, and is related to pH and structure of compound employed as the buffer. We urge readers to carefully

consider buffer choice when conducting experiments on nucleophile-electrophile reactions in aqueous solution. Although we could observe the sum effect of added nucleophile, hydration, and buffer reaction on loss of electrophilic substrate, determining individual rate constants for each process will most likely require time course data of the reaction products.

Nucleophilic addition reactions that occur in sediments, soil, and water treatment processes deserves mechanistic study. We expect that the effects molecular structure and pH exert on nucleophilicity, electrophilicity, and protonation state are key to determining the importance of these reaction pathways. We studied Michael addition reactions with *p*-benzoquinone in buffered 99% aqueous solutions to simulate the slow irreversible binding of nucleophiles to natural organic matter (*42*), which had previously been studied in mixed solvents (*8*). We determined that a Hammett relationship also exists for patulin, a natural toxic compound, that undergoes a more complex addition pathway than does *p*-benzoquinone (*29*, *43*). As we become more aware of potential water quality impacts of mycotoxins arising from crop fields (*25*) we will need to consider the ramifications of electrophilic and nucleophilic properties on their environmental fate and transport. Lastly, we proposed that *p*-benzoquinone loss rate could be a simple tool to predict loss of any contaminants possessing a nucleophilic functional group such as the herbicides chloramben, aminopyralid and clopyralid.

References

(1) B. Gevao, K. Semple, K. Jones. Bound pesticide residues in soils: A review. *Environmental Pollution* **2000**, *108*, 3–14.

(2) D. Barraclough, T. Kearney, A. Croxford. Bound residues: Environmental solution or future problem? *Environmental Pollution* **2005**, *133*, 85–90.

(3) J. Bollag, M. J. Loll. Incorporation of Xenobiotics Into Soil Humus. *Experientia* **1983**, *39*, 1221–1231.

(4) E. Barriuso, P. Benoit, I. G. Dubus. Formation of pesticide nonextractable (bound) residues in soil: Magnitude, controlling factors and reversibility. *Environmental Science and Technology* **2008**, *42*, 1845–1854.

(5) E. J. Weber, D. Colon, G. Baughman. Sediment-associated reactions of aromatic amines. 1. Elucidation of sorption mechanisms. *Environmental Science and Technology* **2001**, *35*, 2470–2475.

(6) J. R. Fábrega-Duque, C. T. Jafvert, H. Li, L. S. Lee. Modeling abiotic processes of aniline in water-saturated soils. *Environmental Science and Technology* **2000**, *34*, 1687–1693.

(7) K. A. Thorn, P. Pettigrew, W. S. Goldenberg, E. J. Weber. Covalent binding of aniline to humic substances. 2. ^{15}N NMR studies of nucleophilic addition reactions. *Environmental Science and Technology* **1996**, *30*, 2764–2775.

(8) G. E. Parris. Covalent binding of aromatic amines to humates. 1. Reactions with carbonyls and quinones. *Environmental Science and Technology* **1980**, *14*, 1099–1106.

(9) K. A. Thorn, W. S. Goldenberg, S. Younger, E. J. Weber. Covalent binding of aniline to humic substances - Comparison of nucleophilic addition, enzyme-, and metal-catalyzed reactions by N-15 NMR. *Humic And Fulvic Acids* **1996**, *651*, 299–326.

(10) K. A. Thorn, W. S. Goldenberg, S. Younger, E. J. Weber, *Covalent binding of aniline to humic substances. Comparison of nucleophilic addition, enzyme-, and metal-catalyzed reactions by* ^{15}N *NMR* in *Humic and Fulvic Acids: Isolation, Structure and Environmental Role*, J. S. Gaffney, N. A. Marley, S. B. Clark (Eds.), American Chemical Society, Washington, DC, **1996**, pp. 299–326.

(11) D. Colon, E. J. Weber, G. Baughman. Sediment-associated reactions of aromatic amines. 2. QSAR development. *Environmental Science and Technology* **2002**, *36*, 2443–2450.

(12) M. Uchimiya, A. T. Stone. Reversible redox chemistry of quinones: Impact on biogeochemical cycles. *Chemosphere* **2009**, *77*, 451–458.

(13) M. Uchimiya, *Electron Transfer Reactions Between Quinones and Iron in Aqueous Environments*, Ph.D. thesis, Johns Hopkins University, Baltimore, Maryland, **2006**.

(14) J. Nurmi, P. G. Tratnyek. Electrochemical properties of natural organic matter (NOM), fractions of NOM, and model biogeochemical electron shuttles. *Environmental Science and Technology* **2002**, *36*, 617–624.

(15) S. P. Mathur. Evaluation of a reductiometric titration method for determining quinones in soil humus. *Soil Science Society of America Journal* **1972**, *36*, 175–176.

(16) N. Ratasuk, M. A. Nanny. Characterization and quantification of reversible redox sites in humic substances. *Environmental Science and Technology* **2007**, *41*, 7844–7850.

(17) L. Klapper, D. M. McKnight, J. R. Fulton. Fulvic acid oxidation state detection using fluorescence spectroscopy. *Environmental Science and Technology* **2002**, *36*, 3170–3175.

(18) K. A. Thorn, J. B. Arterburn, M. A. Mikita. Nitrogen-15 and carbon-13 NMR investigation of hydroxylamine-derivatized humic substances. *Environmental Science and Technology* **1992**, *26*, 107–116.

(19) A. Kutyrev. Nucleophilic reactions of quinones. *Russian Chemical Reviews* **1991**, *60*, 72–88.

(20) M. Bedner, W. A. MacCrehan. Transformation of acetaminophen by chlorination produces the toxicants 1,4-benzoquinone and N-acetyl-p-benzoquinone imine. *Environmental Science and Technology* **2006**, *40*, 516–522.

(21) B. Beretta, A. Gaiaschi, C. L. Galli, P. Restani. Patulin in apple-based foods: occurrence and safety evaluation. *Food Additives And Contaminants* **2000**, *17*, 399–406.

(22) J. Bennett, M. Klich. Mycotoxins. *Clinical Microbiology Reviews* **2003**, *16*, 497–516.

(23) P. M. Scott, W. F. Miles, P. Toft, J. G. Dube. Occurrence of patulin in apple juice. *Journal of Agricultural and Food Chemistry* **1972**, *20*, 450–451.

(24) P. W. Brian, G. W. Elson, D. Lowe. Production of patulin in apple fruits by *Penicillium expansum*. *Nature* **1956**, *178*, 263–264.

(25) T. D. Bucheli, F. E. Wettstein, N. Hartmann, M. Erbs, S. Vogelgsang, H.-R. Forrer, R. P. Schwarzenbach. Fusarium mycotoxins: Overlooked aquatic micropollutants? *Journal of Agricultural and Food Chemistry* **2008**, *56*, 1029–1034.

(26) N. Hartmann, M. Erbs, H.-R. Forrer, S. Vogelgsang, F. E. Wettstein, R. P. Schwarzenbach, T. D. Bucheli. Occurrence of zearalenone on *Fusarium graminearum* infected wheat and maize fields in crop organs, soil, and drainage water. *Environmental Science and Technology* **2008**, *42*, 5455–5460.

(27) R. Mahfoud. The mycotoxin patulin alters the barrier function of the intestinal epithelium: mechanism of action of the toxin and protective effects of glutathione. *Toxicology and Applied Pharmacology* **2002**, *181*, 209–218.

(28) A. Ciegler, A. C. Beckwith, L. K. Jackson. Teratogenicity of patulin and patulin adducts formed with cysteine. *Applied and Environmental Microbiology* **1976**, *31*, 664–667.

(29) R. Fliege, M. Metzler. Electrophilic properties of patulin. N-Acetylcysteine and glutathione adducts. *Chemical Research in Toxicology* **2000**, *13*, 373–381.

(30) L. Bergström, A. McGibbon, S. Day, M. Snel. Leaching potential and decomposition of clopyralid in Swedish soils under field conditions. *Environmental Toxicology and Chemistry* **1991**, *10*, 563–571.

(31) U.S. EPA Office of Pesticide Programs; Fact Sheet for Aminopyralid. **2005**, 1–56.

(32) L. Hammett. Reaction rates and indicator acidities. *Chemical Reviews* **1935**, *16*, 67–79.

(33) L. Hammett. Some relations between reaction rates and equilibrium constants. *Chemical Reviews* **1935**, *17*, 125–136.

(34) T. S. Hsu, R. Bartha. Interaction of Pesticide-Derived Chloroaniline Residues with Soil Organic-Matter. *Soil Science* **1973**, *116*, 444–452.

(35) M. L. Iskander, H. A. A. Medien, S. Nashed. A thermodynamic assessment on the reaction of aromatic amines versus reactivity with p-benzoquinone from a kinetic study. *Zeithschrift für physikalische Chemie* **1988**, *269*, 1183–1193.

(36) H. Li, L. Lee, C. T. Jafvert, J. G. Graveel. Effect of substitution on irreversible binding and transformation of aromatic amines with soils in aqueous systems. *Environmental Science and Technology* **2000**, *34*, 3674–3680.

(37) G. E. Parris. Environmental and metabolic transformations of primary aromatic amines and related compounds. *Residue Reviews* **1980**, *76*, 1–30.

(38) R. H. Thomson. Studies in the juglone series. III. Addition reactions. *The Journal of Organic Chemistry* **1951**, *16*, 1082–1090.

(39) J. A. Perlinger, V. Kalluri, R. Venkatapathy, W. Angst. Addition of hydrogen sulfide to juglone. *Environmental Science and Technology* **2002**, *36*, 2663–2669.

(40) H. Metiu, *Physical Chemistry: Kinetics*, Taylor & Francis Group, LLC, New York, NY, **2006**.

(41) D. McDaniel, H. Brown. An extended table of Hammett substituent constants based on the ionization of substituted benzoic acids. *The Journal of Organic Chemistry* **1958**, *23*, 420–427.

(42) E. J. Weber, D. L. Spidle, K. A. Thorn. Covalent binding of aniline to humic substances. 1. Kinetic studies. *Environmental Science and Technology* **1996**, *30*, 2755–2763.

(43) R. Fliege, M. Metzler. Electrophilic properties of patulin. Adduct structures and reaction pathways with 4-bromothiophenol and other model nucleophiles. *Chemical Research in Toxicology* **2000**, *13*, 363–372.

Table 2.1. Second-order rate constants determined for reactions of added nucleophiles with *p*-benzoquinone and patulin Michael acceptor. Rate constants (k_{Nu^-}) corrected to reflect the deprotonated form of the nucleophile (Equation 2.4). Half-life calculated for 1 mM of the deprotonated form of the nucleophile.

Michael Acceptor	Nucleophile	k_{Nu^-} (M^{-1} s^{-1})	Half-life (hr)
p-Benzoquinone	Aminopyralid	1.7×10^{-3}	113
	Clopyralid	1.8×10^{-3}	107
	4-Nitroaniline	6.2×10^{-3}	31
	Chloramben	1.2×10^{-2}	15
	4′-Aminoacetophenone	1.8×10^{-2}	11
	3-Hydroxypyridine	1.6×10^{-1}	1.2
	4-Methylimidazole	2.2×10^{-1}	0.9
	Aniline	2.3×10^{-1}	0.8
	4-Ethylaniline	5.4×10^{-1}	0.3
	4-Methoxyphenol	1.14	0.2
Patulin	4-Nitroaniline	4.4×10^{-4}	430
	4′-Aminoacetophenone	7.1×10^{-4}	270
	Aniline	3.0×10^{-3}	65
	Hydroxylamine	4.1×10^{-3}	47
	4-Methoxyaniline	8.0×10^{-3}	24
	4-Aminophenol	9.8×10^{-3}	19
	4-Methoxyphenol	4.1×10^{-2}	5

Table 2.2. Hammett reaction constants (ρ) for para-substituted anilines determined in this study and available in the literature.

Reference	Substrate	ρ (σ)
This Study	*p*-Benzoquinone[a]	-2.1
This Study	Patulin	-1.2
Parris 1980 (*8*)	*p*-Benzoquinone[b]	-1.5
Iskander et al. 1988 (*35*)	*p*-Benzoquinone[c]	-1.4
Li et al. 2000 (*36*)		
Fast Step	Soil Samples	-1.3
Slow Step		-1.25
Colón et al. 2002 (*11*)		
Fast Step	Sediment Sample	-1.75
Slow Step		-0.45

[a] in aqueous solution containing $< 1\%$ methanol. [b] in methanol. [c] in ethanol.

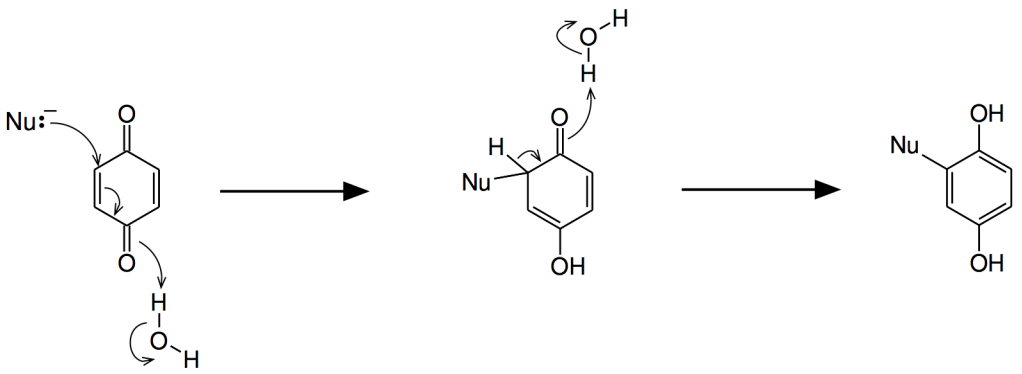

Figure 2.1. Proposed mechanism for Michael addition of a nucleophile ($Nu:^-$) to *p*-benzoquinone.

Buffers

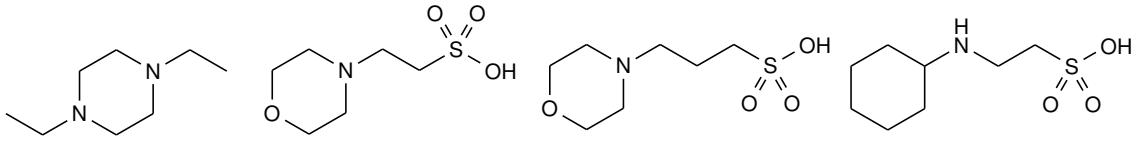

DEPP MES MOPS CHES

Electrophilic Substrates

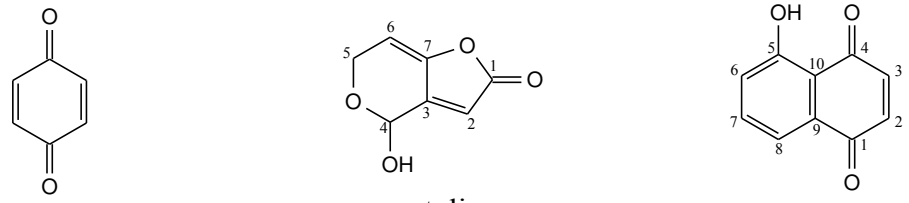

p-benzoquinone patulin juglone

Added Nucleophiles

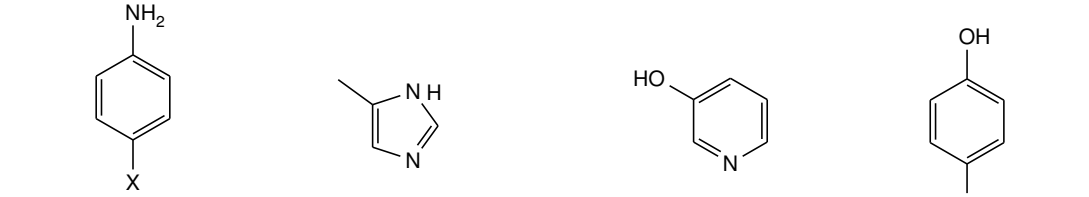

aromatic amines
X = H, OH, OCH_3,
CH_2CH_3, COOH, NO_2

4-methylimidazole 3-hydroxypyridine 4-methoxyphenol

Nucleophilic Contaminants

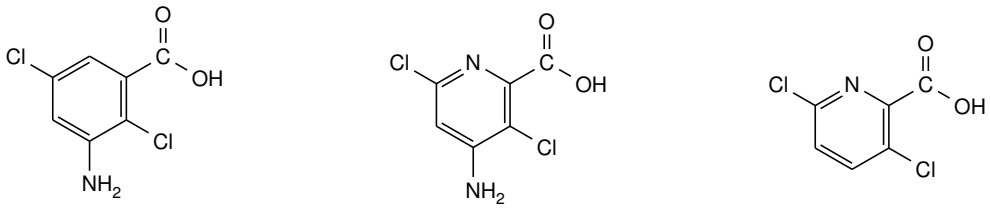

chloramben aminopyralid clopyralid

Figure 2.2. Structures of organic compounds discussed in this study.

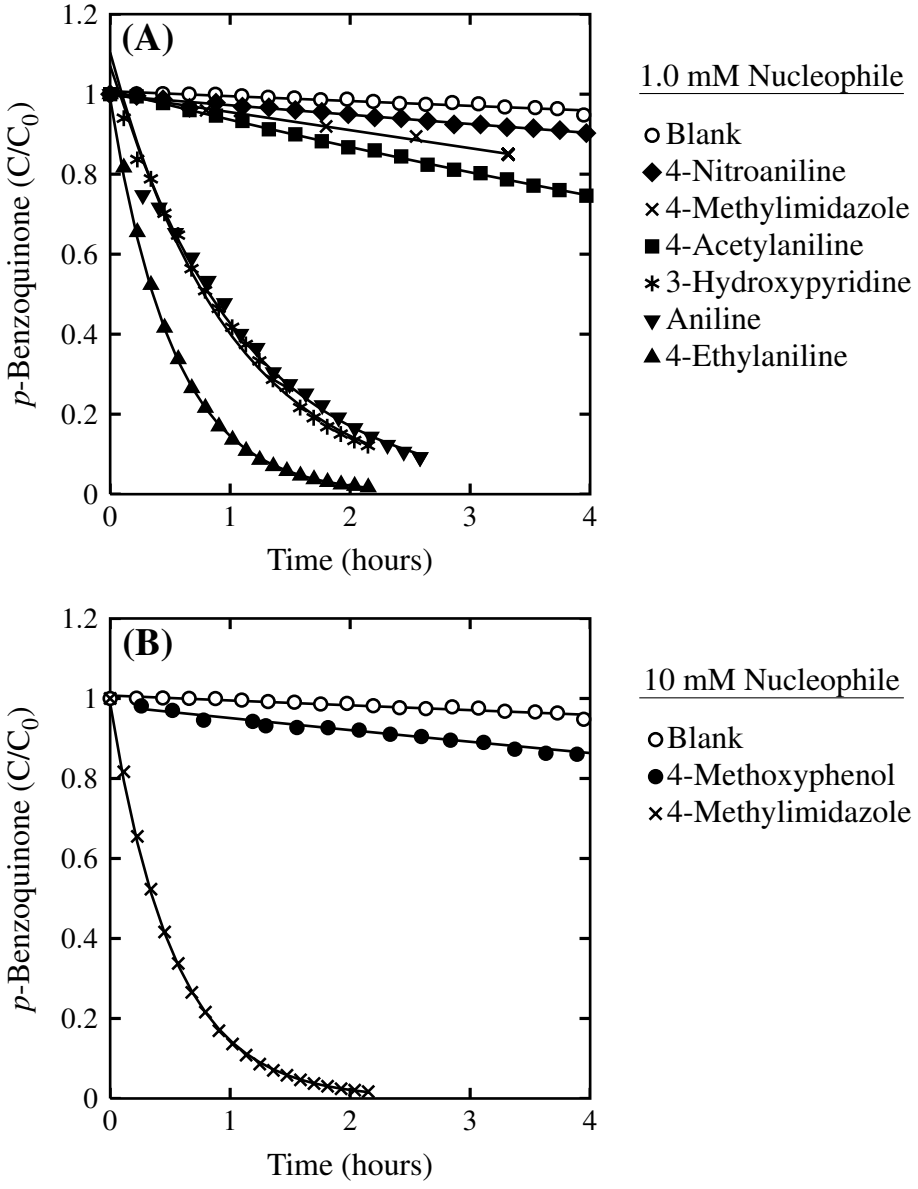

Figure 2.3. *p*-Benzoquinone loss in the presence of an added nucleophile: (A) approximately 1 mM added nucleophile, and (B) approximately 10 mM added nucleophile. Conditions: 100 μM *p*-benzoquinone, 5 mM MOPS adjusted to pH 7.0 and 10 mM NaCl. The blank contains no added nucleophile.

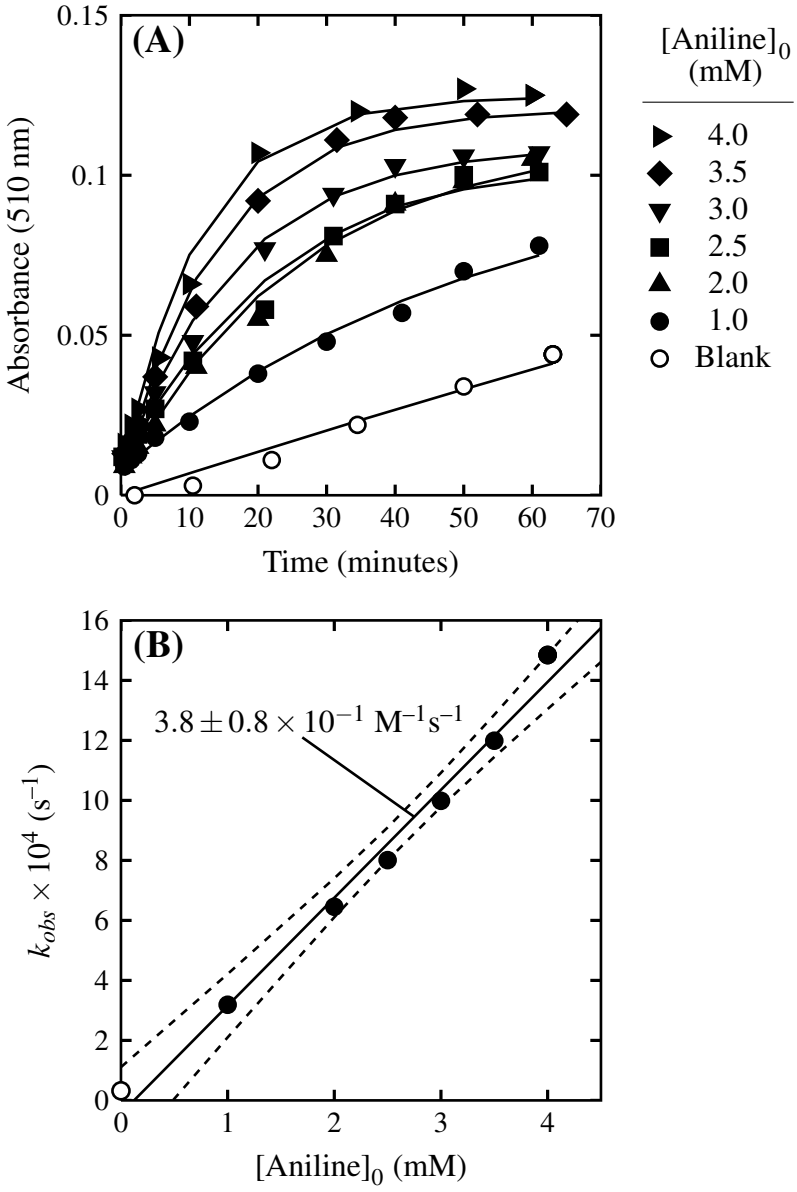

Figure 2.4. (A) Increase in absorbance at 510 nm absorbance in a solution containing 100 μM *p*-benzoquinone and aniline. Conditions: 5.2 mM MOPS buffer adjusted to pH 7.0, 10 mM NaCl. (B) Observed rate constants (k_{obs}) determined from increase in 510 nm absorbance.

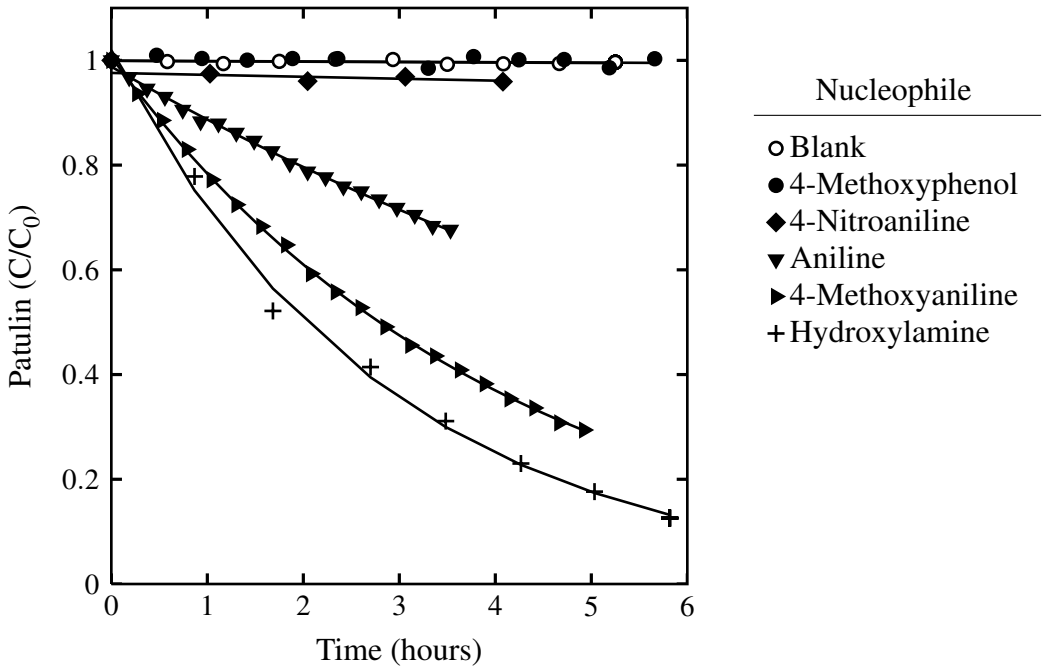

Figure 2.5. Patulin loss in the presence of an added nucleophile. Conditions: 100 μM *p*-benzoquinone, 1 mM added nucleophile, 5 mM MOPS adjusted to pH 7.0 and 10 mM NaCl.

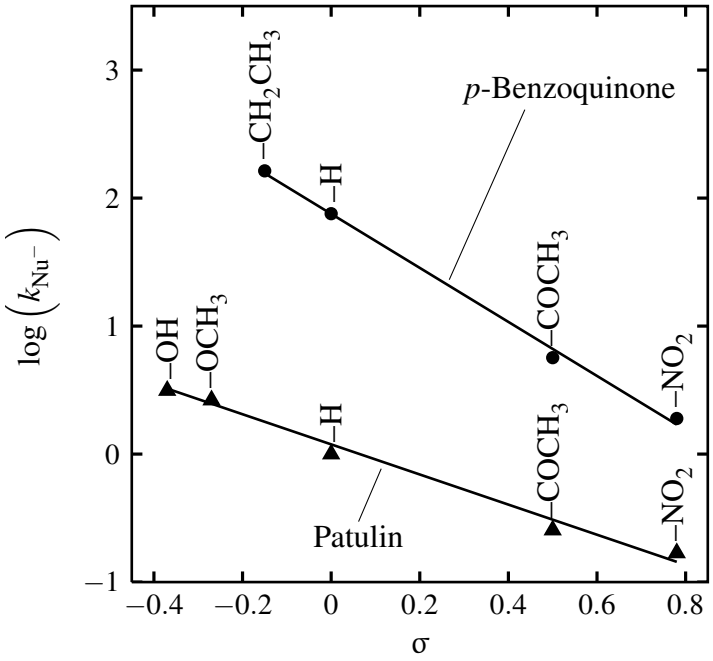

Figure 2.6. Correlation of Hammett constant (σ) and rate constant (k_{Nu^-}) for loss of p-benzoquinone or patulin in the presence of monosubstituted anilines. The substituent is marked for each point. The slope, ρ, for *p*-benzoquinone is -2.1 ± 0.3. For patulin the slope is -1.2 ± 0.2. Rate constants are reported in Table 2.1.

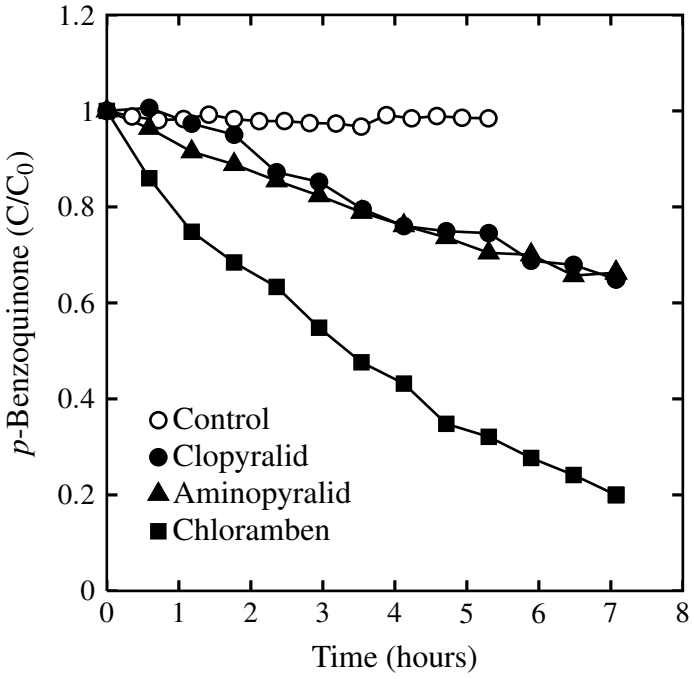

Figure 2.7. *p*-Benzoquinone consumption in the presence of aminopyralid, clopyralid, or chloramben: measured *p*-benzoquinone concentration (C) normalized by initial *p*-benzoquinone concentration (C_0). Conditions: 100 μM *p*-benzoquinone, 1 mM aminopyralid, clopyralid, or chloramben in 5.0 mM MOPS buffer adjusted to pH 7.0.

2.5 Supporting Information

Supporting information for Chapter 2 contains a description of the nucleophilic addition to patulin mechanism proposed by Fliege and Metzler (*1*, *2*), apparent rate constants for loss of *p*-benzoquinone in the presence of nucleophiles (Table S2.1), and for patulin (Table S2.2), 510 nm absorbance in solutions of *p*-benzoquinone and DEPP (Figure S2.5), MES (Figure S2.6) and MOPS (Figure S2.7), and a table of available acid dissociation constants (pK_a values) for chemical compounds used in this chapter.

2.5.1 Patulin Michael Addition Mechanism Proposed by Fliege and Metzler

Fliege and Metzler (*1*, *2*) observed Michael addition reactions of patulin (Figure 2.2) and excess concentrations of glutathione, N-acetyl-L-cysteine, *p*-bromothiophenol, ethanolamine, mercaptoethanol, and bromoaniline nucleophiles during incubations in 50 mM or 1M phosphate buffered (pH 7) water-methanol solutions. All nucleophiles reacted with patulin to form a short-lived monoadduct. For bromothiophenol, the first addition occurs at C-6. They isolated the resulting adduct and confirmed its structure using ^{1}H and ^{13}C NMR (*2*).Glutathione, N-acetyl-L-cysteine, and mercaptoethanol produced monoadducts where addition occurred at C-6 or C-2. The monoadducts transform via rearrangements and eliminations to form intermediates containing electrophilic α,β-unsaturated carbonyl substructures. The hemiacetal (C-4) can tautomerize to an electrophilic aldehyde. Another nucleophilic addition step can occur, potentially leading to a second round of rearrangements and a third addition step. Utlimately, Fliege and Metzler observed four types of products: lactones, thioenolether ketones, dihydropyranones, and ketohexanoic acids. NAC and GSH

formed thioenolether ketones at C-2 and C-6, but lactones were not observed; they were either too short lived or lacked strong UV chromophores required to be detected by UV/HPLC. Methyl ester products were reported arising from methanolysis of lactone rings in the presence of methanol solvent. The dihydropyranone products do not add another nucleophile despite containing an α,β-unsaturated carbonyl backbone. Fliege and Metzler reasoned that the ring oxygen suppresses its electrophilicity and deactivates it. 4-Bromoaniline reacted more slowly than the other nucleophiles tested. Both mono and diadducts were identified.

Fliege and Metzler reported that **1**, **2**, and **3** were the identifiable products of the reaction between aniline and patulin (*1*, *2*). The following is a more detailed description of the mechanism that they proposed. These products arise from nucleophilic attack by aniline or water. There are two nucleophilic attack steps in the proposed mechanism. Nu_1 is represents the nucleophile that attacks first (either aniline or water) and Nu_2 represent the second nucleophile. In this case, Nu_1 or Nu_2 in the products (**1**, **2**, and **3**) represents either a hydroxyl group or aniline.

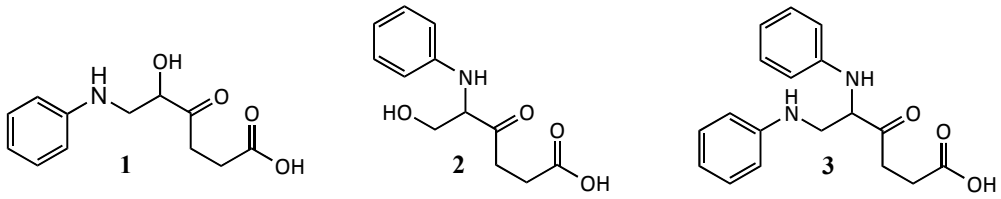

The first step is Michael-type 1,6 addition to C-6. The resulting zwitterion undergoes proton exchange. The enol then tautomerizes to the more stable keto form.

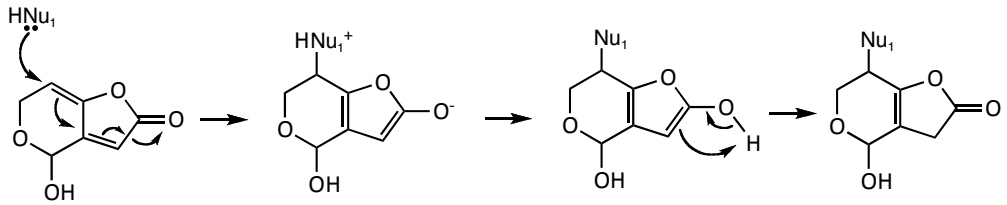

(S2.1)

Lactones are susceptible to hydrolysis. The hydrolysis product undergoes keto-enol tautomerization to the more stable keto form. This reaction can be base catalyzed:

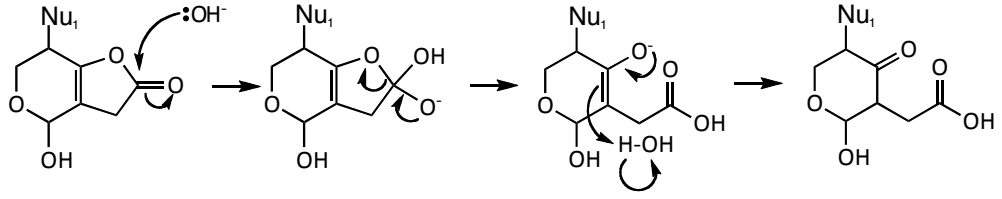

(S2.2)

This step could also be acid catalyzed, following protonation of the carbonyl oxygen:

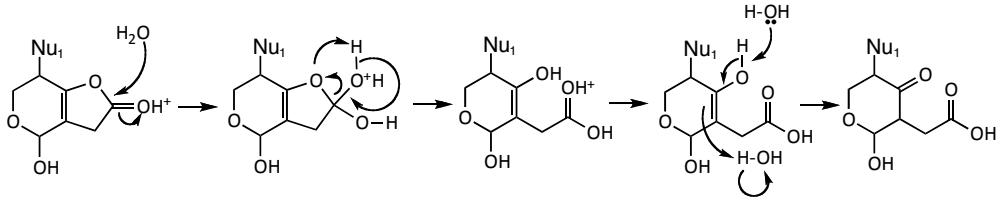

(S2.3)

In the next step, a six-member transition state allows proton transfer from the hemiacetal oxygen to the keto oxygen, opening the hemiacetal ring. The ketone reforms through keto-enol tautomerization.

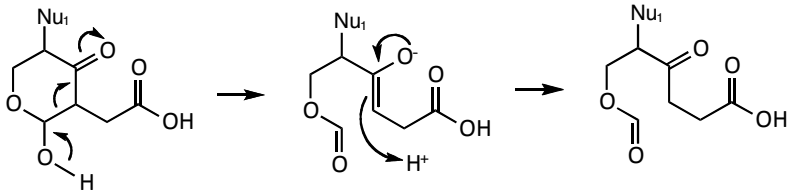

(S2.4)

C-4 can now be eliminated by an E2 mechanism. The leaving group is a formate ion consisting of C-4 and two adjoining oxygens.

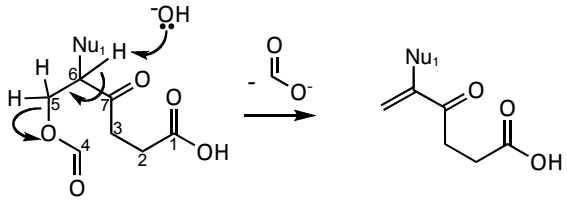

(S2.5)

The elimination product is an α,β-unsaturated carbonyl. Michael-type 1,4-addition of a second nucleophile (Nu_2) and a keto-enol tautomerization leads to the products (**1**, **2**, and **3**).

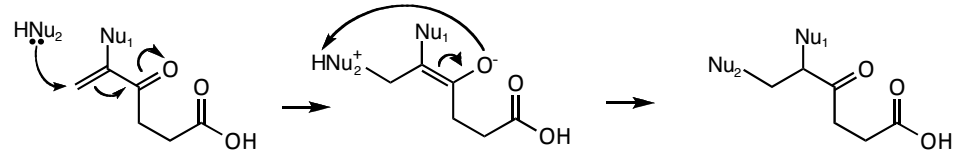

(S2.6)

2.5.2 *p*-Benzoquinone and Reactions with Buffer Compounds

Absorbance of solutions of *p*-benzoquinone and aniline at 510 nm has been attributed to the formation of the Michael-type adduct: anilinohydroquinone (*3*). However, in the absence of aniline, some 510 nm absorbance was observed after 2 hours of contact time in buffered 1 mM *p*-benzoquinone solutions, regardless of whether the buffer was MOPS, phosphate, or maleate at pH 7.0 (Figure S2.2). At pH 2.0, no significant absorbance was observed above 500 nm, regardless of buffer identity. Both phosphate and maleate have buffer capacity near pH 2.0, their pK_a values are 2.148 and 1.92, respectively (25°C and zero ionic strength, *4*). MOPS does not have a pK_a near pH 2, but the solution pH did not change significantly in 2 hours. At pH 7 and pH 2, MOPS buffered solutions exhibited higher absorbance than solutions of the other buffers. At 5 mM buffer concentration, 510 nm absorbance was 2 times higher in MOPS solution than in phosphate or maleate solutions. Increasing the buffer

concentration by an order of magnitude strongly increased absorbance of MOPS solutions, somewhat for phosphate, but only slightly for maleate: 510 nm absorbance was 3 times higher for 50 mM MOPS than 5.0 mM MOPS, 1.76 times higher for 50 mM phosphate versus 5 mM phosphate, and 1.24 times higher for 50 mM maleate versus 5.0 mM maleate.

Tentatively, we can attribute the absorbance observed above 500 nm in maleate solution to products of hydration, and not products arising from addition of maleate. If this absorbance indicated a maleate addition product then increasing the maleate concentration by an order-of-magnitude we expect that the absorbance at 500 nm would have greatly increased. However, the increase in absorbance above 500 nm with increased maleate concentration close to insignificant. Instead of a maleate addition product, we attribute this to a hydration product. In contrast, increased MOPS concentration lead to a much higher absorbance, suggesting that a product that absorbs at 510 nm is formed by reaction of MOPS and *p*-benzoquinone.

The spectrum of the expected hydration product, 1,2,4-trihydroxybenzene is shown in Figure S2.3. A solution of 1,2,4-trihydroxybenzene in 5.0 mM MOPS buffer adjusted to pH 7.0 rapidly changed color before the spectrum could be recorded. One potential explanation for the color change is oxidation of 1,2,4-trihydroxybenzene to 2-hydroxybenzoquinone by O_2 (*5*). Either this benzoquinone (*6*) or subsequent polymerization products may cause the absorbance observed around 500 nm. In methanol, where we do not expect significant O_2 oxidation, no peak around 500 nm is observed (Figure S2.3).

Near the p^aK_a of MOPS (7.184, *4*), solution pH strongly affected absorbance spectra of solutions containing 1 mM *p*-benzoquinone and 5.0 mM MOPS (Figure S2.4). Absorbance at 510 nm increased from pH 6.2 to 7.8. The spectrum taken at pH 5.5, outside the buffer range of MOPS, has much lower absorbance above 500 nm and is similar to the spectrum observed at pH 2.0.

Assuming that the absorbance at 510 nm is due to a MOPS reaction product, the relationship between absorbance and pH near the pK_a of MOPS reflects the influence of protonation. At pH 7.8, 80% of the MOPS in solution is deprotonated and the highest absorbance is observed. At pH 6.2, only 10% of the MOPS is deprotonated and the absorbance is considerably lower. Protonation of MOPS and nucleophilic attack by MOPS occurs at the same atom, likely the tertiary nitrogen, blocking the nucleophilic center by protonation and diminishing its ability to react with electrophiles.

We performed a series of time course experiments observing increase in absorbance at 510 nm of *p*-benzoquinone solutions buffered by DEPP at pH 4.6 (Figure S2.5), MES at pH 6.2 (Figure S2.6 and MOPS at pH 7.0 (Figure S2.7) with increasing concentration of buffer. For all three buffers, solutions of *p*-benzoquinone and MOPS at pH 7.0 (near the pK_a of MOPS) the 510 absorbance slowly increased over time. Also, increasing the concentration of MOPS or MES increased the rate of absorbance increase. Compared to Figure 2.4 higher concentrations of *p*-benzoquinone and MOPS were required to yield the same absorbance that was observed with *p*-benzoquinone and aniline: 1 mM *p*-benzoquinone and 30 mM MOPS yield and absorbance of 0.14 after 70 min, where only 100 μM *p*-benzoquinone and 3 mM aniline are required to yield the same absorbance after 60 min (note that 5 mM MOPS was also present). However, this effect could be due to differences in the rate of adduct formation or differences in the molar absorptivity of the adducts. Authentic standards are not available for these adducts so we cannot determine their molar absorptivity. We speculate that these adducts would be hydroquinones with one hydrogen replaced with a C-N bond linking it to a molecule of buffer. In 5 mM MOPS (pH 7), only negligible absorbance at 510 nm was observed from 100 μM *p*-benzoquinone in the absence of aniline. MES solutions at pH 6.2 gave the same trend as MOPS, but the observed absorbance was lower in the same time frame (Figure S2.6). Solutions buffered using DEPP at pH 4.6 exhibited increases of

absorbance at 510 nm, but the increase was approximately 4 times slower than with MES (Figure S2.5).

MOPS, MES, and DEPP concentration dependence of the rate of increase in 510 nm absorbance suggests that at least some of this absorbance is due to a reaction product between these compounds and *p*-benzoquinone. Some absorbance is likely contributed by products that form by a parallel pathway. Importantly, to achieve the same absorbance the concentration of both *p*-benzoquinone and MOPS needs to be 10 times greater than when aniline is present: the contribution of a potential MOPS adduct or hydration product is an order of magnitude lower than that of the aniline adduct. Still, reactions of MOPS, MES, and DEPP with *p*-benzoquinone do complicate the interpretation of our data more than if the buffer compounds we used had been truly nonnucleophilic. Future researchers should be wary of these potential pitfalls and choose compounds to use as pH buffers wisely.

We expect that the observed rate of *p*-benzoquinone loss depends on (1) the pH, which controls [OH^-] and speciation of the buffer; and (2) the identity and concentration of the buffer. Both hydration and addition of buffer compounds occur simultaneously so it is only possible to discuss them in aggregate when considering loss of *p*-benzoquinone (Figure S2.8). DEPP and MES were used at 5 mM concentration to buffer pH in the range of 4 – 7. The half-life for loss of *p*-benzoquinone at these pH ranged from 74 to 250 hours, which corresponds to less than 10% loss of *p*-benzoquinone after 10 hours. The observed pseudo-first-order rate constant did not exceed 3×10^{-6} s^{-1}. At pH 7.02 in 5.0 mM MOPS buffer the half-life was 41 hours, which corresponds to 15% loss after 10 hours. At higher pH, loss of *p*-benzoquinone in 5.0 mM MOPS solution is more significant: at pH 7.6 and pH 8.1 the half-lives were 21 and 4 hours, respectively. In solutions buffered at pH 8.5-9.5 using 5 mM CHES, loss of *p*-benzoquinone was too fast to measure. Pseudo-first-order rate constants (k_{obs}) determined from the time course shown in Figure S2.8 are plotted as

a function of pH in Figure S2.9. The pH dependence of loss rate is readily apparent in Figure S2.9. In DEPP or MES solutions below pH 6.5 the k_{obs} is smaller than 5×10^{-6}. For MOPS, this is consistent with Figure S2.4: *p*-benzoquinone loss and absorbance increase. Perhaps this is due to adduct formation that is faster at pH higher than the pK_a of MOPS than at pH below it. At pH 4 – 6.5, much slower loss of *p*-benzoquinone indicates that (1) MES and DEPP react slowly with *p*-benzoquinone, (2) [OH^-] is too small to cause significant hydration, (3) the rate contribution of water is less than 3×10^{-6} s^-1, and (4) and the product of rate constant and concentration of H^+ is smaller than 3×10^{-6} s^-1 at these pH.

There is still doubt about the identity of the product that absorbs at 510 nm in the above experiments, and what mechanism leads to increase of absorbance at 510 nm. The absorbance increase could be due to the formation of an adduct between one of the compounds used as a buffer. However, a general base catalysis mechanism could also be active in which DEPP, MES, or MOPS deprotonation of a water molecule and nucleophile attack from that water molecule to *p*-benzoquinone both occur in the rate determining step. Unfortunately, insufficient evidence currently exists to reach either conclusion.

2.5.3 Patulin and Reactions with Buffer Compounds

Patulin is stable in buffered solutions lacking an added nucleophile in buffered solutions consisting of 5.0 mM acetate at pH 5.0, 5.0 mM MES at pH 6.0, and 5.0 mM MOPS at pH 7.0 (Figure S2.10). The slight increase in patulin concentration observed at pH 5.0, 6.0, and 7.0 is most likely due to evaporation of the solution. At pH 9.0 there was significant loss of patulin (Figure S2.10). This time course fits a pseudo-first-order model (Equation 2.3) with a measured k_{obs} of 2.46×10^{-5} s^{-1}. The data for pH 9.0 in Figure S2.10 yield a

k_{OH^-} of 2.35 M^{-1} s^{-1}. However, 5 mM CHES was also present to buffer the solution at pH 9.0. CHES contains a secondary amine functional group that could react with patulin as a nucleophile (Figure 2.2). Unfortunately, it is not possible with these data to tell how much of the loss of patulin was due to reaction with OH^-, CHES, another solution constituent, or by oxidation by O_2 which may be significant at this pH.

Table S2.1. Pseudo-first-order rate constants observed for *p*-benzoquinone loss in the presence of nucleophiles (k_{obs}). Second order rate constants (k) determined by normalizing k_{obs} by concentration of deprotonated nucleophile (Equation 2.4). Error shown determined from 95% confidence intervals for the slope of the best-fit line. Conditions: 5 mM MOPS and 10 mM NaCl. pK_a values from Table S2.3. Hammett σ constants (*7*) shown for aromatic amines.

Nucleophile	[Nucleophile] (mM)	pH	pK_a	σ	k_{obs} (s^{-1})	k (M^{-1} s^{-1})
None		7.06			$3.4 \pm 0.5 \times 10^{-6}$	
4-Ethylaniline	1.01	6.94	5.00	-0.151	$5.0 \pm 0.1 \times 10^{-4}$	$5.0 \pm 0.1 \times 10^{-1}$
Aniline	1.09	7.04	4.58	0	$2.5 \pm 0.1 \times 10^{-4}$	$2.3 \pm 0.1 \times 10^{-1}$
3-Hydroxypyridine	1.81	6.98	5.10		$2.5 \pm 0.1 \times 10^{-5}$	$1.38 \pm 0.05 \times 10^{-1}$
4′-Aminoacetophenone	1.18	6.99	2.75	0.502	$2.05 \pm 0.04 \times 10^{-5}$	$1.74 \pm 0.03 \times 10^{-2}$
4-Nitroaniline	1.16	6.94	1.0	0.778	$6.8 \pm 0.4 \times 10^{-6}$	$5.8 \pm 0.4 \times 10^{-3}$
4-Methylimidazole	10.87	6.91	7.52		$2.4 \pm 0.1 \times 10^{-5}$	$2.2 \pm 0.1 \times 10^{-3}$
4-Methoxyphenol	12.18	7.02	10.21		$9.3 \pm 0.8 \times 10^{-6}$	$7.6 \pm 0.6 \times 10^{-4}$

Table S2.2. Pseudo-first-order rate constants observed for patulin loss in the presence of nucleophiles (k_{obs}). Second order rate constants (k) determined by normalizing k_{obs} by concentration of deprotonated nucleophile (Equation 2.4). Error shown determined from 95% confidence intervals for the slope of the best-fit line. Conditions: 5 mM MOPS and 10 mM NaCl. References for pK_a values given in Table S2.3. Hammett σ constants (*7*) shown for aromatic amines.

Nucleophile	[Nucleophile] (mM)	pH	pK_a	σ	k_{obs} (s^{-1})	k (M^{-1} s^{-1})
Control		7.06			$2 \pm 4 \times 10^{-7}$	
4-Methoxyphenol	10.24	7.02	10.21		$2 \pm 3 \times 10^{-7}$	$4 \pm 5 \times 10^{-2}$
4-Aminophenol	9.98	7.16	5.64	−0.37	$9.6 \pm 0.3 \times 10^{-5}$	$9.8 \pm 0.3 \times 10^{-3}$
4-Methoxyaniline	8.77	7.02	5.32	−0.268	$6.91 \pm 0.04 \times 10^{-5}$	$8.04 \pm 0.05 \times 10^{-3}$
Hydroxylamine	11.05	7.08	5.97		$4.18 \pm 0.07 \times 10^{-5}$	$4.07 \pm 0.07 \times 10^{-3}$
Aniline	10.10	7.12	4.58	0	$3.00 \pm 0.07 \times 10^{-5}$	$2.97 \pm 0.07 \times 10^{-3}$
4′-Aminoacetophenone	10.06	7.02	2.75	0.502	$7.1 \pm 0.7 \times 10^{-6}$	$7.1 \pm 0.7 \times 10^{-4}$
4-Nitroaniline	2.37	7.11	1.0	0.778	$1.05 \pm 0.05 \times 10^{-6}$	$4 \pm 1 \times 10^{-4}$

Table S2.3. Selected pK_a values of chemicals discussed in this chapter.

Chemical	pK_a[a]	s	Reference
Hydroxylamine	5.96		*8*
	13.74		*8*
Acetate	4.756		*4*
DEPP	4.67		*9*
	8.83		*9*
MES	6.270		*4*
MOPS	7.184		*4*
CHES	9.384		*4*
H_3PO_4	2.148		*4*
	7.198		*4*
	12.35		*4*
Maleate	1.92		*4*
	6.27		*4*
Chloramben	3.40[b]		*10*
Clopyralid	2.3[b]		*11*
Aminopyralid	2.56[b]		*12*
3-Hydroxypyridine	4.82		*8*
	8.78		*8*
4-Ethylaniline	5.00		*8*
4-Methoxyaniline	5.357		*8*
para-Aminophenol	5.64		*13*
4-Chloroaniline	3.979		*8*
4′-Aminoacetophenone	2.29		*8*
Aniline	4.601		*8*
4-Nitroaniline	1.015		*8*
4-Methoxyphenol	10.21		*8*
4-Methylimidazole	7.54		*8*

[a] Acid dissociation constants were corrected to zero ionic strength using the Davies equation (*14*), when necessary. [b] Ionic strength not reported.

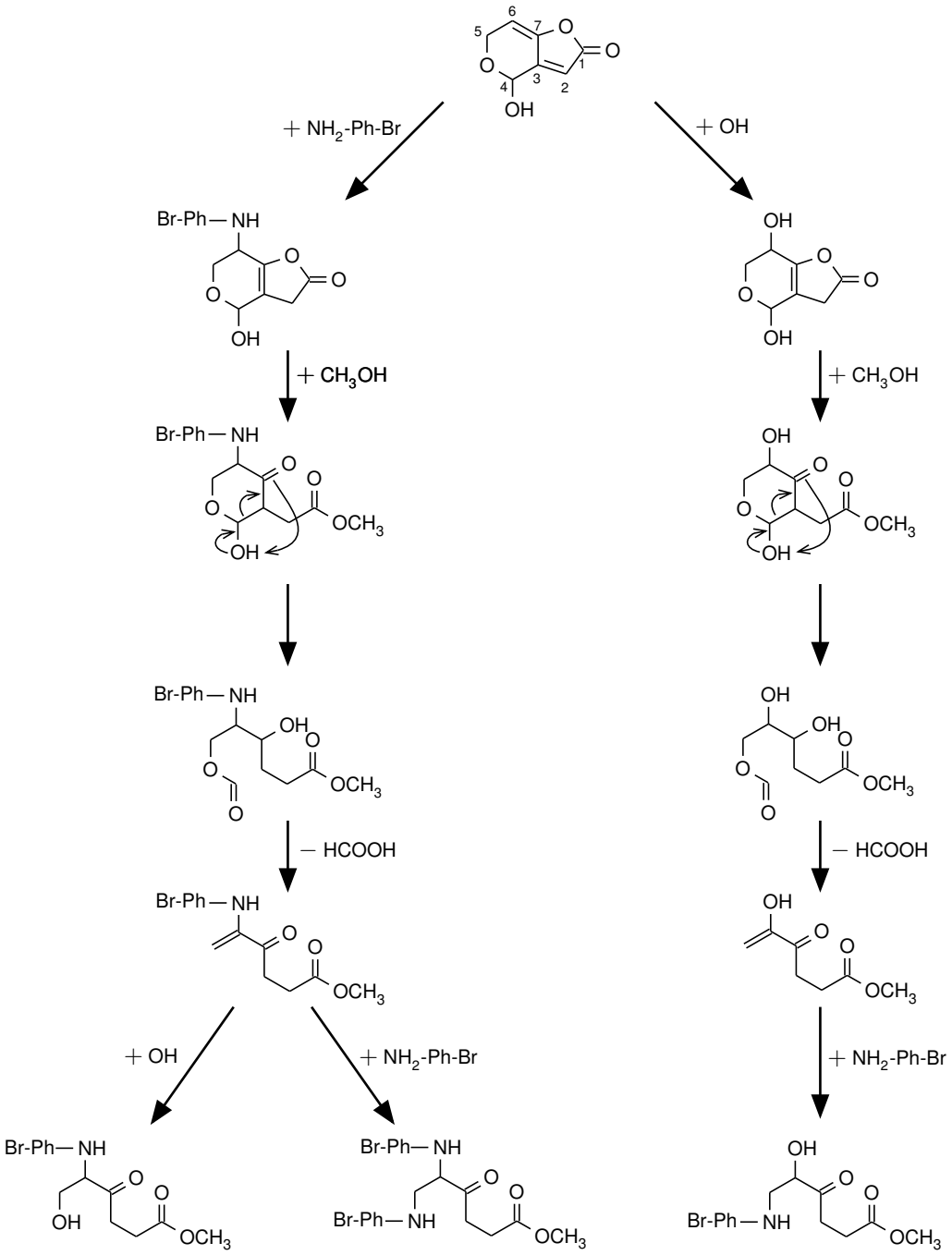

Figure S2.1. Proposed reaction scheme for reaction of patulin with 4-bromoaniline (Br-Ph-NH_2). Adapted from reference *1*.

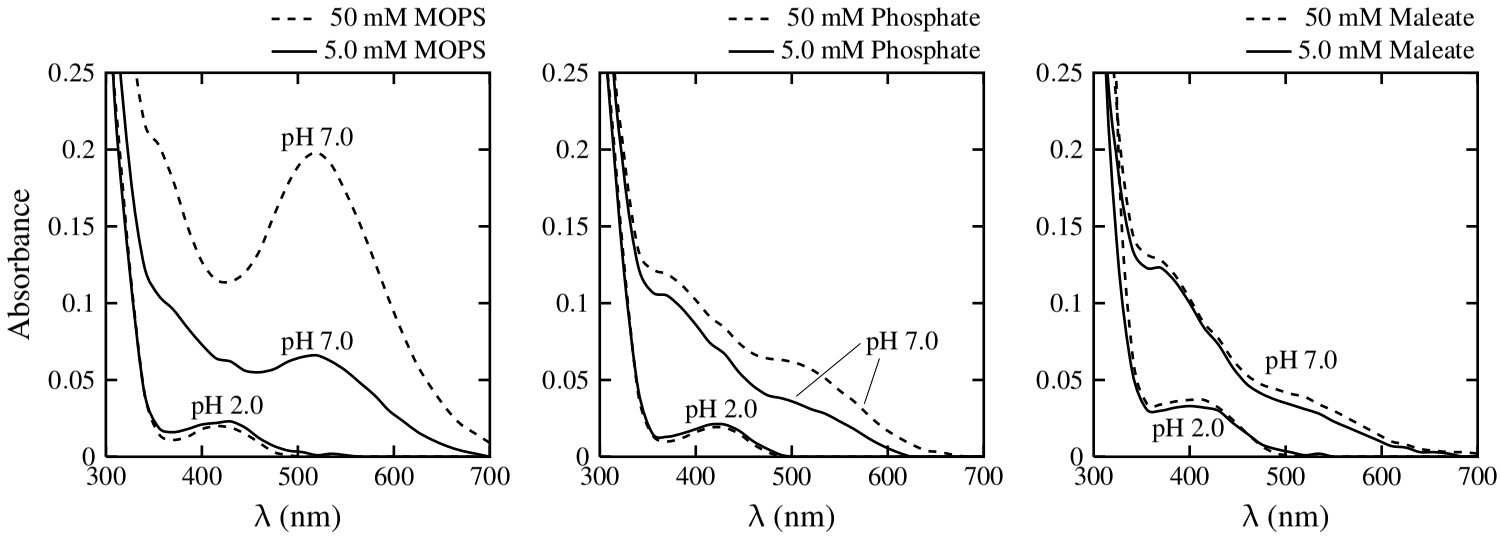

Figure S2.2. Spectra of 1 mM *p*-benzoquinone solutions recorded 2 hours after addition to each medium. Solutions also included 10 mM NaCl.

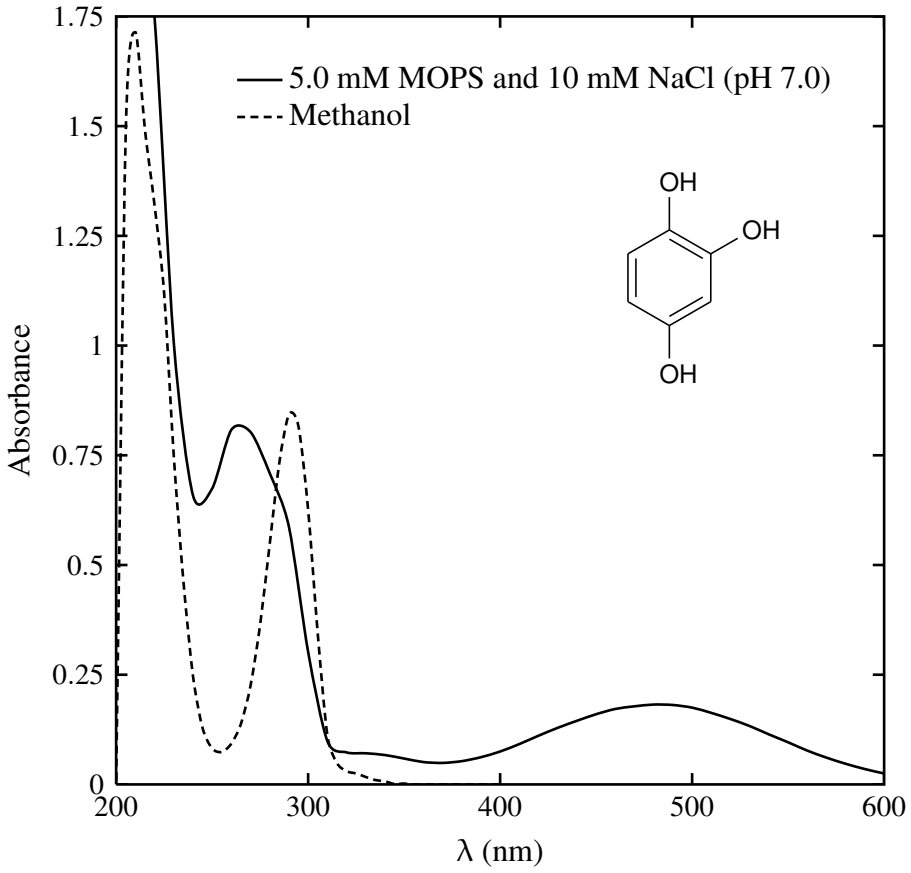

Figure S2.3. Spectra of 250 μM 1,2,4-trihydroxybenzene. In MOPS solution, the spectrum is taken following a rapid color change that occurred despite N_2 sparging.

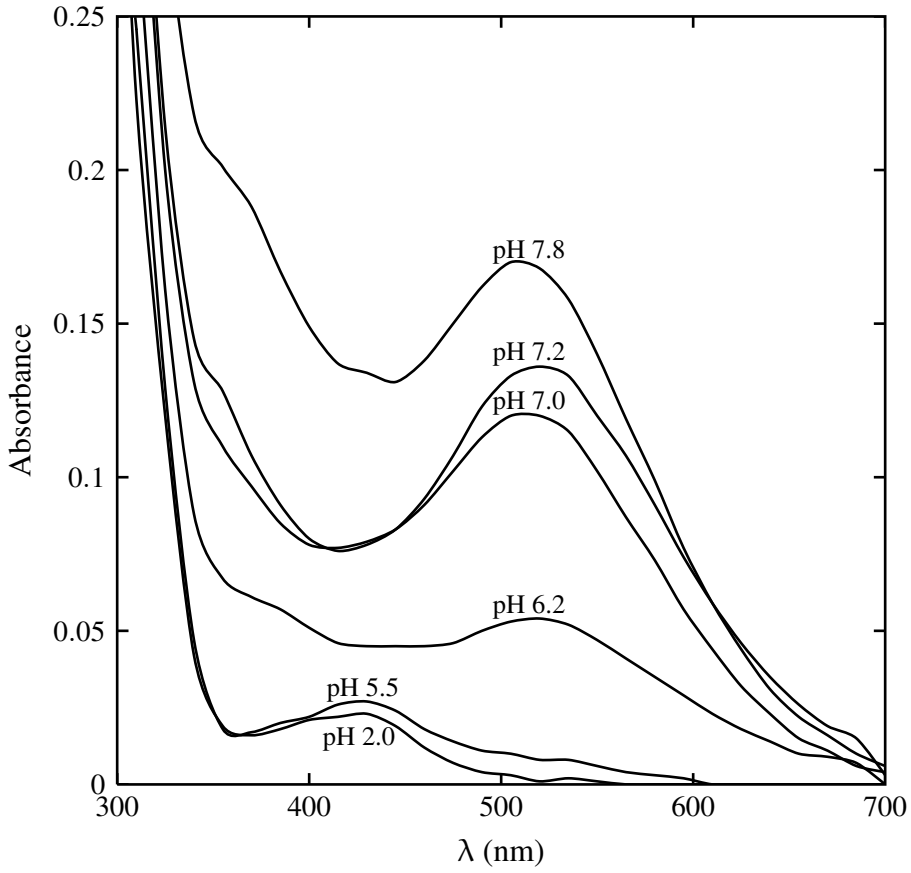

Figure S2.4. Effect of pH on spectra of 1.0 mM *p*-benzoquinone collected 1 hour after addition to pH adjusted solution of 5.0 mM MOPS and 10 mM NaCl.

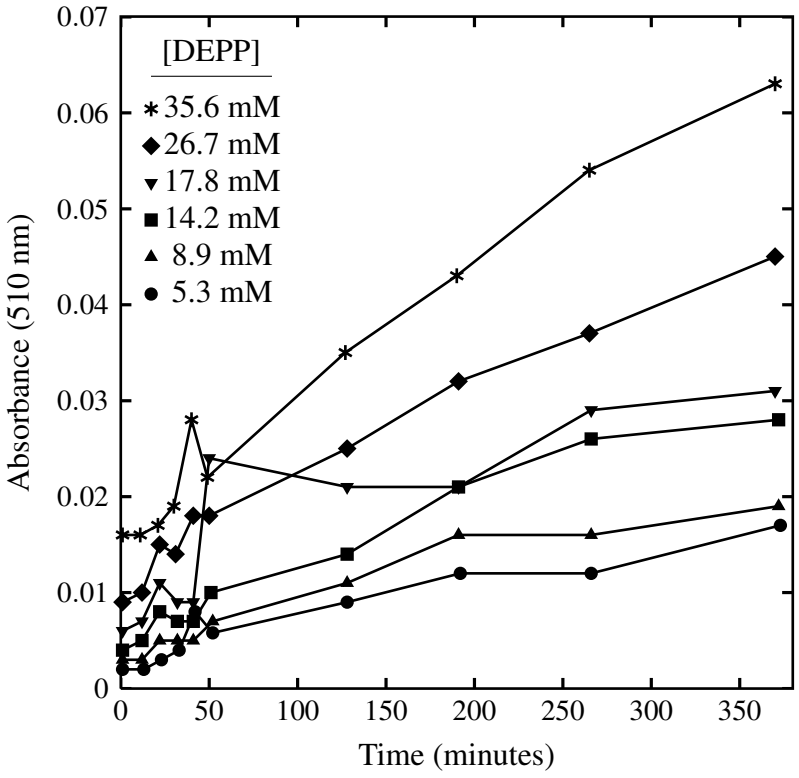

Figure S2.5. 510 nm absorbance increase of 1 mM *p*-benzoquinone solution as a function of DEPP concentration. Solutions were adjusted to pH 4.6 and also contained 10 mM NaCl.

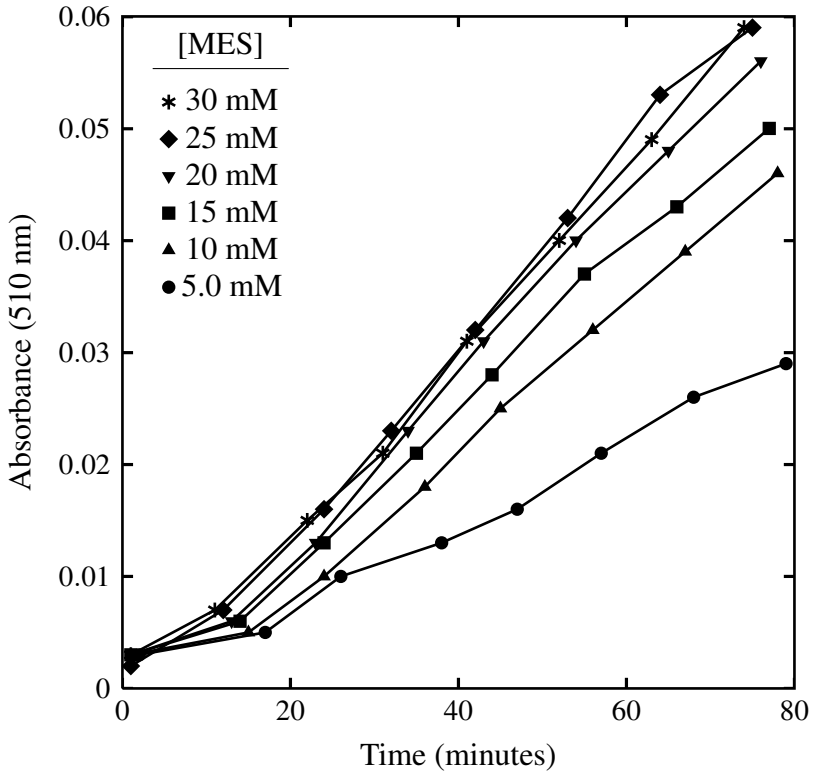

Figure S2.6. Increase in 510 nm absorbance of 1 mM *p*-benzoquinone solutions as a function of MES concentration. Solutions were adjusted to pH 6.2 and also contained 10 mM NaCl.

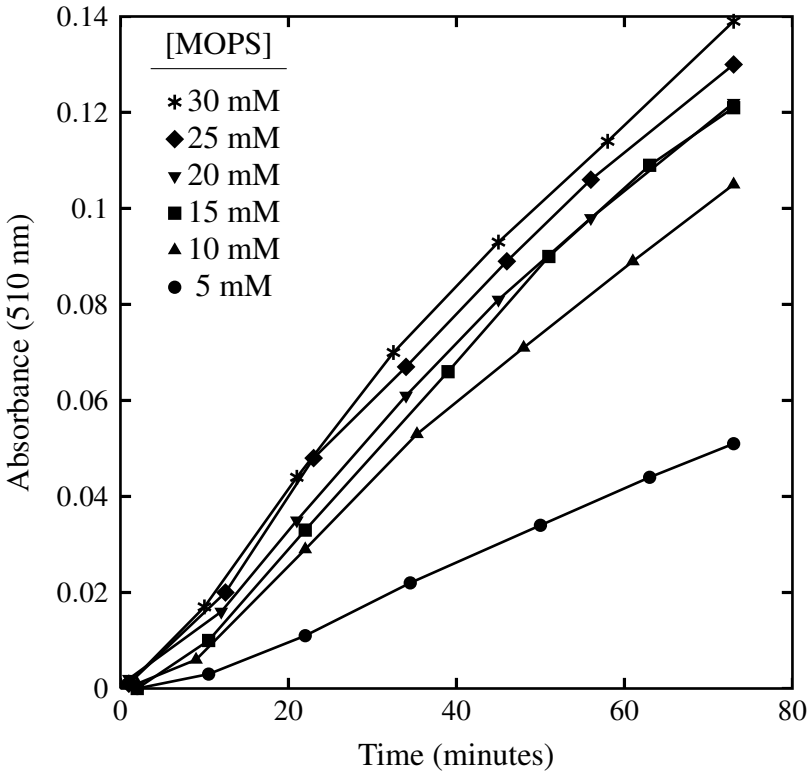

Figure S2.7. Increase in 510 nm absorbance of 1 mM *p*-benzoquinone solutions as a function of MOPS concentration. Solutions were adjusted to pH 7.0 and also contained 10 mM NaCl.

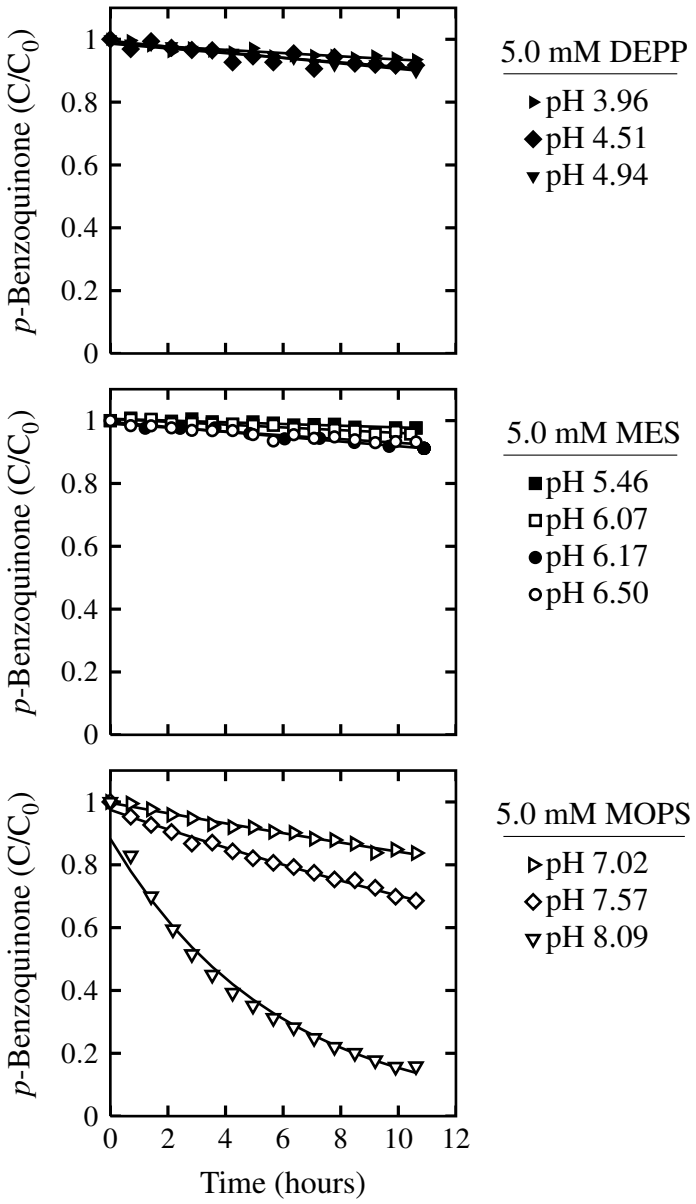

Figure S2.8. *p*-Benzoquinone loss in the absence of added nucleophile. DEPP, MES, and MOPS were employed as buffers. Conditions: 100 μM *p*-benzoquinone, 5 mM buffer, 10 mM NaCl.

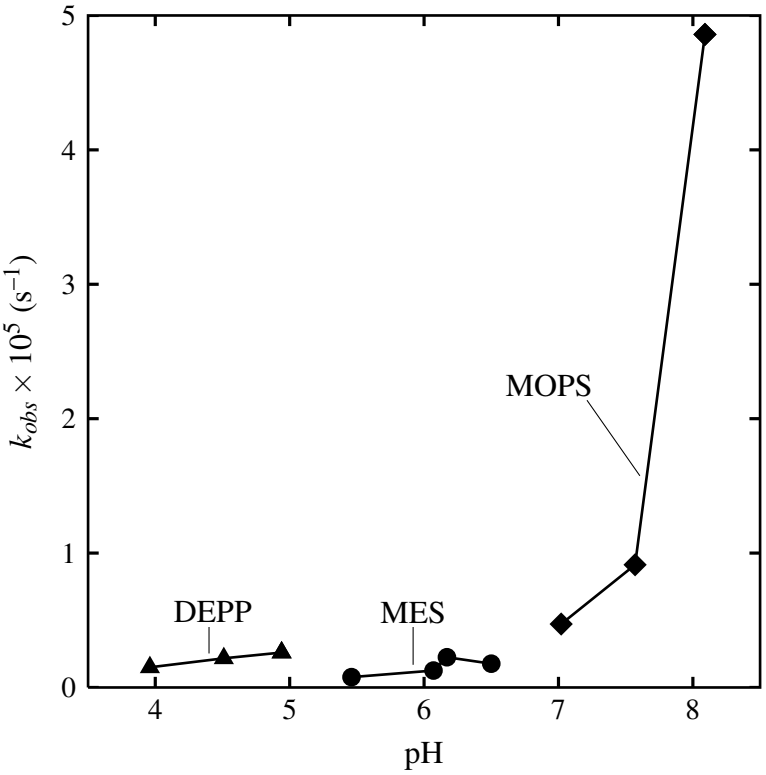

Figure S2.9. Pseudo-first-order rate constants for loss of *p*-benzoquinone calculated using the data in Figure S2.8.

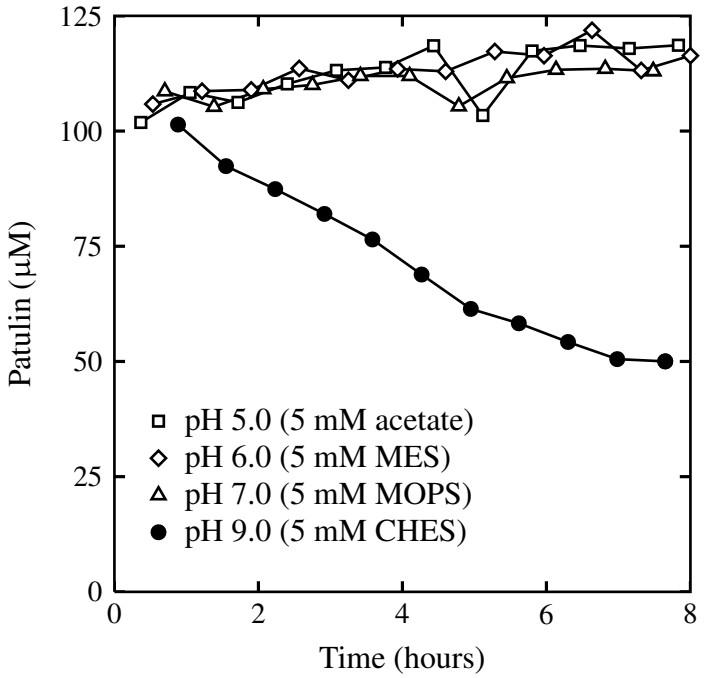

Figure S2.10. Time course for patulin loss in four different buffer systems. Conditions: 100 μM patulin, 5 mM buffer, 10 mM NaCl.

References

(1) R. Fliege, M. Metzler. Electrophilic properties of patulin. Adduct structures and reaction pathways with 4-bromothiophenol and other model nucleophiles. *Chemical Research in Toxicology* **2000**, *13*, 363–372.

(2) R. Fliege, M. Metzler. Electrophilic properties of patulin. N-Acetylcysteine and glutathione adducts. *Chemical Research in Toxicology* **2000**, *13*, 373–381.

(3) M. L. Iskander, H. A. A. Medien. A spectrophotometric kinetic study of the reaction of amino acids with p-benzoquinone. *Anales de Química* **1997**, *93*, 3–7.

(4) R. N. Goldberg, N. Kishore, R. M. Lennen. Thermodynamic quantities for the ionization reactions of buffers. *Journal of Physical and Chemical Reference Data* **2002**, *31*, 231–370.

(5) J. F. Corbett. The chemistry of hydroxy-quinones. Part VI. Formation of 2-hydroxysemiquinones during the autoxidation of benzene-1,2,4-triols in alkaline solution. *Journal of the Chemical Society C: Organic* **1970**, 2101–2106.

(6) B. Philipp, M. Hoff, F. Germa, B. Schink, D. Beimborn, V. Mersch-Sundermann. Biochemical interpretation of quantitative structure-activity relationships (QSAR) for biodegradation of N-heterocycles: A complementary approach to predict biodegradability. *Environmental Science and Technology* **2007**, *41*, 1390–1398.

(7) D. McDaniel, H. Brown. An extended table of Hammett substituent constants based on the ionization of substituted benzoic acids. *The Journal of Organic Chemistry* **1958**, *23*, 420–427.

(8) A. E. Martell, R. M. Smith, R. J. Motekaitis, *Critically Selected Stability Constants of Metal Complexes Database; Version 8.0*, U.S. Department of Commerce, National Institute of Standards and Technology, Gaithersburg, MD, **2004**.

(9) Q. Yu, A. Kandegedara, Y. Xu, D. B. Rorabacher. Avoiding interferences from good's buffers: a contiguous series of noncomplexing tertiary amine buffers covering the entire range of pH 3–11. *Analytical Biochemistry* **1997**, *253*, 50–56.

(10) J. B. Weber, *Interaction of Organic Pesticides with Particulate Matter in Aquatic and Soil Systems* in *Advances in Chemistry*, American Chemical Society, Washington, D. C., **1972**, pp. 55–120.

(11) J. Comer, K. Chamberlain, A. Evans. Validation of pH-Metric Technique for Measurement of pK_a and log P_ow of Ionizable Herbicides. *SAR and QSAR in Environmental Research* **1995**, *3*, 307–313.

(12) U.S. EPA Office of Pesticide Programs; Fact Sheet for Aminopyralid. **2005**, 1–56.

(13) H. Demirelli, F. Köseoğlu. Solvent and Substituent Effects on the Protonation of Anilines in Dioxane–Water Mixtures. *Journal of Solution Chemistry* **2004**, *33*, 1501–1515.

(14) W. Stumm, J. J. Morgan, *Aquatic Chemistry: Chemical Equilibria and Rates in Natural Waters 3rd ed.*, Wiley, New York, New York, **1996**.

Chapter 3

Highly Reactive *p*-Benzoquinone Electrophiles Generated by the Oxidation of Substituted Hydroquinones Using MnO_2(s, pyrolusite) as an Oxidant

3.1 Introduction

In Chapter 2, we discussed nucleophilic addition reactions of phenol and aniline compounds with *p*-benzoquinone which is an experimentally convenient electrophile because it is stable enough to use as a reagent in experimental solutions that include an added nucleophile of interest. In contrast, when a carboxyl group is present on the *p*-benzoquinone ring, the compound is so electrophilic it cannot be readily isolated and used as a substrate in experiments like those in Chapter 2. In fact, carboxy-*p*-benzoquinone can only be isolated in anhydrous chloroform because it is quickly degraded in aqueous solutions or as a neat solid (*1*).

However, carboxy-*p*-benzoquinone can be generated via oxidation of 2,4-dhydroxy-benzoic acid:

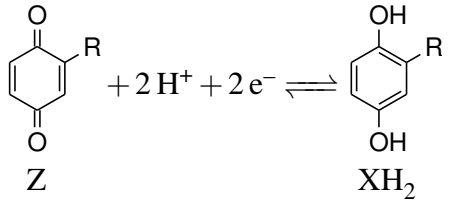

Z XH_2 (3.1)

Collectively we refer to this family of compounds as "quinones," following the convention of Uchimiya and Stone (*2*, *3*). We will refer to the hydroquinone form as XH_2 and the oxidized form as the benzoquinone or Z regardless of the presence of substituents. XH_2 are "proelectrophiles" which are transformed into electrophiles when they become oxidized. Oxidation of XH_2 can be achieved enzymatically consuming H_2O_2 or O_2 (*4–6*), electrochemically (*7*, *8*), or by reaction with $Mn^{III,IV}$ (hydr)oxides (*4*).

In this work, we employ model proelectrophiles as substrates to mimic proelectrophile functional groups with electron withdrawing group substituents within natural organic matter (NOM). Hydroquinone and catechol moieties present in NOM could behave as proelectrophiles and become electrophilic following oxidation. NOM is thought to contain quinone functional groups that are active in reduction and oxidation reactions (*9–11*). Ratasuk et al. (*12*) divided quinone groups in NOM into two fractions: one that has electron-withdrawing substituents and one that has electron donating group substituents or is sterically hindered. We hypothesize that highly reactive electrophiles could be generated in soils and sediments from small molecule proelectrophiles like 2,4-dihydroxybenzoic acid or electron-withdrawing group substituted quinone groups in NOM. The electrophilic form could then react with nucleophiles, and potentially be an important removal mechanism for nucleophilic contaminants in the water column.

Several authors have reported that addition reactions of nucleophilic contaminants, particularly anilines, renders them biologically inactive by forming covalent bonds with natural organic matter in soils and sediments (*4*, *13–22*). Weber et al. (*14*, *16*) observed covalent binding of aniline to humic substances (*16*), and confirmed covalent bond formation using ^{15}N NMR (*14*). Similar studies have reported irreversible sorption of aniline and α-naphthylamine to soils either directly (*23*) or enhanced by oxidation of organic matter by manganese present in soils accompanied by an increase in exchangeable Mn^{2+} (*24*, *25*). Bialk et al. (*4*, *17*) used ^{15}N NMR to show that nucleophilic addition between sulfonamide antimicrobials and humic substances occurred via oxidation reactions caused by the manganese oxide solid birnessite and catalyzed by phenoloxidase enzymes.

Once an electrophile (Z) is generated it can be consumed by the same pathways discussed for *p*-benzoquinone in Chapter 2. Z can react with an added nucleophile to form an adduct (X-Nu). In aqueous solution, OH^- or water can act as a nucleophile and react with Z; we call this "hydration" to distinguish it from reaction with non-solvent nucleophiles. Added nucleophiles compete with H_2O or OH^- to react with benzoquinones (acid catalyzed hydration is not expected; *26*). Hydration occurs via the same mechanism shown in Figure 2.1.

When XH_2 proelectrophiles are oxidized in the presence of nucleophiles the resulting adducts (X-Nu and X-OH) are themselves substituted hydroquinones. X-Nu and X-OH and can be oxidized to benzoquinones (Z-Nu and Z-OH). Z-Nu and Z-OH are second generation electrophiles because they result from a second oxidation step. For an XH_2 with two substituents, a third generation of Z can also be generated (Figure 3.1). Another round of addition/hydration–oxidation reactions is possible when the proelectrophile XH_2 has only 1 substituent. Figure 3.2 shows the sequence of reactions that leads to triadducts and fourth generation benzoquinones that are possible for monosubstituted XH_2 proelectrophiles. In this case, there are 52 possible products (Figure S3.3 in the Supporting Information).

Multiple addition products arising from sequential oxidiation and addition steps have been reported for glutathione and *p*-benzoquinone (*27*) and glutathione with 2-bromohydroquinone (*28*). Glutathione adducts represent a detoxification pathway for quinone compounds, but they can also contribute toxicity, especially in the liver, by causing redox cycles that generate reactive oxygen species (*29*).

Generation of monoadduct and diadducts has been observed as new peaks in cyclic voltammograms when catechol and hydroquinone proelectrophiles are electrochemically oxidized in the presence of nucleophiles (*30–33*).

Replacing ring substituents with more electron-withdrawing substituents yields XH_2 with higher reduction potentials making them more difficult to oxidize (Table 3.1). A carboxylic acid substituent gives XH_2(**III**) a reduction potential of 0.769 V (*34*) which is 0.07 V greater than XH_2(**I**) which has a reduction potential of 0.699 V (*35*). Ring Substituents also influence electrophilicity of the benzoquinone (Z form). Electron-withdrawing substituents increase the rate of nucleophilic addition by increasing electron deficiency of the benzoquinone, while electron-donating substituents have the opposite effect (*26*, *31*). Nucleophilicity is also subject to substituent effects: electron-donating substituents increase nucleophilicity and rates of nucleophilic reactions and electron-withdrawing substituents result in a decrease (*31*, *36*). Lastly, regioselectivity is controlled by electronic effects of substituents. *p*-Benzoquinones with electron-withdrawing ring substituents preferably form adducts ortho to the substituent, while electron donating ring substituents favor adducts para to the substituent (*33*, *37*). The electron-withdrawing or donating properties of ring substituents will also tune pK_a values for a given compound.

2,5-Dihydroxybenzoic acid (XH_2(**III**)), also known as gentisic acid, is an example hydroquinone proelectrophile possessing an electron-withdrawing carboxylic acid substituent. XH_2(**III**) is biosynthesized and by some plants and exuded into the soil near the plant

roots (*38*). Metabolic degradation of carbamate and polycyclic aromatic hydrocarbons can also results in XH_2(**II**) in groundwater (*39*).

Papouchado et al. (*40*, *41*) reported hydroxylation products of EWG substituted hydroquinones that were oxidized electrochemically in an 0.10 M $HClO_4$ medium during cyclic voltammetry. The solvent, H_2O, is the only relevant nucleophile under these conditions because ClO_4^- is a poor nucleophile and the OH^- concentration is 10^{-13} M at this pH. The hydroxylated adduct does become oxidized under their conditions, but they noted that the electron-donating nature of the -OH group in the hydroxylated product prevents further hydroxylation reactions from occurring: no reaction of the 2 nd generation benzoquinone was observed. Under our experimental conditions we expect that hydration products such as those detected by Papouchado and colleagues will be generated along with addition products with nucleophiles intentionall added to experiments. Also, because no second addition product was detected, their results confirm that EDG substituents, in this case $-OH$, decreases electrophilicity of 2 nd generation benzoquinones relative to the 1 st generation.

In our experiments, we employed a $Mn^{III,IV}$ (hydr)oxide as the oxidant to generate benzoquinone electrophiles from hydroquinone proelectrophiles. Phenolic compounds, such as hydroquinone and catechol, have been reported to be oxidized by metal oxides and enzymes present in soil samples (*42*, *43*), including manganese(III,IV) (hydr)oxides (*44–46*). Manganese(III,IV) (hydr)oxides are especially important oxidants in soils and at the oxic/anoxic interface in sediments. Near the oxic/anoxic interface manganese cycles through the +II and +III/+IV oxidation states via abiotic and microbial processes, causing hundreds of redox reactions before ultimate burial (*47*, *48*). Manganese(II) is highly soluble and diffuses to the oxic zone where it is oxidized by microorganisms or O_2 to manganese(III,IV) solids that settle back to the oxic/anoxic zone (*47–53*). Although $Mn^{III,IV}$ (hydr)oxides are thought to be ubiquitous in soils and sediments, they are less abundant in nature than

Fe^{III} oxides (*54*). Despite being less abundant, $Mn^{III,IV}$ (hydr)oxides have higher reduction potentials than Fe^{III} oxides (*54–57*), so they are likely to represent the active oxidant for proelectrophiles such as hydroquinone moieties within NOM.

Synthesized MnO_2(pyrolusite) particles are available to us that contain essentially all Mn^{IV} and no Mn^{III} (*58–61*); reducing this solid will generate one Mn^{II}(aq) for each Mn^{IV} which requires two electrons to be transferred:

$$Mn^{IV}O_2 + 2e^- + 4H^+ \rightleftharpoons Mn^{2+}(aq) + 2H_2O \tag{3.2}$$

Henceforth, we will refer to MnO_2(s, pyrolusite) as MnO_2 for simplicity. We expect MnO_2 will oxidize hydroquinone XH_2 proelectrophiles at pH $<$12 based on thermodynamic considerations. An E_h–pH diagram (Figure S3.2 in the Supporting Information) shows graphically that MnO_2 can oxidize three model hydroquinone proelectrophiles at pH $<$12 but the reduction potential of goethite (Fe^{III}OOH(s) is too low to oxidize hydroquinone proelectrophiles above pH 3.5.

Sulfur, nitrogen, and oxygen atoms are the most common nucleophilic sites within organic compounds. Lone pair electrons residing on these atoms are donated during reaction mechanisms including Michael addition (*62*, *63*). Nucleophilic addition reactions with quinones in conditions representative of aquatic environments have been reported for hydrogen sulfide (*64*), sulfite (*65*), and anilines (*4*, *66–69*). Also, nucleophilic addition reactions between glutathione and *p*-benzoquinone have been studied under physiologic conditions (*27*).

Many nucleophilic organic compounds are oxidizable by MnO_2, including phenolic compounds (*46*) and anilines (*70*). The mechanism shown in Figure 3.1 and Figure 3.2 does not account for oxidative consumption of the nucleophile or reactions of the oxidation

products of the nucleophile. We avoid this complication by carefully selecting model nucleophiles that are not appreciably oxidized under our experimental conditions.

In this study, we conduct kinetic experiments using 4-ethylaniline (An) and 4-methylimidazole (Im) as convenient added nucleophiles. These model nucleophiles are not significantly oxidized under our experimental conditions, they are amenable to analysis by HPLC, and they contain only one potentially nucleophilic atom. Using these model nucleophiles will allow us to compare adduct formation and multiple generations for two different N-donor nucleophiles. An possesses a pK_a of 5.00 (*71*) and serves as a model aromatic amine.

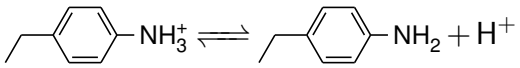

(3.3)

Im serves as a model for histidine and other heterocyclic nitrogen compounds. Im has a pK_a of 7.54 (*71*):

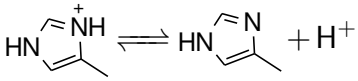

(3.4)

In Chapter 2, An was shown to be a stronger nucleophile than Im in terms of observed reaction rate with *p*-benzoquinone. We saw that the rate constant corrected for the deprotonated species (k_{Nu^-}) was 2.5 times larger for An than for Im. In this chapter, our experiments will also be conducted at pH 7.0 and we expect that An will act as a stronger nucleophile than Im.

Our kinetic studies will focus on the effect of increasing the concentration of proelectrophile or nucleophile. Increasing the concentration of proelectrophile will promote the rate of benzoquinone generation, while increasing the concentration of nucleophile will increase the rate of adduct formation. We can indirectly observe multiple generations by monitoring consumption of proelectrophile (XH_2) and nucleophile (Nu), and generation of Mn^{II}(aq). XH_2 is only consumed when it oxidized to the first generation Z, generating

1 Mn^{II} (Figure 3.1 and Figure 3.2). Additional generation of Mn^{II} indicates oxidation of one the adducts. Nu is only consumed by addition to a benzoquinone. Greater consumption of Nu than XH_2 indicates the formation of diadducts or triaddaucts containing Nu (e.g. X–$(Nu)_2$). Ratios of Nu consumption and Mn^{II} generation to XH_2 consumption over reaction time graphically illustrate this effect.

It should be noted that there are a number of possible side reactions that could occur other than those shown on Figure 3.1 or Figure 3.2. It is likely that not all of the intermediates and products will be stable in solution, especially with an oxidant present: they and may also undergo other decomposition reactions such as ring-opening.

Compounds containing aniline as a functional group are capable of forming imine products via a rapid and reversible reaction 1,2-nucleophilic addition reaction (*66*, *72*):

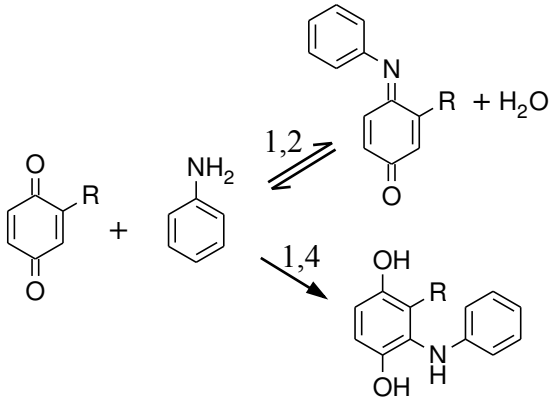

(3.5)

Whether an imine or a Michael type product is favored depends on the electrophilicity of the benzoquinone substrate. In some cases both products are formed: for 4-methylaniline and 2,6-dimethyl-*p*-benzoquinone a 3:1 product ratio of Michael addition product to imine was reported (*72*), while a 3:2 product ratio was reported for benzidine (*73*). We expect that EWG substituted model proelectrophiles will favor Michael-type additions. Any imine products that do form will most likely revert to reactants (*66*) ultimately leading to Michael-type

adducts. In aqueous solutions, the solvent H_2O drives the equilibrium for imine formation (as written in Reaction 3.5) towards the reactants, but H_2O is not involved in the equilibrium for Michael addition.

Radical coupling reactions could also take place in our proelectrophile experiments. Proelectrophile compounds used in this study are phenols (Table 3.1); phenolic compounds are known to undergo oxidative coupling reactions that leads a to a complex array of products (*74*). Anilines can also form radical-coupling products following 1 e^- oxidation (*70*). Whether nucleophilic addition or radical-coupling reactions dominate in our reactions is difficult to discern. Most literature reports support nucleophilic addition because the reported products are consistent with products of a Michael addition pathway, but they have been unable to definitively prove that Michael addition occurs and radical coupling does not (*5*, *16*, *67*, *68*, *75*). We sought to minimize cross-coupling reactions in our experiments by using low concentrations of proelectrophiles and oxidant, anticipating that only extremely low concentration of radicals will be generated. Colarieti et al. (*42*, *43*) observed polymerization caused by oxidants in soil samples when 0.5 g/L (5 mM) of phenol or 5.26 mM and catechol was added to soil samples containing approximately 0.2 g/L (2.3 mM) loading of manganese oxides. In our experiments, the proelectrophile concentration was only 100 μM and never exceeded 1 mM and the loading of MnO_2 was 200 μM. Unfortunately, we are limited in our ability to conclude that only nucleophilic addition occurs and radical addition does not; rather, they more likely occur simultaneously.

In this study we demonstrate that simple experiments consisting of model substituted hydroquinone proelectrophiles and nucleophiles provide evidence of the complex proelectrophile pathway including the generation of multiple addition products and that generating highly reactive electrophiles from electron-withdrawing group bearing proelectrophiles leads to fast rates of nucleophile consumption, despite competition with H_2O and OH^-.

First, we chose a proelectrophile-nucleophile pair to study stoichiometry and kinetics of consumption of the proelectrophile and nucleophile in the presence of MnO_2. Second, we compare four proelectrophiles and two nucleophiles to explore effects of molecular structure on consumption rates and generation of Mn^{II}(aq). Last, we will employ LC/MS to acquire mass spectral evidence of monoadduct formation for nine different nucleophiles with an EWG substituted hydroquinone proelectrophile. By using simple model compounds that represent nucleophilic contaminants and potential binding sites in NOM, we hope to show that electrophiles generated in-situ by oxidation in real soils and sediments may represent an important sink for nucleophilic contaminants.

3.2 Materials and Methods

All aqueous solutions were prepared from reagent grade chemicals and distilled, deionized water (Milli-Q water, 18 MΩ-cm resistivity, Millipore Corp., Milford, MA). All bottles and glassware were rinsed with distilled water, soaked in 5 M nitric acid overnight, rinsed with distilled water and Milli-Q water and then air-dried.

3.2.1 Chemicals

3-(N-Morpholino)propanesulfonic acid (MOPS) and ascorbic acid were purchased from Sigma (St. Louis, MO). 2,5-Dihydroxyterephthalic acid (XH_2(**IV**)), 4-ethylaniline, 4-methylimidazole, 4-aminophenol, L-glutathione, 2-aminobenzyl alcohol, 4-chloroaniline, and 4-nitrophenol were purchased from Aldrich (St. Louis, MO). 4-Nitroaniline was purchased from Alfa Aesar (Pelham, NH). 2′,5′-Dihydroxyacetophenone (XH_2(**II**)), 4-hydroxyphenylacetone and methyl 4-hydroxybenzoate were purchased from TCI America (Portland, OR). NaCl was purchased from Acros Organics (Fair Lawn, NJ). Manganese

atomic absorption standard solution and HPLC and LC/MS Optima grade methanol were purchased from Fisher Scientific (Pittsburgh, PA). 2,5-Dihydroxybenzoic acid (XH_2(**III**)), hydroquinone (XH_2(**I**)), L-cysteine, 2-mercaptoethanol, and ammonium acetate were purchased from Fluka (Buchs, Switzerland). NaOH and acetic acid were purchased from J. T. Baker (Phillipsburg, NJ).

Previously synthesized MnO_2 particles were available for the present work (*58–61*). D-spacings determined using selected area electron diffraction coincided with values reported in the literature for the mineral pyrolusite. The average oxidation state of Mn in the particles was determined to be $+3.98$ by iodometric titration: the Mn in the particles is 98% Mn^{IV} and 2% Mn^{III} (*60*).

3.2.2 Experimental Design

Experiments were conducted in 100 mL polypropylene bottles placed in a constant temperature water bath held at $25 \pm 1°C$ and continuously stirred with Teflon coated stir bars. Sufficient stock solution of MOPS buffer, NaCl, proelectrophile, and nucleophile were added to achieve a total volume of 100 mL and 5 mM MOPS, 10 mM NaCl concentration. Initial concentration of proelectrophile and nucleophile varied between 0 and 1000 μM. To minimize dissolved oxygen, solutions were continuously sparged with N_2(g). HCl and NaOH were added to adjust the pH to 7.0. Solutions were allowed to equilibrate for 30 min. Reaction was initiated by the pipetting a small volume ($<$1 mL) of well mixed 0.22 M MnO_2 stock slurry that was available in our laboratory. In tests lacking MnO_2 only negligible decrease of any proelectrophile or nucleophile concentration was observed within the time scale of our experiments. Following addition of MnO_2, 5 mL samples were periodically withdrawn by syringe and filtered through 0.2 μm track-etch polycarbonate filter membrane

syringe filters (Whatman, UK). Filtration quenches any reaction caused by MnO_2 particles. No other attempt was made to quench reactions in the samples. Filter quenched samples gave the same HPLC, LC/MS and AAS results when analyzed immediately and after 2 days of storage.

Control experiments lacking a proelectrophile were performed for ten nucleophiles. The initial concentration of nucleophile was 100 μM and MnO_2 was spiked to 200 μM concentration in 5 mM MOPS buffer adjusted to pH 7.0 and 10 mM NaCl. After 1 hr, samples were filtered and analyzed for dissolved Mn using flame atomic absorption spectrometry and nucleophile concentration using LC/MS. No significant concentration of dissolved Mn was detected, and no significant change in nucleophile concentration was observed.

3.2.3 Instrumentation and Analysis

Our experiments were performed in the absence of chelating agents, hence dissolved concentrations of Mn^{III} and Mn^{IV} can be assumed to be negligible. Dissolved Mn, measured using flame atomic absorption spectrophotometry (FAAS, AA Analyst 100, Perkin-Elmer, Norwalk, CT), is assumed to consist entirely of Mn^{II}. Any Mn^{2+} adsorped to the MnO_2 particles removed via filtration would not have been detected. The limit of detection (LOD) for FAAS was calculated using the regression residual standard deviation ($S_{y/x}$)

$$\text{LOD} = 3.3\frac{S_{y/x}}{m} \tag{3.6}$$

where m is the slope of the calibration curve (*76–78*).

4-Ethylaniline, 4-methylimidazole and acetylhydroquinone (XH_2(**II**)) concentrations were monitored by an HPLC system (Waters, Milford, MA) using a UV absorbance detection at 230 nm. Run conditions were isocratic using 70% 5 mM ammonium acetate and 30%

methanol as the eluent at a flow rate of 1 mL min^{-1}. Separation was achieved using a μBondapak 5μm 3.6 × 300 mm column (Waters, Milford, MA). Acetyl-*p*-benzoquinone, Z(**II**), was not detected using this method.

LC/MS with electrospray ionization was used to detect addition products in experiments where 2,5-dihydroxybenzoic acid (XH_2III) served as the proelectrophile. LC separation was conducted using a Waters 2795 separation module (Milford, MA) with a 4.6 x 100 mm, 5 μm particle size, Atlantis T3 column (Waters, Milford, MA) run in isocratic mode with 70% 5 mM ammonium acetate and 30% methanol eluent at a flow rate of 200 μL min^{-1}. Adducts were identified based on their molecular ion ($[M-H]^-$) and any detected fragments, typically $[M-COOH]^-$.

Initial rates were calculated for experiments with acetylhydroquinone, 4-ethylaniline, and MnO_2. Initial rates were determined by applying linear regression to XH_2(**II**), 4-ethylaniline, and Mn^{II}(aq) versus time data for the first 4 data points. All data points used in regression were taken within 10 minutes of the start of the reaction. The slope obtained by regression corresponds to initial rate of consumption for nucleophile or proelectrophile or generation of Mn^{II} (r_0 in units of μM min^{-1}). Linear regression analysis yielded correlation coefficients (r^2) that were greater than 0.8, with the exception of one experiment with 500 μM initial concentration of 4-ethylaniline. The time course data and best-fit lines are shown in the Supporting Information (Figure S3.4 and Figure S3.5).

3.3 Results and Discussion

3.3.1 Proelectrophile Experiments with Acetylhydroquinone, 4-Ethylaniline, and MnO_2

We chose test nucleophiles that were not significantly oxidized by MnO_2 under the conditions and timescales of our experiments. We chose nucleophiles that yielded Mn^{II}(aq) below the detection limit (3 μM) after one hour of contact time with MnO_2. Our final set of nucleophiles includes substituted phenols, anilines, and 4-methylimidazole (Table S3.1). Nucleophiles containing thiol groups are quickly oxidized by MnO_2 and were not used in any further experiments.

In one series of kinetic and stoichiometric experiments acetylhydroquinone (XH_2(**II**), Table 3.1) served as the test proelectrophile and 4-ethylaniline (An) served as the test nucleophile. Oxidation of aniline and related compounds by $Mn^{III,IV}$ (hydr)oxide minerals, such as MnO_2, has been reported (*70*). Under the conditions and timescale of our experiments, no Mn^{II} was detected in slurries containing An and MnO_2 (Table S3.1). We chose XH_2(**II**) as the proelectrophile because the acetyl group (–C(=O)CH_3) has similar electron-withdrawing properties as a carboxyl group, which are believed to be highly prevalent in NOM. The Hammett constant, σ_p, is a way to quantify electron withdrawing properties of a substituent group. For a carboxylic acid (–C(=O)OH) σ_p is close to σ_p for the acetyl group: +0.45 and +0.5, respectively *79*). Also, the carboxyl group in XH_2(**III**) imparts a negative charge at pH 7, but XH_2(**II**) is neutral at that pH avoiding electrostatic affects related to charge. In experimental solutions lacking MnO_2 no change in XH_2(**II**) or An concentration was observed within 2 hours. Also, no change in XH_2(**II**) concentration was observed in buffered

solutions lacking MnO_2 and An. Similarly, no change in An concentration was observed in buffered solutions lacking MnO_2 and XH_2(**II**).

An example time course is shown in Figure 3.3A where the initial concentrations were 225 μM XH_2(**II**), 100 μM An, and the MnO_2 loading was 200 μM in 5 mM MOPS buffer (pH 7.0) and 10 mM NaCl. Under these conditions the Mn^{II}(aq) concentration exceeded 130 μM after 90 min. XH_2(**II**) and An were not completely consumed, their concentrations approached 30 μM and 15 μM, respectively.

The ratios of Mn^{II} generated to XH_2(**II**) consumed and An consumed to XH_2(**II**) consumed give insight into what reactions occur following the oxidation of XH_2(**II**) to the benzoquinone (Z) form, on a per XH_2(**II**) oxidized basis (Figure 3.3B). The ratio of Mn^{II}(aq) generated to XH_2(**II**) consumed (R_A) reflects the number of oxidation steps the proelectrophile undergoes, on average.

$$R_A = \frac{Mn^{II}(aq)\text{ generated}}{XH_2(\mathbf{II})\text{ consumed}} = \frac{Mn^{II}(aq)}{[XH_2(\mathbf{II})]_0 - [XH_2(\mathbf{II})]} \tag{3.7}$$

This ratio would be equal to 1 if the proelectrophile was only oxidized once because of the one-to-one stoichiometry of MnO_2 oxidation of hydroquinones. R_A greater than 1 imply that adducts are becoming oxidized, consuming more MnO_2 and generating more Mn^{II}. Note that R_A would be confounded by adsorption of Mn^{II}: the observed values would be too low. The ratio of An consumed to XH_2(**II**) consumed (R_B) gives the average number of An molecules that reacted with the Z form of XH_2(**II**), because An is only consumed by forming adducts with Z.

$$R_B = \frac{\text{An consumed}}{XH_2(\mathbf{II})\text{ consumed}} = \frac{[An]_0 - [An]}{[XH_2(\mathbf{II})]_0 - [XH_2(\mathbf{II})]} \tag{3.8}$$

If R_B is equal to 1, then one Z reacted with one An, presumably leading to a monoadduct. If R_B is less than 1, we expect that some of Z reacted with H_2O or OH^- to form hydration products. R_B greater than 1 suggests that diadducts were formed. Note that if the oxidized form or Z persists in solution the ratio would be lower than expected.

In Figure 3.3B, R_A approaches 1.4, while R_B approaches 0.5. Both ratios are approximately 0.75 at the onset of reaction and stop changing significantly after 30 min.

The ratios shown in Figure 3.3B change depending on the concentration of An and XH_2(**II**) (Figure 3.4). R_B increases with increasing concentration of An, but was relatively constant with time. In Figure 3.4A, the concentration of An is increased from 50 to 1000 μM, the concentration of XH_2(**II**) was 100 μM, and the MnO_2 loading was 200 μM. When An was 50 μM (half the concentration of XH_2(**II**)) the ratio was close to 0.5. The remaining 50 μM of Z(**II**) that is generated most likely reacts with OH^- or H_2O to form hydration products. When An was 100 μM, R_B starts at 1, but decreases over time. As An is consumed hydration becomes more favorable and R_B decreases. At higher An concentrations R_B was consistently higher than 1. High concentrations of An will favor formation of the adducts over hydration products and should promote the formation of diadducts.

R_A exceeded 1 for all concentrations of An (Figure 3.4B). The ratio of Mn^{II} generated to XH_2 consumed reflects the number of generations of benzoquinones (Z) that are formed via oxidation. Using our $Mn^{IV}O_2$ pyrolusite, R_A would not exceed 1.0 if only a first generation formed. Even in the absence of An, R_A was higher than 1 after 10 min, suggesting that the Z form reacts with H_2O or OH^- forming the hydration product (hydroxylated acetylhydroquinone). The hydration product is oxidized leading to a second generation benzoquinone, a second Mn^{II}, and a larger Mn^{II} to XH_2 ratio. When An is present, R_A increases with increasing concentration of An. In other words, more Mn^{II} is generated when 4-ethylaniline forms an addition product with acetyl benzoquinone than when only hydration

occurs. An did not reduce MnO_2 in experiments lacking XH_2, but oxidation of An in these experimental slurries would increase the observed concentration of Mn^{II}(aq) and increase R_A.

R_A represents oxidation steps and R_B represents An addition steps that occur following oxidation of XH_2(**II**) by MnO_2 (on average). Increasing $[Nu]_0$ increases both ratios, evidence that the formation of second-generation benzoquinones and diadducts is promoted (Figure 3.4). Forming an adduct with An could promote subsequent oxidation and addition reactions because the redox properties of the monoadduct (X-Nu) differ from the parent XH_2(**II**) and likely also differ from the hydration product (X-OH). In the monoadduct, An is a substituent of the aromatic ring (replacing a hydrogen in XH_2(**II**)). In the hydration product, a hydrogen in XH_2(**II**) has been replaced with a hydroxyl group. An and hydroxyl groups should both be electron-donating groups (EDG) which would give X-Nu a lower reduction potential than XH_2(**II**), making it more easily oxidized. Recall that Hammett constants are a way to quantify electronic influence of substituents. For a hydroxyl group the Hammett substituent constant, σ_p, is -0.37 (*80*). Although we could not locate a σ_p that would represent An as a substituent, the σ_p for the somewhat similar $-NHCH_3$ group is -0.7 (*80*). A $-NHCH_3$ substituted addition product should be approximately twice as easily oxidized as the –OH substituted hydration product assuming that the Hammett relationship is linear for this reaction. The second-generation addition products (diadducts) have another An or –OH substituent furthering lowering their reduction potential. When the concentration of An is increased the formation of X-Nu will be favored over X-OH, favoring more the more easily oxidizable products which could lead to further oxidation by MnO_2.

Initial rates for consumption of An and XH_2(**II**) and generation of Mn^{II}(aq) increased when the concentration of XH_2(**II**) was increased from 0 to 1000 μM and the concentration of An was 100 μM (Figure 3.5A). The rate of generation of Mn^{II} is similar to the rate

of consumption of XH_2(**II**) at $[XH_2(\mathbf{II})]_0$ lower than 250 μM. At $[XH_2(\mathbf{II})]_0$ greater than 500 μM, generation of Mn^{II} is faster than consumption of XH_2(**II**).

At low $[XH_2(\mathbf{II})]_0$ Mn^{II} might be generated only from oxidation of XH_2(**II**). At higher $[XH_2(\mathbf{II})]_0$, oxidation of adducts would lead to more Mn^{II} being generated than XH_2 being consumed.

The consumption rate of An is tied to the rate of XH_2 oxidation because the reaction of An with Z can only occur after oxidation. However, the rate consumption of An is consistently slower than the rate of consumption of XH_2(**II**) and generation of Mn^{II} (Figure 3.5A). An competes with H_2O or OH^- to react with available Z. The concentration of An is 100 μM in Figure 3.5A which will also limit the increase in rate of consumption of An.

When the concentration of An was increased from 0 to 1000 μM and the concentration of XH_2(**II**) was 100 μM, the initial rate of consumption of XH_2(**II**) and generation of Mn^{II} did not depend on the concentration of An, but the initial rate of consumption of An did increase nonlinearly (Figure 3.5B).

There may be several explanations for the limited increase in rate of consumption of An with increasing $[An]_0$. Consumption of An could be limited by available surface sites; however, the rate of consumption of XH_2(**II**) should decrease with increasing $[An]_0$ as surface sites become occupied by An unless adsorption of An does not affect adsorption of XH_2(**II**). The generation of Mn^{II} and consumption of XH_2(**II**) did not depend on $[An]_0$, suggesting that the amount of Z available may have limited the rate of consumption of An. At low $[An]_0$, An competes with H_2O/OH^- to react with Z and the rate of consumption of An increases with $[An]_0$. At high $[An]_0$ all Z the rate of consumption of An is limited by the rate of generation of Z.

3.3.2 Influence of Proelectrophile and Nucleophile Structure

Time course data for proelectrophile experiments employing 160 μM 4-ethylaniline (An) or 4-methylimidazole (Im) as the nucleophile are shown in Figure 3.6. Reaction slurries contained 100 μM of a single proelectrophile (shown in Table 3.1) and 200 μM MnO_2 in 10 mM NaCl and 5 mM MOPS adjusted to pH 7. After 90 min of contact time, total An consumed depended on proelectrophile identity: XH_2(**III**) >XH_2(**I**) >XH_2(**II**) >XH_2(**IV**) (Figure 3.6A). When Im was the nucleophile the order was XH_2(**III**) >XH_2(**II**) >XH_2(**IV**) >XH_2(**I**) (Figure 3.6B). Regardless of proelectrophile identity consumption of An was greater than Im after 90 min. Note that no reaction was observed between any of the proelectrophiles and either nucleophile in the absence of MnO_2.

Protonation state could explain the greater consumption of An than Im (Figure 3.6): the pK_a of Im is 7.54 and the pK_a of An is 5.00 (*71*). Thus, at pH 7.0, 77% of Im is protonated while only 1% of An is protonated. Protonation blocks nucleophilic attack by occupying the lone-pair electrons on atom of the nucleophile that would donate those electrons during nucleophilic attack.

For both An and Im, we observed the greatest consumption of nucleophile when XH_2(**III**) was the proelectrophile (Figure 3.6A and B) and the least with XH_2(**I**). Z(**I**) lacks an electron-withdrawing substituent and should be the least electrophilic among the four benzoquinones. The electron-withdrawing carboxylic acid substituent on Z(**III**) leads to the greater consumption of nucleophile.

More An was consumed when the proelectrophile was XH_2(**III**) than when it was XH_2(**II**). As mentioned previously, the Hammett constant, σ_p, is +0.45 for a carboxylic acid (–C(=O)OH), and +0.5 for a acetyl group (–C(=O)CH_3): acetyl groups should be slightly more electron withdrawing than carboxylic acids (*79*). However, at pH 7 carboxylic

acid groups would be deprotonated and σ_p is only +0.11 for carboxylate (–C(=O)O$^-$). At pH 7, Z(**III**) would be significantly less electrophilic than Z(**II**). Figure 3.6C shows less Mn^{II}(aq) was generated with XH_2(**II**) than XH_2(**III**): less Z(**II**) was generated than Z(**III**). The consumption of nucleophile will depend on both the concentration of Z and the rate constant for nucleophilic attack. In this case, even though we expect Z(**II**) to be more electrophilic than Z(**III**), less generation of Z(**II**) from XH_2(**II**) ultimately lead to less consumption of An.

Similarly, less Mn^{II} was generated when XH_2(**IV**) was the proelectrophile than for XH_2(**II**) (Figure 3.6C), but more An was consumed after 90 min (Figure 3.6A). Electronic effects of proelectrophile substituents influence both the rate of oxidation of the XH_2 form and the rate of nucleophilic addition to the Z form. Both rates will influence the extent of nucleophile consumption: XH_2(**IV**) is more difficult to oxidize than XH_2(**II**), but the corresponding Z form should be a stronger electrophile.

With XH_2(**I**), the least An and Im was consumed, and Mn^{II} increased quickly but plateaued near 100 μM within 15 min (Figure 3.6C and D). If all 100 μM of XH_2(**I**) were consumed, 100 μM Mn^{II} would be generated if only the parent proelectrophile was oxidized and not for any addition or hydration products. Mn^{II} approached 100 μM for both An amd Im when XH_2(**I**) or XH_2(**IV**) served as the proelectrophile. With XH_2(**III**) and An Mn^{II} exceeded 100 μM, but not with XH_2(**III**) and Im. The 100 μM limit was exceeded for both nucleophiles when XH_2(**II**) was the proelectrophile.

In the case of An and XH_2(**I**), 50 μM of An is consumed, presumably forming addition products with the generated *p*-benzoquinone (Figure 3.6A). However, the addition and hydration products have not been further oxidized, which would have lead to Mn^{II} concentration in excess of the 100 μM limit. For XH_2(**IV**), the 100 μM Mn^{II} limit was not exceeded within 90 min for either nucleophile (Figure 3.6C and D). Because it contains two electron-

withdrawing carboxylic acid functional groups, 2,5-dihydroxyterephthalic acid, XH_2(**IV**), should be the most difficult of these proelectrophiles to oxidize; accordingly, 160 μM of An or Im had no appreciable affect on oxidation rate. For XH_2(**II**), the 100 μM Mn^{II} limit was exceeded within 30 min. Similar results for XH_2(**II**) are obtained in the absence of an added nucleophile. Oxidation of XH_2(**III**) in the presence of Im quickly approached the limit, but did not exceed it. This was also observed in the absence of nucleophile. In contrast, the 100 μM Mn^{II} limit was quickly exceeded when An was present. It is difficult to tell why the presence of Im limited the amount of Mn^{II} that was generated (Figure 3.6D) but An did not (Figure 3.6C). Perhaps the lower reduction potential, and thus increased oxidizability, of an An adduct over XH_2(**III**) lead to further reduction of MnO_2. Im did not form adducts as well as An, so there were no adducts to reduce any available MnO_2.

It is important to note that under conditions where MnO_2 is not completely reduced to Mn^{II} the fraction that is adsorped to MnO_2 particles would not be detected. However, our results still show that hydroquinone proelectrophiles act as more than two equivalent reductant via multiple generations of adducts. Oxidation of hydroquinone proelectrophiles to benzoquinone electrophiles requires two electron transfer. Reduction of MnO_2 to Mn^{II} also requires two electron transfer because our MnO_2 particles contain almost entirely Mn^{IV}. The balanced redox reaction is:

$$MnO_2(s) + XH_2(aq) + 2H^+ \rightleftharpoons Mn^{II}(aq) + Z(aq) + 2H_2O \qquad (3.9)$$

Thus if XH_2 could only be a two-equivalent reductant, the maximum amount of Mn^{II} that could be generated would be equal to the initial concentration of XH_2 or loading of MnO_2, whichever is smaller. However, this threshold is exceeded in many of our experimental results (for example, Figure 3.6). If the measured concentrations of Mn^{II} are too small

because of adsorption the number of generations observed would increase, but our conclusion that multiple generations occur is unchanged.

3.3.3 LC/MS Evidence of Monoadducts

We obtained mass spectral evidence for nine monoadducts using LC/MS with XH_2(**III**) as the proelectrophile. Figure 3.7 shows two example spectra taken after 12 hours of contact time from separate reaction slurries with 50 μM XH_2(**III**) as the proelectrophile, 100 μM 4-hydroxybenzoate as the nucleophile, 220 μM MnO_2 in 10 mM NaCl and 5 mM MOPS buffer adjusted to pH 7.0. Negative mode electrospray LC/MS requires analytes to have an ionizable functional group that becomes negatively charged during the electrospray process (*81*). Because XH_2(**III**) has a carboxylic acid group, the products X-Nu and X-OH are amenable to LC/MS detection regardless of the identity of the nucleophile. Figure 3.7A shows the total ion count chromatogram for an experiment where 4-hydroxybenzoate was the nucleophile. Peaks are observed for XH_2(**III**), X-OH, X-Nu, and 4-hydroxybenzoate. The phenolic hydroxy group in methyl 4-hydroxybenzoate is sufficiently ionizable to allow LC/MS detection. The monoadduct could be one of three isomers depending on which ring hydrogen is replaced by the nucleophile. Unfortunately, it is not possible to discern which monoadduct isomer is formed to because mass spectrometry typically cannot discern isomers, especially when peak detection is limited to molecular ion and a single fragment. Electrospray typically does not generate many fragments. Unfortunately, authentic standards are not available for these compounds, and quantification of adducts was not possible.

Negative mode electrospray ionization mass spectrometry gives a signal corresponding to the molecular weight of anionic fragments. For monoadducts of methyl 4-hydroxybenzoate the deprotonated anion, $[M\text{-}H]^-$, and an anion resulting from loss of a carboxyl group,

[M-COOH]$^-$, were detected (Figure 3.7). (M represents the mass of the total molecular structure.) For methyl 4-hydroxybenzoate, a third anion resulting from loss of a methoxy group, [M-OCH_3]$^-$, was also observed (Figure 3.7A). Note that mass spectra are reported as mass to charge ratio (m/z), under our LC/MS conditions the charge is always -1, so the m/z is equal to the molecular weight of the fragment.

Nucleophile and monoadduct structures are shown in Table 3.2, along with m/z of identifying fragments. [M-H]$^-$ and [M-COOH]$^-$ fragments were detected for all observed adducts, except when *para*-aminophenol was the nucleophile. Mass spectra are shown in the supporting information (Figure S3.7). Only one of the three possible isomers is shown in Table 3.2. A peak with an m/z of 169, corresponding to the hydration product, was also observed (Figure 3.7A). We did not obtain any mass spectral evidence for diadducts.

Prior researchers have focused on anilines for their environmental significance (*4*, *13*, *14*, *24*, *67*, *82*). Also, we observed monoadducts for four para-substituted anilines with our model proelectrophile XH_2(**III**), supporting the conclusion that anilines could be removed by addition reactions to electrophilic sites in natural organic matter (NOM) generated by oxidation (Table 3.2). We observed a monoadduct with 4-methylimidazole, a N-heterocycle. Previously, it was reported that the N-heterocycle pyridine did not bind irreversibly to sediment samples (*13*). Our data suggests that perhaps irreversible binding might have been observed if an oxidant had been added to (or present in) the soil samples.

Despite the slow rate of addition of phenols to *p*-benzoquinone at pH 7.0 (Table 2.1), we detected monoadducts of three phenolic nucleophiles with XH_2(**III**) as the proelectrophile (Table 3.2). Nucleophilic reactions of phenolic compounds have received less attention in the literature than anilines. This observation could have implications for the environmental behavior of phenolic compounds, given the ubiquity of both manganese (hydr)oxides in soils and sediments and phenolic functional groups in NOM, natural compounds and synthetic

compounds. Perhaps this is another mechanism that could explain phenolic coupling reactions. Phenols (*42*) and catechols (*43*) oxidized by metal oxides and enzymes present in soil samples polymerize when the phenol or catechol is in excess. This is usually attributed to fast radical coupling reactions, but a proelectrophile pathway could also be active. Whether the radical coupling or addition pathway dominates will depend on the competitive reactions of the phenoxy radical formed by one electron oxidation. Because radicals are so reactive, the unpaired electron will be either quickly donated to another phenol via a cross-coupling reaction or lost to oxidation. In the case of hydroquinone, catechol and other 1,2- or 1,4-dihydroxybenzenes, losing the second electron to oxidation generates an electrophilic benzoquinone. Once the electrophilic form is generated it can react with phenolic nucleophiles leading to Michael addition products. Ultimately, reaction conditions control the dominant pathway: excess phenol or catechol favors donating the unpaired electron in radical reactions, while excess oxidant favors losing the electron via oxidation.

3.4 Conclusions

We explored the proelectrophile pathway by employing simple substituted hydroquinone proelectrophiles and nucleophiles as model compounds using MnO_2 as an oxidant. We used 4-ethylaniline (An) and 4-methylimidazole (Im) as model nucleophiles because they are not oxidized significantly by MnO_2 under the conditions of our experiments and represent some key nitrogen-containing functional groups in organic contaminants and biologically relevant compounds. Experiments investigating reaction stoichiometry of proelectrophile experiments with An and acetylhydroquinone (XH_2(**II**)) show that increasing An increases the fraction of Z(**II**) that undergoes nucleophilic addition of An instead of hydration and

increase the likelihood that di or triadducts are generated. Lastly, using LC/MS we were able to acquire mass spectral evidence of monoadducts formed between MnO_2 oxidized XH_2(**III**) and nine nucleophiles, including ones we previously found to react very slowly with *p*-benzoquinone.

Hydroquinone functional groups within NOM could be capable of acting as proelectrophiles when an oxidant is available, such as $Mn^{III,IV}$ (hydr)oxides. These groups would be particularly electrophilic when bonded to electron-withdrawing carboxylic acid functional groups. The prevalence of hydration versus nucleophile addition product as well as the formation of multiple addition products depends on reaction conditions. Higher concentrations of added nucleophiles favors Michael addition over hydration and promotes the generation of multiple addition products.

Acknowledgments

The authors thank Dr. Zhi Shi for synthesizing the MnO_2(s,pyrolusite) particles used in this project.

References

(1) T. J. Holmes, V. John, J. Vennerstrom, K. E. Choi. Solution characterization of carboxybenzoquinone and the isolation of derived quinhydrones. *The Journal of Organic Chemistry* **1984**, *49*, 4736–4738.

(2) M. Uchimiya, A. T. Stone. Aqueous oxidation of substituted dihydroxybenzenes by substituted benzoquinones. *Environmental Science and Technology* **2006**, *40*, 3515–3521.

(3) M. Uchimiya, A. T. Stone. Reversible redox chemistry of quinones: Impact on biogeochemical cycles. *Chemosphere* **2009**, *77*, 451–458.

(4) H. M. Bialk, A. J. Simpson, J. A. Pedersen. Cross-Coupling of Sulfonamide Antimicrobial Agents with Model Humic Constituents. *Environmental Science and Technology* **2005**, *39*, 4463–4473.

(5) H. M. Bialk, C. Hedman, A. Castillo, J. A. Pedersen. Laccase-mediated Michael addition of ^{15}N-sulfapyridine to a model humic constituent. *Environmental Science and Technology* **2007**, *41*, 3593–3600.

(6) A. Gulkowska, M. Sander, J. Hollender, M. Krauss. Covalent Binding of Sulfamethazine to Natural and Synthetic Humic Acids: Assessing Laccase Catalysis and Covalent Bond Stability. *Environmental Science and Technology* **2013**, 130226141339002.

(7) H. Beiginejad, D. Nematollahi, F. Varmaghani, M. Bayat. Efficient Factors on the Hydrolysis Reaction Rate of Some Para-Aminophenol Derivatives in Acidic pHs. *Journal of the Electrochemical Society* **2013**, *160*, H469–H473.

(8) L. Papouchado, G. Petrie, J. H. Sharp, R. N. Adams. Anodic hydroxylation of aromatic compounds [8]. *The Journal of the American Chemical Society* **1968**, *90*, 5620–5621.

(9) R. Sutton, G. Sposito. Molecular structure in soil humic substances: The new view. *Environmental Science and Technology* **2005**, *39*, 9009–9015.

(10) Z. Struyk, G. Sposito. Redox properties of standard humic acids. *Geoderma* **2001**, *102*, 329–346.

(11) J. Nurmi, P. G. Tratnyek. Electrochemical properties of natural organic matter (NOM), fractions of NOM, and model biogeochemical electron shuttles. *Environmental Science and Technology* **2002**, *36*, 617–624.

(12) N. Ratasuk, M. A. Nanny. Characterization and quantification of reversible redox sites in humic substances. *Environmental Science and Technology* **2007**, *41*, 7844–7850.

(13) E. J. Weber, D. Colon, G. Baughman. Sediment-associated reactions of aromatic amines. 1. Elucidation of sorption mechanisms. *Environmental Science and Technology* **2001**, *35*, 2470–2475.

(14) K. A. Thorn, P. Pettigrew, W. S. Goldenberg, E. J. Weber. Covalent binding of aniline to humic substances. 2. ^{15}N NMR studies of nucleophilic addition reactions. *Environmental Science and Technology* **1996**, *30*, 2764–2775.

(15) K. A. Thorn, W. S. Goldenberg, S. Younger, E. J. Weber, *Covalent binding of aniline to humic substances. Comparison of nucleophilic addition, enzyme-, and metal-catalyzed reactions by ^{15}N NMR* in *Humic and Fulvic Acids: Isolation, Structure and Environmental Role*, J. S. Gaffney, N. A. Marley, S. B. Clark (Eds.), American Chemical Society, Washington, DC, **1996**, pp. 299–326.

(16) E. J. Weber, D. L. Spidle, K. A. Thorn. Covalent binding of aniline to humic substances. 1. Kinetic studies. *Environmental Science and Technology* **1996**, *30*, 2755–2763.

(17) H. M. Bialk, J. A. Pedersen. NMR investigation of enzymatic coupling of sulfonamide antimicrobials with humic substances. *Environmental Science and Technology* **2008**, *42*, 106–112.

(18) A. Saxena, R. Bartha. Binding of 3,4-Dichloroaniline By Humic-Acid and Soil - Mechanism and Exchangeability. *Soil Science* **1983**, *136*, 111–116.

(19) T. S. Hsu, R. Bartha. Hydrolyzable and nonhydrolyzable 3,4-dichloroaniline-humus complexes and their respective rates of biodegradation - Journal of Agricultural and Food Chemistry (ACS Publications). *Journal of Agricultural and Food Chemistry* **1976**.

(20) T. S. Hsu, R. Bartha. Interaction of Pesticide-Derived Chloroaniline Residues with Soil Organic-Matter. *Soil Science* **1973**, *116*, 444–452.

(21) A. Saxena, R. Bartha. Modeling of the covalent attachment of chloroaniline residues to quinoidal sites of soil humus. *Bulletin Of Environmental Contamination And Toxicology* **1983**, *30*, 485–491.

(22) B. Gevao, K. Semple, K. Jones. Bound pesticide residues in soils: A review. *Environmental Pollution* **2000**, *108*, 3–14.

(23) H. Li, L. Lee. Sorption and abiotic transformation of aniline and α-naphthylamine by surface soils. *Environmental Science and Technology* **1999**, *33*, 1864–1870.

(24) H. Li, L. Lee, D. Schulze, C. A. Guest. Role of soil manganese in the oxidation of aromatic amines. *Environmental Science and Technology* **2003**, *37*, 2686–2693.

(25) H. Li, L. Lee, C. T. Jafvert, J. G. Graveel. Effect of substitution on irreversible binding and transformation of aromatic amines with soils in aqueous systems. *Environmental Science and Technology* **2000**, *34*, 3674–3680.

(26) A. Kutyrev. Nucleophilic reactions of quinones. *Russian Chemical Reviews* **1991**, *60*, 72–88.

(27) S. S. Lau, B. A. Hill, R. J. Highet, T. J. Monks. Sequential oxidation and glutathione addition to 1,4-benzoquinone: Correlation of toxicity with increased glutathione substitution. *Molecular Pharmacology* **1988**, *34*, 829–836.

(28) T. J. Monks, S. S. Lau, R. J. Highet, J. R. Gillette. Glutathione conjugates of 2-bromohydroquinone are nephrotoxic. *Drug Metabolism and Disposition* **1985**, *13*, 553–559.

(29) T. Monks, R. Hanzlik, G. Cohen, D. Ross, D. Graham. Quinone chemistry and toxicity. *Toxicology and Applied Pharmacology* **1992**, *112*, 2–16.

(30) L. Fotouhi, S. Asadi, E. Tammari, M. M. Heravi, D. Nematollahi. Electrochemical oxidation of catechol and 4-tert-butylcatechol in the presence of 1-methyl-1h-imidazole-2-thiol: synthesis and kinetic study. *Journal Of The Iranian Chemical Society* **2008**, *5*, 712–717.

(31) L. Fotouhi, E. Tammari, S. Asadi, M. M. Heravi, D. Nematollahi. Estimation of Heterogeneous Rate Constants of Reaction of Electrochemically Generated o-Benzoquinones with Various Nucleophiles Containing Thiol Group. *International Journal Of Chemical Kinetics* **2009**, *41*, 426–431.

(32) D. Nematollahi, A. Ariapad, M. Rafiee. Electrochemical nitration of catechols: Kinetic study by digital simulation of cyclic voltammograms. *Journal of Electroanalytical Chemistry* **2007**, *602*, 37–42.

(33) H. Beiginejad, D. Nematollahi, F. Varmaghani, M. Bayat, H. Salehzadeh. Efficient Factors on the Reaction Rate and Site-Selectivity in Sulfonylation of Catechol and Hydroquinone Derivatives: Experimental and Theoretical Studies. *Journal of the Electrochemical Society* **2013**, *160*, G3001–G3007.

(34) E. Pelizzetti, E. Mentasti, C. Baiocchi. Kinetics and mechanism of oxidation of quinols by hexachloroiridate(IV) in aqueous acidic perchlorate media. *Journal of Physical Chemistry* **1976**, *80*, 2979–2982.

(35) W. M. Clark, *Oxidation-Reduction Potentials of Organic Systems*, Williams & Wilkins, Baltimore, MD, **1960**.

(36) D. Nematollahi, B. Dadpou. Electrochemical pyridination of hydroquinone in aqueous solution. *Monatshefte Fur Chemie* **2011**, *142*, 1235–1239.

(37) M. D. Rozeboom, I. M. Tegmo-Larsson, K. N. Houk. Frontier molecular orbital theory of substitutent effects on regioselectivities of nucleophilic additions and cycloadditions to benzoquinones and naphthoquinones. *The Journal of Organic Chemistry* **1981**, *46*, 2338–2345.

(38) L. A. Griffiths. On The Distribution of Gentisic Acid in Green Plants. *Journal Of Experimental Botany* **1959**, *10*, 437–442.

(39) K. Hanna, B. Rusch, L. Lassabatere, A. Hofmann, B. Humbert. Reactive transport of gentisic acid in a hematite-coated sand column: Experimental study and modeling. *Geochimica et Cosmochimica Acta* **2010**, *74*, 3351–3366.

(40) L. Papouchado, G. Petrie, R. N. Adams. Anodic oxidation pathways of phenolic compounds. Part I. Anodic hydroxylation reactions. *Journal of Electroanalytical Chemistry* **1972**, *38*, 389–395.

(41) L. Papouchado, R. W. Sandford, G. Petrie, R. N. Adams. Anodic oxidation pathways of phenolic compounds Part 2. Stepwise electron transfers and coupled hydroxylations. *Journal of Electroanalytical Chemistry* **1975**, *65*, 275–284.

(42) M. L. Colarieti, G. Toscano, G. Greco, Jr. Soil-catalyzed polymerization of phenolics in polluted waters. *Water Research* **2002**, *36*, 3015–3022.

(43) M. L. Colarieti, G. Toscano, M. R. Ardi, G. Greco, Jr. Abiotic oxidation of catechol by soil metal oxides. *Journal of Hazardous Materials* **2006**, *134*, 161–168.

(44) A. T. Stone, J. J. Morgan. Reduction and dissolution of manganese(III) and manganese(IV) oxides by organics: 2. Survey of the reactivity of organics. *Environmental Science and Technology* **1984**, *18*, 450–456.

(45) A. T. Stone, J. J. Morgan. Reduction and dissolution of manganese (III) and manganese (IV) oxides by organics. 1. Reaction with hydroquinone. *Environmental Science and Technology* **1984**, *18*, 450–456.

(46) A. T. Stone. Reductive dissolution of manganese(III/IV) oxides by substituted phenols. *Environmental Science and Technology* **1987**, *21*, 979–988.

(47) D. Canfield, B. Thamdrup, J. Hansen. The anaerobic degradation of organic matter in Danish coastal sediments: Iron reduction, manganese reduction, and sulfate reduction. *Geochimica et Cosmochimica Acta* **1993**, *57*, 3867–3883.

(48) K. Nealson, D. Saffarini. Iron and manganese in anaerobic respiration: Environmental significance, physiology, and regulation. *Annual Review of Microbiology* **1994**, *48*, 311–343.

(49) B. Thamdrup, H. Fossing, B. Jørgensen. Manganese, iron and sulfur cycling in a coastal marine sediment, Aarhus Bay, Denmark. *Geochimica et Cosmochimica Acta* **1994**, *58*, 5115–5129.

(50) T. G. Spiro, J. R. Bargar, G. Sposito, B. M. Tebo. Bacteriogenic Manganese Oxides. *Accounts Of Chemical Research* **2010**, *43*, 2–9.

(51) P. van Cappellen, Y. Wang. Cycling of iron and manganese in surface sediments: A general theory for the coupled transport and reaction of carbon, oxygen, nitrogen, sulfur, iron, and manganese. *American Journal of Science* **1996**, *296*, 197–243.

(52) S. Emerson, S. Kalhorn, L. Jacobs, B. Tebo, K. Nealson, R. Rosson. Environmental oxidation rate of manganese(II): bacterial catalysis. *Geochimica et Cosmochimica Acta* **1982**, *46*, 1073–1079.

(53) B. Tebo, S. Emerson. Microbial manganese(II) oxidation in the marine environment: a quantitative study. *Biogeochemistry* **1986**, *2*, 149–161.

(54) J. E. Post. Manganese oxide minerals: Crystal structures and economic and environmental significance. *Proceedings Of The National Academy Of Sciences Of The United States Of America* **1999**, *96*, 3447–3454.

(55) C. Negra, D. Ross, A. Lanzirotti. Oxidizing behavior of soil manganese: Interactions among abundance, oxidation state, and pH. *Soil Science Society of America Journal* **2005**, *69*, 87–95.

(56) P. Anschutz, K. Dedieu, F. Desmazes, G. Chaillou. Speciation, oxidation state, and reactivity of particulate manganese in marine sediments. *Chemical Geology* **2005**, *218*, 265–279.

(57) O. Bricker. Some Stability Relations in the System Mn-O_2-H_2O at 25°C and One Atmosphere Total Pressure. *American Mineralogist* **1965**, *50*, 1296–1354.

(58) A. T. Stone, Z. Shi. Reductive dissolution of PbO_2(s, plattnerite) and MnO_2(s, pyrolusite) by biofluid constituents. *Geochimica et Cosmochimica Acta* **2008**, *72*, A903–A903.

(59) A. T. Stone, Z. Shi. Oxidation of biofluid constituents by higher valent (hydr)oxide nanoparticles. *Geochimica et Cosmochimica Acta* **2009**, *73*, A1279–A1279.

(60) Z. Shi, *Redox Surface Reactions Occurring at PbO_2(plattnerite), MnO_2(pyrolusite), and Hydrous Manganese Oxide Particle - Water Interfaces Relevant to Water Supply Systems and Biochemical Systems*, Ph.D. thesis, Johns Hopkins University, Baltimore, MD, **2010**.

(61) J. W. Murray. The surface chemistry of hydrous manganese dioxide. *Journal of Colloid and Interface Science* **1974**, *46*, 357–371.

(62) R. P. Schwarzenbach, P. M. Gschwend, D. M. Imboden, *Environmental Organic Chemistry, 2nd ed. 2nd ed.*, John Wiley and Sons, New York, NY, **2003**.

(63) E. V. Anslyn, D. A. Dougherty, *Modern Physical Organic Chemistry* , University Science Books, Sausalito, CA, **2006**.

(64) J. A. Perlinger, V. Kalluri, R. Venkatapathy, W. Angst. Addition of hydrogen sulfide to juglone. *Environmental Science and Technology* **2002**, *36*, 2663–2669.

(65) M. P. Youngblood. Kinetics and mechanism of the addition of sulfite to p-benzoquinone. *The Journal of Organic Chemistry* **1986**, *51*, 1981–1985.

(66) G. E. Parris. Covalent binding of aromatic amines to humates. 1. Reactions with carbonyls and quinones. *Environmental Science and Technology* **1980**, *14*, 1099–1106.

(67) D. Colon, E. J. Weber, G. Baughman. Sediment-associated reactions of aromatic amines. 2. QSAR development. *Environmental Science and Technology* **2002**, *36*, 2443–2450.

(68) A. Gulkowska, M. Krauss, D. Rentsch, J. Hollender. Reactions of a Sulfonamide Antimicrobial with Model Humic Constituents: Assessing Pathways and Stability of Covalent Bonding. *Environmental Science and Technology* **2012**, *46*, 2102–2111.

(69) M. L. Iskander, H. A. A. Medien, S. Nashed. A thermodynamic assessment on the reaction of aromatic amines versus reactivity with p-benzoquinone from a kinetic study. *Zeithschrift für physikalische Chemie* **1988**, *269*, 1183–1193.

(70) S. Laha, R. G. Luthy. Oxidation of aniline and other primary aromatic amines by manganese dioxide. *Environmental Science and Technology* **1990**, *24*, 363–373.

(71) A. E. Martell, R. M. Smith, R. J. Motekaitis, *Critically Selected Stability Constants of Metal Complexes Database; Version 8.0*, U.S. Department of Commerce, National Institute of Standards and Technology, Gaithersburg, MD, **2004**.

(72) A. I. Ononye, J. G. Graveel. Modeling the reactions of 1-naphthylamine and 4-methylaniline with humic acids: Spectroscopic investigations of the covalent linkages. *Environmental Toxicology and Chemistry* **1994**, *13*, 537–541.

(73) A. I. Ononye, J. G. Graveel, J. D. Wolt. Kinetic and Spectroscopic Investigations of the Covalent Binding of Benzidine to Quinones. *Environmental Toxicology and Chemistry* **1989**, *8*, 303–308.

(74) W. Waters. Comments on the mechanism of one-electron oxidation of phenols: A fresh interpretation of oxidative coupling reactions of plant phenols. *Journal Of The Chemical Society B-Physical Organic* **1971**, 2026–2029.

(75) J. Park, J. Dec, J. Kim, J. Bollag. Effect of humic constituents on the transformation of chlorinated phenols and anilines in the presence of oxidoreductive enzymes or birnessite. *Environmental Science and Technology* **1999**, *33*, 2028–2034.

(76) G. L. Long, J. D. Winefordner. Limit of Detection A Closer Look at the IUPAC Definition - Analytical Chemistry (ACS Publications). *Analytical Chemistry* **1983**.

(77) J. Vial, A. Jardy. Experimental Comparison of the Different Approaches To Estimate LOD and LOQ of an HPLC Method - Analytical Chemistry (ACS Publications). *Analytical Chemistry* **1999**.

(78) A. Shrivastava, V. Gupta. Methods for the determination of limit of detection and limit of quantitation of the analytical methods. *Chronicles of Young Scientists* **2011**, *2*, 21.

(79) D. McDaniel, H. Brown. An extended table of Hammett substituent constants based on the ionization of substituted benzoic acids. *The Journal of Organic Chemistry* **1958**, *23*, 420–427.

(80) C. Hansch, A. Leo, D. Hoekman, *Exploring QSAR: Hydrophobic, Electronic, and Steric Constants*, *Vol. 2*, American Chemical Society, Washington, DC, **1995**.

(81) W. M. A. Niessen, *Liquid Chromatography - Mass Spectrometry 3rd ed.*, Vol. 97 of *Chromatographic Science*, CRC/Taylor & Francis, Boca Raton, FL, **2006**.

(82) T. H. J. Niedermeyer, A. Mikolasch, M. Lalk. Nuclear amination catalyzed by fungal laccases: Reaction products of p-hydroquinones and primary aromatic amines. *Journal of Organic Chemistry* **2005**, *70*, 2002–2008.

(83) R. Arnaud. Acidity and Basicity Constants for some Dihydroxyacetophenones. *Bulletin de la Societe chimique de France* **1967**, 4541–4551.

Table 3.1. Hydroquinone proelectrophiles (XH_2) discussed in this chapter and available chemical properties. E°_H is the standard reduction potential at 25°C for the reaction $Z + 2\,H^+ + 2\,e^- \rightleftharpoons XH_2$. pK_{a1} and pK_{a2} correspond to the phenolic hydrogens. pK_{aR} refers to the side group of the reduced form (XH_2). pK_a values reported for zero ionic strength and 25°C.

	XH_2	Z	pK_{a1}	pK_{a2}	pK_{aR}	E°_H (V)
I	hydroquinone 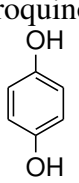	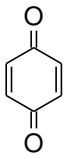	10.16[a]	12.02[a]	N/A	0.699[a]
II	acetylhydroquinone 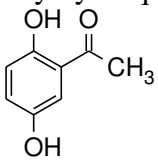	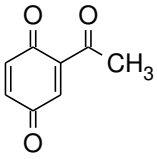	9.48[b]	12.90[b]	N/A	[e]
III	2,5-dihydroxybenzoic acid 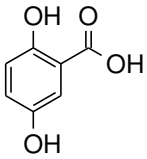	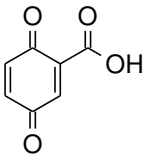	10.47[c]	[e]	2.96[c]	0.769[d]
IV	2,5-dihydroxyterephthalic acid 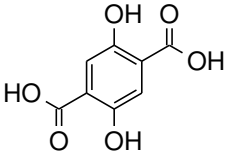	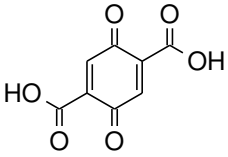	[e]	[e]	[e]	[e]

[a] Ref. *35*. [b] Ref. *83*. [c] Ref. *71* [d] Ref. *34*. [e] Data not available.

Table 3.2. Addition products for nine nucleophiles and MnO_2 oxidized XH_2(**III**) detected by negative-mode electrospray LC/MS after 12 hours of contact time. Only one of three possible isomers is shown. "n.d." indicates nucleophiles that are not detectable by electrospray LC/MS in negative mode. The molecular weight (MW) in g mol^{-1}, molecular ion mass to charge ratio (m/z) and major fragment m/z are shown for each structure.

Nucleophile		Adduct	
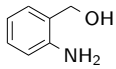 2-aminobenzyl alcohol	MW = 123 $[M-H]^-$ = 122	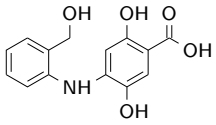	MW = 275 $[M-H]^-$ = 274
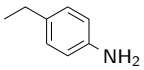 4-ethylaniline	MW = 121 n.d.	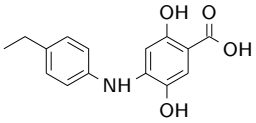	MW = 273 $[M-H]^-$ = 272 $[M-COOH]^-$ = 228
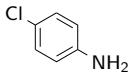 4-chloroaniline	MW = 127 n.d.	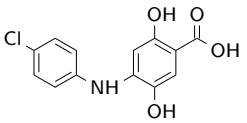	MW = 279 $[M-H]^-$ = 278 $[M-COOH]^-$ = 234
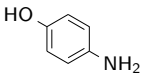 4-aminophenol	MW = 109 $[M-H]^-$ = 108	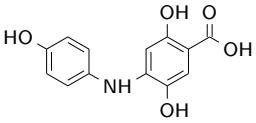	MW = 261 $[M-H]^-$ = 260
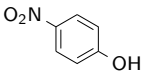 4-nitrophenol	MW = 139 n.d.	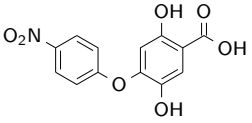	MW = 291 $[M-H]^-$ = 290 $[M-COOH]^-$ = 246
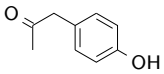 4-hydroxyphenyl acetone	MW = 150 $[M-H]^-$ = 149	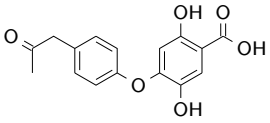	MW = 302 $[M-H]^-$ = 301 $[M-COOH]^-$ 257
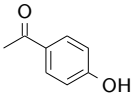 4-hydroxyacetophenone	MW = 136 $[M-H]^-$ = 135	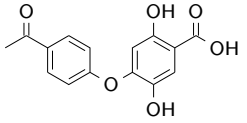	MW = 288 $[M-H]^-$ = 287 $[M-COOH]^-$ 242
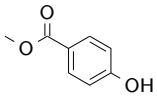 methyl 4-hydroxybenzoate	MW = 152 $[M-H]^-$ = 151	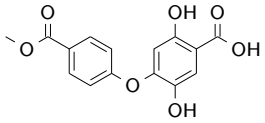	MW = 304 $[M-H]^-$ = 303 $[M-COOH]^-$ 258 $[M-OCH_3]^-$ = 273
 4-methylimidazole	MW = 82 n.d.	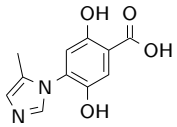	MW = 234 $[M-H]^-$ = 233 $[M-COOH]^-$ 189

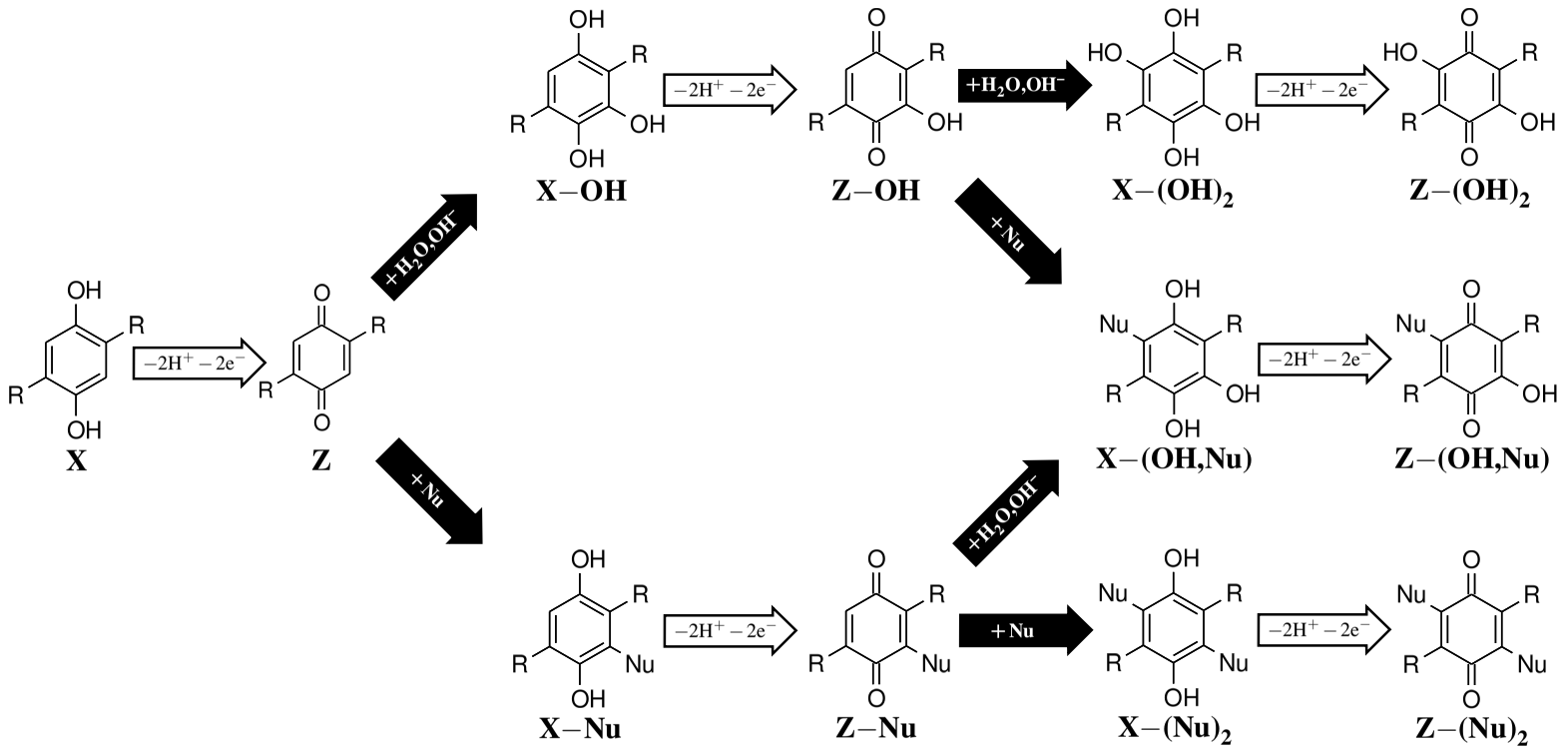

Figure 3.1. Starting with a di-substituted hydroquinone, oxidation followed by Michael addition can occur sequentially. Abbreviations are provided below each intermediate product denoting hydroquinone (X) and benzoquinone (Z) structures.

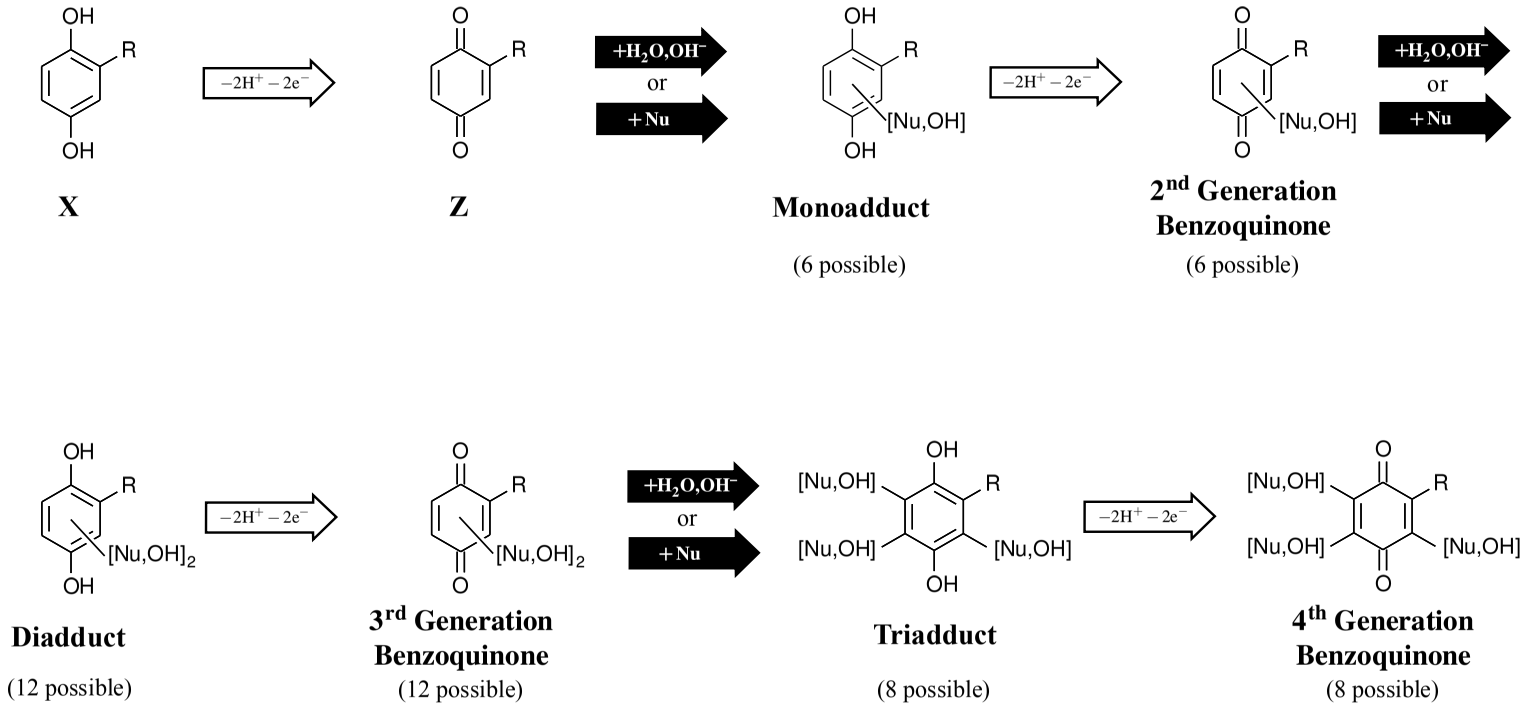

Figure 3.2. Starting with a monosubstituted hydroquinone, oxidation followed by Michael addition can occur sequentially. Abbreviations are provided below each intermediate and product denoting hydroquinone (X) and benzoquinone (Z) structures. All possible products are shown in Figure S3.3.

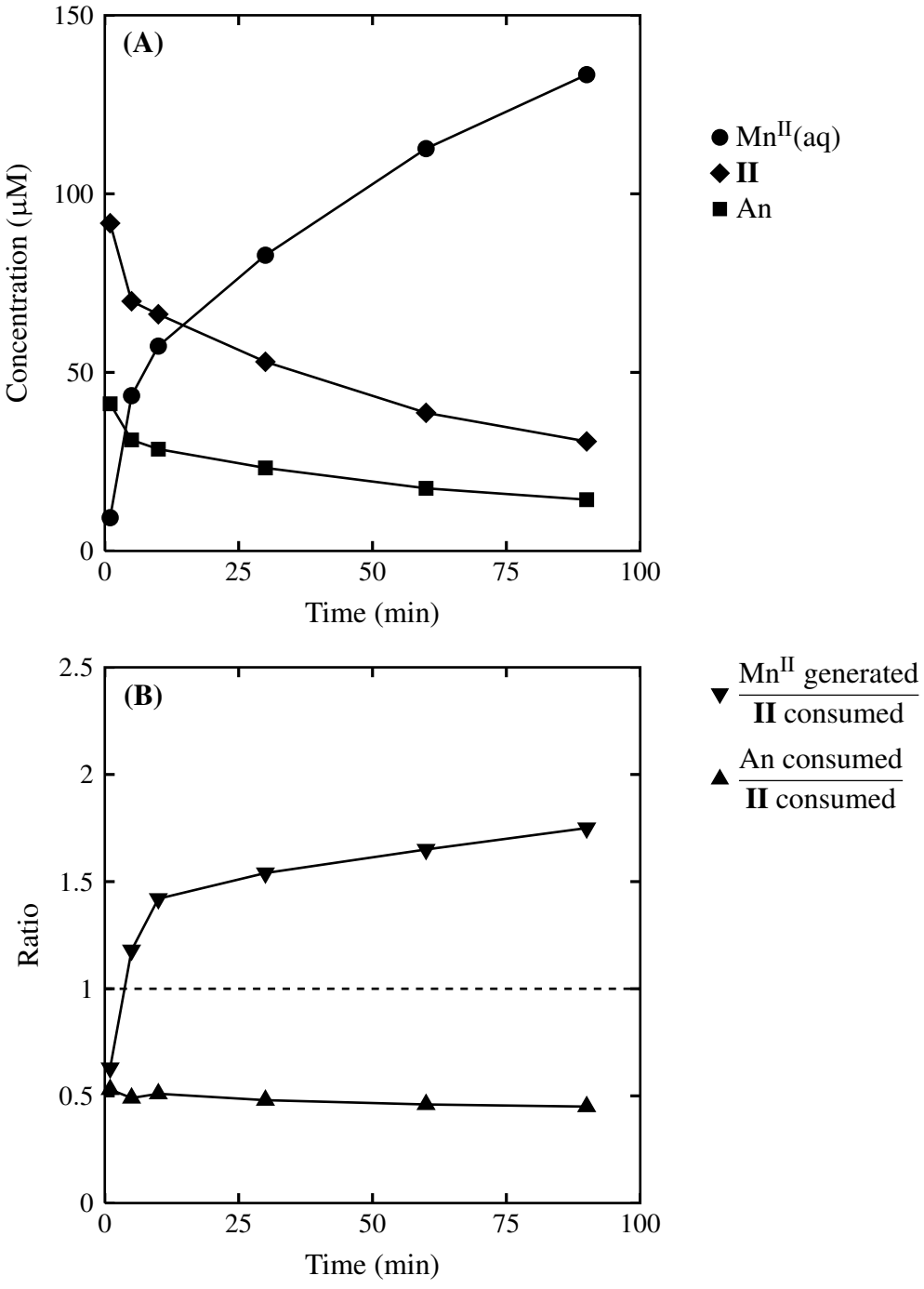

Figure 3.3. (A) Example time course for experimental slurry containing 4-ethylaniline (An) and acetylhydroquinone (XH_2(**II**)) in the presence of MnO_2. Initial conditions: 50 μM An, 100 μM XH_2(**II**), 200 μM MnO_2 in 5 mM MOPS buffer adjusted to pH 7.0 and 10 mM NaCl. (B) Mn^{II} to XH_2(**II**) and An to XH_2(**II**) ratio.

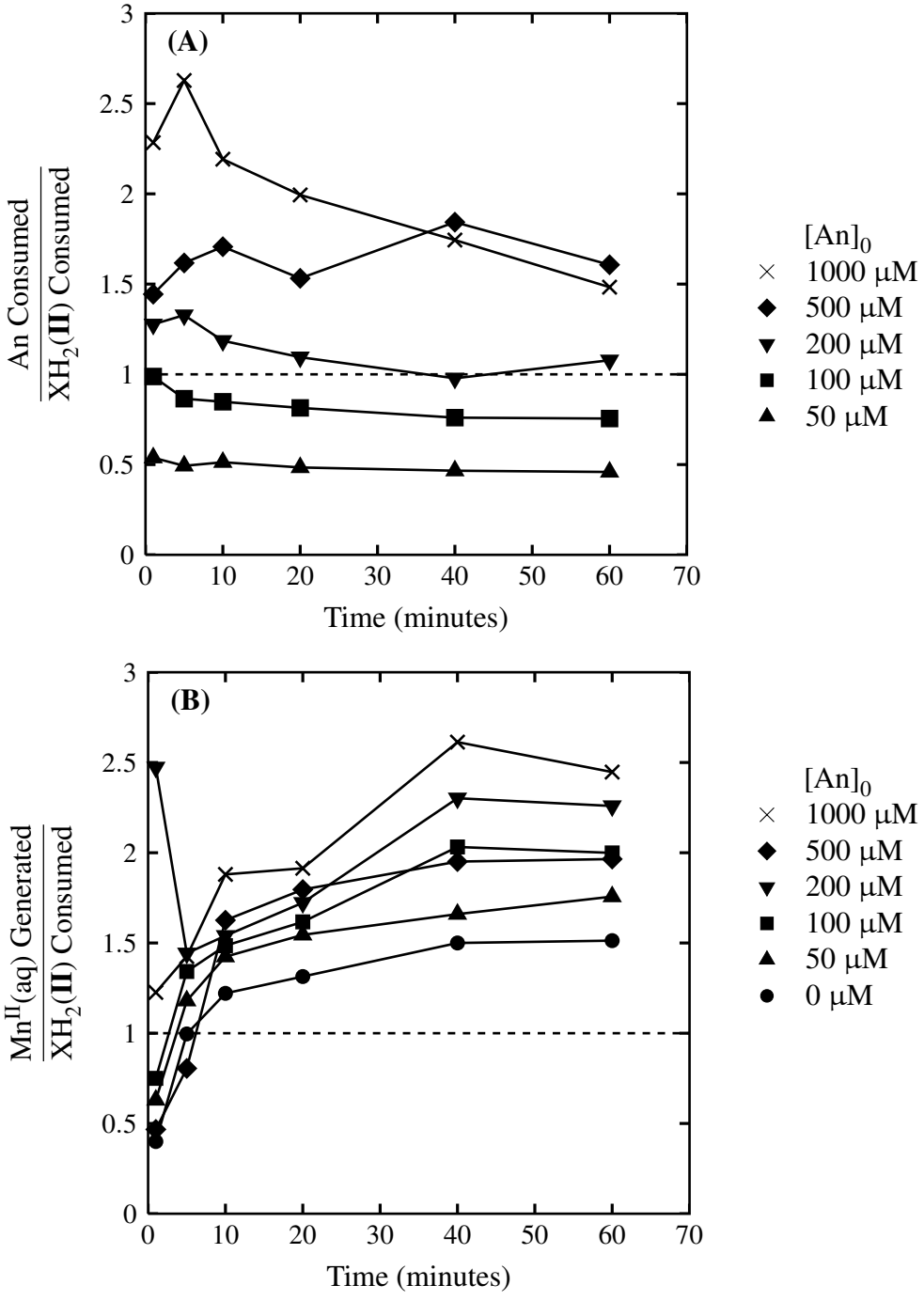

Figure 3.4. (A) R_A, $Mn^{II}(aq)$ generated to acetylhydroquinone (XH_2(**II**)) consumed. (B) R_B, 4-ethylaniline (An) consumed to acetylhydroquinone (XH_2) consumed. Initial conditions: 100 μM XH_2 and 200 μM MnO_2 in 5 mM MOPS buffer adjusted to pH 7.0 and 10 mM NaCl. Dashed lines mark one-to-one ratio.

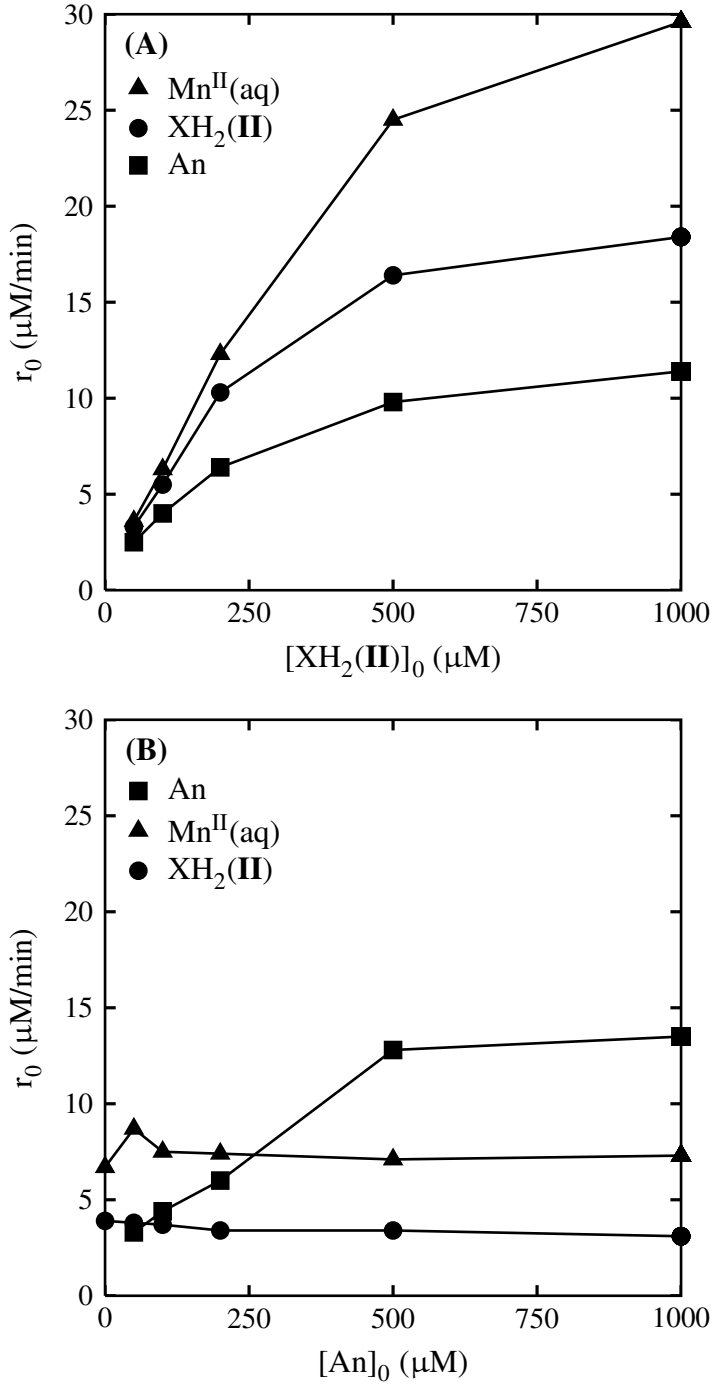

Figure 3.5. Initial rate (r_0) of consumption of XH_2(**II**), consumption of 4-ethylaniline (An) and generation of Mn^{II}(aq). For simplicity, both generation and consumption are shown as positive. (A) 100 μM An. (B) 100 μM XH_2(**II**). Conditions: 5 mM MOPS adjusted to pH 7.0, 10 mM NaCl, 200 μM MnO_2.

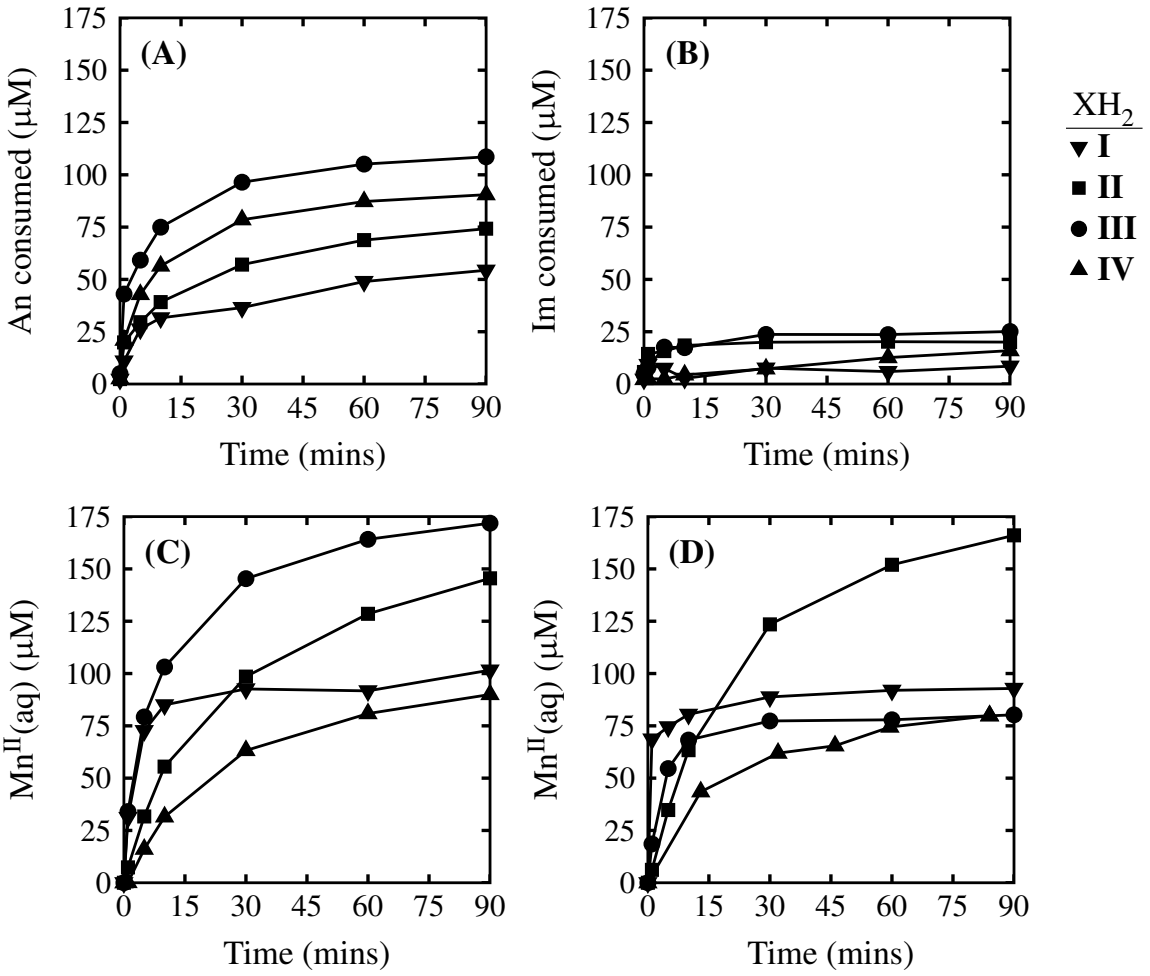

Figure 3.6. Nucleophile consumption and $Mn^{II}(aq)$ generation for 4-ethylaniline (An, A and C) and 4-methylimidazole (Im, B and D) in the presence of one of four proelectrophiles (Table 3.1). Conditions: 100 μM proelectrophile, 160 μM nucleophile, and 200 μM MnO_2 in 5 mM MOPS adjusted to pH 7 and 10 mM NaCl.

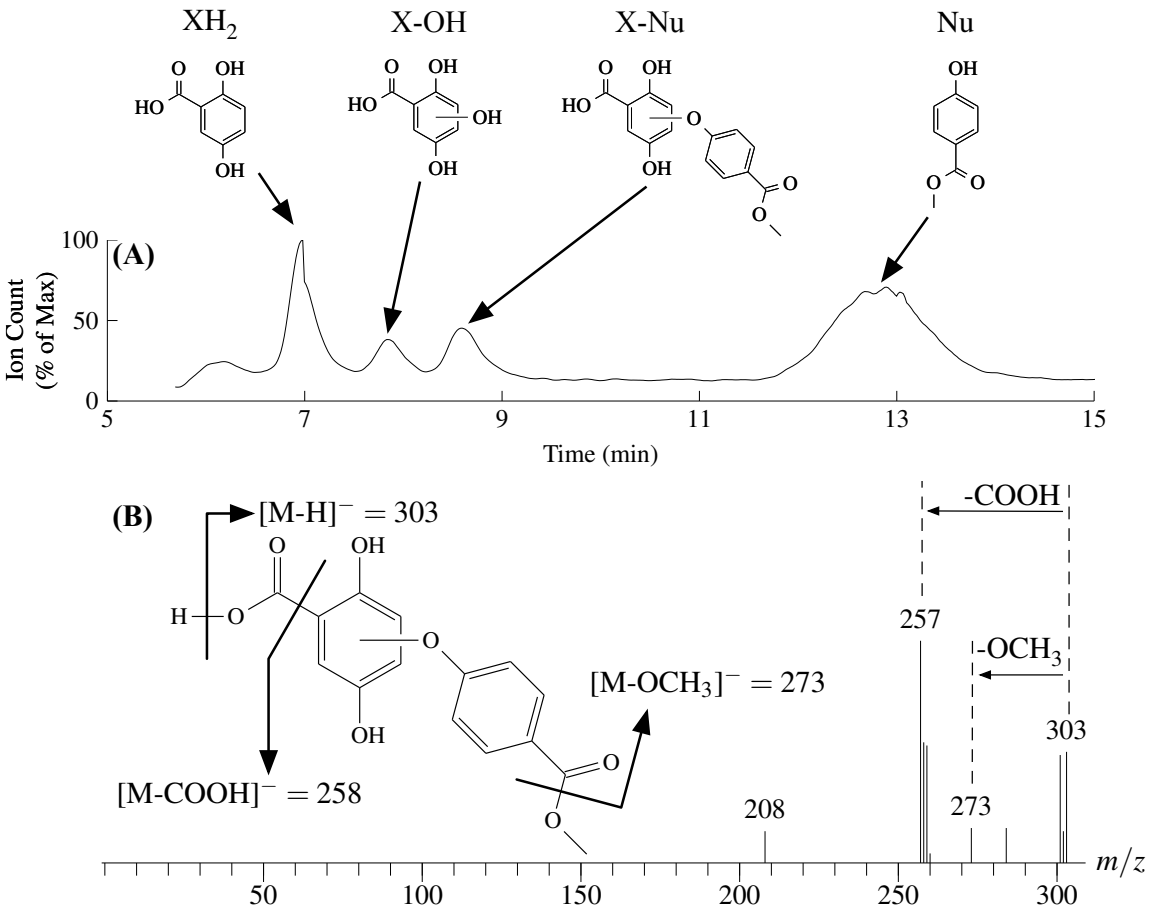

Figure 3.7. Example chromatogram (A) and mass spectrum (B) collected by LC/MS after 12 hours of contact time from a slurry containing 50 μM XH_2(**III**), 220 μM MnO_2, and 100 μM methyl 4-hydroxybenzoate. The mass spectrum in B corresponds to the peak in A with retention time of 12.8 min. Conditions: 5.0 mM MOPS adjusted to pH 7.0, 10 mM NaCl.

3.5 Supporting Information

Supporting information for Chapter 3 includes a section discussing an application of the Langmuir-Hinshelwood-Hougan-Watson kinetic model, an E_h-pH diagram depicting the dependence of redox potential for reduction of MnO_2 and goethite and oxidation of three substituted hydroquinones (Figure S3.2) as well as tabulated equilibrium constants used to generate Figure S3.2 (Table S3.3, Table S3.4, and Table S3.5), tabulated 1 hour Mn^{II} concentration measured in slurries of candidate nucleophiles in the absence of an XH_2 proelectrophile (Table S3.1), structures of all possible hydroquinone and benzoquinone adducts that can be generated from proelectrophile experiments with an XH_2 proelectrophile containing a single substituent group (Figure S3.3), a graphical determination of the initial rates shown in Figure 3.5 (Figure S3.4 and Figure S3.5), additional time course data where the MnO_2 loading was 80 or 160 μM (Figure S3.6), mass spectra supporting Table 3.2 (Figure S3.7), and a table of available acid dissociation constants (pK_a) for chemical compounds studied in this chapter (Table S3.2).

3.6 Application of the Langmuir-Hinshelwood-Hougan--Watson kinetic model

The Langmuir-Hinshelwood-Hougan-Watson (LHHW) kinetic model, which was developed for surface-catalyzed reactions, can be applied to redox reactions at mineral surfaces (*1–3*). The LHHW model considers a reaction at a surface that involves three steps: adsorption to an available surface site, reaction at the surface (in this case electron transfer), and desorption of the product. We can apply the LHHW model to oxidation of XH_2(**II**) at the

surface of MnO_2 and using initial rate data to discern the rate-determining step from one of those three processes (*2*). The relationship between initial rate of XH_2(**II**) consumption and initial XH_2(**II**) concentration is mathematically different depending on which process is rate determining. In the adsorption-limited case, sorption of XH_2(**II**) to the surface determines the rate of consumption of XH_2(**II**). The initial rate (r_0^a) is linearly dependent on initial concentration:

$$r_0^a = -\frac{d[\mathrm{XH_2(II)}]}{dt} = k_{ads}[\mathrm{S}][\mathrm{XH_2(II)}]_0 \tag{S3.1}$$

where k_{ads} is the rate constant for adsorption, and S represents surface sites. If oxidation of XH_2(**II**) at the surface is rate-determining step then the initial rate depends on the amount of XH_2(**II**) that is adsorbed to the surface. In this case, adsorption will reach equilibrium conditions because XH_2(**II**) can adsorb to the surface faster than it can react at the surface.

$$r_0^s = -\frac{d[\mathrm{XH_2(II)}]}{dt} = \frac{k_{ox}[\mathrm{S}][\mathrm{XH_2(II)}]_0}{1 + \mathrm{K_{XH_2(II)}}[\mathrm{XH_2(II)}]_0} \tag{S3.2}$$

where k_{ox} is the rate constant for oxidation at the surface of MnO_2. Adsorption of XH_2(**II**) is represented by the equilibrium constant ($K_{XH_2(II)}$) because the amount of XH_2(**II**) that adsorbs is not kinetically controlled. In the third case, where consumption of XH_2(**II**) is limited by desorption of Z(**II**) and not by adsorption of XH_2(**II**) or oxidation at the surface, the rate of desorption is independent of the concentration of XH_2(**II**). Under initial conditions, the concentration of Z(**II**) is zero, so the rate expression becomes:

$$r_0^d = -\frac{d[\mathrm{XH_2(II)}]}{dt} = k_{des}[\mathrm{S}] \tag{S3.3}$$

Where k_{des} is the rate constant for desorption of the oxidation product. Equations S3.1, S3.2, and S3.3 predict different dependence of initial rate of consumption of XH_2(**II**) on the initial

concentration of XH_2(**II**). Depending on which equation best describes the data, the LHHW model gives some evidence of whether adsorption, reaction at the surface, or desorption of the product is rate determining for consumption of the substrate. Note that Equation S3.2 can mimic Equation S3.1 under conditions where the product of $K_{XH_2(\mathbf{II})}[XH_2(\mathbf{II})]_0$ is small.

The above equations assume that electron transfer at the surface is so fast that XH_2 is oxidized to Z(**II**) and MnO_2 is reduced to Mn^{II} in a single step. In other words, the first electron transfer is not modeled separately from the second electron transfer step. This assumption describes a situation where the semiquinone radical intermediate and with $Mn^{(}III$) form Z(**II**) and Mn^{II} faster than any other potential reactions.

In Figure S3.1, lhe nonlinear increase in initial rate of consumption of XH_2(**II**) with increasing XH_2(**II**) concentration is consistent with the surface-reaction limited case (Equation S3.2, shown as a line Figure S3.1A). Values for $k_{ox}[S]$ and $K_{XH_2(\mathbf{II})}$ are determined by nonlinear least squares regression. Individual values for k_{ox} and [S] cannot be determined using this method, but the aggregate parameter $k_{ox}[S]$ was determined to be 3.4×10^{-7} M s^{-1}. $K_{XH_2(\mathbf{II})}$ was 4×10^6 M^{-1}. This suggests that oxidation of XH_2(**II**) at the surface of MnO_2 controls the overall rate of reaction. Increasing the concentration of XH_2(**II**) in the bulk solution increases the rate of reaction until the concentration is high enough to saturate the surface.

Figure S3.1A and Equation S3.2 concern the oxidation of XH_2(**II**) on the surface of MnO_2. What is not addressed is whether the adduct-forming reaction of Z(**II**) with An occurs on the surface or if Z(**II**) must desorb to react with An in the bulk phase. A relationship similar to Equation S3.2 can written for consumption of An. Consider the case where An must adsorb to the surface of MnO_2 prior to reaction with adsorbed Z(**II**). The initial rate of consumption of An would be described by an equation similar to Equation S3.2 for the

surface reaction between An and Z(**II**).

$$r_0 = -\frac{d[\mathrm{An}]}{dt} = \frac{k[\mathrm{Z}(\mathbf{II})][\mathrm{S}][\mathrm{An}]_0}{1 + \mathrm{K_{An}}[\mathrm{An}]_0} \tag{S3.4}$$

where $\mathrm{K_{An}}$ is the adsorption equilibrium constant. Alternatively, consider the case where Z(**II**) must desorb to react with An in the bulk phase. The rate of consumption of An should increase linearly with increasing concentration of An:

$$r_0 = -\frac{d[\mathrm{An}]}{dt} = k[\mathrm{An}][\mathrm{Z}(\mathbf{II})] \tag{S3.5}$$

Note that we expect that Z(**II**) will not accumulate, so [Z(**II**)] should be small and independent of $[\mathrm{An}]_0$.

The rate of consumption of An shown in Figure S3.1B is not consistent with Equation S3.5; it appears to follow Equation S3.4, such that the amount of An available to react is limited by the adsorption coefficient and available adsorption sites. Similar to Equation S3.2, the parameters in Equation S3.4 can be determined from least squares regression. In this case, the aggregate parameter is $k[\mathrm{Z}(\mathbf{II})][\mathrm{S}]$ and its value was 2×10^{-7} M s^{-1}. K_{An} was 6×10^6 $\mathrm{M}^{-}1$. The rate of consumption of An cannot continually increase with increasing $[\mathrm{An}]_0$ because the number of surface sites is limited. Because Z(**II**) is generated on the solid surface, it might not persist long enough to desorb to the bulk phase. It would react with a nearby adsorbed nucleophile or $\mathrm{H_2O/OH^-}$. Unfortunately, it is not possible to discern if the increase in An consumption in Figure S3.1B is due to this surface effect, or if increasing the concentration of An increases the rate of nucleophilic addition of An over hydration. Most likely, time course data for the products (X-Nu and X-OH) would be required to separate these two effects.

It is important to note that the LHHW model was developed for simple irreversible reactions at surfaces that act as catalysts and are not consumed during the reaction (*1*). MnO_2 is subject to reduced to Mn^{II} and is dissolved during our experiments. When XH_2(**II**) is present in excess of MnO_2 the solid particles become completely dissolved (Figure S3.5) and heterogeneous kinetics no longer apply. However, we applied the LHHW model only to initial rates. Under initial conditions there is still MnO_2 surface present regardless of the concentration of XH_2(**II**). Also, the LHHW model only provides meaningful relationships between the initial rate of XH_2(**II**) and $[XH_2(\mathbf{II})]_0$ and between the initial rate of An consumption and $[An]_0$ because it was developed to model A $\longrightarrow$ B reactions at catalyst surfaces. For this reason only equations S3.2 and S3.4 are plotted on Figure S3.1.

The results of our LHHW modeling exercise imply a reaction mechanism where both the rate of consumtion of XH_2(**II**) and An are limited by the rate of reaction at the MnO_2 surface. Before any reaction occurs, XH_2(**II**) and An sorb and accumulate on the surface of MnO_2. The first electron transfer takes place where XH_2(**II**) is oxidized to the semiquinone radical and an Mn^{IV} atom at the surface is reduced to Mn^{III}. Both the semiquinone and Mn^{III} are sufficiently reactive that they are quickly transformed to Z(**II**) and Mn^{II}, respectively. The highly electrophilic Z(**II**) reacts quickly with either An, OH^-, or H_2O to form the monoadduct (X-An) or the hydration product (X-OH). At some unknown later time, Mn^{II} and X-An or X-OH desorb from the MnO_2 surface.

Table S3.1. Mn^{II}(aq) after 1 hour in filtered samples of candidate nucleophiles and MnO_2, which serves as a measure of the extent of reaction. ND indicates that Mn^{II}(aq) was below the 3 μM limit of detection. Conditions: 100 μM candidate nucleophile, 200 μM MnO_2, 5 mM MOPS buffer (pH 7.0) and 10 mM NaCl. Acid dissociation values pK_a are shown for 25°C and zero ionic strength when available (*4*).

Nucleophile		pK_a	Mn^{II}(aq) (μM)
Methyl 4-hydroxy-benzoate	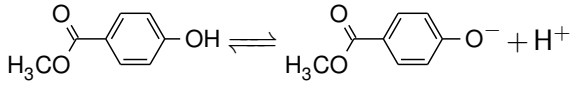		ND
4-Hydroxy-phenylacetone	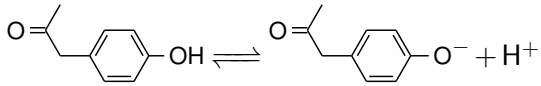		ND
4′-Hydroxy-acetophenone	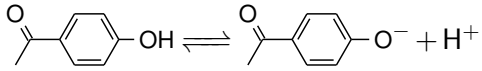	8.05	ND
4-Nitrophenol	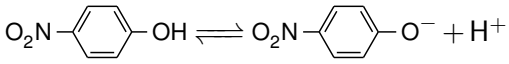	7.15	ND
4-Ethylaniline	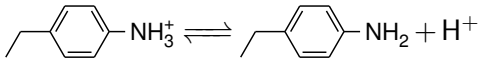	5.00	ND
4-Chloro-aniline	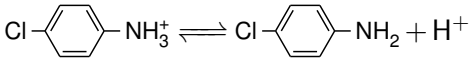	4.06	ND
4-Methyl-imidazole	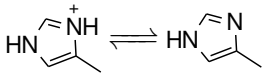	7.54	ND
No added nucleophile			ND

Table S3.2. Selected acid dissociation constants reported at 25 °C. Values adjusted to zero ionic strength using the Davies equation when necessary (*5*).

Use	Chemical	log K	Ref.
Nucleophile			
	Hydroxylamine	5.96	*4*
		13.74	*4*
	4-Ethylaniline	5.00	*4*
	4-Methoxyaniline	5.357	*4*
	p-Aminophenol[a]	5.64	*6*
	4-Chloroaniline	4.07	*4*
	4′-Aminoacetophenone	2.29	*4*
	Aniline	4.601	*4*
	4-Nitroaniline	1.015	*4*
	4-Methylimidazole	7.54	*4*
	2-Mercaptoethanol[a]	9.72	*4*
	4-Nitrophenol	7.15	*4*
	4′-Hydroxyacetophenone	8.05	*4*
Proelectrophile			
	Hydroquinone	10.16	*4*
		12.02	*4*
	Gentisic acid[b]	2.96	*4*
		10.47	*4*
	Acetylhydroquinone	9.48	*7*
		12.9	*7*
Buffer			
	Acetate	4.784	*8*
	MES	6.270	*8*
	MOPS	7.184	*8*
	CHES	9.384	*8*

[a] Data only available for one of two pK_a values. [b] Data only available for two of three pK_a values.

Table S3.3. Reduction potential thermodynamic data used to generate Figure S3.2. Values reported for 25°C No activity corrections were made.

Reduction potential	E°_{H} (V)	Ref.
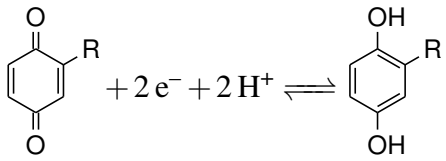		
$Z{-}R + 2\,e^- + 2\,H^+ \rightleftharpoons H_2X{-}R$		
R = COOH	0.769	*9*
R = H	0.699	*10*
R = CH_3	0.644	*10*
$Fe^{3+} + e^- \rightleftharpoons Fe^{2+}$	0.777	*5*
$MnO_2(\text{pyrolusite}) + 2\,e^- + 4\,H^+ \rightleftharpoons Mn^{2+} + 2\,H_2O$	1.229	*11*
$O_2 + 4\,e^- + 4\,H^+ \rightleftharpoons 2\,H_2O$	1.23[a]	*5*
$2\,H^+ + 2\,e^- \rightleftharpoons H_2$	0.00	*5*

[a] Calculated from reported $p\epsilon^{\circ}$: $E_{\circ} = \frac{2.303RT}{F} p\epsilon^{\circ}$.

Table S3.4. Equilibrium thermodynamic data used to generate Figure S3.2. Acid dissociation constants adjusted for zero ionic strength using the Davies equation when necessary (*5*). Values reported at 25°C.

Equilibrium expression	log K	Ref.
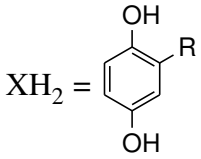		
R = COOH		
$H_3X \rightleftharpoons H_2X^- + H^+$	2.96[a]	*12*
$H_2X^- \rightleftharpoons HX^{2-} + H^+$	10.77[b]	*13*
$HX^{2-} \rightleftharpoons X^{3-} + H^+$	[c]	
R = H		
$H_2X \rightleftharpoons HX^- + H^+$	10.16[b]	*10*
$HX^- \rightleftharpoons X^{2-} + H^+$	12.02[d]	*10*
$R = CH_3$		
$H_2X \rightleftharpoons HX^- + H^+$	10.36[b]	*4*
$HX^- \rightleftharpoons X^{2-} + H^+$	12.25[d]	*4*

[a] Acid dissociation constant for carboxylic acid side group. [b] Acid dissociation for first phenolic proton (−OH). [c] Data not available. [d] Acid dissociation constant for second phenolic proton.

Table S3.5. Stability constants[a] for Fe^{II} and Fe^{III} hydrolysis used to generate Figure S3.2 (*14*).

Equilibrium Expression	logK	Ref.
$Fe^{II}OH^{+} \rightleftharpoons Fe^{2+} + OH^{-}$	9.397	*4*
$Fe^{II}(OH)_2^{0} \rightleftharpoons Fe^{2+} + 2\,OH^{-}$	20.494	*4*
$Fe^{II}(OH)_3^{-} \rightleftharpoons Fe^{2+} + 3\,OH^{-}$	28.494	*4*
$Fe^{II}(OH)_4^{2-} \rightleftharpoons Fe^{2+} + 4\,OH^{-}$	45.988	*4*
$Fe^{III}OH^{2+} \rightleftharpoons Fe^{3+} + OH^{-}$	2.187	*4*
$Fe^{III}(OH)_2^{+} \rightleftharpoons Fe^{3+} + 2\,OH^{-}$	4.594	*4*
$Fe^{III}(OH)_3^{0} \rightleftharpoons Fe^{3+} + 3\,OH^{-}$	13.600	*4*
$Fe^{III}(OH)_4^{-} \rightleftharpoons Fe^{3+} + 4\,OH^{-}$	21.588	*4*
$Fe_2^{III}(OH)_2^{4+} \rightleftharpoons 2\,Fe^{3+} + 2\,OH^{-}$	2.854	*4*
$Fe_3^{III}(OH)_4^{5+} \rightleftharpoons 3\,Fe^{3+} + 4\,OH^{-}$	6.288	*4*
$Mn^{II}(OH)^{+} \rightleftharpoons Mn^{2+} + OH^{-}$	10.0	*4*
$Mn^{II}(OH)_3^{-} \rightleftharpoons Mn^{2+} + 3\,OH^{-}$	34.2	*4*
Solubility product constants		
$FeOOH(s,geothite) + H_2O \rightleftharpoons Fe^{3+} + 3\,OH^{-}$	0.200	*5*
$Mn^{II}(OH)_2(s) \rightleftharpoons Mn^{2+} + OH^{-}$	14.50	*5*

[a] 25°C. Adjusted for zero ionic strength using the Davies equation (*5*).

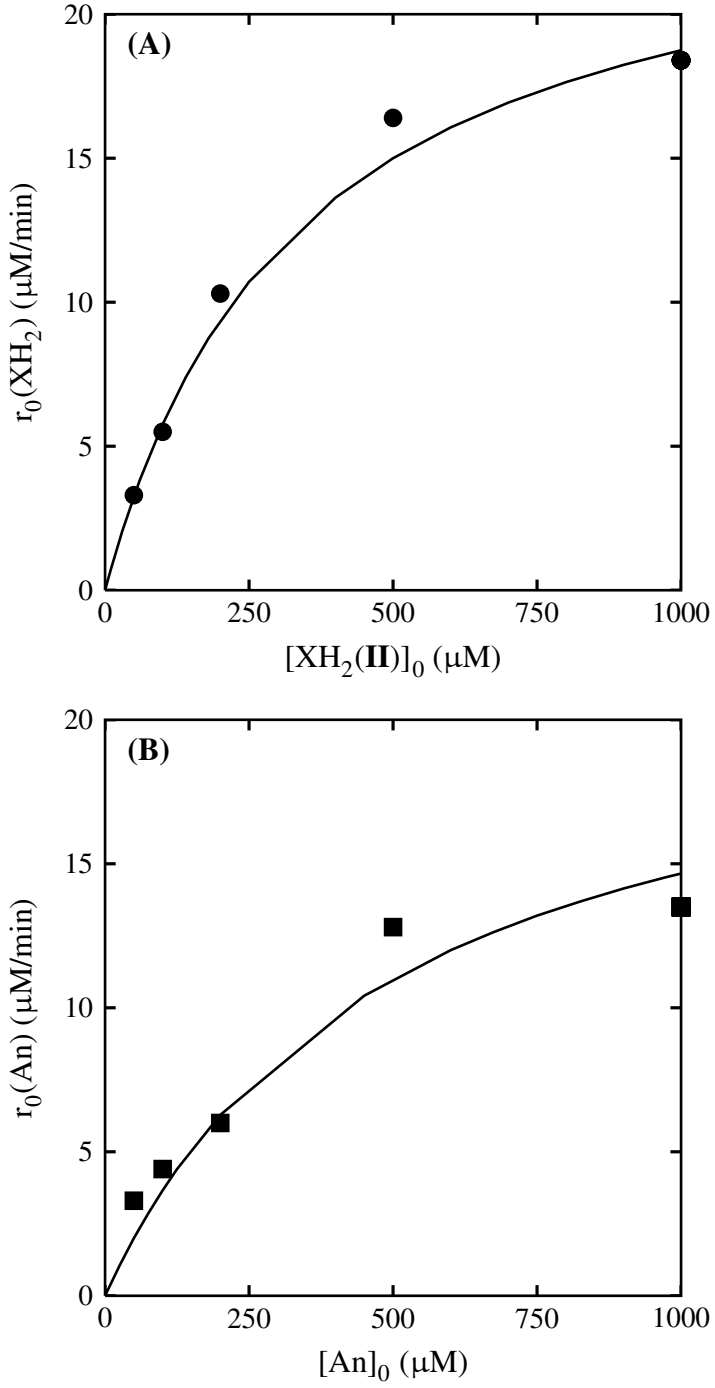

Figure S3.1. (A) Initial rate of consumption of XH_2(**II**), $r_0(XH_2)$. (B) Initial rate of consumption of 4-ethylaniline, r_0(An). For simplicity, rates of consumption are shown as positive. (A) 100 μM An, line represents Equation S3.2. (B) 100 μM XH_2(**II**), line represents Equation S3.4. Conditions: 5 mM MOPS adjusted to pH 7.0, 10 mM NaCl, 200 μM MnO_2.

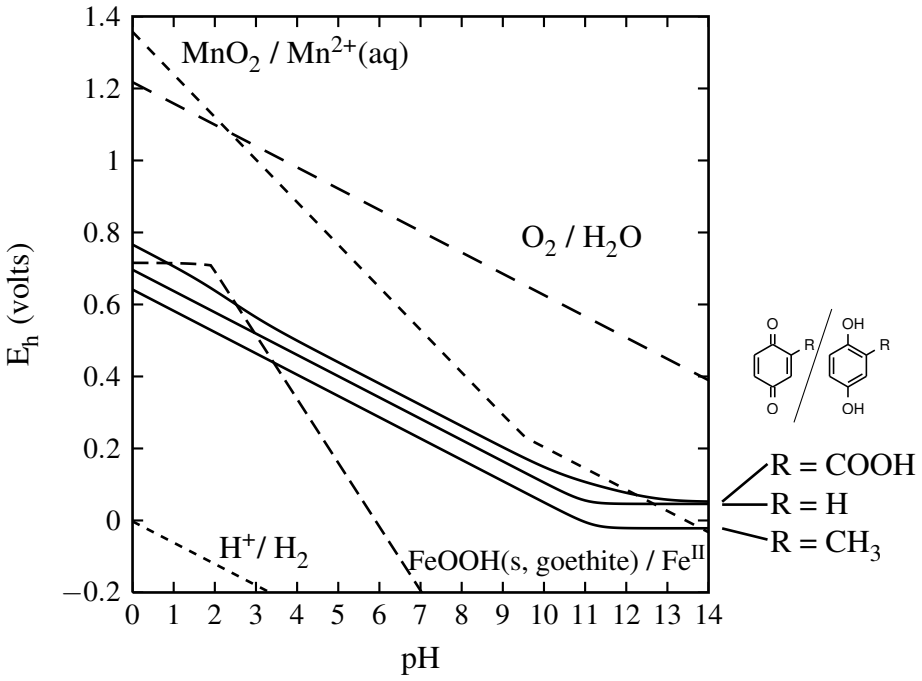

Figure S3.2. E_h-pH diagram for three benzoquinone/hydroquinone half-reactions including MnO_2 / Mn^{2+}(aq), FeOOH(s, goethite), and O_2 / H_2O half-reactions as reference. Conditions: 50 μM of each hydroquinone and benzoquinone, 50 μM Mn^{2+}(aq) and total Fe^{II}, the activity of MnO_2 or FeOOH(s, goethite) is set to 1.0, $P_{O_2} = 0.21$ atm, 10 mM NaCl and 25°C temperature.

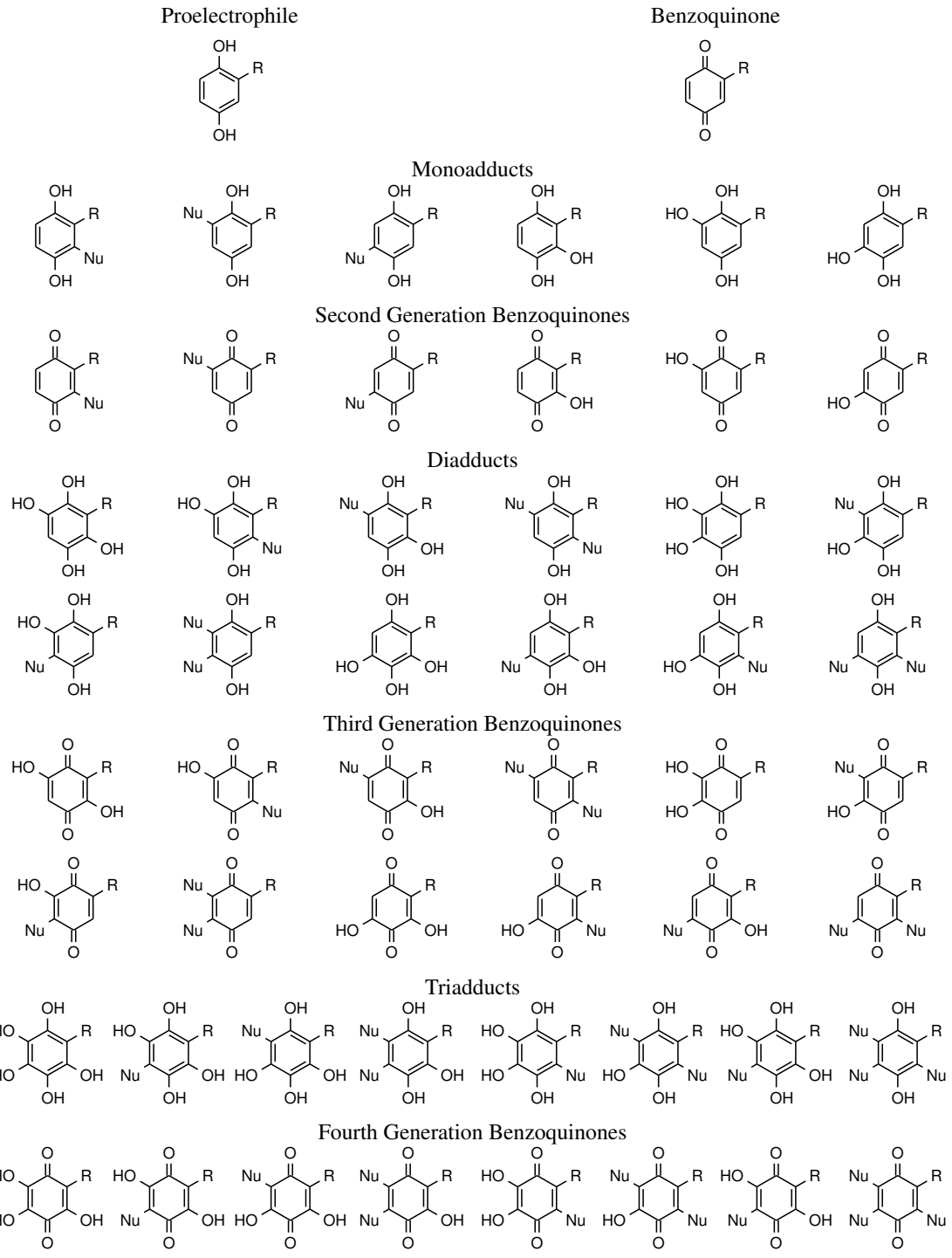

Figure S3.3. Molecular structures of all possible adducts and benzoquinone electrophiles that could result from a hydroquinone electrophile with a single substituent (R).

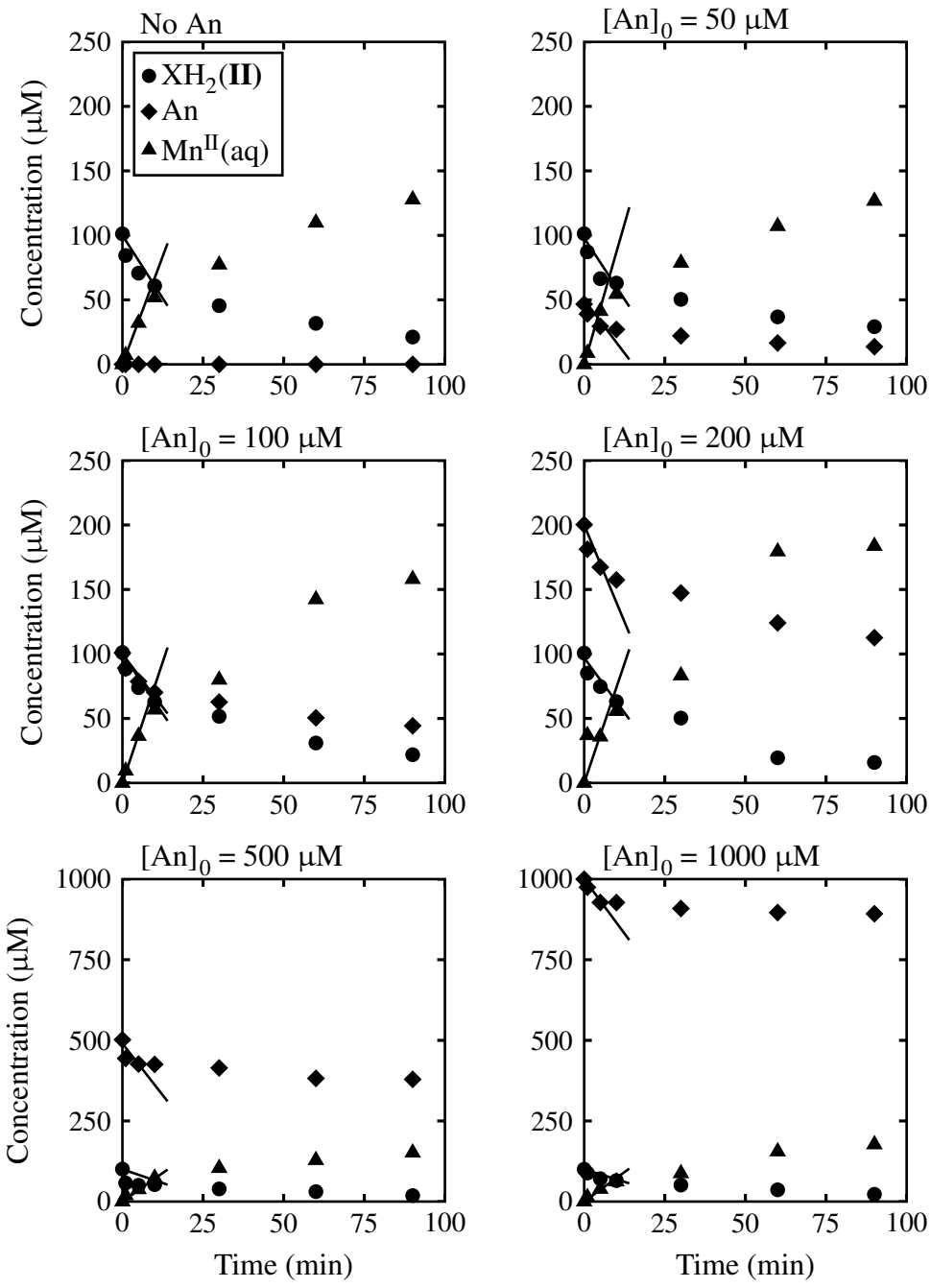

Figure S3.4. Proelectrophile experiments consisting of 4-ethylaniline (An) as the nucleophile and acetylhydroquinone (XH_2(**II**)) as the proelectrophile. Lines represent linear fits used to determine initial rate. Conditions: 100 μM XH_2(**II**), 200 μM MnO_2, 5 mM MOPS adjusted to pH 7.0, and 10 mM NaCl.

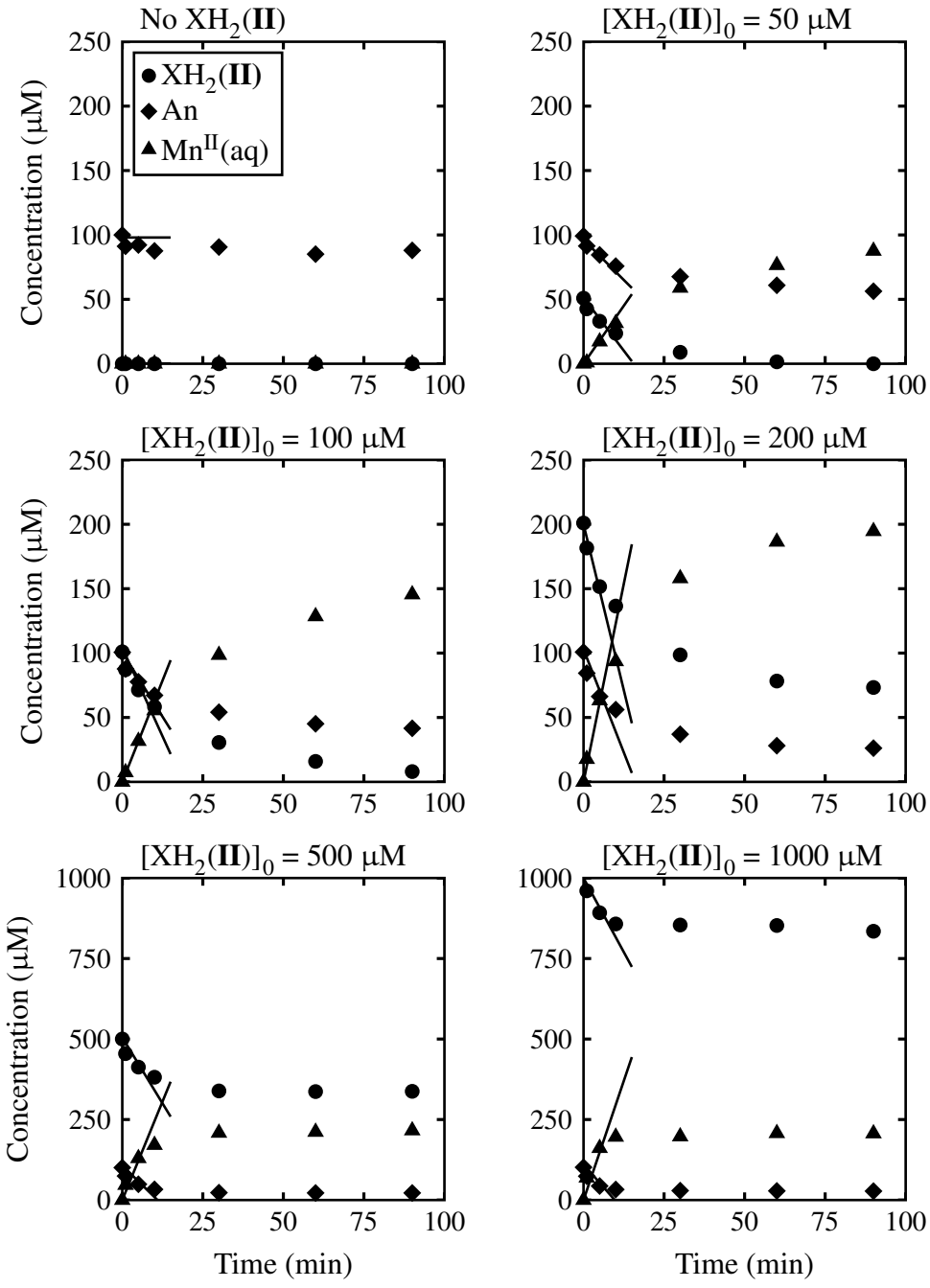

Figure S3.5. Proelectrophile experiments consisting of 4-ethylaniline (An) as the nucleophile and acetylhydroquinone (XH_2(**II**)) as the proelectrophile. Lines represent linear fits used to determine initial rate. Conditions: 100 μM An, 200 μM MnO_2, 5 mM MOPS adjusted to pH 7.0, and 10 mM NaCl.

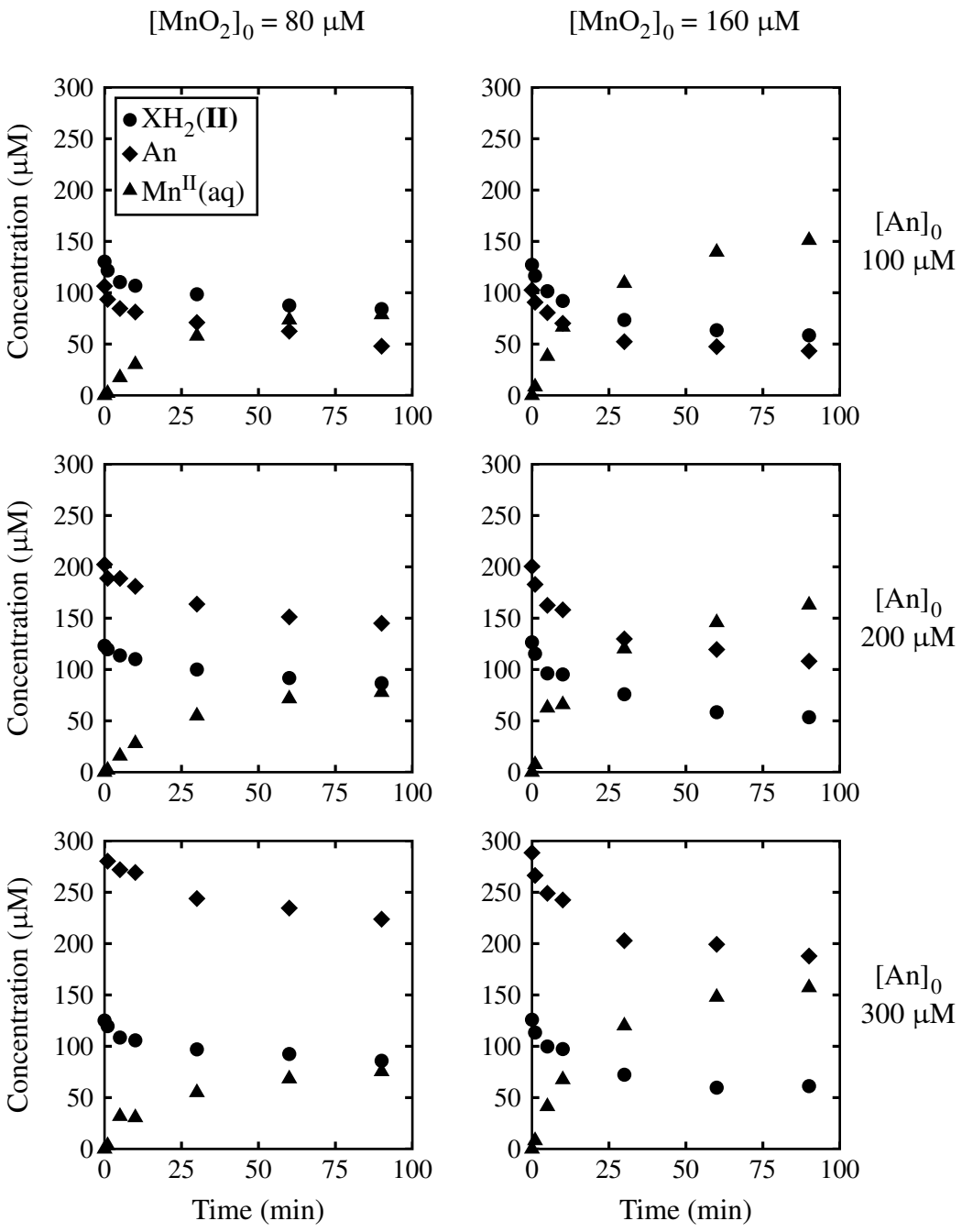

Figure S3.6. Proelectrophile experiments consisting of 4-ethylaniline (An) as the nucleophile and acetylhydroquinone (XH_2(**II**)) as the proelectrophile. Conditions: 130 μM XH_2(**II**), 5 mM MOPS adjusted to pH 7.0, and 10 mM NaCl.

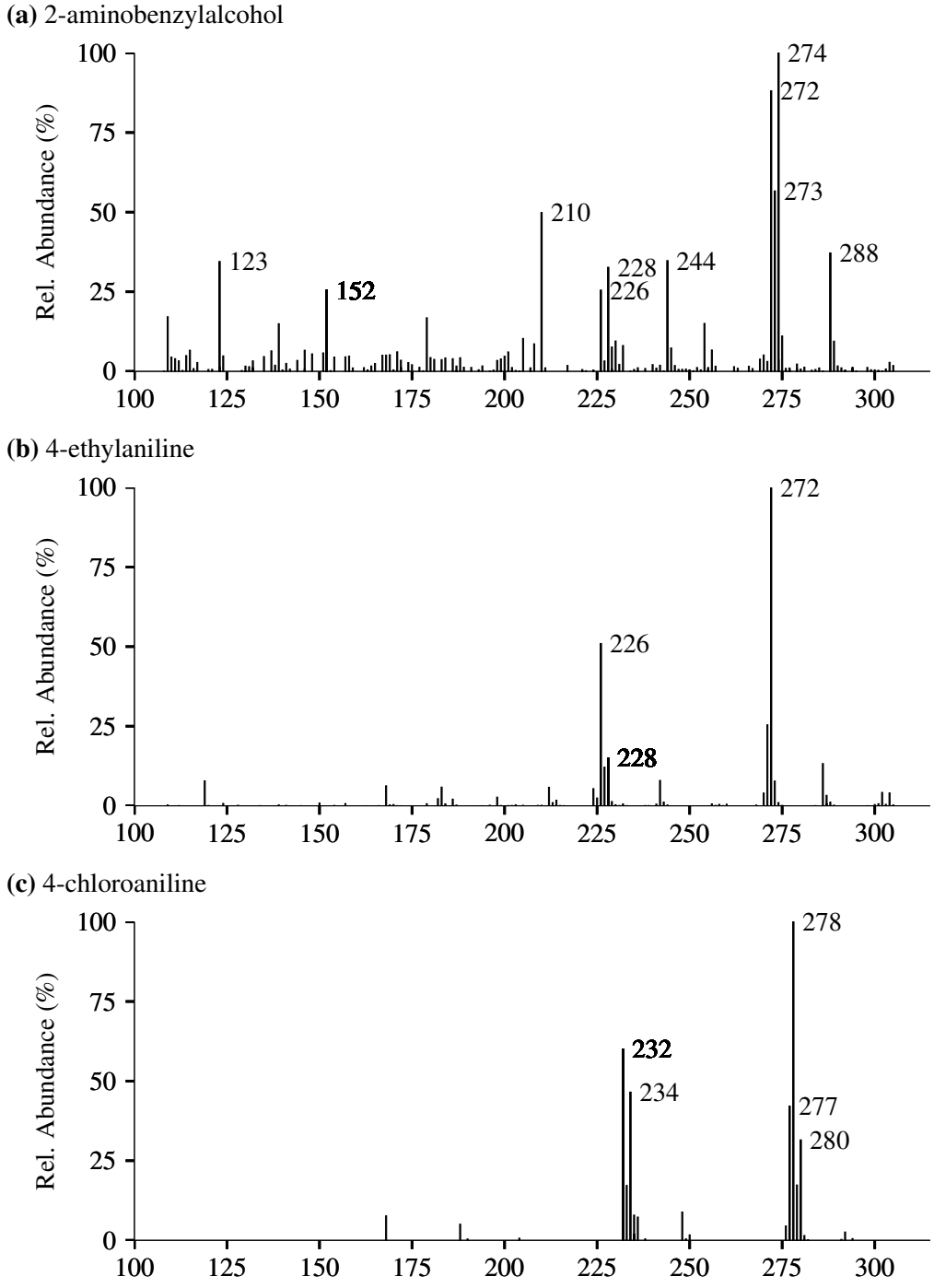

Figure S3.7. Mass spectra corresponding to monoadducts in Table 3.2 collected after 12 hrs . Conditions: 50 μM gentisic acid proelectrophile, 100 μM nucleophile, 220 μM MnO_2, 5 mM MOPS (pH 7.0), and 10 mM NaCl.

(a) 4-aminophenol

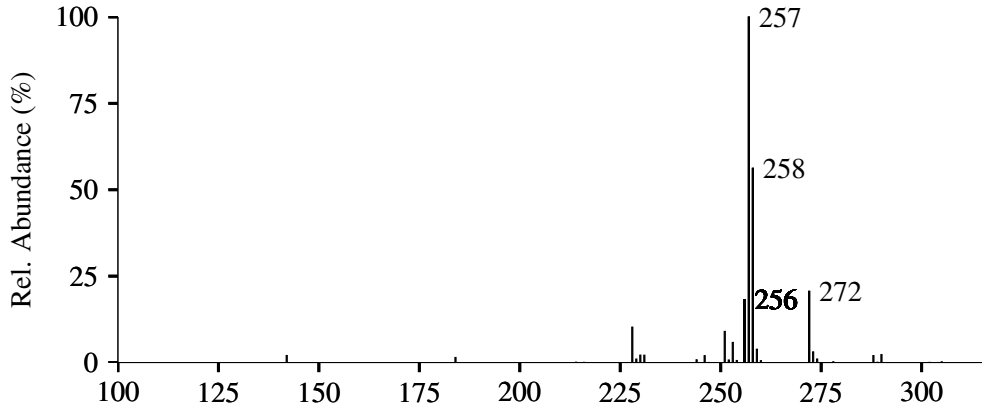

(b) 4-nitrophenol

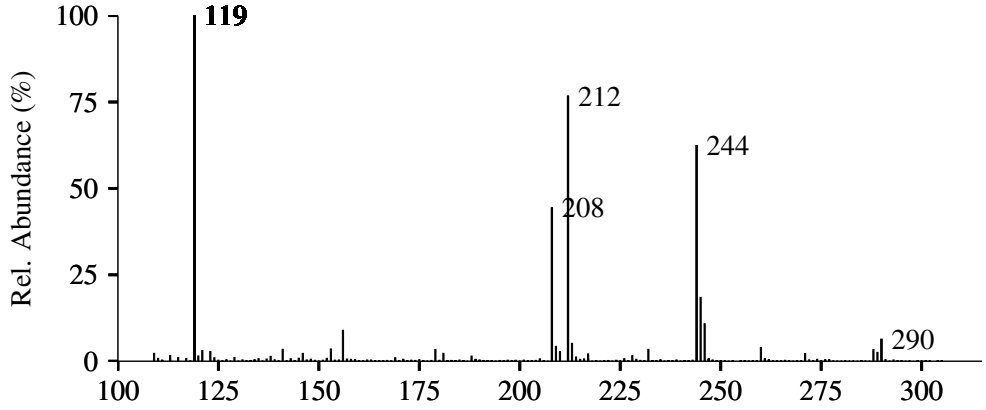

(c) 4-hydroxyphenylacetone

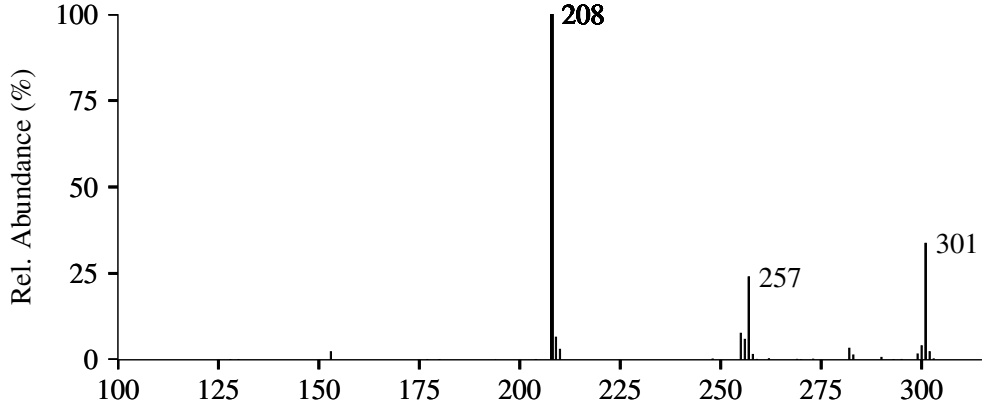

Figure S3.8. Continued.

(a) 4-hydroxyacetophenone

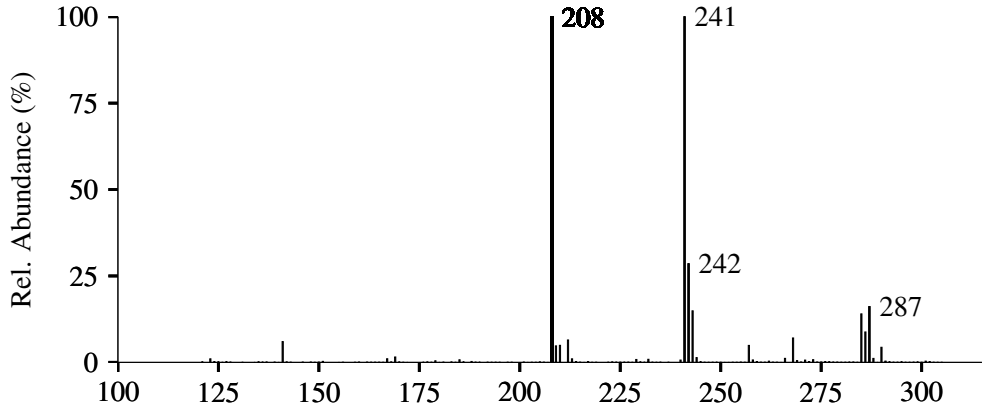

(b) methyl 4-hydroxybenzoate

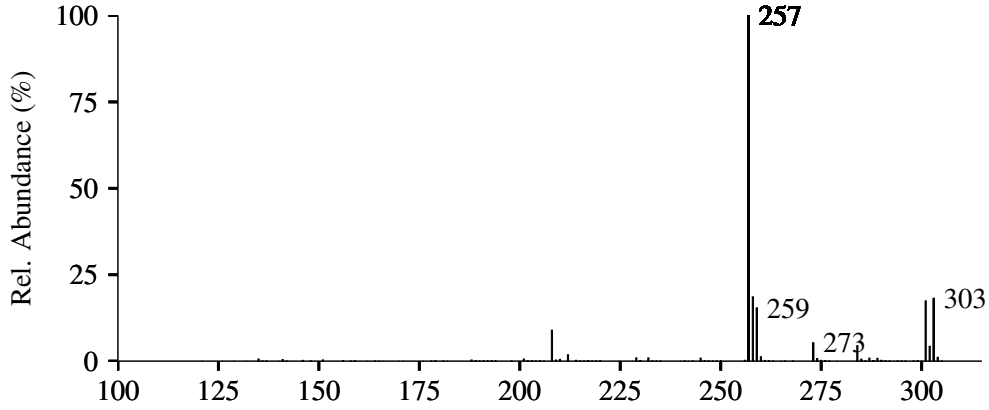

(c) 4-methylimidazole

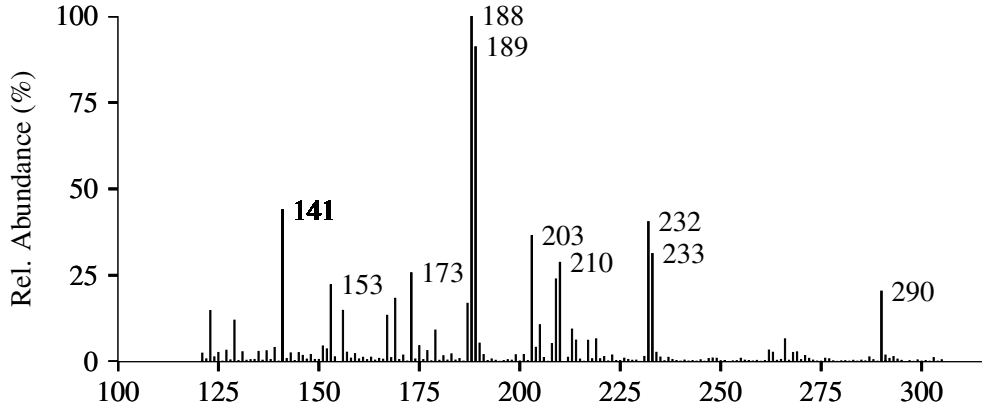

Figure S3.9. Continued.

References

(1) H. S. Fogler, *Essentials of Chemical Reaction Engineering 4th ed.*, Prentice Hall, Upper Saddle River, NJ, **2011**.

(2) W. A. Arnold, *Kinetics And Pathways Of Chlorinated Ethylene and Chlorinated Ethane Reaction with Zero-Valent Metals.*, Ph.D. thesis, Johns Hopkins University, Baltimore, MD, **2000**.

(3) W. A. Arnold, A. L. Roberts. Pathways and kinetics of chlorinated ethylene and chlorinated acetylene reaction with Fe(0) particles. *Environmental Science and Technology* **2000**, *34*, 1794–1805.

(4) A. E. Martell, R. M. Smith, R. J. Motekaitis, *Critically Selected Stability Constants of Metal Complexes Database; Version 8.0*, U.S. Department of Commerce, National Institute of Standards and Technology, Gaithersburg, MD, **2004**.

(5) W. Stumm, J. J. Morgan, *Aquatic Chemistry: Chemical Equilibria and Rates in Natural Waters 3rd ed.*, Wiley, New York, New York, **1996**.

(6) H. Demirelli, F. Köseoğlu. Solvent and Substituent Effects on the Protonation of Anilines in Dioxane–Water Mixtures. *Journal of Solution Chemistry* **2004**, *33*, 1501–1515.

(7) R. Arnaud. Acidity and Basicity Constants for some Dihydroxyacetophenones. *Bulletin de la Societe chimique de France* **1967**, 4541–4551.

(8) R. N. Goldberg, N. Kishore, R. M. Lennen. Thermodynamic quantities for the ionization reactions of buffers. *Journal of Physical and Chemical Reference Data* **2002**, *31*, 231–370.

(9) E. Pelizzetti, E. Mentasti, C. Baiocchi. Kinetics and mechanism of oxidation of quinols by hexachloroiridate(IV) in aqueous acidic perchlorate media. *Journal of Physical Chemistry* **1976**, *80*, 2979–2982.

(10) W. M. Clark, *Oxidation-Reduction Potentials of Organic Systems*, Williams & Wilkins, Baltimore, MD, **1960**.

(11) O. Bricker. Some Stability Relations in the System Mn-O_2-H_2O at 25°C and One Atmosphere Total Pressure. *American Mineralogist* **1965**, *50*, 1296–1354.

(12) T. J. Holmes, V. John, J. Vennerstrom, K. E. Choi. Solution characterization of carboxybenzoquinone and the isolation of derived quinhydrones. *The Journal of Organic Chemistry* **1984**, *49*, 4736–4738.

(13) J. D. Clemmer, G. K. Hogaboom, R. A. Holwerda. Reduction Of The Bis(2,9-Dimethyl-1,10-Phenanthroline)Copper(Ii) Ion By Substituted Hydroquinones. *Inorganic Chemistry* **1979**, *18*, 2567–2572.

(14) M. Uchimiya, *Electron Transfer Reactions Between Quinones and Iron in Aqueous Environments*, Ph.D. thesis, Johns Hopkins University, Baltimore, Maryland, **2006**.

Chapter 4

Permanganate Oxidation of Alkenes: Studying Product Distribution Using *cis*-Stilbenedicarboxylic Acid as a Convenient Model Compound

4.1 Introduction

Permanganate (MnO_4^-) is used in many ways in water treatment and environmental remediation (*1*). It is employed in a third of water treatment facilities in the United States. MnO_4^- can remove Mn^{II} and Fe^{II} from drinking water (*2*) as well as remedy taste and odor problems (*3*). MnO_4^- can be used to help remove arsenic from drinking water by oxidizing arsenite (As^{III}) to arsenate (As^{V}) which is more easily removed by precipitation or adsorption (*4*). It can remove precursors to trihalomethanes and other disinfection byproducts (*5*). It promotes coagulation and flocculation in waters with high organic content improving removal of organic carbon (*6*, *7*). MnO_4^- in-situ chemical oxidation can effectively treat many contaminants in the subsurface including chlorinated ethylenes (*8–10*), cyclotrimethylenetrinitramine (RDX, *11*, *12*), chlorophenols (*13*), and methyl-*tert*-butyl ether (*14*). Researchers are discovering that many pollutants that are effectively removed

by MnO_4^- including the cyanobacterial toxin microcystin-LR (*15–18*), estradiol related endocrine-disrupting compounds (*19*), the antibacterial triclosan (*20*), carbamazepine (*21*), ciprofloxacin, lincomycin, and trime- thoprim (*22*, *23*), and pesticides including aldrin, terbufos, metribuzin, permethrin (*24*), and dichlorvos (*25*).

In all of these situations, it is important to recognize (1) the impacts of solution conditions on the efficiency and efficacy of oxidation by MnO_4^- and (2) what the ultimate products are following treatment. Alkenes ($-C{=}C-$) are a simple MnO_4^- oxidizable functional group that occurs in many organic chemicals. We will employ *cis*-stilbenedicarboxylic acid (SDCA) as a model alkene to examine alkene oxidation by MnO_4^-. Using SDCA allows us to probe how pH and reactant concentrations affect kinetics and influence the ultimate product distribution in the laboratory instead of complicated environmental samples.

Alkenes oxidation by MnO_4^- is believed to occur via cyclic Mn^V intermediate that subsequently breaks down via multiple steps into the ultimate products (*26*). Rate expressions are reported to be first-order in both MnO_4^- and in alkene, have small positive enthalpies of activation, and large negative entropies of activation (*27–30*) implying an intermediate formed by attack of one MnO_4^- onto one alkene:

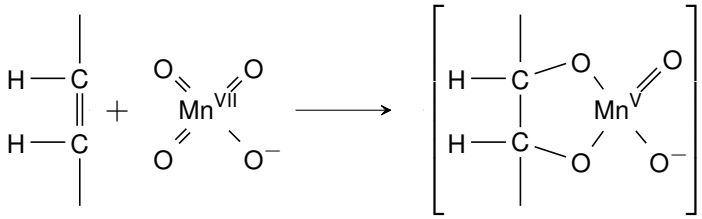

(4.1)

Solution pH within the range of aquatic environments can have a complex effect on alkene oxidation by MnO_4^-. For some compounds, a higher protonation state leads to an increase in reaction rate in the pH range 0.5-5. For example, for substituted maleic acids

the oxidation rate constant of the monoanion (HA^-) was faster than for the neutral (H_2A) or dianion (A^{2-}) species (*31–33*), which was attributed to hydrogen bonding in the monoanion leading to a more rigid planar structure (*33*). Conversely, for fumaric acids the order was $H_2A > HA^- > A^{2-}$ which was attributed to electrostatic effects (*34*). For *trans*-crotonic acid the neutral species reacts faster than the anion (*35*). However, no effect of pH on oxidation rate was observed for trichloroethylene (*10*) or carbamazepine (*21*) in environmentally relevant pH ranges.

The final product distribution depends on solution conditions, in particular pH and the ratio of alkene substrate and MnO_4^- concentrations will determine the dominant reaction pathway. Which products are ultimately generated depends on what reactions occur following the generation of the cyclic Mn^V intermediate. The intermediate can undergo further oxidation by MnO_4^-, intramolecular reactions, acid-base chemistry, or hydrolysis reactions.

An example of further oxidation by MnO_4^- is the formation of a cyclic Mn^{VI} intermediate (*30*, *36*, *37*):

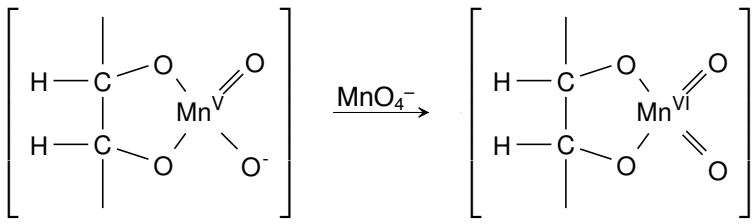

(4.2)

A Mn^{VI} intermediate reportedly formed during oxidation of cinnamic acid at acidic pH (*38*) and for bicyclo[2.2.1]-2-heptene (*39*). Lee and Brownridge (*38*) reasoned that because manganate ($Mn^{VI}O_4^{2-}$) is known to cleave diols, any cleavage of the diol-like cyclic Mn^{VI} intermediate would not occur until after Mn^V is oxidized to Mn^{VI}. To illustrate this point,

they added periodate (IO_4^-), which oxidizes any Mn^V to Mn^{VI}, increasing the yield of cleavage products.

We expect that excess MnO_4^- will favor oxidation by a second MnO_4^-. Wiberg and Saegebarth (*40*) reported UV spectral evidence for a Mn^{VI} intermediate with excess MnO_4^-. However, in the case of oleate and crotonate, a cyclic Mn^{VI} intermediate was reported when the concentration of the substrate was an order of magnitude greater than MnO_4^- (*30*).

A ketol product can be generated from either the Mn^V or Mn^{VI} intermediate (shown for an Mn^{VI} intermediate in Reaction 4.3). First, hydrolysis of the intermediate leads to an acyclic Mn ester. In Reaction 4.3, two-electron reduction of Mn^VI within the ester yields an Mn^{IV} product and the ketol (*39*, *41*).

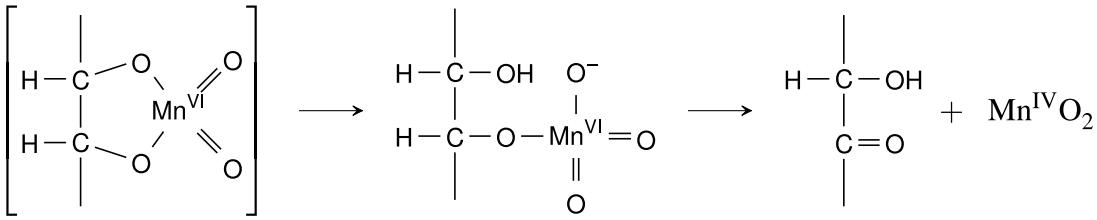

(4.3)

Overall, 4 electrons are transferred from the alkene substrate to MnO_4^-. Ketol products were favored at neutral pH for oleic acid (*39*), maleic acid and fumaric acid (*42*), and methylated uracil derivatives (*41*). The ketol product is not expected to form via oxidation of a diol, as was reported for oleate (*43*), uracil (*41*) and propylene glycol (*44*).

Excess MnO_4^- leads to a dione product. One proposed mechanism (*38*, *45*) involves oxidation of a tertiary hydrogen in the intermediate to a carbocation which is further oxidized

to the dione (Reaction 4.4).

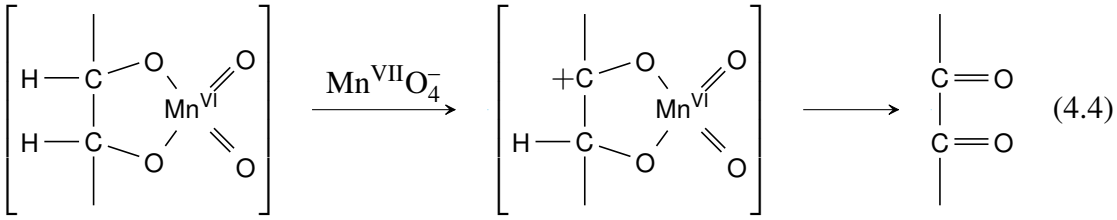

(4.4)

Note that MnO_4^- has been reported to oxidize tertiary hydrogens (*46*). Another possibility is that the dione can result from oxidation of the ketol (Reaction 4.5).

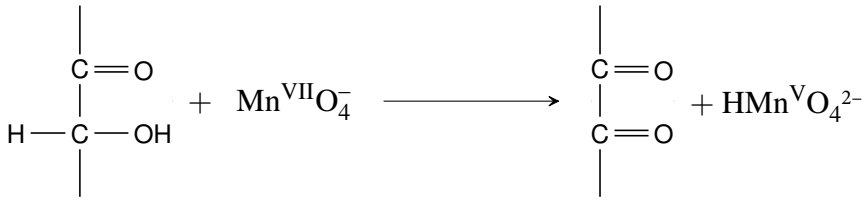

(4.5)

The dione product results from an overall 6 electron transfer from the alkene to MnO_4^-.

Breakdown of either the Mn^V or the Mn^{VI} cyclic intermediate can lead to two aldehyde products by cleaving the C−C bond (*26*). Two aldehyde products result from an overall 4 electron transfer from alkene substrate to MnO_4^-.

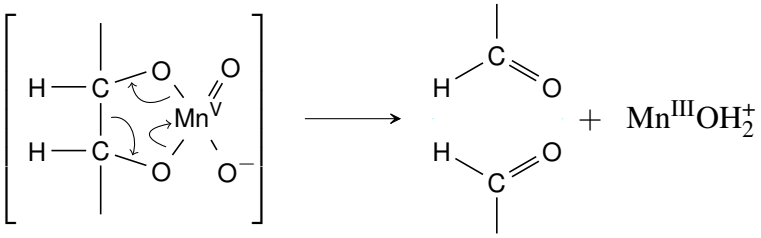

(4.6)

Breakdown of the Mn^V intermediate at acidic pH yielding aldehyde products was reported for acetylene carboxylic acid (*47*), crotonic acid (*35*), maleic acid and fumaric acid (*34*,

48), and cinnamic acid (*38*). Under highly acidic conditions, protonation of the cyclic hypomanganate ester accelerates decomposition (similar to Equation 4.6) by increasing the oxidation potential of Mn^{V} (*45*). UV/Vis spectra of the inorganic products match Rayleigh's law indicating that the inorganic product is particulate or colloidal $Mn^{IV}O_2$ (*27*, *29*). Mn^{III} does not disproportionate when chelated by pyrophosphate and is the ultimate MnO_4^- reduction product when pyrophosphate is present (*34*, *35*, *38*, *49*, *50*). However, in the absence of a chelating ligand disproportionation of Mn^{III} yields $Mn^{IV}O_2$ particles and Mn^{2+}(aq) (*37*).

Carboxylic acids are often reported as the final products of MnO_4^- oxidation of alkenes (*26*). MnO_4^- is known to oxidize aldehydes to carboxylic acids via a pathway where loss of the aldehydic hydrogen is thought to represent the rate-determining step (*51–55*). This reaction can be acid catalyzed

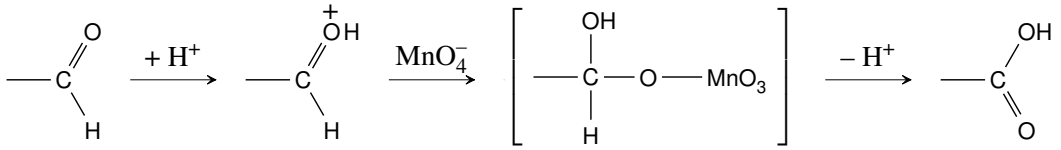

(4.7)

or base catalyzed (*52*, *55*).

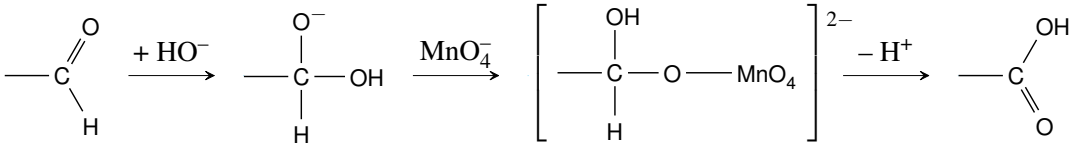

(4.8)

Oxidation of an alkene resulting in C=C bond cleavage and two carboxylic acid final products is an overall 8 electron transfer to MnO_4^- from the alkene substrate.

A diol product can be formed from hydrolysis of either the Mn^{V} or Mn^{VI} cyclic ester intermediate (Equation 4.9). Diol products have been reported from MnO_4^- oxidation of cycloalkanes (*27*, *56–58*), uracils (*41*), bicyclo[2.2.1]-2-heptene (*39*), stilbene (*58*), and oleate (*43*, *59*). At alkaline pH, the high concentration of OH^- favors hydrolysis of the cyclic Mn^{V} intermediate. The diol product forms by an overall 2 electron transfer from the alkene to MnO_4^-.

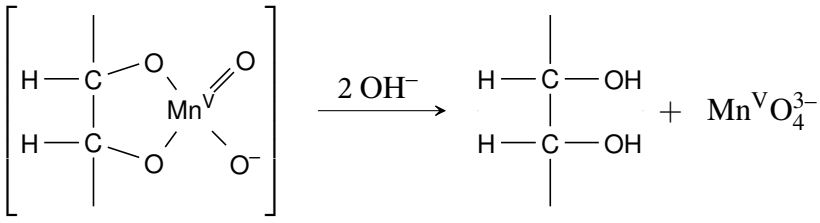

$$+ \quad Mn^{V}O_4^{3-} \qquad (4.9)$$

To summarize, consider that the stoichiometry of MnO_4^- and alkene substrate depends on the number of electrons transferred to form the ultimate reaction products. The possible alkane oxidation products we are considering are two carboxylic acids (resulting from cleavage of the C=C bond), one carboxylic acid and one aldehyde, two aldehydes, dione, ketol, and diol. The MnO_4^- reduction products we will consider are MnO_2(s), MnOOH(s) and Mn^{2+}(aq). Half-reactions show the number of electrons required to oxidize and alkene to each product (Reactions S4.1 – S4.6 in the Supporting Information) and the number required to reduce MnO_4^- to each of the three reduction products (Reactions S4.7 – S4.9 also in the Supporting Information). Note that these reactions are valid for any alkene substrate. Each pair of oxidation and reduction products result in a different number of electrons transferred from the substrate to MnO_4^-. As an example, the half-reaction for oxidation of

an alkene to two carboxylic acids is an 8 electron oxidation of the alkene substrate.

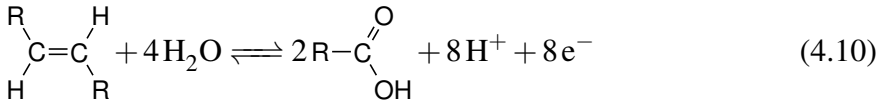

(4.10)

The half-reaction for reduction of MnO_4^- to MnO_2 is a 3 electron reduction of MnO_4^-.

$$MnO_4^-(aq) + 4H^+(aq) + 3e^- \rightleftharpoons Mn^{IV}O_2(s) + 2H_2O \tag{4.11}$$

From the balanced reaction the stoichiometry of moles of MnO_4^- consumed to moles of alkene consumed can be determined to be 2.67.

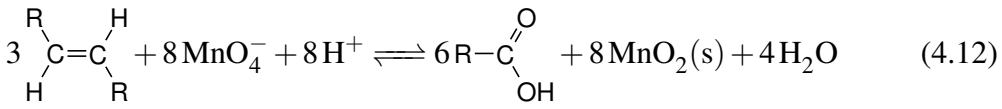

(4.12)

Table 4.1 summarizes the balanced redox reactions by tabulating mole of MnO_4^- consumed per mole of alkene consumed for all combinations of organic oxidation products and inorganic reduction products. The balanced reactions are shown in the Supporting Information (Reactions S4.10 – S4.27).

The number moles of MnO_4^- required is greater when MnO_2 is product because it results from 3 electron reduction where MnO_2 results from 5 electron reduction. The largest value on Table 4.1 corresponds to two carboxylic acids and MnO_2 as the products, and the smallest is for the diol and Mn2+(aq). The high and low values correspond to the greatest and least extent of oxidation of alkene and most and least number of moles of MnO_4^- required to generated the products. In an actual reaction mixture the number of moles consumed per alkene will fall within this range.

In this study we employ *cis*-Stilbenedicarboxylic acid (SDCA) as a model alkene. SDCA is an ideal model compound because it is commercially available, it is at least somewhat

water soluble, it reacts on an observable time-scale, and it some of its oxidation products are commercially available or synthesizable. SDCA has carboxylic acid functional groups that make it and its expected MnO_4^- oxidation products amenable to detection by liquid-chromatography and mass-spectrometry (LC/MS) with electrospray ionization.

Figure 4.1 shows the structure of SDCA and the anticipated MnO_4^- oxidation products. Authentic standards are available for the C=C double bond cleavage products: 4-carboxybenzaldehyde and terephthalic acid. Authentic standards are not available for the diol, ketol, and dione products, but peak areas can be reported from LC/MS analysis.

In this study, we show that SDCA can be used to study how solution conditions affect the final product distribution from MnO_4^- oxidation of alkenes: in particular pH and the ratio of MnO_4^- and SDCA concentration. We will compare the product distribution resulting from one set of solution conditions to another by analyzing the oxidation products of SDCA by LC/MS and by investigating Mn speciation using a modified iodometric titration method. We will conduct both time-course and reaction quench experiments to explore both kinetics and product distribution.

4.2 Materials and Methods

All aqueous solutions were prepared from reagent grade chemicals and distilled, deionized water (Milli-Q water, 18 MΩ-cm resistivity, Millipore Corp., Milford, MA). All bottles and glassware were rinsed with distilled water, soaked in 5 M nitric acid overnight, rinsed with distilled water and Milli-Q water and then air-dried.

4.2.1 Chemicals

Ascorbic acid and 3-(N-morpholino)propanesulfonic acid (MOPS) were purchased from Sigma (St. Louis, MO). Sodium acetate, terephthalic acid, and benzoic acid were purchased from Aldrich (St. Louis, MO). 4,4′-*cis*-Stilbenedicarboxylic acid (SDCA), 4-carboxybenzaldehyde, and hydroxylamine hydrochloride were purchased from Alfa Aesar (Pelham, NH). NaCl was purchased from Acros Organics (Fair Lawn, NJ). HCl and LC/MS Optima grade methanol were purchased from Fisher Scientific (Pittsburgh, PA). Potassium permanganate ($KMnO_4$), sodium hydrogen carbonate ($NaHCO_3$), and ammonium acetate were purchased from Fluka (Buchs, Switzerland). Sodium thiosulfate ($Na_2S_2O_3$), sodium hydroxide (NaOH), potassium iodide (KI), dibasic anhydrous sodium phosphate (Na_2HPO_4), and acetic acid were purchased from J. T. Baker (Phillipsburg, NJ).

4-Carboxybenzaldehyde oxime was synthesized using the following procedure. An excess of hydroxylamine hydrochloride (2 g) was added to a continuously stirred solution of 4-carboxybenzaldehyde (0.545 g) dissolved in 100 mL of 0.1 M NaOH in an Erlenmeyer flask. The solution was left to react for 24 hrs. Then, 5 M HCl was added to lower the pH below 3, where the oxime product precipitates but unreacted hydroxylamine remains dissolved. Crystals of the oxime were collected by vacuum filtration, washed with 0.1 M HCl, and rinsed with Milli-Q water, and allowed to air dry until the mass of crystals and filter paper no longer decreased due to evaporation of water. This method gave 0.431 g of product or 86% yield. LC/MS analysis of a 50 μM aqueous solution of the product crystals yielded one peak with m/z corresponding to 4-carboxybenzealdehyde oxime.

4.2.2 Reaction Medium and Experimental Design

All experiments were performed in 100 mL polypropylene bottle reactors placed in a 25 $\pm$ 1°C constant temperature bath. Reaction solutions were continuously stirred with Teflon-coated stir bars and sparged with N_2(g). The N_2(g) sparge line is bubbled through water before reaching the experimental solution to minimize evaporation of the solution. Before every experiment, fresh stock solutions of SDCA, $KMnO_4$, NaCl, and the buffer of interest were prepared in Milli-Q water. Solutions contained 5.0 mM acetate to maintain pH between 4.0 and 5.0, 5.0 mM phosphate at pH 7.0, and 5.0 mM carbonate at pH 10.0. NaCl was added to set the ionic strength. For comparison purposes, some pH 7.0 experiments were performed without added buffer. Instead HCl and NaOH additions were used to maintain pH. All buffer stock solutions were adjusted to desired pH with NaOH or HCl before adding to reactors.

A quenching method was used because the reaction between SDCA and MnO_4^- was too fast to be observed directly using LC/MS. Hydroxylamine (NH_2OH) reduces MnO_4^- to Mn^{2+} (*60*), which quenches the samples before they are analyzed by LC/MS. NH_2OH is oxidized by MnO_4^- to nitrite and nitrous oxide in strongly alkaline solution, nitric acid in strong acidic solution, and nitrogen gas under "weakly alkaline" conditions (*60*). Samples were taken by pipetting a 1 mL aliquot from the reactor to an autosampler vial containing 100 μL of "quench solution." The quench solution consisted of 11.3 mM hydroxylamine, 300 μM benzoic acid, and 111 mM phosphate buffer adjusted to pH 7.0 and was prepared freshly before each experiment. The vials were shaken vigorously and analyzed by LC/MS. Control experiments showed that SDCA and terephthalic acid did not react with the agents in the quenching solution. Concentrations and peak areas detected by LC/MS did not change after quenching for up to two days of storage time. Benzoic acid serves as an LC/MS

internal standard. Hydroxylamine reacts with 4-carboxybenzaldehyde to form an oxime; the oxime was detected by LC/MS using a synthesized standard. No 4-carboxybenzaldehyde was detected in any experimental sample indicating that it was completely derivatized to the oxime. For simplicity, the concentration of 4-carboxybenzaldehyde oxime will be reported as 4-carboxybenzaldehyde from here on.

4.2.3 Time Course Experiments and Kinetic Analysis

A series of time course experiments was performed using solutions of SDCA, NaCl, and buffer of interest which were prepared as described above. The stock of MnO_4^- was added last to initiate reaction. Samples were taken periodically, quenched, and analyzed by LC/MS. No concentration data was collected for MnO_4^- or other Mn compounds. The concentration of SDCA, terepthalic acid, and 4-carboxybenzaldehyde were determined by LC/MS. The concentration of the ketone, diol, and dione products were determined by considering the mass balance. The following mass balance expression equates the SDCA initially added to the solution ($[SDCA]_0$) to the sum of any SDCA remaining at the time of quenching and the oxidation products.

$$[SDCA]_0 = [SDCA] + 0.5[\text{4-carboxybenzaldehyde}] + 0.5[\text{terephthalic acid}] + [\text{ketol}] + [\text{dione}] + [\text{diol}] \quad (4.13)$$

4-Carboxyaldehyde and terephthalic acid arise from cleavage of the carbon-carbon double bond in SDCA. Because SDCA is symmetric, two molecules of 4-carboxybenzaldehyde are generated for each SDCA that is cleaved. The stoichiometric ratio is represented by the coefficient of 0.5 in Equation 4.13. A coefficient of 0.5 is also required for terephthalic acid because of the one-to-one stoichiometry of 4-carboxybenzaldehyde oxidation to terephthalic

acid. LC/MS analysis of calibration standards of SDCA, 4-carboxybenzaldehyde, and terephthalic acid demonstrate that concentration was linearly related to peak area. For these three compounds, the slope of the calibration curve was determined using the standards. Equations 4.14 – 4.16 assume that concentration is linearly related to peak area for the ketol, dione, and diol oxidation products.

$$[\text{ketol}] = m_{\text{ketol}} A_{\text{ketol}} \tag{4.14}$$

$$[\text{dione}] = m_{\text{dione}} A_{\text{dione}} \tag{4.15}$$

$$[\text{diol}] = m_{\text{diol}} A_{\text{diol}} \tag{4.16}$$

where m_{i} is the slope of the calibration curve for compound i and A_{i} is the peak area for i. Substituting Equations 4.14 – 4.16 into Equation 4.13 gives

$$\begin{aligned}[\text{SDCA}]_0 = {} & [\text{SDCA}] + 0.5[\text{4-carboxybenzaldehyde}] + \\ & 0.5[\text{terephthalic acid}] + m_{\text{ketol}} A_{\text{ketol}} + m_{\text{dione}} A_{\text{dione}} + m_{\text{diol}} A_{\text{diol}}\end{aligned} \tag{4.17}$$

Equation 4.17 can be used to determine best-fit values of each slope by nonlinear least-squares regression where the three slopes are the fitting parameters. The slopes were assumed to be constant for all samples analyzed on the same day. Duplicate analysis of standards for SDCA, 4-carboxybenzaldehyde, and terephthalic acid show that the slopes for these compounds do not change significantly when samples are analyzed on the same day. It was assumed that the slopes for ketol, dione, and diol would also be consistent within the same day. A system of equations was set up consisting of a version of Equation 4.17 for each sample collected and analyzed on the same day by incorporating concentration data for SDCA, 4-carboxybenzaldehyde, and terephthalic acid and peak area of ketol, dione, and

diol. Optimal values for each slope were determined using the Solver tool within Microsoft Excel (*61*). Values were selected that most closely achieved mass balance and that, were all greater than or equal to zero, and that resulted in concentrations of ketol, dione, and diol that made physical sense.

In a separate experiment, the kinetics of MnO_4^- oxidation of 4-carboxybenzaldehyde to terephthalic acid were investigated using solutions prepared identically to the solutions above, except that the substrate was changed from SDCA to 4-carboxybenzaldehyde. Concentrations of 4-carboxybenzaldehyde and terephthalic acid were monitored using the hydroxylamine quenching method and LC/MS. Pseudo-first-order kinetic modeling was used to determine the rate constant because the concentration of MnO_4^- was more than an order of magnitude greater than the concentration of 4-carboxybenzaldehyde.

4.2.4 Reaction Quench Experiments and Oxidizing Equivalents

A second series of experiments was conducted where reaction was initiated by MnO_4^- addition and allowed to proceed for 30 min in order to test product distribution and reaction stoichiometry under varying pH conditions. Reaction solutions were prepared as above. Following the reaction time, one 100 μL aliquot of the reaction slurry was quenching solution as described above and analyzed by LC/MS determine concentration of SDCA, terephthalic acid, 4-carboxybenzaldehyde, and peak areas of ketol, diol, and dione. Iodometric titration (*62*) was adapted to determine the number of oxidizing equivalents (OE) in an unfiltered and filtered aliquot, where OE is the number of moles of electrons per liter of sample slurry or solution obtained by reducing all oxidants to their fully reduced forms by addition of a reductant. Iodometric titration has been used previously to determine the average oxidation state of $Mn^{III,IV}$ (hydr)oxide solids (*63*). Here, iodide was used to reduce MnO_4^-,

Mn^{IV}, and Mn^{III} to Mn^{2+}, which also quenches the sample. Concentrations or loadings of Mn^{VI} and Mn^{V} were assumed to be negligible. Reaction of MnO_4^- in excess iodide (I^-) at acidic pH proceeds quantitatively to Mn^{2+} (*64*, *65*). I^- is oxidized to iodine (I_2), which forms triiodide ion (I_3^-) in the presence of excess I^- (*64*). Hypoiodous acid (HOI) and periodate (IO_4^-) can also be products of MnO_4^- oxidation of I^-, but excess I^- and acidic pH are expected to favor I_3^- (*64*). In tests, no change was detected in the concentration of SDCA, 4-carboxybenzaldehyde, terephthalic acid or peak area of ketol, diol, or dione that resulted from any step of iodometric analysis that could not be accounted for by dilution.

Iodometric titration was performed on 2 aliquots of each reaction slurry. The analysis of samples is depicted as a flow chart in the supporting information (Figure S4.3). For the first aliquot, approximately 15 mL of slurry were filtered into a flask using a 0.2 μm pore diameter track-etched polycarbonate filter membranes (Whatman, UK). A 10 mL aliquot of this filtered solution was pipetted into to an Erlenmeyer flask. This aliquot served as the filtered sample. A second 10 mL aliquot of the reaction slurry was pipetted into a second Erlenmeyer flask and served as the unfiltered sample. To each flask, 500 μL of 1 M HCl and 0.5 gram of KI was added, yielding a yellow or brown solution. The resulting solutions were titrated with 1 mM sodium thiosulfate ($Na_2S_2O_3$). Just before reaching the colorless endpoint, several drops of 1 % starch solution were added resulting in a blue solution. More $Na_2S_2O_3$ titrant was added until the endpoint was reached.

OE is related to concentration of MnO_4^-, Mn^{IV}, and Mn^{III} by the number of electrons transferred in the half-reaction representing reduction to Mn^{2+}:

$$MnO_4^-(aq) + 8H^+(aq) + 5e^- \rightleftharpoons Mn^{2+}(aq) + 4H_2O \tag{4.18}$$

$$Mn^{IV}O_2(s) + 4H^+(aq) + 2e^- \rightleftharpoons Mn^{2+}(aq) + 2H_2O \tag{4.19}$$

$$Mn^{III}OOH(s) + 3H^{+}(aq) + e^{-} \rightleftharpoons Mn^{2+}(aq) + 2H_2O \tag{4.20}$$

Before any reaction with SDCA occurs, all of the OE are present as MnO_4^-. Initial OE (OE_0) can be calculated from $[MnO_4]_0$:

$$OE_0 = 5[MnO_4^-]_0 \tag{4.21}$$

Also consider the Mn mass balance equation:

$$Mn_{TOT} = [MnO_4^-]_0 = [MnO_4^-] + [Mn^{IV}] + [Mn^{III}] + [Mn^{2+}] \tag{4.22}$$

where Mn_{TOT} is the total amount of manganese present in the slurry. Combining Equations 4.21 and 4.22 gives the following expression for OE initially present in the solution:

$$OE_0 = 5[MnO_4^-]_0 = 5[MnO_4^-] + 5[Mn^{IV}] + 5[Mn^{III}] + 5[Mn^{2+}] \tag{4.23}$$

The OE measured in the unfiltered sample represents residual MnO_4^-, and any Mn^{IV} or Mn^{III} in the suspension

$$OE(\text{unfiltered}) = 5[MnO_4^-] + 2[Mn^{IV}] + [Mn^{III}] \tag{4.24}$$

where OE(unfiltered) is the number of oxidizing equivalents determined by iodometric titration of the unfiltered sample. The coefficients in Equation 4.24 arise from Equations 4.18, 4.19, and 4.20. In the filtered sample, the measured OE are assumed to arise from

MnO_4^-. The residual MnO_4^- concentration can be calculated using Equation 4.25.

$$OE(\text{filtered}) = 5[MnO_4^-] \tag{4.25}$$

Combining Equations 4.21 and 4.25 yields the amount of MnO_4^- (in concentration units) that had been consumed by the quench time:

$$MnO_4^-(\text{consumed}) = \frac{OE_0 - OE(\text{filtered})}{5} \tag{4.26}$$

Subtracting OE(filtered) from OE(unfiltered) gives the OE from Mn^{III} and Mn^{IV} particles that are trapped by the filter.

$$OE(\text{particulate}) = OE(\text{unfiltered}) - OE(\text{filtered}) = 2[Mn^{IV}] + [Mn^{III}] \tag{4.27}$$

Finally, subtracting Equation 4.24 from Equation 4.23 gives the number of OE that were transferred during the alotted reaction time.

$$OE(\text{transferred}) = OE_0 - OE(\text{unfiltered}) = 3[Mn^{IV}] + 4[Mn^{III}] + 5[Mn^{2+}] \tag{4.28}$$

This method has some limitations. The OE assigned to Mn^{III} and Mn^{IV} depend on the filter cutoff size. Thus OE(particulate) can only be operationally defined and would not account for any particulates that pass through the filter. Other solution constituents can stabilize or destabilize the $Mn^{III,IV}$ (hyrdr)oxide solid particles against aggregation impacting whether or not they are removed by filtration. For example, pyrophosphate can chelate Mn^{III} (*66*) forming a dissolved complex that would pass through the filter. Any Mn^{III} and Mn^{IV} that pass through the filter would be reported as MnO_4^-.

Electron equivalents of SDCA oxidized can be calculated by considering the stoichiometry and number of electrons transferred in each half-reaction shown in Table 4.1 and the product calculations determined using Equation 4.17. These equivalents will be called reducing equivalents (RE) to contrast them with OE described above.

$$\begin{aligned} \text{RE(transferred)} = 4[\text{terephthalicacid}] + 2[\text{4-carboxybenzaldehyde}] + \\ 6[\text{dione}] + 4[\text{ketol}] + 2[\text{diol}] \end{aligned} \tag{4.29}$$

4.2.5 Instrumental Analysis

Concentrations of the SDCA, 4-carboxybenzaldehyde oxime, and terephthalic acid as well as peak areas of ketol, diol, and dione oxidation products were determined by LC/MS. Benzoic acid served as an internal standard. The LC/MS system consisted of a Waters 2795 Alliance separation module and a Micromass Quattro Micro Triple Quadrupole Mass Spectrometer (Waters, Milford, MA). Separation was achieved using a Waters Atlantis T3 column (4.6 x 100 mm, 5 μm particle size). Gradient elution at a flow rate of 1 mL min^{-1} was used where mobile phase A was 0.2% v/v acetic acid adjusted to pH 4.0 by addition of ammonium hydroxide and mobile phase B was methanol. The gradient run method was: 0–6 min 10% B, 6–9 min increase to 80% B, and 9–9.5 min decrease to 10% B. The mass spectrometer was equipped with an electrospray ion source, which was operated in negative mode. All compounds were detected based on their molecular ions ($[M\text{-}H]^-$). The cone voltage setting was between -25 and -15 V depending on the analyte. Single ion recording mode was used to detect each compound set to the mass to charge ratio (m/z) of the molecular ion, the values used for SDCA and each product are given in Figure 4.1.

4.3 Results

4.3.1 Time Course Experiments

Hydroxylamine quenching made it possible to investigate the kinetics of 20 μM SDCA oxidation by MnO_4^- (Figure 4.2). A MnO_4^- concentration of 200 μM lead to complete consumption of SDCA within 10 minutes of reaction. At 20 μM MnO_4^-, only 15 μM of SDCA was consumed; 5 μM SDCA remained after 1 hour of reaction. Any effects of buffer identity or pH (performed at pH 5.0, 7.0, and 10) were too small to discern using the quenching technique. In control experiments lacking MnO_4^-, no loss of SDCA was detected at pH 7.0 (with or without 5 mM phosphate buffer) or pH 10.0 (5 mM carbonate buffer); however, at pH 5.0 (5 mM acetate buffer) approximately 18% loss of this model alkene was observed (Figure S4.4 in the Supporting Information).

Terephthalic acid, 4-carboxybenzaldehyde, ketol and dione we detected in solutions of 20 μM SDCA 200 μM MnO_4^- in 5 mM acetate (pH 5.0) buffered solutiom with ionic strength adjusted to 10 mM with NaCl (Figure 4.3). As in Figure 4.2, SDCA was consumed in less than 10 minutes. LC/MS evidence suggests that aldehyde, acid, ketol, and dione are the only significant products at pH 5.0. Aldehyde and ketol oxidation products reach a maximum concentration between 5 and 10 min then decrease somewhat over the remaining contact time. After 1 hour, aldehyde and ketol were the major products. The concentration of dione and carboxylic acid products increased gradually over time.

The hydroxylamine quench method was also used to monitor loss of 20 μM SDCA with increasing the concentration of MnO_4^- (Figure 4.4). These solutions also contained 5.0 mM acetate adjusted to pH 4.0 and 10 mM ionic strength adjusted by addition of NaCl. SDCA was completely consumed within 11 min at MnO_4^- concentrations greater than 170 μM. The

dependence of aldehyde, ketol, and acid product concentration on initial concentration of MnO_4^- was complex. For ketol and aldehyde, the 11 min concentration was greater at 170 and 85 μM Mn_{04}^- than at 42 or 218 μM Mn_{04}^-. For terephthalic acid, both the initial rate of generation and the 11 min concentration did not change with increasing concentration of MnO_4^-, except that a slightly higher 11 min concentration was detected when $[MnO_4^-]_0$ was 85 μM than at the other concentrations tested.

In Figure 4.3, only 2.5 μM of terephthalic acid was detected after 60 min, which is consistant with a rate of oxidation of the 4-carboxybenzaldehyde to terephthalic acid that is significantly slower than the rate of oxidation of SDCA. We can directly observe the rate of this reaction experimentally because authentic standards are available for both the 4-carboxybenzaldehyde and terephthalic acid. We monitored the loss of 4-carboxybenzaldehyde and generation of terephthalic acid with $[Mn_4^-]_0$ of 200 and 400 μM in 5 mM acetate (pH 5.0) with ionic strength adjusted to 10 mM using NaCl (Figure 4.5). When $[MnO_4^-]_0$ was 200 μM (as in Figure 4.3) the half-life was approximately 160 min. Doubling $[MnO_4^-]_0$ to 400 μM shortened the half-life to 80 min. The rate constant was determined to be $k = 3.6 \pm 0.6 \times 10^{-1}$ M^{-1} s^{-1} by regression using a pseudo-first-order kinetic model. Excellent mass balance was maintained throughout both experiments. In a separate experiment, 400 μM MnO_4^- and 20 μM terephthalic acid were added to a solution containing 5.0 mM acetate buffer (pH 5.0) with ionic strength adjusted to 10.0 mM using NaCl. No loss of terephthalic acid was observed using the quenching method over 5 hours of reaction.

4.3.2 Reaction Quench Experiments and Oxidizing Equivalents

Concentrations of residual MnO_4^- and the $Mn^{III,IV}$ solids and Mn^{2+}(aq) generated after 30 min was measured using iodometry in a series of experiments employing SDCA. In Figure 4.3B, manganese speciation was determined for one time point in the reaction, at 30 minutes. When $[MnO_4^-]_0$ is 200 μM, the total number of oxidizing equivalents added is 1 mEq L^{-1}. After 30 min, OE(filtered) was 710 μEq L^{-1}. The filtered sample corresponds to 142 μM MnO_4^- meaning that 58 μM of MnO_4^- was consumed after 30 min. OE(particulate), representing Mn^{III} and Mn^{IV} particulates removed by filtration, accounted for 199 μEq L^{-1}. The remaining oxidizing equivalents 91 μEq L^{-1} were transferred during MnO_4^- oxidation of SDCA.

MnO_4^- was added to 20 μM of SDCA solutions and were quenched after 30 min. Manganese speciation and organic product yield are shown in Figure 4.6, and in tabular form in the supporting information (Table S4.3). Five buffer systems were employed: 5.0 mM acetate (pH 5.0), 5.0 mM phosphate (pH 7.0), 5.0 mM pyrophosphate (pH 7.0), pH 7.0 maintained by adding small amounts of HCl or NaOH (termed "unbuffered"), and 5.0 mM carbonate (pH 10). There was significant OE(particulate) measured in the pH 5.0 buffer and at pH 7 in the absence of buffer, but not in the pH 10.0 buffer or at pH 7.0 in either phosphate and pyrophosphate buffer. No OE(filtered) was detected in pH 5.0 and pH 7.0 (unbuffered) solutions when $[MnO_4^-]_0$ was 20 μM or less. At the 30 minute quench time, pH 5.0, pH 7.0 (unbuffered) and pH 7.0 (5 mM phosphate) samples were brown, but pH 7.0 (5 mM pyrophosphate) and pH 10.0 were red.

Aldehyde and ketol were the major organic oxidation products detected at the 30 minute quench time for all pH and buffer systems tested (Figure 4.6). Figure 4.6 shows the products by contribution to mass balance based on Equation 4.13, these data are shown as concen-

tration versus initial MnO_4^- concentration in Figure S4.5 in the Supporting Information. Regardless of pH and buffer identity, all SDCA was consumed at $[MnO_4^-]_0$ greater than 40 μM. The 30 minute concentrations of ketol and 4-carboxybenzaldehyde were the largest in solutions with 40 μM initial concentration of MnO_4^-. At $[MnO_4^-]_0$ greater than 40 μM, the 30 minute concentration of 4-carboxybenzaldehyde decreased with increasing $[MnO_4^-]_0$, with the exception of the absence of buffer at pH 7.0. Ketol concentration did not decrease at $[MnO_4^-]_0$ higher than 40 μM. Terephthalic acid was detected in all buffer systems, but the concentration did not exceeded 3.5 μM. No significant concentration of the dione or diol was detected.

OE(transferred) and RE(transferred) after 30 minutes of contact time are compared in Table 4.2. The values of OE(transferred) are typically similar or larger than RE(transferred) at high concentrations of MnO_4^-. RE(transferred) was larger than OE(transferred) at low MnO_4^-.

Regardless of pH the ratio of MnO_4^- consumed to SDCA consumed increased with increasing concentration of MnO_4^- (Figure 4.7A) except for the solution adjusted to pH 7.0 without a buffer with 10 μM initial concentration of MnO_4^-. The presence of 5.0 mM carbonate (pH 10.0) or 5.0 mM pyrophosphate (pH 7.0) kept the MnO_4^- to SDCA consumption ratio near 1, but the ratio was higher for pH 7.0 (5.0 mM phosphate), pH 5.0 (5.0 mM acetate), and pH 7 in the absence of a buffer (Figure 4.7), with no ligand present some MnO_4^- was reduced to $Mn^{III,IV}$ solids. Solid formation was also favored at pH 5.0 (Figure 4.6).

The ratio of OE(transferred) to SDCA consumed (Figure 4.7B) also generally increased with increasing concentration of MnO_4^-. The unbuffered pH 7.0 solution had the highest values for both ratios. The 5.0 mM acetate (pH 5.0) solution had the second highest values

for the ratio of MnO_4^- consumed to SDCA consumed (Figure 4.7A), but the lowest values for the ratio of OE(transferred) to SDCA consumed (Figure 4.7B).

4.4 Discussion

We expect that oxidation of SDCA by MnO_4^- occurs in a series of steps. The first step is formation of an intermediate that we could not detect. The first intermediate is expected to be the cyclic Mn^V intermediate shown in Figure 4.1. The second step is one of two reactions: the reaction that generates 4-carboxybenzaldehyde from the intermediate or the reaction that generates ketol from the intermediate.

If 4-carboxybenzaldehyde is the product of the second step, then the third step is oxidation of 4-carboxybenzaldehyde to terephthalica acid. For ketol, the thirds step is oxidation of ketol to dione. We will examine how our experimental results support this proposed scheme and consider the effect of pH and the concentration of MnO_4^-.

Solution pH did not influence the rate of the first step, Figure 4.2, at both initial concentrations of MnO_4^-. The lack of pH effect on substrate consumption rate was also reported for trichloroethylene (*10*) and carbamazepine (*21*). MnO_4^- has a pK_a of MnO_4^- is -2.24 (*67*) and exists as an anion at all pH we tested.

The first proposed reaction step involves both SDCA and MnO_4^- and accordingly the rate of SDCA consumption increased with increasing concentration of MnO_4^- (Figure 4.2 and Figure 4.4). However, the stoichiometry is greater than one to one: on the time scales we considered (less than 60 minutes) 20 μM SDCA was not completely consumed in solutions of 20 μM MnO_4^-. MnO_4^- is expected to be involved in the second and third steps, which could consume MnO_4^- before SDCA is completely consumed.

The consumption of SDCA, generation of 4-carboxybenzaldehyde and generation of ketol represent reactions that generate and consume the first intermediate. In Figure 4.3A the concentration of SDCA fell below the detection limit in less than 10 min while the aldehyde and ketol oxidation products reached their highest concentration on roughly the same time scale. These similar rates of generation and consumption are indicative of the short-lived nature of the cyclic Mn^{V} intermediate.

We would expect that the rates of the two possible reactions that happen in the second step (either oxidation of the cyclic Mn^{V} intermediate to either ketol or two molecules of 4-carboxybenzaldehyde) would also increase with increasing MnO_4^- concentration. However, Figure 4.4 contains peculiar results for 4-carboxybenzaldehyde and ketol. The highest MnO_4^- concentration did not yield the highest 11 minute concentration of ketol, 4-carboxybenzaldehyde, or terephthalic acid. Perhaps 4-carboxybenzaldehyde and ketol are quickly oxidized at the highest concentration of MnO_4^- at pH 4.0, but this was not observed at pH 5.0 (Figure 4.3). Significantly higher concentration of terephthalic acid was observed at pH 4.0 (Figure 4.4 than at any other pH we tested (Figure 4.6). We speculate that low pH would promote terephthalic acid generation. Toland et al. (*68*) reported that oxidation of SDCA with permanganate yielded terephthalic acid "almost quantitatively."

Solution pH did not significantly influence the distribution of organic products (Figure 4.6). Perhaps pH outside of the range 5.0 $<$pH $<$10.0 would be required to observe a significant influence of pH on both the reaction rate and the distribution of products.

The subsequent oxidation steps leading to final products may be much slower than oxidation of SDCA. The rate of 4-carboxybenzaldehyde oxidation depends on the initial concentration of MnO_4^- (Figure 4.5). This is reflected in the decrease of 4-carboxybenzaldehyde concentration and increase of Terephthalic acid concentration at initial MnO_4^- concentrations

greater than 40 μM: In Figure 4.6, increasing the concentration of MnO_4^- lead to greater oxidation of 4-carboxybenzaldehyde to terephthalic acid.

In our proposed scheme, 4-carboxybenzaldehyde is generated from the cyclic intermediate and consumed by oxidation to terephthalic acid. The generation step is fast, leading to a maximum concentration in 3.5 minutes in Figure 4.3. After reaching a maximum, the 4-carboxybenzaldehyde concentration slowly decreases which we attribute to oxidation of 4-carboxybenzaldehyde. The concentration of 4-carboxybenzaldehyde decreases by 1.85 μM between the maximum and 60 minutes. Over the same time period (3.5 to 60 minutes), terephthalic acid concentration increases by 1.54 μM. The close agreement in these values is consistent with the slow oxidation of 4-carboxybenzaldehyde to terephthalic acid, which we also observed directly in solutions of 4-carboxybenzaldehyde and MnO_4^-.

Concentrations of 4-carboxybenzaldehyde in 30 minute quench experiments (Figure 4.6) also reflect that the oxidation of 4-carboxybenzaldehyde by MnO_4^- to terephthalic acid is slow and dependent on the concentration of MnO_4^-. Regardless of pH and buffer identify, only small concentrations of terephthalic acid were observed after 30 minutes. The concentration of 4-carboxybenzaldehyde in Figure 4.6 decreased at high concentrations of MnO_4^-, consistent with more oxidation to terephthalic acid in the same time period. If more contact time had been allowed, we would expect larger concentration of terephthalic acid and lower concentration of 4-carboxybenzaldehyde.

The time course for ketol was similar to 4-carboxybenzaldehyde consistent with fast generation of ketol of the cyclic Mn^V intermediate and slow consumption via oxidation to dione (Figure 4.3). We could not perform an experiment to determine the rate constant of ketol oxidation to dione because of the lack of authentic standards. We hypothesize that this oxidation reaction is similarly slow. We can only base that hypothesis on Figure 4.3

because no significant concentration of dione was observed in the 30 minute quenching data Figure 4.6.

At pH 5.0 and order-of-magnitude excess of MnO_4^- in Figure 4.3, the amount of MnO_4^- consumed was almost triple the initial concentration of SDCA (Figure 4.2B). When MnO_4^- is in excess, we expect that the stoichiometry will be higher than 1:1 because of MnO_4^- oxidation of the intermediate and some of the products. The 200 OE that remain as solids may have come from the 4 electron oxidation of SDCA to aldehyde or ketol: the corresponding 4 electron reduction of MnO_4^- would give Mn^{III} as the product (S4.8).

Solutions buffered with 5 mM phosphate or pyrophosphate at pH 7.0 suppressed the $Mn^{III,IV}$ solids that were detected in the absence of a buffer (Figure 4.6). Both phosphate and pyrophosphate are known to adsorb strongly to oxide surfaces, which could prevent aggregation resulting in particles small enough to pass through the filter. Jiang et al. (*19*, *69*) confirmed the presence of a Mn^{III} pyrophosphate species generated during MnO_4^- oxidation of phenolic endocrine disrupting compounds. Pyrophosphate chelates Mn^{III} rendering it soluble and stable, preventing disproportionation to MnO_2(s) and Mn^{2+}(aq) (*50*). Phosphate should exhibit the same effect, albeit to a lesser extent.

Higher initial concentration of MnO_4^- favors more highly oxidized products. Oxidation of aldehyde to acid consumes MnO_4^- without affecting SDCA, causing the ratio in Figure 4.7A to increase. $Mn^{III,IV}$ solids are products of 3 or 4 electron reduction of MnO_4^- (Equations S4.8 and S4.7), while Mn^{2+} is the 5 electron reduction product (Equation S4.9). Under conditions where no solid formed, each MnO_4^- consumed transferred 5 e^- to the reductants. Each MnO_4^- that is reduced to Mn^{III} or Mn^{IV} only transfers 3 or 4 electrons, so more MnO_4^- must be reduced to achieve the same amount of electron transfer. The extent of oxidation of SDCA and generation of products was similar regardless of pH and buffer identity

(Figure 4.6). To achieve the same extent of oxidation when $Mn^{III,IV}$ solids are generated more MnO_4^- must be consumed, increasing the ratio shown on Figure 4.7.

Ideally, OE(transferred) and RE(transferred) would be equal and confirm that the number of electrons that were transferred from SDCA via oxidation equaled the number of electrons transferred to MnO_4^- via reduction (Table 4.2). The discrepancy between the two could reflect limitations in the iodometric method. Although we did not observe any other peaks using LC/MS that would correspond to other oxidation products, any undetected product that is oxidized by MnO_4^- would increase OE(transferred) but would not be accounted for in RE(transferred).

4.5 Conclusions

Using SDCA as a model alkene with a hydroxylamine quench model and modified iodometry, we have demonstrated a means monitoring manganese speciation and the identity and yields of organic oxidation products. Oxidation of SDCA is much faster than the oxidation of the aldehyde containing products to the corresponding carboxylic acids. Aldehydes and ketols are the major products of SDCA oxidation by MnO_4^-. Carboxylic acids and diones may be significant products on longer time scales at high doses of MnO_4^-. Within the range 5 <pH <10, pH had a significant effect, but the identity of the buffer had a less pronounced effect. Nonzero RE(transferred) in the absence of MnO_4^- may indicate that some other oxidant, likely O2, can oxidize SDCA and generate the same products.

References

(1) J. Walton, P. Labine, A. Reidies, *The Chemistry of Permanganate in degradative oxidations* in *Chemical Oxidation: Technologies for the Nineties*, W. W. Eckenfelder, J. A. Roth, A. R. Bowers (Eds.), CRC Press, Lancaster, **1992**, pp. 205–230.

(2) L. Rader. How to operate and maintain manganese greensand treatment units. *On Tap* **2003**, *2*, 31–32.

(3) A. M. Dietrich, R. C. Hoehn, L. C. Dufresne, L. W. Buffin, D. M. C. Rashash, B. C. Parker. Oxidation of odorous and nonodorous algal metabolites by permanganate, chlorine, and chlorine dioxide. *Water Science and Technology* **1995**, *31*, 223–228.

(4) S. Sorlini, F. Gialdini. Conventional oxidation treatments for the removal of arsenic with chlorine dioxide, hypochlorite, potassium permanganate and monochloramine. *Water Research* **2010**, *44*, 5653–5659.

(5) K. J. Ficek, J. E. Boll. Potassium permanganate: an alternative to prechlorination. *Aqua* **1980**.

(6) J. Ma, G. Li. Laboratory and full-scale plant studies of permanganate oxidation as an aid in coagulation. *Water Science and Technology* **1993**, *27*, 47–54.

(7) J. Ma, G. B. Li, Z. L. Chen, G. R. Xu, G. Q. Cai. Enhanced coagulation of surface waters with high organic content by permanganate preoxidation. *Water Science and Technology: Water Supply* **2001**, *1*, 51–61.

(8) M. Schnarr, C. Truax, G. Farquhar, E. Hood, T. Gonullu, B. Stickney. Laboratory and controlled field experiments using potassium permanganate to remediate trichloroethy-

lene and perchloroethylene DNAPLs in porous media. *Journal of Contaminant Hydrology* **1998**, *29*, 205–224.

(9) Y. E. Yan, F. W. Schwartz. Oxidative degradation and kinetics of chlorinated ethylenes by potassium permanganate. *Journal of Contaminant Hydrology* **1999**, *37*, 343–365.

(10) Y. E. Yan, F. W. Schwartz. Kinetics and Mechanisms for TCE Oxidation by Permanganate. *Environmental Science and Technology* **2000**, *34*, 2535–2541.

(11) J. Albano, S. Comfort, V. Zlotnik, T. Halihan, M. Burbach, C. Chokejaroenrat, S. Onanong, W. Clayton. In situ chemical oxidation of RDX-Contaminated groundwater with permanganate at the nebraska ordnance plant. *Ground Water Monitoring and Remediation* **2010**, *30*, 96–106.

(12) T. Halihan, J. Albano, S. Comfort, V. A. Zlotnik. Electrical resistivity imaging of a permanganate injection during in situ treatment of RDX-contaminated groundwater. *Ground Water Monitoring and Remediation* **2012**, *32*, 43–52.

(13) S. M. G. Hossain, R. G. McLaughlan. Oxidation of Chlorophenols in Aqueous Solution by Excess Potassium Permanganate. *Water, Air, and Soil Pollution* **2011**, *223*, 1429–1435.

(14) J. H. Damm, C. Hardacre, R. M. Kalin, K. P. Walsh. Kinetics of the oxidation of methyl tert-butyl ether (MTBE) by potassium permanganate. *Water Research* **2002**, *36*, 3638–3646.

(15) W. Li, J. Duan, D. Mulcahy. Kinetic characteristics of oxidation of microcystin-LR at low concentration by chlorine and permanganate. *Journal Of Water Supply Research And Technology-Aqua* **2012**, *61*, 82–93.

(16) J. Acero, E. Rodríguez, M. E. Majado, A. Sordo, J. Meriluoto. Oxidation of microcystin-LR with chlorine and permanganate during drinking water treatment. *Journal Of Water Supply Research And Technology-Aqua* **2008**, *57*, 371–380.

(17) E. Rodríguez, J. Acero, L. Spoof, J. Meriluoto. Oxidation of MC-LR and -RR with chlorine and potassium permanganate: Toxicity of the reaction products. *Water Research* **2008**, *42*, 1744–1752.

(18) G. D. Onstad, S. Strauch, J. Meriluoto, G. A. Codd, U. von Gunten. Selective oxidation of key functional groups in cyanotoxins during drinking water ozonation. *Environmental Science and Technology* **2007**, *41*, 4397–4404.

(19) J. Jiang, S.-Y. Pang, J. Ma, H. Liu. Oxidation of phenolic endocrine disrupting chemicals by potassium permanganate in synthetic and real waters. *Environmental Science and Technology* **2012**, *46*, 1774–1781.

(20) J. Jiang, S.-Y. Pang, J. Ma. Oxidation of triclosan by permanganate (Mn(VII)): Importance of ligands and in situ formed manganese oxides. *Environmental Science and Technology* **2009**, *43*, 8326–8331.

(21) L. Hu, H. Martin, O. Arce-Bulted, M. Sugihara, K. Keating, T. J. Strathmann. Oxidation of carbamazepine by Mn(VII) and Fe(VI): Reaction kinetics and mechanism. *Environmental Science and Technology* **2009**, *43*, 509–515.

(22) L. Hu, A. M. Stemig, K. H. Wammer, T. J. Strathmann. Oxidation of Antibiotics during Water Treatment with Potassium Permanganate: Reaction Pathways and Deactivation. *Environmental Science and Technology* **2011**, *45*, 3635–3642.

(23) L. Hu, H. M. Martin, T. J. Strathmann. Oxidation Kinetics of Antibiotics during Water Treatment with Potassium Permanganate. *Environmental Science and Technology* **2010**, *44*, 6416–6422.

(24) E. Chamberlain, H. Shi, T. Wang, Y. Ma, A. Fulmer, C. Adams. Comprehensive screening study of pesticide degradation via oxidation and hydrolysis. *Journal of Agricultural and Food Chemistry* **2012**, *60*, 354–363.

(25) C. Liu, Z. Qiang, C. Adams, F. Tian, T. Zhang. Kinetics and mechanism for degradation of dichlorvos by permanganate in drinking water treatment. *Water Research* **2009**, *43*, 3435–3442.

(26) S. Dash, S. Patel, B. Mishra. Oxidation by permanganate: synthetic and mechanistic aspects. *Tetrahedron* **2009**, *65*, 707–739.

(27) F. Freeman, J. C. Kappos. Permanganate ion oxidations. 19. Hexadecyltrimethylammonium permanganate oxidation of cycloalkenes. *Journal of Organic Chemistry* **1989**, *54*, 2730–2734.

(28) F. Freeman, L. Y. Chang. Permanganate Ion Oxidations .17. Kinetics and Mechanism of the Oxidation of (E)-3-(2-Thienyl)-2-Propenoates and (E)-3-(3-Thienyl)-2-Propenoates in Phosphate-Buffered Solutions. *The Journal of the American Chemical Society* **1986**, *108*, 4504–4509.

(29) F. Freeman, J. C. Kappos. Permanganate Ion Oxidations .15. Additional Evidence for Formation of Soluble (Colloidal) Manganese-Dioxide During the Permanganate Ion Oxidation of Carbon-Carbon Double-Bonds in Phosphate-Buffered Solutions. *The Journal of the American Chemical Society* **1985**, *107*, 6628–6633.

(30) K. B. Wiberg, R. D. Geer. Kinetics of Permanganate Oxidation of Alkenes. *The Journal of the American Chemical Society* **1966**, *88*, 5827–5832.

(31) M. Jáky, L. I. Simándi. Mechanism of the permanganate oxidation of unsaturated compounds. Part VI. Kinetic investigation of the oxidation of methylmaleic acid, methylfumaric acid, and dimethylmaleic acid. *Journal Of The Chemical Society-Perkin Transactions 2* **1976**, 939–943.

(32) L. I. Simándi, M. Jáky. Mechanism of the permanganate oxidation of unsaturated compounds. Part 7. Kinetics of the oxidation of propiolic and phenylpropiolic acids. *Journal Of The Chemical Society-Perkin Transactions 2* **1977**, 630.

(33) Z. Szeverényi, L. I. Simándi, M. Jáky. Rate Constants of Permanganate Oxidation of Dimethylmaleic Acid and Dimethylmaleic Anhydride. *Inorganica Chimica Acta* **1977**, *23*, L31–L32.

(34) L. I. Simándi, M. Jáky. Mechanism of the permanganate oxidation of unsaturated compounds. Part IV. Kinetic investigation of the oxidation of maleic and fumaric acid. *Journal Of The Chemical Society-Perkin Transactions 2* **1973**, 1856.

(35) K. Polgar, M. Jáky, L. I. Simándi. Kinetics and mechanism of the permanganate oxidation of trans-crotonic acid. *Reaction Kinetics and Catalysis Letters* **1976**, *5*, 489–495.

(36) D. G. Lee, T. Chen. Oxidation of hydrocarbons. 18. Mechanism of the reaction between permanganate and carbon-carbon double bonds. *The Journal of the American Chemical Society* **1989**, *111*, 7534–7538.

(37) L. I. Simándi, M. Jáky. Nature of the detectable intermediate in the permanganate oxidation of trans-cinnamic acid. *The Journal of the American Chemical Society* **1976**, *98*, 1995–1997.

(38) D. G. Lee, J. R. Brownridge. Oxidation of Hydrocarbons .4. Kinetics and Mechanism of Oxidative Cleavage of Cinnamic Acid by Acidic Permanganate. *The Journal of the American Chemical Society* **1974**, *96*, 5517–5523.

(39) K. B. Wiberg, K. A. Saegebarth. The mechanisms of permanganate oxidation. iv. hydroxylation of olefins and related reactions. *The Journal of the American Chemical Society* **1957**, *79*, 2822–2824.

(40) K. B. Wiberg, C. Deutsch, J. Roček. Permanganate oxidation of crotonic acid. Spectrometric detection of an intermediate [13]. *The Journal of the American Chemical Society* **1973**, *95*, 3034–3035.

(41) F. Freeman, C. O. Fuselier, C. R. Armstead, C. E. Dalton, P. A. Davidson, E. M. Karchesfski, D. E. Krochman, M. N. Johnson, N. K. Jones. Permanganate Ion Oxidations .13. Soluble Manganese(Iv) Species in the Oxidation of 2,4(1h,3h)-Pyrimidinediones (Uracils). *The Journal of the American Chemical Society* **1981**, *103*, 1154–1159.

(42) L. I. Simándi, M. Jáky. Mechanism of Permanganate Oxidation of Unsaturated-Compounds .4. Kinetic Investigation of Oxidation of Maleic and Fumaric Acids. *Journal Of The Chemical Society-Perkin Transactions 2* **1973**, 1856–1860.

(43) G. King. alpha-ketol carboxylic acids Part I 9-Hydroxy-10-keto- and 10-hydroxy-9-keto-stearic acids. *Journal of The Chemical Society (Resumed)* **1936**, 1788–1792.

(44) W. L. Evans. The oxidation of propylene glycol with potassium permanganate. *The Journal of the American Chemical Society* **1923**, *45*, 171–176.

(45) D. G. Lee, N. S. Srinivasan. Oxidation of hydrocarbons. X. Concerning the formation of ketols and diones during the oxidation of alkenes by permanganate ion. *Canadian Journal of Chemistry-Revue Canadienne De Chimie* **1981**, *59*, 2146–2149.

(46) K. B. Wiberg, A. S. Fox. The mechanisms of permanganate oxidation. Oxidation of tertiary hydrogens. *The Journal of the American Chemical Society* **1963**, *85*, 3487–3491.

(47) M. Jáky, L. I. Simándi. Mechanism of the permanganate oxidation of unsaturated compounds. Part I. Short-lived intermediates of the oxidation of acetylenedicarboxylic acid. *Journal Of The Chemical Society-Perkin Transactions 2* **1972**, 1481–1486.

(48) L. I. Simándi, M. Jáky. Mechanism of Permanganate Oxidation of Unsaturated-Compounds .4. Kinetic Investigation of Oxidation of Maleic and Fumaric Acids. *Journal Of The Chemical Society-Perkin Transactions 2* **1973**, 1856–1860.

(49) M. Jáky, L. I. Simándi, L. Maros, I. Molnár-Perl. Mechanism of the permanganate oxidation of unsaturated compounds. Part III. Intermediates in the oxidation of maleic and fumaric acids. *Journal Of The Chemical Society-Perkin Transactions 2* **1973**, 1565–1569.

(50) J. K. Klewicki, J. J. Morgan. Kinetic behavior of Mn(III) complexes of pyrophosphate, EDTA, and citrate. *Environmental Science and Technology* **1998**, *32*, 2916–2922.

(51) R. Stewart. The mechanisms of permanganate oxidation. III. the oxidation of benzhydrol. *The Journal of the American Chemical Society* **1957**, *79*, 3057–3061.

(52) K. B. Wiberg, R. Stewart. The mechanisms of permanganate oxidation. I. The oxidation of some aromatic aldehydes. *The Journal of the American Chemical Society* **1955**, *77*, 1786–1795.

(53) M. Jáky, J. Szammer. Oxidation of aldehydes with permanganate in acidic and alkaline media. *Journal of Physical Organic Chemistry* **1997**, *10*, 420–426.

(54) F. Freeman, J. Brant, N. Hester, A. Kamego, M. Kasner, T. Mclaughlin, E. Paull. Permanganate oxidations. III. Kinetics and mechanisms of the oxidation of furfurals in alkaline mediax. *Journal of Organic Chemistry* **1970**, *35*, 982–985.

(55) K. B. Wiberg, F. Freeman. Kinetics of the base-catalyzed permanganate oxidation of benzaldehyde. *Journal of Organic Chemistry* **2000**, *65*, 573–576.

(56) J. Taylor, T. Janini, O. Elmer. Aqueous permanganate oxidations of cycloalkenes to cis-glycols and cis to trans conversions. *Organic Process Research & Development* **1998**, *2*, 147–150.

(57) J. E. Taylor, D. Williams, K. Edwards, D. Otonnaa, D. Samanich. Permanganate peroxidation of cyclohexene. 1. The unusual effect of turbulent stirring and dilution upon glycol yields. *Canadian Journal of Chemistry-Revue Canadienne De Chimie* **1984**, *62*, 11–15.

(58) J. Boeseken. Sur la Configuration des α-Glycols Formés par Oxydation des Alkylènes. *Recueil des Travaux Chimiques des Pays-Bas* **1928**, *47*, 683–693.

(59) J. Coleman, C. Ricciuti, D. Swern. Improved preparation of 9(10),10(9)-ketohydroxystearic acids by oxidation of oleic acid with potassium permanganate

in neutral solution. *The Journal of the American Chemical Society* **1956**, *78*, 5342–5345.

(60) J. W. Ladbury, C. F. Cullis. Kinetics and mechanism of oxidation by permanganate. *Chemical Reviews* **1958**, *58*, 403–438.

(61) Microsoft Excel for Mac 2011. **2010**.

(62) L. S. Clesceri, A. D. Eaton, A. E. Greenberg, *Standard Methods for the Examination of Water and Wastewater*, American Public Health Assocation, American Water Works Association, Water Pollution Control Federation, Washington, DC, **2000**.

(63) J. W. Murray, L. S. Balistrieri, B. Paul. The oxidation state of manganese in marine sediments and ferromanganese nodules. *Geochimica et Cosmochimica Acta* **1984**, *48*, 1237–1247.

(64) L. J. Kirschenbaum, J. R. Sutter. Kinetic Studies of Permanganate Oxidation Reactions. I. Reaction with Iodide Ion. *The Journal of Physical Chemistry* **1966**.

(65) O. A. Songina, V. A. Zakharov, G. B. Bekturova, L. I. Smirnova. Amperometric-Titration of Permanganate, Chromate, and Vanadate with Potassium Iodide. *Journal of Analytical Chemistry of the USSR* **1974**, *29*, 1377–1380.

(66) I. M. Kolthoff, J. I. Watters. Polarographic determination of manganese as tri-dihydrogen pyrophosphatomanganiate. *Industrial and Engineering Chemistry-Analytical Edition* **1943**, *15*, 8–13.

(67) W. W. Y. Lam, W. L. Man, C. F. Leung, C. Y. Wong, T. C. Lau. Solvent effects on the oxidation of RuIV=O to O=Ru VI=O by MnO4 -. Hydrogen-atom versus oxygen-atom transfer. *The Journal of the American Chemical Society* **2007**, *129*, 13646–13652.

(68) W. G. Toland, J. B. Wilkes, F. J. Brutschy. Reactions of toluic acids with aulfur. I. Stilbenedicarboxylic acids. *The Journal of the American Chemical Society* **1953**, *75*, 2263–2264.

(69) J. Jiang, S.-Y. Pang, J. Ma. Role of Ligands in Permanganate Oxidation of Organics. *Environmental Science and Technology* **2010**, *44*, 4270–4275.

Table 4.1. Moles of MnO_4^- consumed per mol of alkene consumed required to generate specific organic oxidation and inorganic reduction products based on balanced redox reactions. Half-reactions are shown for oxidation of an alkene substrate. The number of electrons required to reduce MnO_4 to each reduction product are shown. Balanced redox reactions are shown in 4.6.1 in the Supporting Information.

	MnO_4^- reduction product		
	MnO_2(s)	MnOOH(s)	Mn^{2+}(aq)
Alkene Oxidation Product Half-Reaction	3 e^-	4 e^-	5 e^-
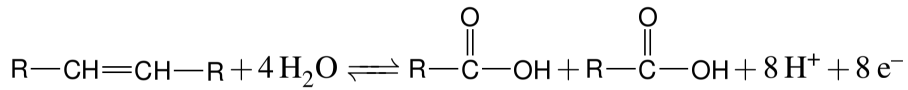	2.67	2	1.6
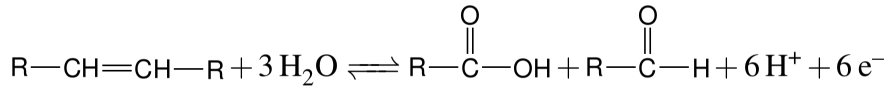	2	1.5	1.2
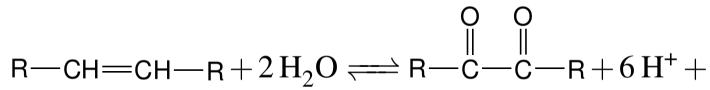	2	1.5	1.2
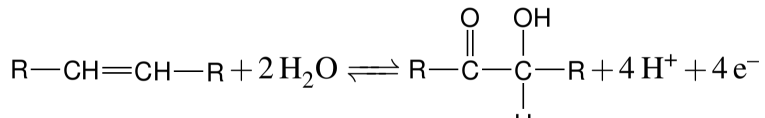	1.33	1	0.8
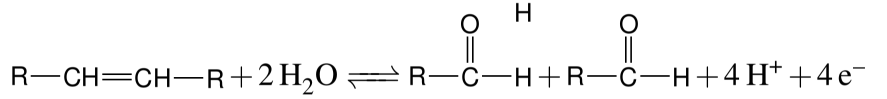	1.33	1	0.8
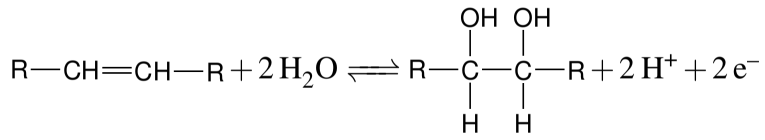	0.67	0.5	0.4

Table 4.2. Comparison of equivalents of MnO_4^- reduced, shown as OE(transferred), and equivalents of SDCA oxidized, shown as RE(transferred), measured after 30 minutes of contact time in buffered solutions of 20 μM SDCA and MnO_4^- with ionic strength adjusted to 10 mM with NaCl.

Buffer (pH)	$[MnO_4^-]_0$ (μM)	OE(transferred) (μEq L^{-1})	RE(transferred) (μEq L^{-1})
	0	0	4.8
5.0 mM	10	28	27
Acetate	20	49	48
(pH 5.0)	40	44	70
	100	58	74
	200	91	75
	0	0	4
	10	10	18
Unbuffered	20	53	53
(pH 7.0)	40	88	85
	100	192	90
	200	200	84
	0	0	6
5.0 mM	10	26	32
Phosphate	20	50	64
(pH 7.0)	40	80	82
	100	113	86
	200	145	90
	0	0	3
5.0 mM	10	40	36
Pyrophoshpate	20	70	71
(pH 7.0)	40	90	77
	100	103	82
	200	120	85
	0	0	6
5.0 mM	10	31	35
Carbonate	20	60	58
(pH 10.0)	40	92	97
	100	87	98
	200	128	110

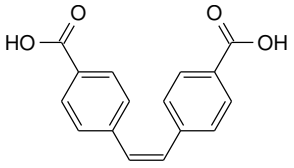

cis-Stilbenedicarboxylic acid
$[\text{M-H}]^- = 267$

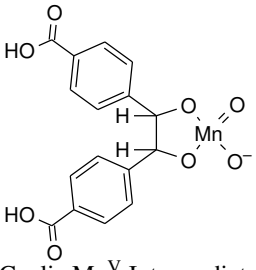

Cyclic Mn^V Intermediate

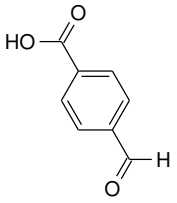

4-Carboxybenzaldehyde
4 electrons
$[\text{M-H}]^- = 164$

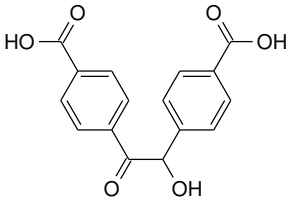

Ketol
4 electrons
$[\text{M-H}]^- = 299$

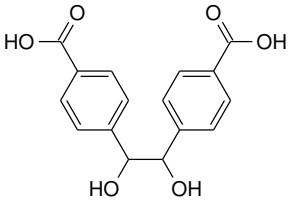

Diol
2 electrons
$[\text{M-H}]^- = 301$

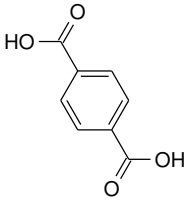

Terephthalic acid
8 electrons
$[\text{M-H}]^- = 165$

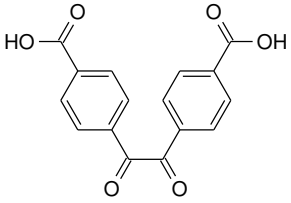

Dione
6 electrons
$[\text{M-H}]^- = 297$

Figure 4.1. Molecular structure of *cis*-stilbenedicarboxylic acid (SDCA), proposed cyclic Mn^V intermediate, and products. Each product is labeled with the required number of electrons SDCA must be oxidized by to generate it and the mass-to-charge ratio (m/z) of the molecular ion used to detect it by electrospray mass spectrometry.

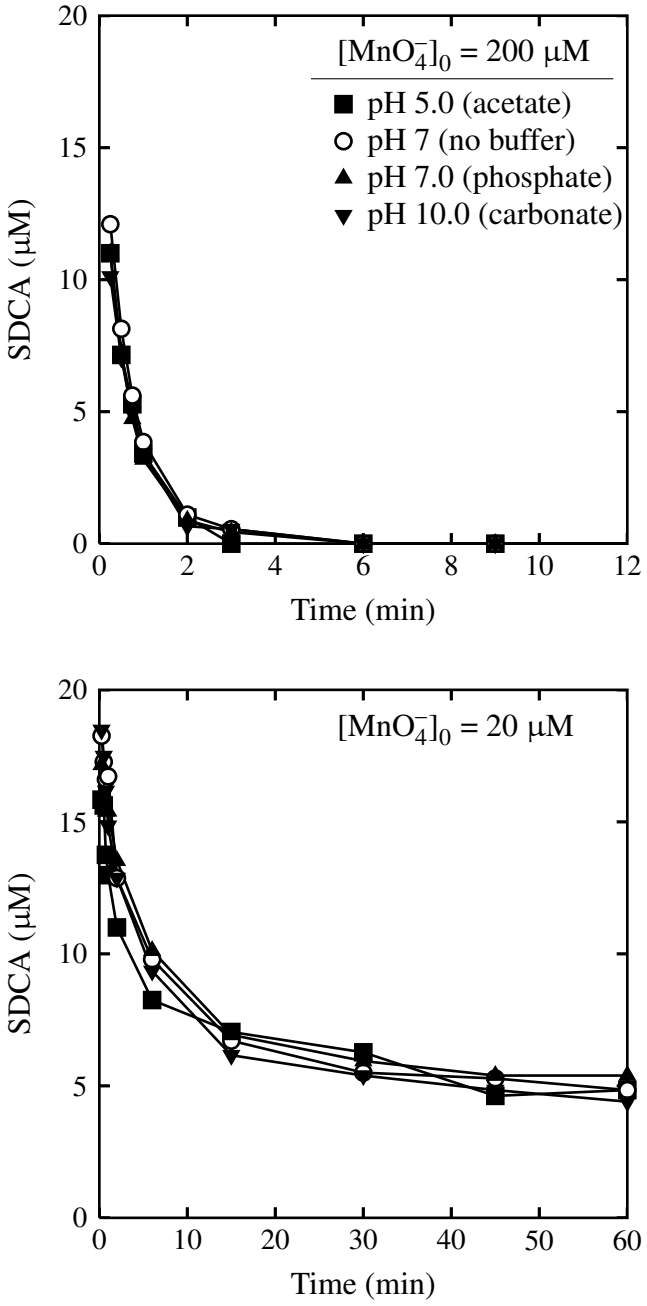

Figure 4.2. Loss of *cis*-stilbenedicarboxylic acid in the presence of MnO_4^-. Conditions: 20 μM SDCA, ionic strength adjusted to 10 mM with NaCl.

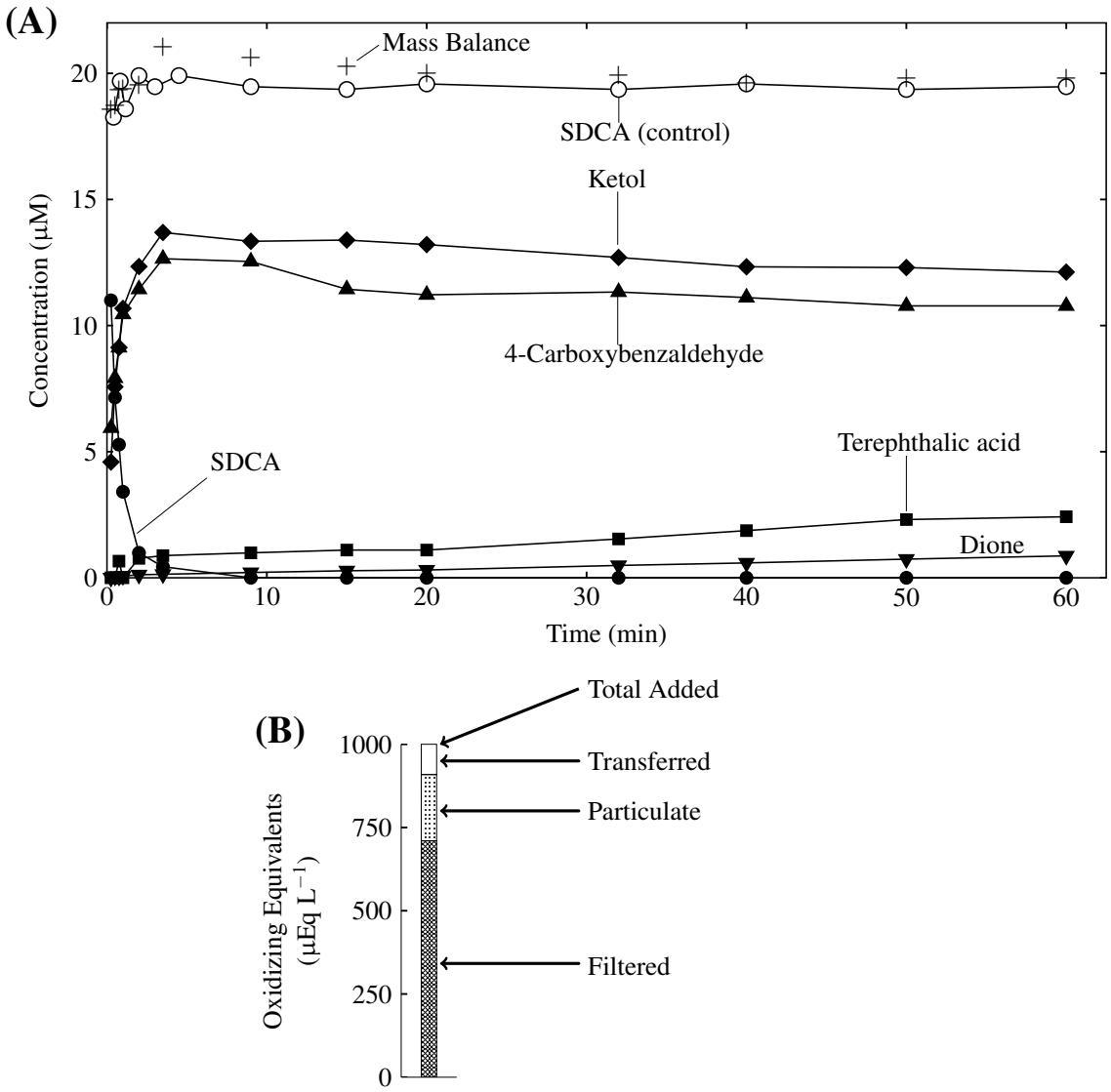

Figure 4.3. (A) *cis*-Stilbenedicarboxylic acid (SDCA) loss in the presence of 200 μM MnO_4^-. Conditions: 20 μM SDCA, 5 mM acetate buffer (pH 5.0), and ionic strength adjusted to 10 mM using NaCl. The concentration of SDCA in a separate control experiment lacking MnO_4^- is shown for comparison. (B) Results obtained from iodometric titration of filtered and unfiltered aliquots collected after 30 min of contact time.

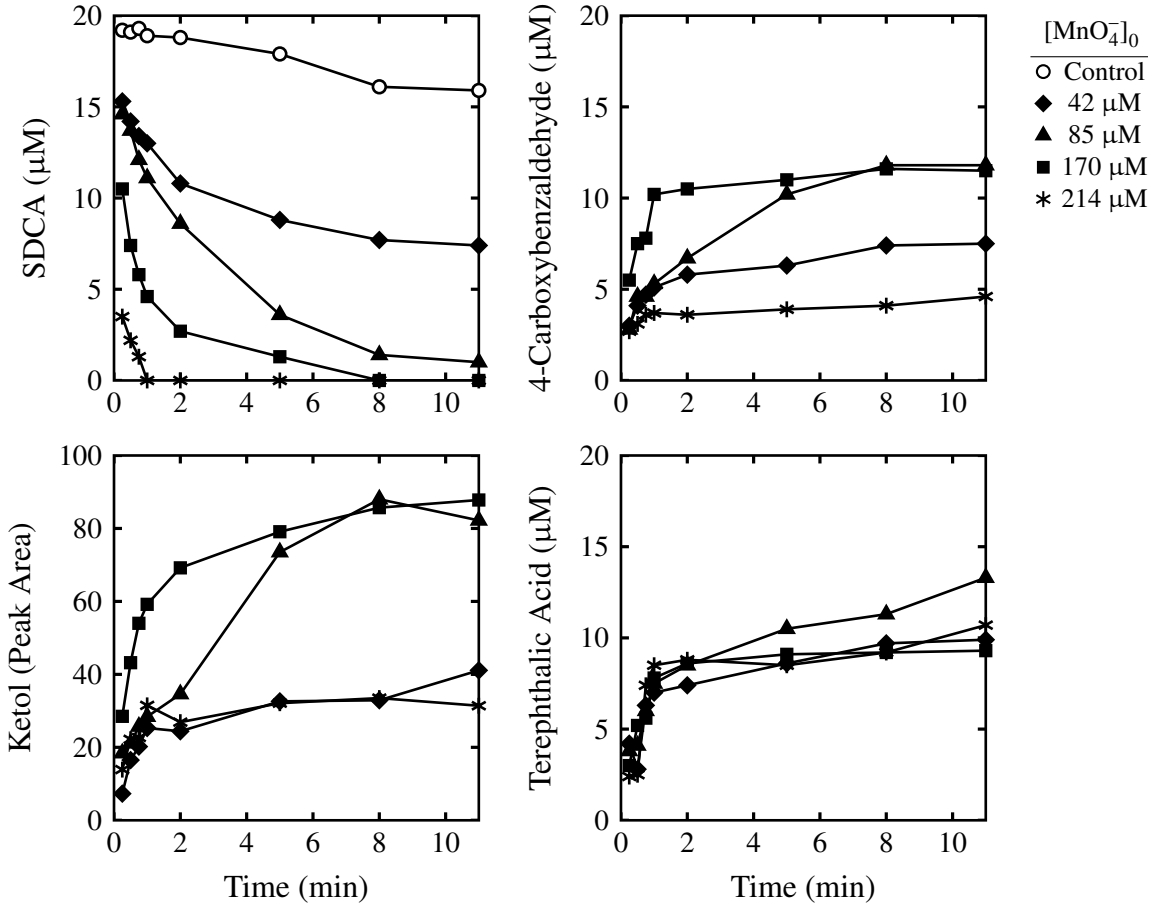

Figure 4.4. Time course plots for reaction of 20 μM *cis*-Stilbenedicarboxylic acid (SDCA) and generation of 4-carboxybenzaldehyde, terephthalic acid and ketol in the presence of increasing amounts of MnO_4^-. The reaction medium contained 5.0 mM acetate (pH 4.0) with ionic strength adjusted to 10 mM using NaCl. The concentration of SDCA in a control experiment lacking MnO_4^- is shown for comparison.

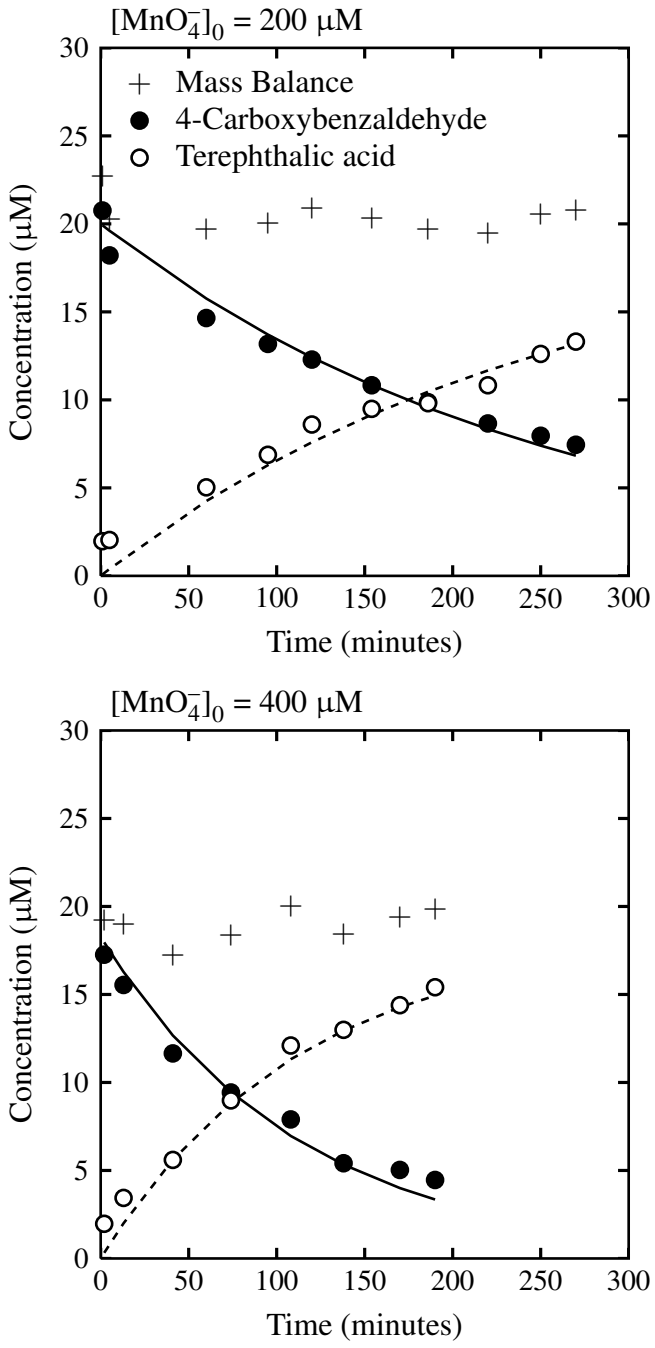

Figure 4.5. Time course plots for oxidation of 20 μM 4-carboxybenzaldehyde to terephthalic acid by (A) 200 μM Mno_4^- and (B) 400 μM MnO_4^-. The reaction medium contained 5.0 mM acetate (pH 5.0) with ionic strength was adjusted to 10 mM using NaCl. Lines represent a pseudo-first-order model of 4-carboxybenzaldehyde consumption. Dashed lines a represent model of terephthalic acid generation. The sum of 4-carboxybenzaldehyde and terephthalic acid concentrations is shown as the mass balance.

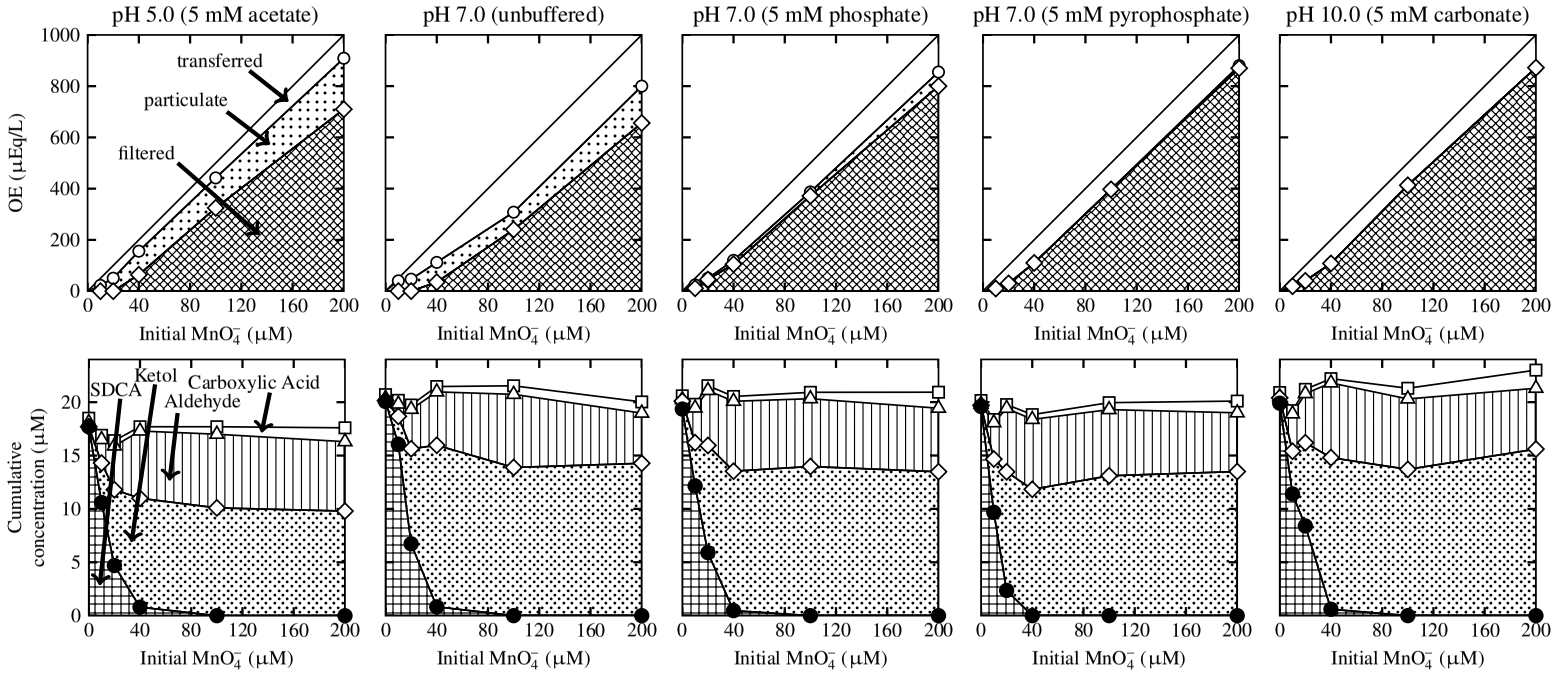

Figure 4.6. Oxidizing equivalents (OE), unreacted *cis*-stilbenedicarboxylic acid (SDCA) and organic oxidation product concentrations after 30 min of contact time. Conditions: 20 μM SDCA, ionic strength adjusted to 10 mM using NaCl.

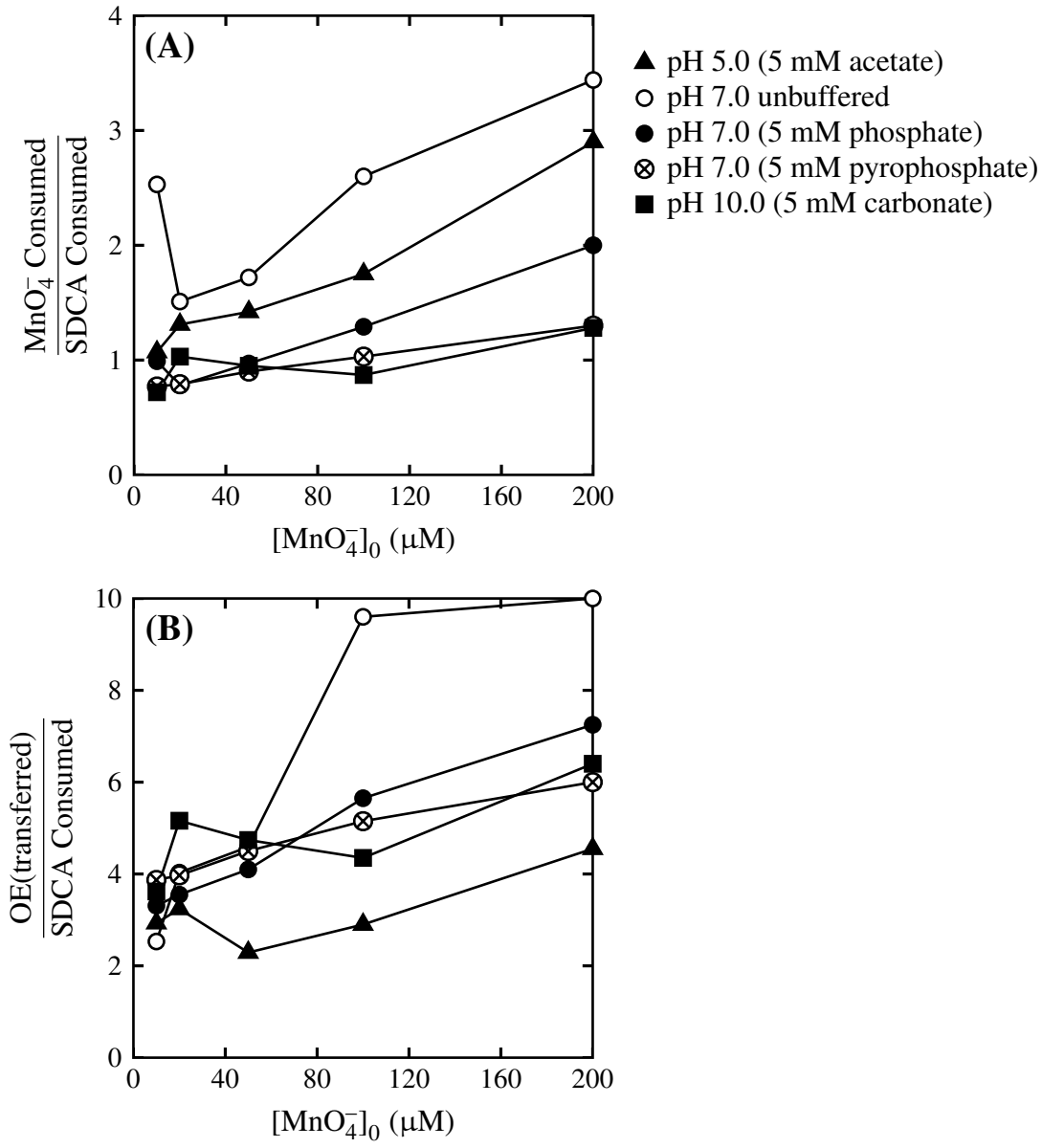

Figure 4.7. (A) Ratio of MnO_4^- consumed to *cis*-stilbenedicarboxylic acid (SDCA) consumed and (B) ratio of OE(transferred) to SDCA consumed. Conditions: 20 μM SDCA, ionic strength adjusted to 10 mM using NaCl, reaction was quenched after 30 min of contact time.

4.6 Supporting Information

Supporting information for Chapter 4 includes half-reactions balanced reactions for redox reactions between alkenes and MnO_4^- leading to the possible organic oxidation and inorganic reduction products that were referred to in Table 4.1, results from a series of experiments using 3-cyclopentene-1-carboxylic acid as a model alkene (4.6.2), a flow diagram of the sampling procedure for iodometry and LC/MS analysis in quenched experiments (Figure S4.3), time course results for control experiments showing loss of SDCA in the absence of MnO_4^- (Figure S4.4), tabulated data shown on Figure 4.6, and a table of available acid dissociation constants (pK_a) for chemical compounds used in this study (Table S4.4).

4.6.1 Redox Reactions for Permanganate Oxidation of an Alkene

This section gives six half-reactions for oxidation of an alkene substrate and three for reduction of MnO_4. Following the half-reactions, eighteen balanced reactions are shown for each pair of alkene oxidation product and MnO_4^- reduction product. These reactions were used to determine the stoichiometric ratios of MnO_4^- consumed to alkene consumed shown in Table 4.1.

The half-reaction for two carboxylic acid final products requires 8 electron transfer overall from the alkene to MnO_4^-.

$$\mathrm{R\text{-}CH{=}CH\text{-}R} + 4\,\mathrm{H_2O} \rightleftharpoons \mathrm{R\text{-}\overset{\overset{O}{\|}}{C}\text{-}OH} + \mathrm{R\text{-}\overset{\overset{O}{\|}}{C}\text{-}OH} + 8\,\mathrm{H^+} + 8\,\mathrm{e^-} \tag{S4.1}$$

If one carboxylic acid and one aldehyde are the final products then 6 electron transfer is required.

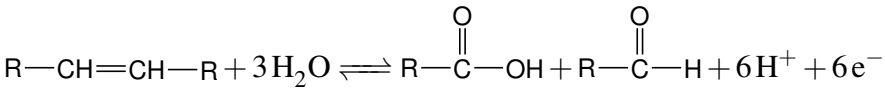

(S4.2)

The half-reaction for dione formatation also requires 6 electron transfer.

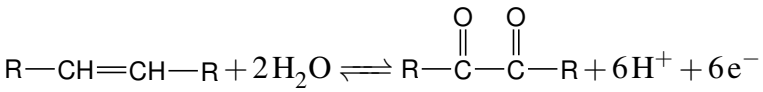

(S4.3)

Formation of the ketol product requires 4 e⁻transfer

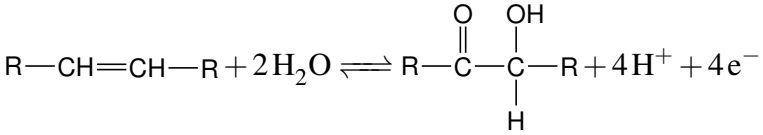

(S4.4)

and so does forming two aldehydes.

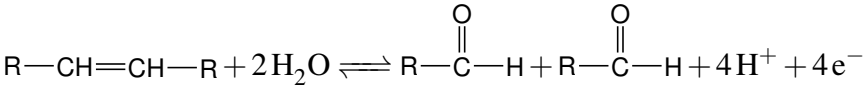

(S4.5)

Diol products result from only 2 electron transfer.

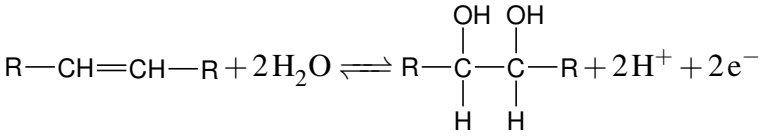

(S4.6)

In summary, oxidative C=C double bond cleavage to two carboxylic acids requires transfer of 8 electrons, while one carboxylic acid and one aldehyde requires 6 electrons. Oxidation to a ketol product is a 4 electron transfer and the diol is a 2 electron transfer.

Now, we will list the half-reactions for reduction of MnO_4^-. The potential products of MnO_4^- reduction are Mn^{IV} solids, Mn^{III} solids, and Mn^{2+}(aq). The half-reactions show that these products result from 3, 4, and 5 electron reductions, respectively.

$$MnO_4^-(aq) + 4H^+(aq) + 3e^- \rightleftharpoons Mn^{IV}O_2(s) + 2H_2O \tag{S4.7}$$

$$MnO_4^-(aq) + 5H^+(aq) + 4e^- \rightleftharpoons Mn^{III}OOH(s) + 2H_2O \tag{S4.8}$$

$$MnO_4^-(aq) + 8H^+(aq) + 5e^- \rightleftharpoons Mn^{2+}(aq) + 4H_2O \tag{S4.9}$$

The balanced redox reactions for all possible combinations of MnO_4^- reduction products and alkene oxidation products are shown below. *Two Carboxylic Acids*

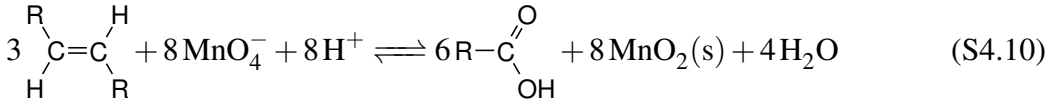

(S4.10)

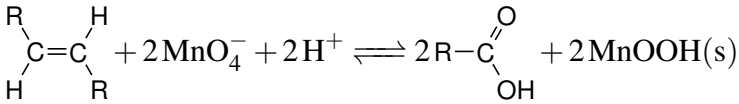

(S4.11)

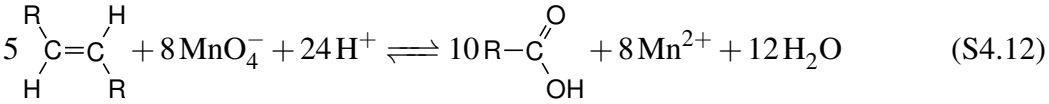

(S4.12)

One Carboxylic Acid and One Aldehyde

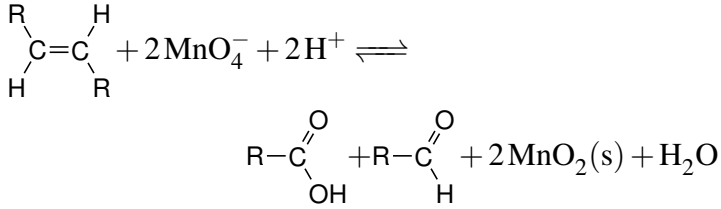

(S4.13)

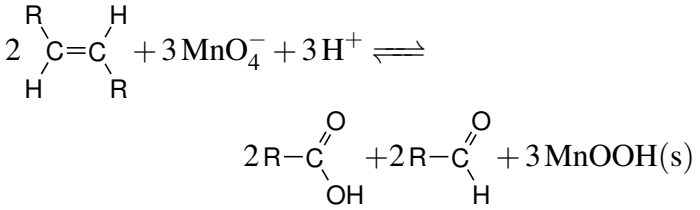

(S4.14)

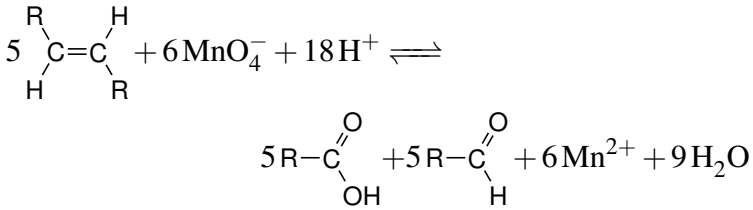

(S4.15)

Dione

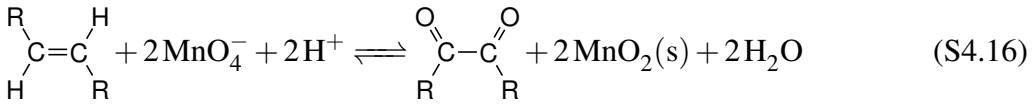

(S4.16)

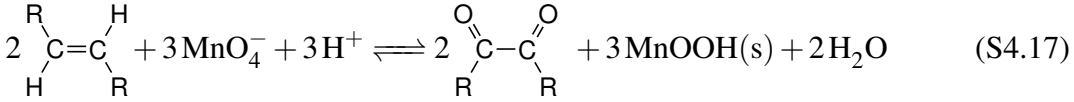

(S4.17)

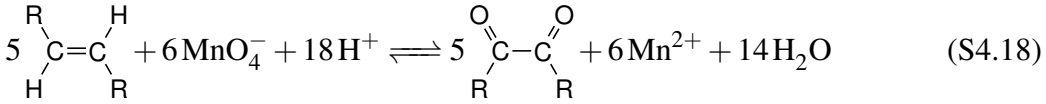

(S4.18)

Ketol

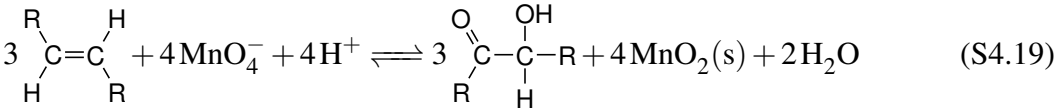

(S4.19)

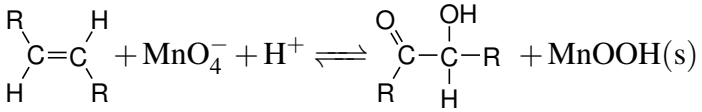

(S4.20)

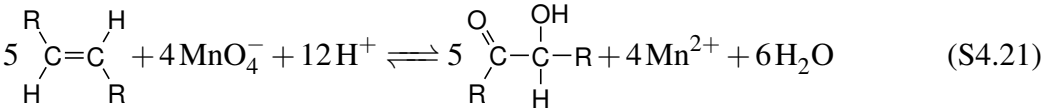

(S4.21)

Two Aldehydes

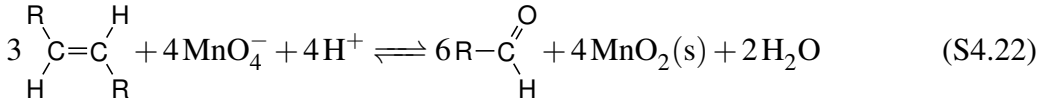

(S4.22)

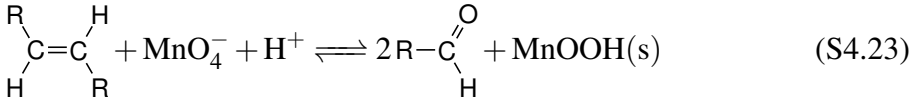

(S4.23)

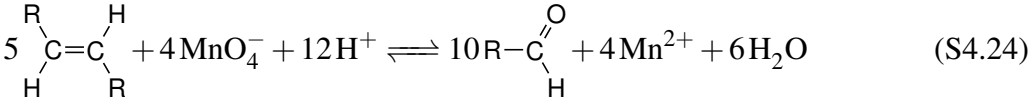

(S4.24)

Diol

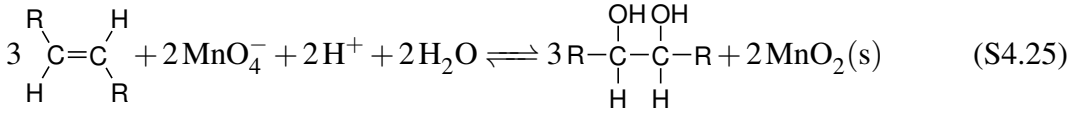

(S4.25)

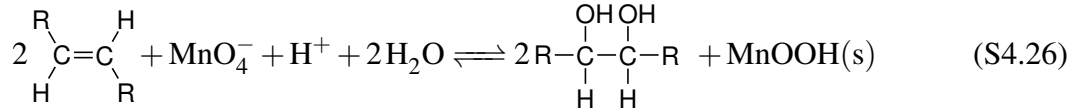

(S4.26)

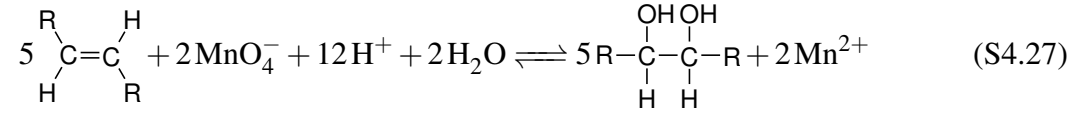

(S4.27)

4.6.2 3-Cyclopentene-1-carboxylic acid

A second model compound we employed was 3-cylcopentenecarboxylic acid (CPCA). Figure S4.1 show a proposed pathway for MnO_4^- oxidation of CPCA. The fully oxidized product where the alkene double bond has been broken and oxidized to two carboxylic acid groups known as "tricarballylic acid" is commercially available. We report peak areas for the acid-aldehyde intermediate, and the diol product.

Methods for CPCA

All aqueous solutions were prepared from reagent grade chemicals and distilled, deionized water (Milli-Q water, 18 MΩ-cm resistivity, Millipore Corp., Milford, MA). All bottles and glassware were rinsed with distilled water, soaked in 5 M nitric acid overnight, rinsed with distilled water and Milli-Q water and then air-dried.

3-Cylcopentene-1-carboxylic acid and tricarballlic acid were purchased from Aldrich (St. Louis, MO). All other chemicals used were from the same suppliers mentioned in 4.2.1.

All experiments were performed in 100 mL polypropylene bottle reactors placed in a $25 \pm 1^{\circ}C$ constant temperature bath. Reaction solutions were continuously stirred with Teflon-coated stir bars and sparged with $N_2(g)$. The $N_2(g)$ sparge line is bubble through water before reaching the experimental solution to minimize evaporation of the solution. Before every experiment, fresh stock solutions of CPCA, $KMnO_4$, NaCl, and the buffer of interest were prepared in Milli-Q water. Solutions contained 5.0 mM acetate buffer to maintain pH at 4.25 and 5.0 mM carbonate buffer at pH 10.0. Sufficient stock of NaCl was added to adjust the ionic strength to 10 mM.

Samples were taken after 12 hours of contact time and filtered with 0.2 μm pore diameter track-etched polycarbonate filter membranes (Whatman, UK). The quenching solution was not used. LC/MS analysis was used to determine concentration of CPCA and tricarballylic acid oxidation product. Peak areas a peaks with m/z corresponding to diol product and acid-aldehyde intermediate were also measured. Concentration cannot be determined for diol product and acid-aldehyde because authentic standards were unavailable. HPLC separation was conducted using a Waters 2795 separation module (Milford, MA) with a 4.6 x 250 mm, 5 μm particle size, Atlantis T3 column (Waters, Milford, MA). HPLC eluent was

isocratic 85% 0.2% acetic acid, 15% methanol at a 1 mL min^{-1} flow rate. MS detection was conducted in the same manner as described for SDCA (4.2.5).

Results and Discussion for CPCA

The products generated from MnO_4^- oxidation of 3-cyclopentencarboxylic acid (CPCA) were starkly different at pH 4.25 than at pH 10.0 Figure S4.2. In both solutions, complete loss of CPCA was observed after 24 hours when $[MnO_4^-]_0$ was greater than 300 μM. The diol product was detected at pH 10.0, but not at pH 4.25. The largest peak area for diol was observed at 400 μM $[MnO_4^-]_0$ and then decreased with increasing $[MnO_4^-]_0$. At pH 4.25, concentrations of tricarballylic acid were below 5 μ when $[MnO_4^-]_0$ was less than 500 μM. Tricarballylic acid concentration increased to between 50 and 63 μM at permanganate concentrations between 1000 and 1800 μM. At pH 10, tricarballylic acid increased slightly with increasing $[MnO_4^-]_0$, but did not exceed 7.2 μM. Note that in control experiments in solutions of MnO_4^- and tricarballylic acid no loss of either compound was observed. At pH 4.25, the largest peak areas of acid/aldehyde arose when $[MnO_4^-]_0$ was in the range of 250 – 750 μM, but it decreased at higher $[MnO_4^-]_0$. Only small peak areas of acid-aldehyde were detected at pH 10.0.

At pH 4.25, we expect that tricarballylic acid will be the fully oxidized product, and that acid/aldehyde would be an intermediate (Figure S4.1). Consistent with this, tricarballylic acid is favored at high $[MnO_4^-]_0$, and acid/aldehyde is favored at intermediate $[MnO_4^-]_0$ (Figure S4.2). However, even at the highest $[MnO_4^-]_0$ (1800 μM), only 62 μM tricarballylic acid has been generated out of 150 μM of CPCA initially added. Even though the MnO_4^- concentration was in greater than an order-of-magnitude excess, CPCA was not fully oxidized to tricarballylic acid within 24 hours. The dialdehyde intermediate, which we did not monitor, may account for some CPCA that was oxidized by MnO_4^-, but not to

acid/aldehyde or tricarballylic acid. Because dialdehyde, acid/aldehyde, and tricarballylic acid are members of a series of oxidation reactions the amount generated after 24 hours will depend on the rate of the two aldehyde oxidation reactions (k_4 and k_5 on Figure S4.1). If k_4 is smaller k_5 the concentration of dialdehyde will increase over time and the concentration of acid/aldehyde and tricarballylic acid will be limited. Unfortunately, we could not determine k_4 and k_5 directly, but they must be very slow because not all of CPCA is converted to tricarballylic acid in 24 hours despite the excess of MnO_4^-. Of course, CPCA may have been converted into a different product. Notably, we did not monitor the ketol. The ketol was a major product for SDCA (Figure 4.6), and may also be a major product for CPCA.

At pH 10.0, tricarballylic acid is not expected to be the major product: only 7.2 μM was generated at the highest $[MnO_4^-]_0$. Instead of acid/aldehyde and tricarballylic acid, the diol product was detected. High concentrations of OH^- at pH 10.0 should favor the diol, which results from hydrolysis of the cyclic hypomanganate ester (Equation 4.9). The decrease in diol peak area after reaching a maximum at 400 μM $[MnO_4^-]_0$ could be due to higher oxidant dose favoring ketol, which is a more highly oxidized product than the diol (Table 4.1).

Table S4.1. Oxidizing equivalents (OE) measured after 30 minutes of contact time in solutions of 20 μM *cis*-stilbenedicarboxylic acid (SDCA) and MnO_4^- (Figure 4.6). All OE reported in μEq L^{-1}.

Buffer (pH)	$[MnO_4^-]_0$	Initial	Unfiltered	Filtered	Particulate	Transferred
	0	0	0	0	0	0
5.0 mM	10	50	22.5	0	22.5	27.5
Acetate	20	100	50.5	0	50.5	49.5
(pH 5.0)	40	200	156	64	92	44
	100	500	442	325	117	58
	200	1000	909	710	199	91
	0	0	0	0	0	0
	10	50	40	0	40	10
Unbuffered	20	100	46.5	0	46.5	53.5
(pH 7.0)	40	200	112	35	77	88
	100	500	308	240	68	192
	200	1000	800	656	144	200
	0	0	0	0	0	0
5.0 mM	10	50	24	11	13	26
Phosphate	20	100	50	45	5	50
(pH 7.0)	40	200	120	105	15	80
	100	500	387	371.5	15.5	113
	200	1000	855	800	55	145
	0	0	0	0	0	0
5.0 mM	10	50	10	10	0	40
Pyrophospate	20	100	30	30	0	70
(pH 7.0)	40	200	110	110	0	90
	100	500	397	397	0	103
	200	1000	880	870	10	120
	0	0	0	0	0	0
5.0 mM	10	50	19	19	0	31
Carbonate	20	100	40	40	0	60
(pH 10.0)	40	200	108	108	0	92
	100	500	413	413	0	87
	200	1000	872	872	0	128

Table S4.2. Concentrations and peak areas determined using LC/MS. Same conditions as Figure 4.6.

Buffer (pH)	$[MnO_4^-]_0$ (μM)	SDCA (μM)	Ald[a] (μM)	Ac[b] (μM)	K[c] (Area)	Diol (Area)	Dione (Area)	B[d] (Area)
5.0 mM Acetate (pH 5.0)	0	17.7	0.8	0.8	0	22		40495
	10	10.6	4.3	0.8	883	6	8	39065
	20	4.7	8.2	0.9	1725	17	71	39853
	40	0.8	12.5	0.9	2470	21		39668
	100	0.0	13.8	1.4	2513		112	40846
	200	0.0	13	2.5	2450	10	116	40949
Unbuffered (pH 7.0)	0	20.1	0.4	0.7	24			44239
	10	16.0	2.3	0.7	704			44114
	20	6.7	7.4	0.8	2253			41466
	40	0.8	10	1	3906			42313
	100	0.0	13.7	1.6	2956	5	126	41242
	200	0.0	9.4	2.1	3687			42356
5.0 mM Phosphate (pH 7.0)	0	19.4	0.3	0.7	209			46498
	10	12.2	6.5	0.7	1072			43448
	20	5.9	10.3	0.9	2560	47		41795
	40	0.5	13.1	0.9	3420	78	154	42945
	100	0.0	12.7	1.2	5258	112	426	45649
	200	0.0	11.9	3	3958	97	218	40763
5.0 mM Pyrophosphate (pH 7.0)	0	19.6	0.2	0.7	33	65		46596
	10	9.7	6.8	0.6	1555	4		51032
	20	2.4	11.9	0.7	3331	13	132	49174
	40	0.0	13.1	0.9	3493	6	155	48390
	100	0.0	12.4	1.3	3893		136	48712
	200	0.0	11	2.2	3835			46583
5.0 mM Carbonate (pH 10.0)	0	19.9	0.3	0.8	123			40965
	10	11.4	6.9	0.6	1333	3		47030
	20	8.4	9.3	0.8	2540		126	45680
	40	0.6	14	0.8	4640	80	233	46053
	100	0.0	13.2	1.9	4509	93	584	46288
	200	0.0	11.4	3.5	5106	137	961	46049

[a] Aldehyde (4-carboxybenzaldehyde). [b] Acid (terephthalic acid). [c] Ketol.
[d] Benzoic acid internal standard.

Table S4.3. Concentration of organic products and oxidizing equivalents (OE) after 30 minutes of contact time in solutions of 20 μM *cis*-stilbenedicarboxylic acid (SDCA) and MnO_4^- as shown on Figure 4.6. Concentrations are reported in μM and OE are in μEq L^{-1}

Buffer (pH)	$[MnO_4^-]_0$	SDCA	Ald[a]	Ac[b]	K[c]	MB[d]	OE(t)[e]	OE(p)[f]	OE(f)[g]
5.0 mM Acetate (pH 5.0)	0	17.7	0.8	0.8	0	18.5	0	0	0
	10	10.6	4.3	0.8	3.7	16.9	27.5	22.5	0
	20	4.7	8.2	0.9	7.1	16.4	49.5	50.5	0
	40	0.8	12.5	0.9	10.2	17.7	44	92	64
	100	0	13.8	1.4	10.1	17.8	58	117	325
	200	0	13	2.5	9.8	17.7	91	199	710
Unbuffered (pH 7.0)	0	20.1	0.4	0.7	0.1	20.7	0	0	0
	10	16.1	2.3	0.7	2.6	20.2	10	40	0
	20	6.7	7.4	0.8	8.9	19.7	53.5	46.5	0
	40	0.8	10	1	15.1	21.5	88	77	35
	100	0	13.7	1.6	13.9	21.5	192	68	240
	200	0	9.4	2.1	14.3	20	200	144	656
5 mM Phosphate (pH 7.0)	0	19.4	0.3	0.7	0.7	20.6	0	0	0
	10	12.2	6.5	0.7	4	19.8	26	13	11
	20	5.9	10.3	0.9	10	21.5	50	5	45
	40	0.5	13.1	0.9	13.1	20.7	80	15	105
	100	0	12.7	1.2	14	21.3	113	15.5	371.5
	200	0	11.9	3	13.5	21.1	145	55	800
5 mM Pyrophosphate (pH 7.0)	0	19.6	0.2	0.7	0.1	20.2	0	0	0
	10	9.7	6.8	0.6	5	18.4	40	0	10
	20	2.4	11.9	0.7	11.1	19.9	70	0	30
	40	0	13.1	0.9	11.8	19	90	0	110
	100	0	12.4	1.3	13.1	20.1	103	0	397
	200	0	11	2.2	13.5	20.1	120	10	870
5.0 mM Carbonate (pH 10.0)	0	19.9	0.3	0.8	0.4	20.9	0	0	0
	10	11.4	6.9	0.6	4	19.2	31	0	19
	20	8.4	9.3	0.8	7.8	21.2	60	0	40
	40	0.6	14	0.8	14.2	22.2	92	0	108
	100	0	13.2	1.9	13.7	21.3	87	0	413
	200	0	11.4	3.5	15.6	23	128	0	872

[a] Aldehyde (4-carboxybenzaldehyde). [b] Acid (terephthalic acid). [c] Ketol.
[d] Mass Balance (Equation 4.13). [e] OE(transferred). [f] OE(particulate). [g] OE(filtered).

Table S4.4. Known pK_a values for chemicals used in this chapter. Acid dissociation constants were corrected to zero ionic strength using the Davies equation (*1*), when necessary.

Chemical	pK_a	Reference
$HMnO_4 \rightleftharpoons MnO_4^- + H^+$	−2.24	*2*
Hydroxylamine	5.97	*3*
	13.7	*3*
Acetate	4.784	*4*
H_3PO_4	2.148	*4*
	7.198	*4*
	12.35	*4*
Pyrophosphate	0.83	*4*
	2.26	*4*
	6.72	*4*
	9.46	*4*
Carbonate	6.351	*4*
	10.329	*4*
3-Cyclopentene-1-carboxylic acid	7.11[a]	*5*
Terephthalic acid	3.61	*3*
	4.50	*3*
4-Carboxybenzaldehyde	3.77	*6*

[a] in 50% aqueous ethanol at 25°C.

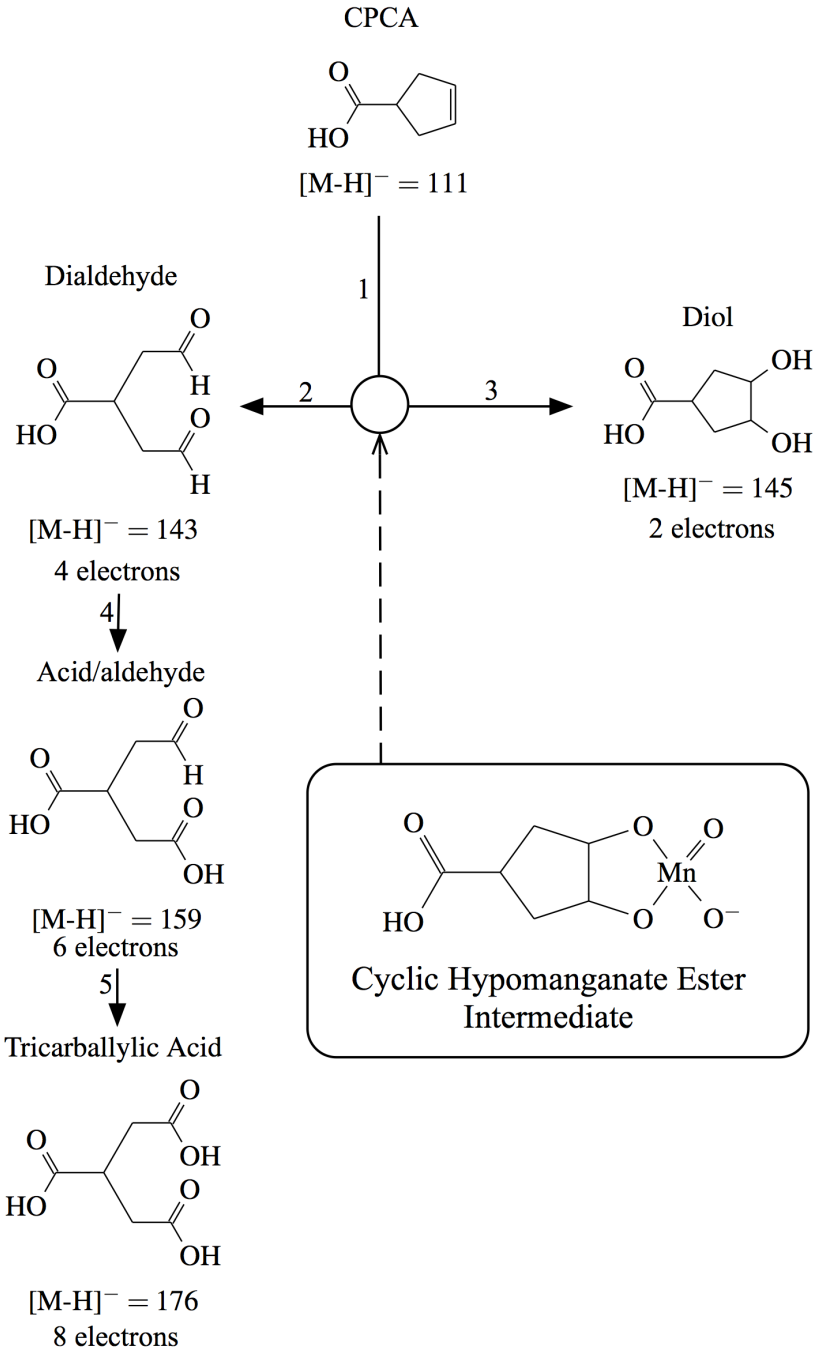

Figure S4.1. Proposed MnO_4^- oxidation pathway of 3-cylcopentenecarboxylic acid. After the cyclic hypomanganate ester intermediate is formed, the pathway can diverge to aldehyde and acid products or a diol. Each compound is labeled with the molecular ion mass to charge ratio for the which was used to detect each species.

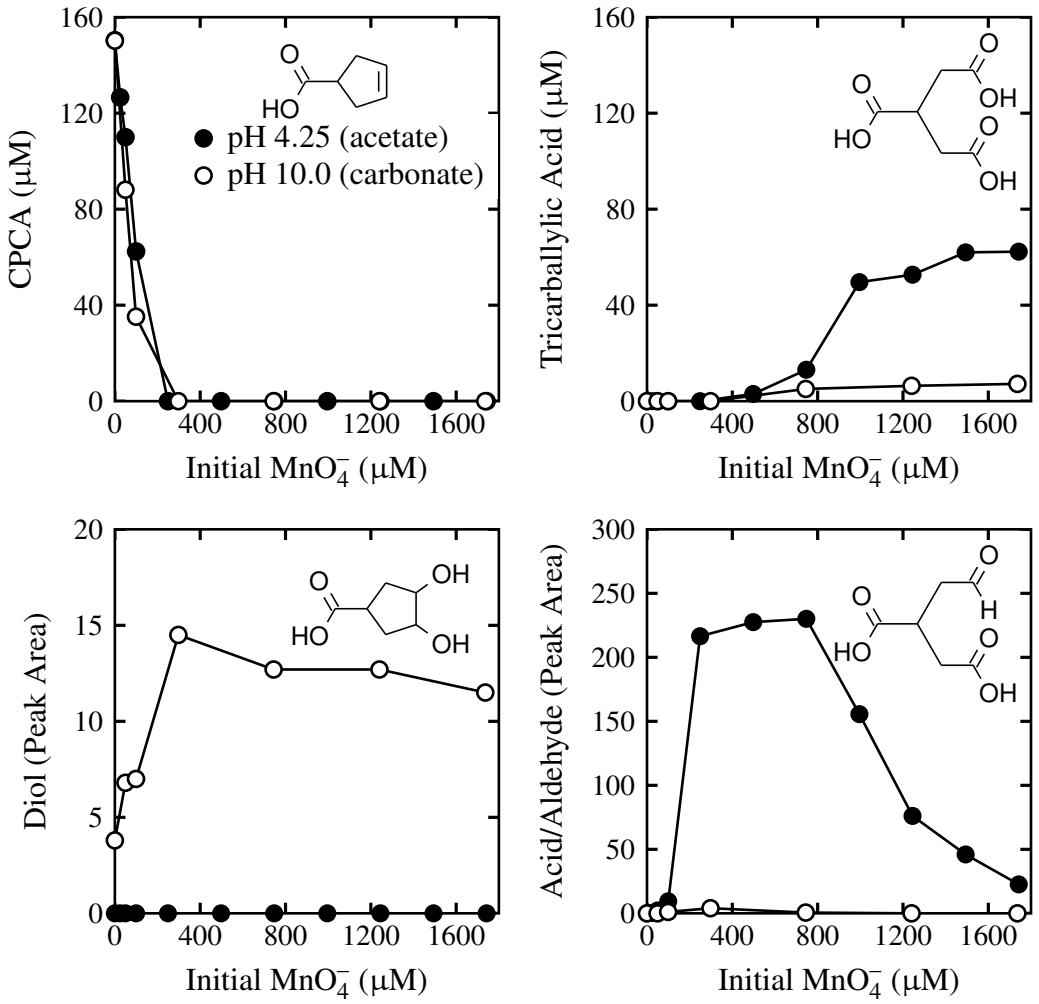

Figure S4.2. 3-cyclopentencarboxylic acid (CPCA) consumed and products generated after 24 hrs. Conditions: 150 μM CPCA, 5 mM buffer, ionic strength adjusted to 10 mM.

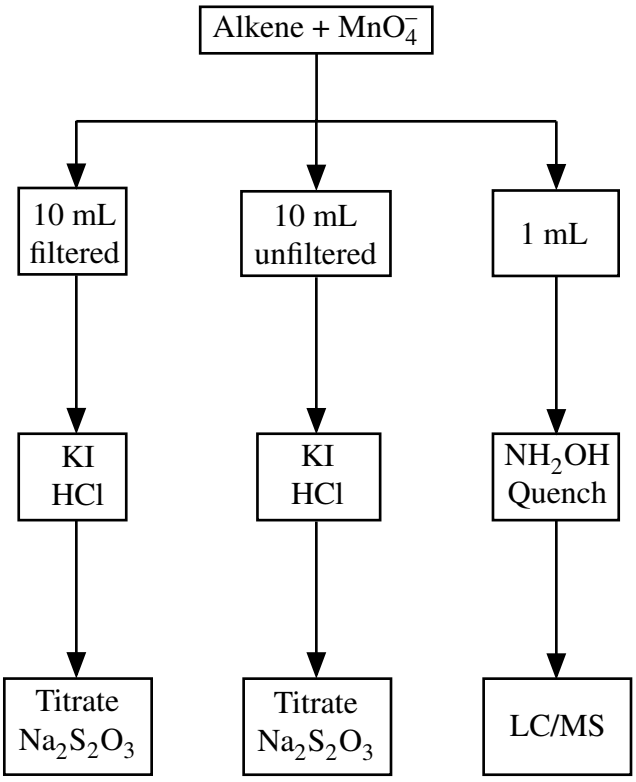

Figure S4.3. Flow diagram for analysis of non-time course experiments using iodometric titration and LC/MS.

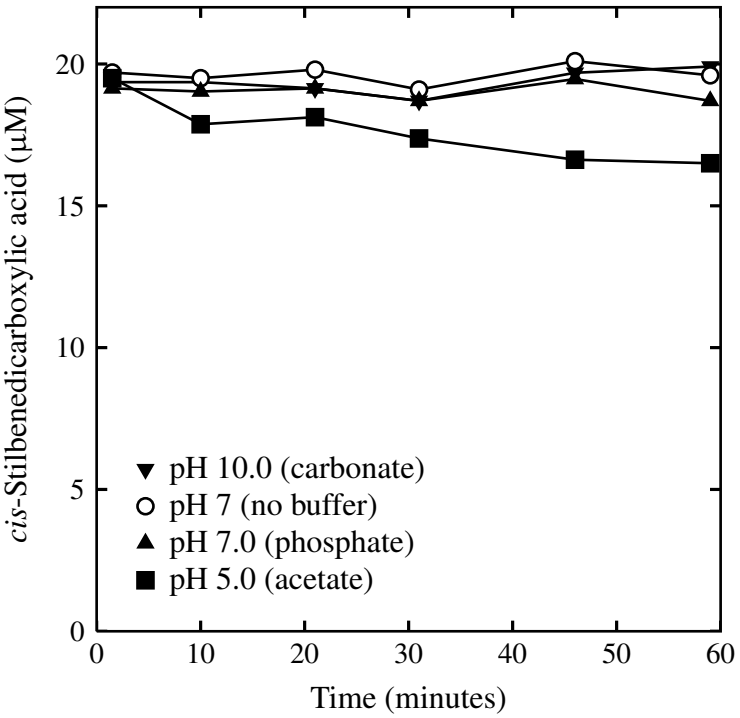

Figure S4.4. *cis*-Stilbenedicarboxylic acid (SDCA) loss in the absence of MnO_4^-. Ionic strength was adjusted to 10 mM by addition of NaCl.

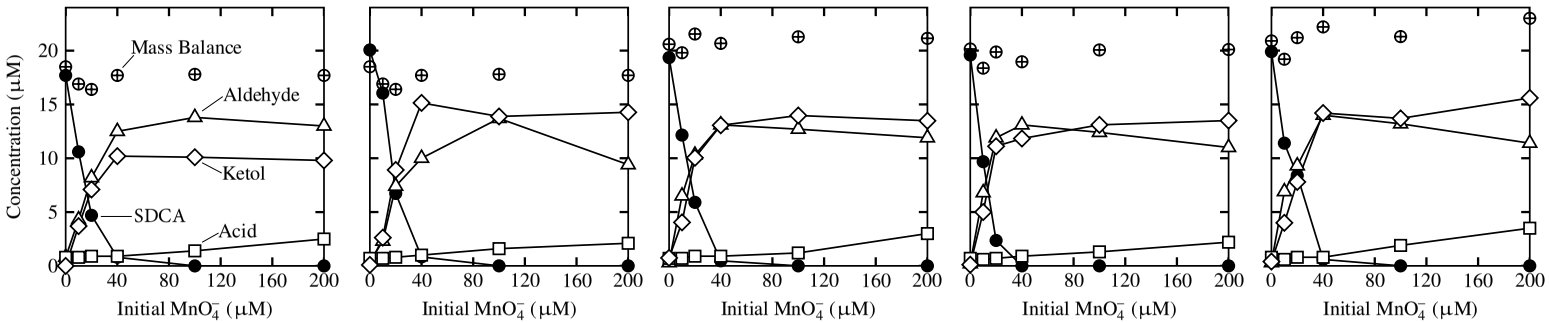

Figure S4.5. Organic oxidation products of *cis*-stilbenedicarboxylic acid (SDCA) after 30 min of contact time (corresponds to Figure 4.6). Mass balance is calculated using Equation 4.13. Conditions: 20 μM SDCA, ionic strength adjusted to 10 mM.

References

(1) W. Stumm, J. J. Morgan, *Aquatic Chemistry: Chemical Equilibria and Rates in Natural Waters 3rd ed.*, Wiley, New York, New York, **1996**.

(2) W. W. Y. Lam, W. L. Man, C. F. Leung, C. Y. Wong, T. C. Lau. Solvent effects on the oxidation of RuIV=O to O=Ru VI=O by MnO4 -. Hydrogen-atom versus oxygen-atom transfer. *The Journal of the American Chemical Society* **2007**, *129*, 13646–13652.

(3) A. E. Martell, R. M. Smith, R. J. Motekaitis, *Critically Selected Stability Constants of Metal Complexes Database; Version 8.0*, U.S. Department of Commerce, National Institute of Standards and Technology, Gaithersburg, MD, **2004**.

(4) R. N. Goldberg, N. Kishore, R. M. Lennen. Thermodynamic quantities for the ionization reactions of buffers. *Journal of Physical and Chemical Reference Data* **2002**, *31*, 231–370.

(5) O. H. Wheeler, I. Lerner. Structure and properties of cyclic compounds. III. Dissociation constants of simple α,β-unsaturated cyclic acids. *The Journal of the American Chemical Society* **1956**, *78*, 63–64.

(6) M. Zedda, J. Tuerk, T. Teutenberg, S. Peil, T. Schmidt. A strategy for the systematic development of a liquid chromatographic mass spectrometric screening method for polymer electrolyte membrane degradation products using isocratic and gradient phase optimized liquid chromatography. *Journal of Chromatography A* **2009**, *1216*, 8910–8917.

Chapter 5

Conclusion

5.1 Summary of Findings

In this dissertation we have detailed our experimental results for two major topics. The first is nucleophilic addition reactions and the proelectrophile pathway. We monitored reactions of nucleophiles with *p*-benzoquinone and patulin electrophiles and hydroquinone proelectrophiles that become electrophilic following oxidation. These reactions deserve detailed study because they could be involved in bound residue formation in soils and sediments. The second topic is MnO_4^- oxidation of alkenes. We identified a model compound where all of the expected oxidation products can be detected by LC/MS. This conclusion chapter will provide a summary of our findings on both of these topics and then propose some future directions for each topic.

5.1.1 Nucleophilic Addition Reactions

Sorption and desorption processes are integral to environmental fate and transport of many contaminants after they are released into the environment. Irreversible binding, often involving formation of a covalent bond, removes certain contaminants from the water column

and renders them biologically unavailable. Irreversibly bound contaminants are sometimes called "bound residues." Nucleophilic addition mechanisms, such as Michael addition, allow contaminants containing nucleophilic functional groups to form covalent bonds.

In Chapter 2, we sought to explore structure-reactivity relationships for Michael addition by monitoring loss of two model Michael acceptor electrophiles: *p*-benzoquinone and patulin. We monitored loss of Michael acceptor in the presence of a suite of added nucleophiles which were para-substituted anilines, 4-methylimidazole, and 4-methoxyphenol in MOPS buffered solution at pH 7.0. Our results are consistent with pH, nucleophilicity and electrophilicity being the key factors that control reaction rate between nucleophiles and Michael acceptors. We also confirmed that aromatic amines with electron-donating group substituents are stronger nucleophiles than those with electron-withdrawing substituents. Loss of *p*-benzoquinone is observed in the presence of aminopyralid, clopyralid, and chloramben herbicides may indicate that these more complex nucleophiles can also form bound residues. Substituted anilines reacted at least an order-of-magnitude faster with *p*-benzoquinone than with patulin, suggesting that 1,4-addition to *p*-benzoquinone is faster than 1,6-addition to patulin.

We note experimenters must take care to select buffers carefully when conducting experiments concerning nucleophile-electrophile reactions in aqueous media. In aqueous media, H_2O and OH^- are both capable of acting as nucleophiles, which we call "hydration. We saw absorbance increase in MOPS, MES, and DEPP buffered solutions of *p*-benzoquinone that we attribute to adduct formation. Maleate exhibited no concentration effect, suggesting that it does not react with *p*-benzoquinone and may be a more suitable buffer choice. However, under our experimental conditions in the presence of added nucleophiles the loss rate of *p*-benzoquinone and patulin was much faster than in the absence of added nucleophile.

In Chapter 3, we introduced the concept of "proelectrophiles" and reported on some simple model proelectrophile experiments. In particular, we are interested in highly electrophilic benzoquinones with electron-withdrawing group substituents. Unlike *p*-benzoquinone, which served as a model electrophile in Chapter 2, these substituted benzoquinones must be generated in situ by oxidation of a hydroquinone proelectrophile.

We expect one-to-one stoichiometry for pyrolusite (MnO_2) oxidation of hydroquinone proelectrophiles because reduction of MnO_2 is a 2 electron process and so is oxidation of a hydroquinone proelectrophile to the corresponding benzoquinone. Similarly, the stoichiometry of nucleophilic addition of an added nucleophile to a benzoquinone electrophile should also be 1-to-1. To probe reaction stoichiometry we conducted a series experiments using acetylhydroquinone as the proelectrophile and 4-ethylaniline as the nucleophile where we monitored consumption of acetylhydroquinone, consumption of 4-ethylaniline, and generation of Mn^{II}. Increased generation of Mn^{II} with increasing concentration of added nucleophile indicates that addition products become oxidized to second or third generation benzoquinones and increased consumption of nucleophile indicates that nucleophilic addition leading the adducts (X–Nu) is favored at the expense of hydration. We also considered initial rates of consumption of acetylhydroquinone, consumption of 4-ethylaniline, and generation of Mn^{II}. All three initial rates increased with increasing concentration of proelectrophile. However, only the initial rate of consumption of nucleophile increased with increased concentration of nucleophile. The rate and extent of adduct formation depends on both the concentrations of proelectrophile and nucleophile but also on the rate constants for oxidation and addition. Lastly, we reported LC/MS evidence for monoadducts resulting from experiments with gentisic acid as the proelectrophile and nine different nucleophiles.

Our results expand the mechanistic understanding of the interplay between addition reactions and oxidation reactions. This may represent a significant sink for nucleophilic

contaminants and natural products in environments where $Mn^{III,IV}$ (hydr)oxides oxidize organic matter such as at oxic/anoxic interface in sediments (*1*) or in manganese containing soils (*2*).

5.1.2 Permanganate oxidation of Alkenes

Technologies involving chemical oxidation are invaluable in water/wastewater treatment and subsurface remediation situations. In particular, oxidation by permanganate (MnO_4^-) can be employed to treat taste and odor problems, remove Mn^{II} and Fe^{II}, and remove precursors for disinfection byproducts among other uses.

MnO_4^- can oxidize a variety of inorganic chemicals and functional groups within organic molecules. A simple and common MnO_4^- oxidizable functional group is the alkene carbon-carbon double ($-C{=}C-$). Oxidation is thought to be initiated by MnO_4^- attack on the double bond leading to a cyclic Mn^V intermediate. The ultimate products result from competition of hydrolysis and oxidation reactions the following formation of an intermediate, which result in distribution of products is generated that depends on the pH and the dose of MnO_4^-.

Based on a literature review, the products of MnO_4^- oxidation of alkenes are expected to contain aldehydes, carboxylic acids, ketols, diones, and diol functional groups. However, most existing reports focus on a subset of these products. We monitored a more complete distribution of oxidation products by employing *cis*-stilbenedicarboxylic acid and 3-cyclopentenecarboxylic acid as convenient model alkenes, which could be detected even without authentic standards for some of the products. *cis*-Stilbenedicarboxylic acid was oxidized primarily to a ketol product or broken into two aldehyde products after 30 minutes of contact time and 10 times excess of permanganate. We also observed oxidation of the ketol to a dione and the aldehyde to a carboxylic acid; however this reaction is much slower.

We also used filtration and iodometric titration to attribute oxidizing equivalents remaining after 30 min to $Mn^{III,IV}$ solids and residual MnO_4^-.

Identification of useful model compounds such as *cis*-stilbenedicarboxylic acid and 3-cyclopentenecarboxylic acid (in the Supporting Information for Chapter 4) enhances our ability to observe effects of medium composition and experimental conditions for MnO_4^- oxidation of alkenes in the laboratory.

5.2 Future Research

Our results reported here would benefit from additional experimental data and some suggestions are given to future experimenters. Hopefully, they will spark further research into nucleophilic addition reactions in the environment and oxidation by MnO_4^- that will lead to useful tools for the environmental chemistry community.

5.2.1 Nucleophilic Addition and the Proelectrophile Pathway

The ratio plots (Figure 3.4) are an informative tool for discussing competition between hydration and nucleophilic addition for reaction with the generated benzoquinone electrophile and similar data should be taken for proelectrophiles with other sidegroups, for example hydroquinone or methylhydroquinone. Similar experiments with two nucleophiles from the same family, e.g. 4-nitroaniline and 4-methylaniline, may yield more detailed information about the influence of nucleophilicity and basicity. Blocking surface sites by including phosphate or pyrophosphate could help determine which steps of the proelectrophile pathway take place at the surface or are surface limited.

Pseudo-first-order kinetic studies monitoring loss of *p*-benzoquinone could be used as a simple predictor for rate of bound residue formation. Colón et al (*3*) correlated pK_a,

Hammett σ constant, and half-wave potential with loss rate of aromatic amines in soil samples. While, these molecular descriptors worked well for aromatic amines, they are often not available for complicated compounds like many organic contaminants. Pseudo-first-order rate constant for loss of *p*-benzoquinone could also correlate with loss rate to soils and sediments and can be determined by simple, inexpensive laboratory experiments. Loss of *p*-benzoquinone experiments are much cheaper to perform and containing fewer confounding factors than experiments in the field or experiments using whole soil or sediment samples. Potential nucleophiles could be screened for its rate of reaction with *p*-benzoquinone and the rate would be normalized by the rate of *p*-benzoquinone loss of a "benchmark nucleophile resulting in one weighting factor per nucleophile. A similar approach was taken by U.S. EPA (*4*) when developing toxic weighting factors (TWF) which allow wastewater discharges to be directly compared to each other in terms of toxic-weighted pounds equivalent even when the particular pollutants that the wastewater contains are different. Using a complex dataset of human health criteria and chronic aquatic life toxicity data, EPA developed factors relative to copper where pollutants with TWF greater than copper are more toxic. The weighting factors developed from rate of loss of *p*-benzoquinone would rank the nucleophiles in terms of likelihood to form covalently-bound residues. It could be a basis for selecting "green chemicals when performing an alternatives analysis for chemicals currently being used in industry and commerce. Chemicals that are quickly removed from the water column via binding to organic matter might be preferable to chemicals that do not bind and might persist longer the environment. If necessary, rates for loss of nucleophiles with known weighting factors in a particular location could be estimated by conducting a single whole soil or sediment experiment using the "benchmark nucleophile and a representative soil or sediment sample. Then, the amount of contaminants lost due to irreversible binding could

be estimated in fate and transport models of compounds containing a nucleophilic functional group.

5.2.2 Oxidation by Permanganate

Our experiments were continuously sparged with N_2 to minimize the concentration of O_2 in solution. In water treatment, the source water may contain higher concentrations of O_2 which could oxidize intermediates or products involved in MnO_4^- oxidation. This could change the distribution of the products or lead to new products.

The influence of natural organic matter (NOM) on MnO_4^- oxidation of alkenes should be evaluated, as well as the effect of oxidation by MnO_4^- on the properties and structure of NOM itself. The chemical structure of NOM is complicated and difficult to characterize. Redox properties of NOM samples depend on sampling location, because of differing environmental conditions that lead to NOM formation. Aeschbacher et al. (*5*) reported that electron accepting capacity of humic substance samples was linearly correlated with C/H elemental ratio and aromaticity estimated from ^{13}C NMR spectra. Perhaps a similar correlation exists for MnO_4^- oxidation rate and pathway because MnO_4^- oxidation is selective to certain functional groups. Based on chemical structure, some NOM samples may be more readily oxidized by MnO_4^- than others. Similarly, MnO_4^- may be less effective at promoting aggregation or removing disinfection byproduct precursors depending on the NOM sample origin. Humic acids may also differ from fulvic acids in terms of MnO_4^- oxidation reactivity. Aeschbacher et al. (*5*) also reported that electron accepting capacity was highest for terrestrial humic acids and lowest for aquatic fulvic acids.

References

(1) D. Canfield, B. Thamdrup, J. Hansen. The anaerobic degradation of organic matter in Danish coastal sediments: Iron reduction, manganese reduction, and sulfate reduction. *Geochimica et Cosmochimica Acta* **1993**, *57*, 3867–3883.

(2) H. Li, L. Lee, D. Schulze, C. A. Guest. Role of soil manganese in the oxidation of aromatic amines. *Environmental Science and Technology* **2003**, *37*, 2686–2693.

(3) D. Colon, E. J. Weber, G. Baughman. Sediment-associated reactions of aromatic amines. 2. QSAR development. *Environmental Science and Technology* **2002**, *36*, 2443–2450.

(4) U.S. EPA; Draft Toxic Weighting Factor Development in Support of CWA 304(m) Planning Process. *water.epa.gov* **2005**.

(5) M. Aeschbacher, M. Sander, R. P. Schwarzenbach. Novel electrochemical approach to assess the redox properties of humic substances. *Environmental Science and Technology* **2010**, *44*, 87–93.

Vita

Phillip Martin Flanders was born in St. Louis Park, Minnesota on July 8, 1985. He grew up in Chanhassen, Minnesota and graduated from Chaska High School in Chaska, Minnesota in 2003. He received a B.S. with a double major in Chemical Engineering and Chemistry with a minor in Japanese Language and Culture in 2007 from Rose-Hulman Institute of Technology (Terre Haute, Indiana). His undergraduate research work at Rose-Hulman focusing on reaction pathways of TiO_2 photodegradation of sulfamethoxazole in 2004. He began graduate studies in 2007 at Johns Hopkins University (Baltimore, Maryland) in August of 2007, earning the M.S.E. in Geography and Environmental Engineering in 2009. His research at Johns Hopkins focused on highly electrophilic benzoquinone Michael acceptors generated via MnO_2 oxidation, and the product distribution resulting from permanganate oxidation of alkenes. Upon completion of his graduate studies, Phillip accepted a position as an Environmental Engineer with the U.S. Environmental Protection Agency in the Engineering and Analysis Division of the Office of Water located in Washington, D.C.